

**CONSOLIDATION OF  
GEOLOGIC STUDIES OF  
GEOPRESSURED GEOTHERMAL  
RESOURCES IN TEXAS**

Annual Report

By R. A. Morton, T. E. Ewing, W. R. Kaiser,  
and R. J. Finley

Prepared for the U.S. Department of Energy  
Division of Geothermal Energy  
Contract No. DE-AC08-79ET27111

Bureau of Economic Geology  
W. L. Fisher, Director  
The University of Texas at Austin  
Austin, Texas 78712

March 1983

## DISCLAIMER

This report was prepared as an account of work sponsored by an agency of the United States Government. Neither the United States Government nor any agency thereof, nor any of their employees, makes any warranty, express or implied, or assumes any legal liability or responsibility for the accuracy, completeness, or usefulness of any information, apparatus, product, or process disclosed, or represents that its use would not infringe privately owned rights. Reference herein to any specific commercial product, process, or service by trade name, trademark, manufacturer, or otherwise, does not necessarily constitute or imply its endorsement, recommendation, or favoring by the United States Government or any agency thereof. The views and opinions of authors expressed herein do not necessarily state or reflect those of the United States Government or any agency thereof.

This report has been produced directly from the best available copy.

Available from the National Technical Information Service, U.S. Department of Commerce, Springfield, Virginia 22161.

Price: Printed Copy A10  
Microfiche A01

Codes are used for pricing all publications. The code is determined by the number of pages in the publication. Information pertaining to the pricing codes can be found in the current issues of the following publications, which are generally available in most libraries: Energy Research Abstracts (ERA); Government Reports Announcements and Index (GRA and I); Scientific and Technical Abstract Reports (STAR); and publication NTIS-PR-360, available from NTIS at the above address.

TABLE OF CONTENTS

<b>SECTION I: STRUCTURAL STYLES AND STRUCTURAL EVOLUTION OF THE FRIO GROWTH-FAULT TREND IN TEXAS: CONSTRAINTS ON GEOPRESSURED RESERVOIRS</b> . . . . .	1
ABSTRACT . . . . .	1
INTRODUCTION. . . . .	1
CORPUS CHRISTI STUDY AREA . . . . .	2
Stratigraphy . . . . .	5
Structure and structural development . . . . .	7
Structural constraints on geopressured reservoirs at depth . . . . .	25
SARITA DIP SECTION . . . . .	25
Stratigraphy . . . . .	27
Structure and structural development . . . . .	29
Structural constraints on geopressured reservoirs at depth . . . . .	35
PORT ARTHUR STUDY AREA . . . . .	35
Stratigraphy . . . . .	38
Structure and structural development . . . . .	42
Structural constraints on geopressured reservoirs at depth . . . . .	51
FRIO STRUCTURAL STYLES AND DEEP GEOTHERMAL POTENTIAL . . . . .	54
Comparison of structural styles of five Frio study areas . . . . .	54
Structural constraints on geopressured reservoirs at depth . . . . .	57
OUTLOOK: GEOTHERMAL PROSPECTS IN THE FRIO TREND IN THE NEXT DECADE . . . . .	58
ACKNOWLEDGMENTS . . . . .	59
REFERENCES . . . . .	60

*Figures in Section I*

I-1. Depositional systems of the Frio Formation showing the locations of the Frio geopressured trend study areas. . . . .	3
I-2. Location map of sections and wells used, Corpus Christi study area . . . . .	4
I-3. Stratigraphic diagram of the Frio and related units, Corpus Christi study area, showing the markers used in this study . . . . .	6
I-4. Interval velocity versus depth, Corpus Christi study area . . . . .	8
I-5. Structure map on CC-1 (top of Frio) . . . . .	9

I-6.	Structure map on CC-4 (approximately <u>Nonion struma</u> ) . . . . .	10
I-7.	Structure map on CC-9 (approximately <u>Textularia mississippiensis</u> ) . . . . .	11
I-8.	Structure map on CC-11 (approximately <u>Anomalina bilateralis</u> ). . . . .	12
I-9.	Isopach map of the CC-1 to CC-4 interval (upper Frio) . . . . .	13
I-10.	Isopach map of the CC-4 to CC-9 interval (middle Frio). . . . .	14
I-11.	Isopach map of the CC-9 to CC-11 interval (lower Frio). . . . .	15
I-12.	Interpreted seismic section, Nueces County . . . . .	17
I-13.	Interpreted seismic section, Corpus Christi Bay, Nueces County . . . . .	18
I-14.	Structural section across a shale diapir, San Patricio County . . . . .	19
I-15.	Structural section across Mobil-David dome and the P. Kraft withdrawal basin . . . . .	20
I-16.	Section A-A', true depth, southern Nueces County . . . . .	22
I-17.	Section B-B', true depth, northeastern Nueces County . . . . .	22
I-18.	Section C-C', true depth, San Patricio County. . . . .	22
I-19.	Distribution of fault-well intersections with depth, Corpus Christi study area . . . . .	24
I-20.	Structure map contoured on S5 horizon, Sarita prospect area . . . . .	26
I-21.	Structural dip section H-H', Sarita prospect area . . . . .	28
I-22.	Structural dip section constructed roughly along the seismic line . . . . .	30
I-23.	Seismic reflector facies interpretation of the line . . . . .	32
I-24.	Interpreted seismic section . . . . .	33
I-25.	True-depth structural section constructed from the line confirmed by well data . . . . .	34
I-26.	Palinspastic reconstructions of the western part of the line across the Sarita prospect area . . . . .	36
I-27.	Location map of the Port Arthur area showing well control, general locations of seismic lines, and locations of salt domes . . . . .	37
I-28.	Regional distribution of sand-bearing lower Hackberry channels in the Hackberry Embayment west of Acadia Parish, Louisiana . . . . .	39
I-29.	Interpretation of a strike-oriented seismic line along the shore of Sabine Lake. . . . .	40
I-30.	Stratigraphic diagram of Frio and related strata, Jefferson County study area, showing diagnostic foraminifera, sand-body distribution, and marker horizons used in this study . . . . .	41
I-31.	Structural section C-C' passing by Port Arthur field and Spindletop salt dome . . . . .	43
I-32.	Interval velocity versus depth for two velocity surveys and velocity analyses from seismic data . . . . .	44

I-33.	Isopach map of the A3-Vicksburg interval, Port Arthur area, showing broad uplifts and depressions during lower Frio deposition . . . . .	46
I-34.	Isopach map of the A3-A4 interval, Port Arthur area, showing salt uplifts and major growth faults influencing Hackberry deposition . . . . .	47
I-35.	Structure map contoured on A4 horizon, Port Arthur area . . . . .	48
I-36.	Structure map contoured on A2 horizon, Port Arthur area . . . . .	50
I-37.	Isopach map of the A1-A3 interval, Port Arthur area, showing salt uplifts and significant growth faults influencing upper Frio and Anahuac deposition . . . . .	52
I-38.	Isolith map of the <u>Heterostegina</u> limestone (middle Anahuac) . . . . .	53

**SECTION II: VARIATIONS IN CHEMICAL COMPOSITIONS OF TERTIARY FORMATION WATERS, TEXAS GULF COAST . . . . .**

		62
ABSTRACT . . . . .		62
INTRODUCTION. . . . .		63
WATER CHEMISTRY OF INDIVIDUAL FIELDS . . . . .		63
Willow Slough field . . . . .		63
Red Fish Reef field . . . . .		66
Cedar Point field . . . . .		70
Alta Loma field . . . . .		73
Sugar Valley field . . . . .		76
Maude B. Traylor field . . . . .		80
Red Fish Bay field . . . . .		83
May - South May field . . . . .		83
Tijerina-Canales-Blucher field . . . . .		86
McAllen Ranch field. . . . .		86
North Rincon field . . . . .		88
South Texas fields . . . . .		91
Structure . . . . .		91
Stratigraphy . . . . .		100
Water chemistry . . . . .		104
REGIONAL COMPARISON OF HYDROCHEMISTRY . . . . .		104
Total dissolved solids . . . . .		106
Calcium . . . . .		106
Sodium . . . . .		109
Sodium-calcium ratio . . . . .		109
Alkalinity . . . . .		109

Potassium . . . . .	113
Bromide, chloride-bromide ratio, and chloride-sodium ratio . . . . .	116
SALINITY VARIATIONS AND FLUID FLOW . . . . .	120
Corpus Christi area . . . . .	120
Galveston area . . . . .	122
GEOCHEMICAL REACTIONS AND HYDROLOGICAL PROCESSES . . . . .	122
Water-rock interactions . . . . .	124
Chocolate Bayou field . . . . .	124
McAllen Ranch field . . . . .	127
Alternative interpretations . . . . .	127
CONCLUSIONS . . . . .	128
ACKNOWLEDGMENTS . . . . .	130
REFERENCES . . . . .	131
APPENDIX II-A: CHEMICAL ANALYSES OF WATER SAMPLES . . . . .	134

*Figures in Section II*

II-1. Locations of oil and gas fields from which water samples were collected or chemical analyses obtained . . . . .	64
II-2. Stratigraphic dip section through the Willow Slough field showing the salinities of water produced from two sandstone intervals . . . . .	65
II-3. Concentrations of total dissolved solids, major ions, and ion ratios in the Frio Formation, Willow Slough field . . . . .	67
II-4. Concentrations of total dissolved solids, major ions, and ion ratios in the Frio Formation, Red Fish Reef field . . . . .	71
II-5. Concentrations of total dissolved solids, major ions, and ion ratios in the Cedar Point Field . . . . .	72
II-6. Fence diagram showing structure, stratigraphic markers, and salinity data, Chocolate Bayou, Pleasant Bayou, Halls Bayou, and Alta Loma fields, Brazoria and Galveston Counties . . . . .	74
II-7. Concentrations of total dissolved solids, major ions, and ion ratios in Alta Loma field . . . . .	75
II-8. Structure map of a correlation marker within the lower Frio Formation, Sugar Valley field . . . . .	77
II-9. Electric log patterns of the correlation marker used for figure II-8. . . . .	78
II-10. Equilibrium temperature calculated for depths of the correlation marker in figure II-8 . . . . .	79

II-11.	Concentrations of total dissolved solids, major ions, and ion ratios in Sugar Valley field . . . . .	81
II-12.	Concentrations of total dissolved solids, major ions, and ion ratios in Maude B. Traylor field. . . . .	82
II-13.	Concentrations of total dissolved solids, major ions, and ion ratios in Red Fish Bay field . . . . .	84
II-14.	Concentrations of total dissolved solids, major ions, and ion ratios in the May - South May field. . . . .	85
II-15.	Concentrations of total dissolved solids, major ions, and ion ratios in Tijerina-Canales-Blucher field . . . . .	87
II-16.	Concentrations of total dissolved solids, major ions, and ion ratios in McAllen Ranch field . . . . .	89
II-17.	Concentrations of total dissolved solids, major ions, and ion ratios in North Rincon field . . . . .	90
II-18.	Location map of wells, cross sections, and salinity data sources in the South Texas field area . . . . .	92
II-19.	Structure map of the top of the Frio Formation . . . . .	93
II-20.	Structural dip cross section through the South Texas field area . . . . .	94
II-21.	Structure map of the top of the middle Frio Formation . . . . .	96
II-22.	Stratigraphic cross section through the McAllen field area . . . . .	97
II-23.	Structure map of the top of the lower Frio Formation . . . . .	98
II-24.	Stratigraphic cross section through Donna field . . . . .	99
II-25.	Net-sandstone-thickness map of the middle Frio, South Texas field area . . . . .	101
II-26.	Net-sandstone-thickness map of the upper Frio, South Texas field area . . . . .	102
II-27.	Stratigraphic cross section through Pharr field . . . . .	103
II-28.	Concentrations of total dissolved solids, major ions, and ion ratios in Donna field . . . . .	105
II-29.	Maximum concentrations of total dissolved solids in Tertiary formation waters . . . . .	107
II-30.	Maximum concentrations of calcium in Tertiary formation waters . . . . .	108
II-31.	Maximum concentrations of sodium in Tertiary formation waters . . . . .	110
II-32.	Maximum values of the sodium-calcium ratio in Tertiary formation waters . . . . .	111
II-33.	Locations of known salt domes and shale diapirs beneath the Texas Coastal Plain . . . . .	112
II-34.	Maximum alkalinity of Tertiary formation waters . . . . .	114
II-35.	Maximum concentrations of potassium in Tertiary formation waters . . . . .	115
II-36.	Maximum values of the chloride-bromide ratio in Tertiary formation waters . . . . .	117
II-37.	Maximum values of the chloride-sodium ratio in Tertiary formation waters . . . . .	119

II-38.	Average salinities, equilibrium temperatures, and pressure gradients at 9,000 ft near Corpus Christi Bay . . . . .	121
II-39.	Average salinities, equilibrium temperatures, and pressure gradients at 10,000 ft in western Galveston County . . . . .	123
II-40.	Concentrations of total dissolved solids, major ions, and ion ratios in the Frio Formation, Chocolate Bayou field . . . . .	126

*Table in Section II*

II-1.	Range of ion concentrations and ion ratios of Tertiary formation waters, Texas Gulf Coast . . . . .	68
-------	---	----

**SECTION III: PREDICTING RESERVOIR QUALITY AND DIAGENETIC HISTORY IN THE FRIO FORMATION (OLIGOCENE) OF TEXAS . . . . . 136**

ABSTRACT . . . . .	136
INTRODUCTION. . . . .	137
RESERVOIR QUALITY . . . . .	139
Authigenic minerals . . . . .	139
Thermodynamic data . . . . .	139
Stability relations . . . . .	141
Reaction pairs . . . . .	141
Activity diagrams . . . . .	144
Carbonate equilibrium . . . . .	144
Chloritization . . . . .	146
Kaolinitization . . . . .	152
Cation exchange . . . . .	152
Albitization . . . . .	156
Geopressuring . . . . .	156
DIAGENETIC HISTORY. . . . .	164
Carbonate equilibrium . . . . .	164
Timing of albitization . . . . .	165
Chlorite formation . . . . .	168
CONCLUSIONS . . . . .	168
ACKNOWLEDGMENTS . . . . .	169
REFERENCES . . . . .	169

*Figures in Section III*

III-1. Map of upper, middle, and lower Texas coast and Frio oil and gas fields having analyzed waters . . . . .	138
III-2. Activity diagram of the reaction calcite = ferroan calcite . . . . .	145
III-3. Activity diagram of the reaction kaolinite = chlorite . . . . .	147
III-4. Activity diagram of the reaction kaolinite = chlorite, two Brazoria County waters . . . . .	148
III-5. Activity diagram of the reaction Ca-montmorillonite = chlorite . . . . .	150
III-6. Activity diagram of the reaction illite = chlorite . . . . .	151
III-7. Activity diagram of the reaction plagioclase (An30) = kaolinite . . . . .	153
III-8. Activity diagram of the reaction Ca-montmorillonite = kaolinite . . . . .	154
III-9. Activity diagram of the reaction Ca-montmorillonite = Na-montmorillonite . . . . .	155
III-10. Activity diagram of the reaction plagioclase (An30) = albite . . . . .	157
III-11. Activity diagram of the reaction microcline = albite . . . . .	158
III-12. Ionic strength versus depth . . . . .	160
III-13. Ca <sup>2+</sup> /Na <sup>+</sup> mole ratio versus depth . . . . .	161
III-14. Cl <sup>-</sup> /Ca <sup>2+</sup> mole ratio versus depth . . . . .	162
III-15. Log[Ca <sup>2+</sup> ] <sup>.16</sup> /[Na <sup>+</sup> ] <sup>.33</sup> ratio versus depth . . . . .	163
III-16. Log[Ca <sup>2+</sup> ] <sup>.29</sup> /[Fe <sup>2+</sup> ] <sup>1.85</sup> [Mg <sup>2+</sup> ] <sup>1.85</sup> ratio versus depth . . . . .	166
III-17. Major diagenetic events in the Frio Formation . . . . .	167

*Tables in Section III*

III-1. Mineral composition . . . . .	142
III-2. Reaction pairs . . . . .	143

<b>SECTION IV: DISTRIBUTION AND POSSIBLE DIAGENETIC ORIGIN OF HIGH-RESISTIVITY CAP ROCK SHALE, FRIO FORMATION, TEXAS GULF COAST . . . . .</b>	<b>172</b>
ABSTRACT . . . . .	172
INTRODUCTION. . . . .	172
CAP ROCK DISTRIBUTION . . . . .	173
Thickness . . . . .	174
Peak resistivity . . . . .	174
Delineation of study area . . . . .	178

CAP ROCK - FACIES RELATIONSHIPS . . . . .	178
ANALYSIS OF CAP ROCK . . . . .	178
Total carbonate . . . . .	182
Silica and multi-element analysis . . . . .	182
Clay mineralogy . . . . .	187
DIAGENETIC MECHANISMS . . . . .	187
DISCUSSION AND IMPLICATIONS FOR CAP ROCK DEVELOPMENT . . . . .	188
CONCLUSIONS . . . . .	191
ACKNOWLEDGMENTS . . . . .	191
REFERENCES . . . . .	192

*Figures in Section IV*

IV-1. Shale-resistivity plot for a well in Kenedy County, Texas . . . . .	175
IV-2. Thickness of cap rock intervals within the Frio Formation of the Texas Gulf Coast . . . . .	176
IV-3. Maximum shale resistivity within the Frio Formation of the Texas Gulf Coast . . . . .	179
IV-4. Major depositional systems of the Frio Formation in the Lower Texas Gulf Coast and location of regional cross sections in an area of more detailed study, which includes Sarita East field . . . . .	180
IV-5. Facies interpretation of part of regional cross section 19 (from Dodge and Posey, 1981) . . . . .	181
IV-6. Qualitative interpretation of clay mineral distribution in a well in Kenedy County, Texas, based on X-ray diffraction patterns . . . . .	189

*Tables in Section IV*

IV-1. Criteria for defining cap rock using shale-resistivity plots derived from geophysical well logs . . . . .	177
IV-2. Percent total carbonate in non-cap rock and cap rock interval sediments in a well in Kenedy County, Texas . . . . .	183
IV-3. Percent total carbonate in non-cap rock and cap rock shales in two wells in Kenedy County, Texas . . . . .	184
IV-4. Multi-element analysis of non-cap rock and cap rock shales in a well in Kenedy County, Texas . . . . .	185
IV-5. Percent total silica in non-cap rock and cap rock shales in two wells in Kenedy County, Texas . . . . .	186

## Section I

# STRUCTURAL STYLES AND STRUCTURAL EVOLUTION OF THE FRIO GROWTH-FAULT TREND IN TEXAS: CONSTRAINTS ON GEOPRESSURED RESERVOIRS

*By T. E. Ewing*

*Assisted by R. S. Reed, R. G. Anderson, R. Padilla y Sanchez, and K. Hubby*

## ABSTRACT

Detailed structural mapping at several horizons in selected study areas within the Frio growth-fault trend demonstrates a pronounced variability in structural style. At Sarita in South Texas, shale mobilization produced one or more shale ridges, one of which localized a low-angle growth fault trapping a wedge of deltaic sediments. At Corpus Christi, shale mobilization produced a series of large growth faults, shale-cored domed anticlines, and shale-withdrawal basins, which become progressively younger basinward. At Blessing, major growth faults trap sands of the Greta/Carancahua barrier system, having some discrete shale diapirs but little progradation. At Pleasant Bayou, a major early growth-fault system was overprinted by salt tectonics--the intrusion of Danbury Dome and the development of a salt-withdrawal basin. At Port Arthur, low-displacement, long-lived faults formed on a sand-poor shelf margin contemporaneously with broad salt uplifts and basins. Variability in styles can be related to the nature and extent of Frio sedimentation and shelf-margin progradation and to the presence of salt.

Structural styles that are conducive to large geothermal reservoirs include blocks between widely spaced growth faults having dip reversal, salt-withdrawal basins, and shale-withdrawal basins. These styles are widespread on the Texas Gulf Coast. However, actually finding a large reservoir depends on demonstrating the existence of sufficient sand having adequate quality to support geopressured geothermal energy production.

## INTRODUCTION

Regional studies conducted as part of the geopressured geothermal research program of the Bureau of Economic Geology have assessed the presence of geopressured geothermal resources within the major growth-fault trends of the Texas Gulf Coast (Bebout and others,

1978, 1982; Weise and others, 1981a, 1981b). Because of the methods used, these studies could assess only the part of the rock column that had been extensively drilled in the search for oil and gas. To assess prospective areas that have been inadequately drilled and to define areas that might be prospective in the future, one needs to understand the different structural styles within the growth-fault trends. A regional synthesis also allows the extrapolation of results from detailed prospect areas to the entire trend.

Structural style and evolution can best be analyzed in areas where both dense, deep well control and seismic coverage are available. Seismic lines obtained by the Bureau fall into two categories: (1) grids of data around prospect areas having test well sites, and (2) regional dip-oriented seismic lines that provide representative coverage within the growth-fault trends. The prospect grids of the three identified geopressured geothermal prospect areas have been previously analyzed and combined with well data (Winker and others, 1981); work on the Port Arthur dispersed gas prospect is reported both here and elsewhere (Gregory and others, 1983). Regional lines, however, have never been systematically studied. One line across the Vicksburg growth faults in South Texas has been interpreted by Han (1982) in a study of the McAllen Ranch field and adjacent areas. The other seismic lines have not received full-scale interpretation before the present study.

For this report, two study areas were defined; these areas coincide with acquired seismic data, geothermal fairways, and areas of current interest (fig. I-1). The Corpus Christi study area in Nueces, San Patricio, and adjoining counties contains two regional seismic dip lines. The Port Arthur study area in Jefferson and Orange Counties is centered on the dispersed gas prospect at Port Arthur field and contains a grid of seismic data. In addition, a regional line along the Kleberg-Kenedy county line is interpreted and related to the geology of the Sarita prospect area described by Weise and others (1981a). These areas, together with the Blessing and Pleasant Bayou prospect areas described by Winker and others (1981), span nearly the entire range of Frio depositional systems (as defined by Galloway and others, 1982; fig. I-1). Therefore, this report also summarizes work to date on structural styles along the Frio trend of the Texas Gulf Coast. Similar study areas are defined for the Wilcox growth-fault trend and will be studied in the upcoming year. Quantitative studies of fault-block geometries along the growth-fault trends are also underway but are too preliminary in nature to be reported here.

#### CORPUS CHRISTI STUDY AREA

The Corpus Christi study area (fig. I-2) coincides with the area of the Corpus Christi fairway studied by Weise and others (1981a, 1981b). These authors established a series of 11

3

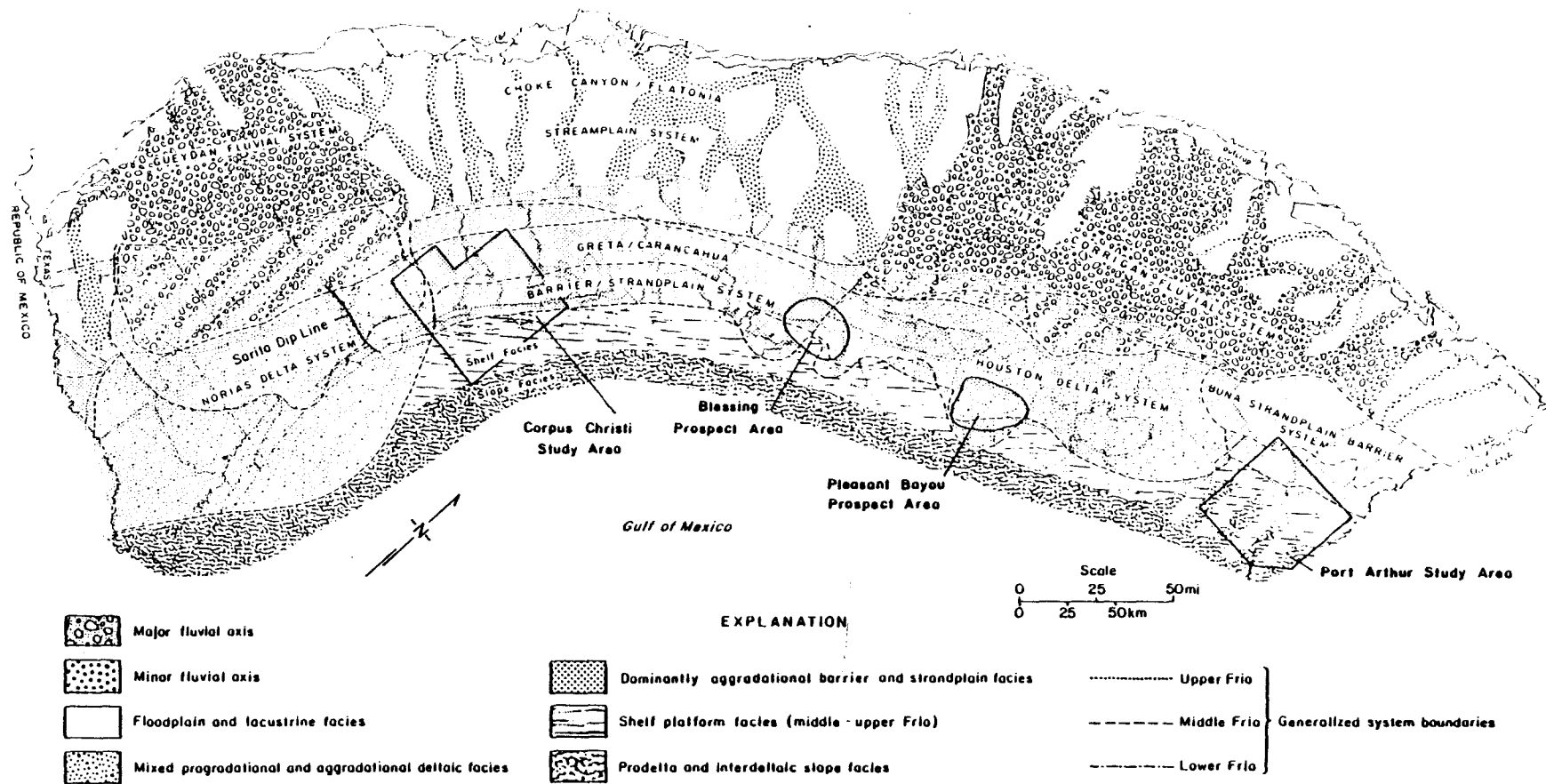


Figure I-1. Depositional systems of the Frio Formation showing the locations of the Frio geopressedured trend study areas (from Galloway and others, 1982).

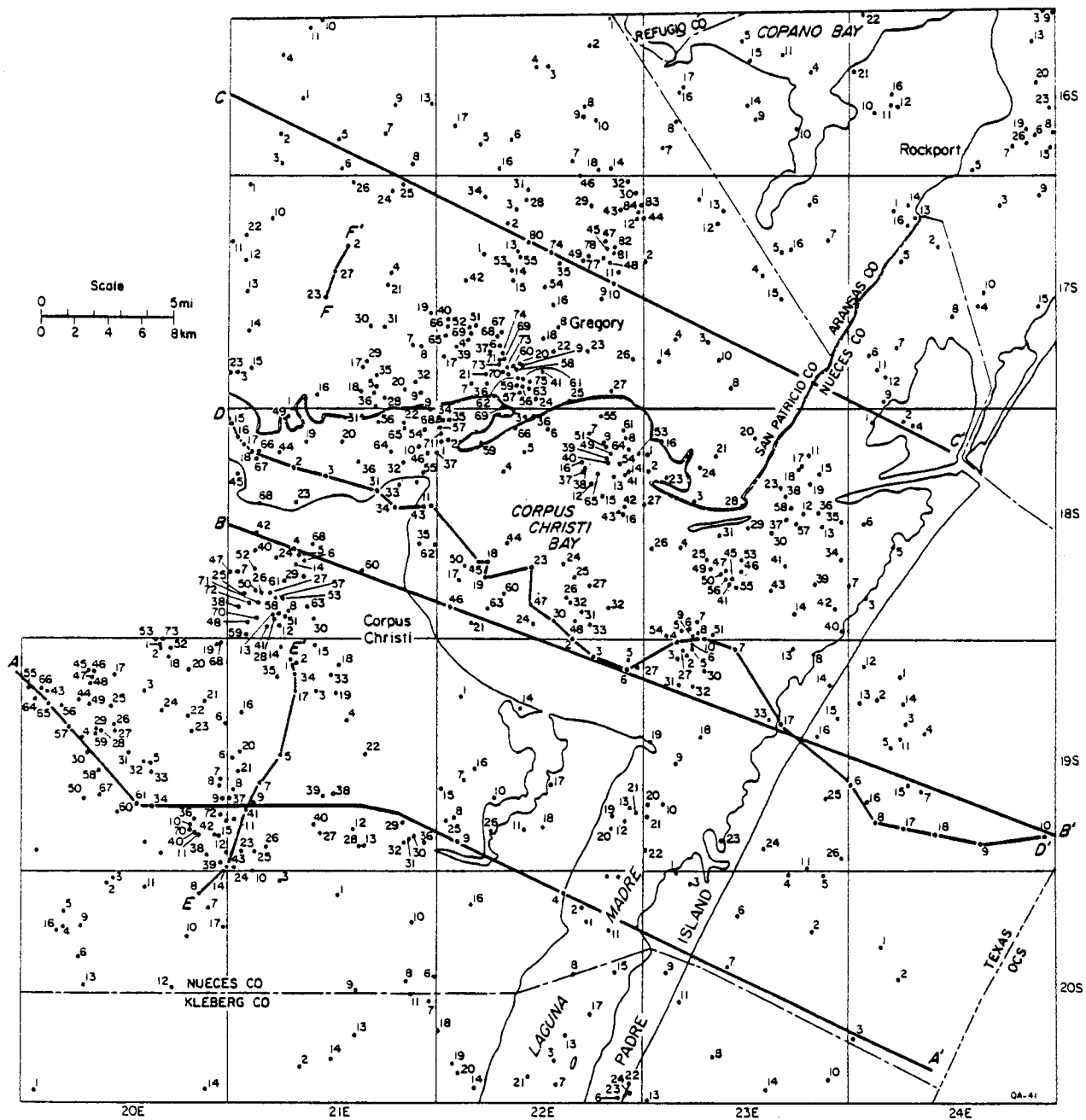


Figure I-2. Location map of sections and wells used, Corpus Christi study area. The area covers most of the Corpus Christi fairway of Weise and others (1981a).

correlation markers, CC-1 through CC-11, throughout most of the area. For the present study, their well log correlations were confirmed and extended. A total of 600 well logs were examined. Two seismic lines have been acquired, one in central Nueces County (roughly along section A-A' in fig. I-2) and the other in Nueces Bay (roughly along section B-B'). These lines have been interpreted interactively with the well log correlation matrix. The combination of dense well control and dip-oriented seismic lines allows a fairly detailed structural and depositional history to be reconstructed.

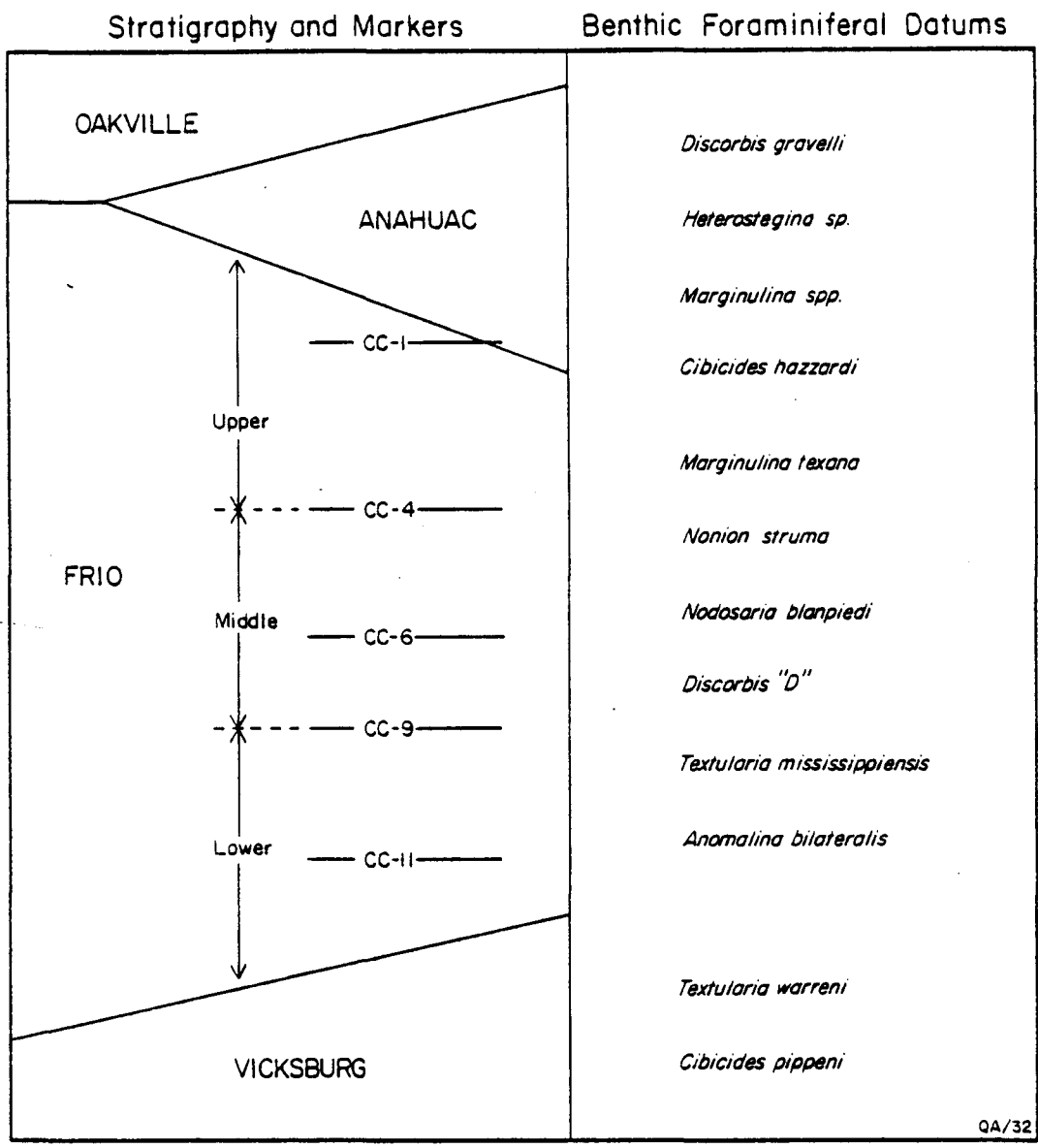
The study area lies within the southern part of the Greta/Carancahua barrier-bar/strandplain depositional system of the Frio Formation, immediately north of the northern margin of the Norias delta system (fig. I-1). Most of the Frio sandstones represent strike-fed barrier-bar and strandplain sand bodies within the system. The sand system in this area prograded eastward from the lowermost Frio (Frio-Vicksburg) of the Vicksburg Fault Zone fields of western Nueces County to the upper Frio (about CC-4) near the present-day shoreline. This progradation, first reported by Boyd and Dyer (1964), apparently kept pace with the rapid eastward progradation of the Norias delta to the south of the area. In contrast, the main Greta/Carancahua sand system to the northeast of the study area appears to have prograded only slightly during Frio time instead stacking to form thick composite sands (Galloway and others, 1982).

Little detailed structural information has been published about the Corpus Christi area. Several of the early-discovered oil fields in the area have been the subject of field studies, but these are of little use in this study. Major fields in the area have been researched in the Railroad Commission of Texas files to improve the rendering of the producing structures.

### Stratigraphy

The Frio Formation in the study area ranges from 3,000 ft to more than 8,000 ft thick. The base of the Frio interval, or the top of the Vicksburg Formation, is arbitrarily taken at the occurrence of Textularia warreni in wells having paleontological data and correlative horizons in other wells (fig. I-3). The Vicksburg has not been penetrated to the southeast of the western major growth fault in the study area, except on Mobil-David dome and in shale diapirs. The top of the Frio is defined as the top of a sandstone-rich sequence overlain by the Anahuac marine shale (Holcomb, 1964); this includes sandstones of the Marginulina and Heterostegina biozones, which pass downdip into Anahuac shale.

Logs from deep geopressured wells show an overall separation into two sections. The upper section consists of thick, upward-coarsening sands or composite sands, which represent the prograding barrier bars. In landward positions, these sands thin and grade into thick,



QA/32

Figure I-3. Stratigraphic diagram of the Frio and related units, Corpus Christi study area, showing the markers used in this study. Approximate benthic foraminiferal correlations are shown; the fossils, however, rise considerably in the section as one proceeds basinward (M. B. Edwards, personal communication, 1981).

sometimes lignitic shales of lagoonal to paludal origin. Below a rather sharp horizon, the sand bodies are thicker and shalier and are interbedded with thick marine shales. These sands may be traced updip across a major growth fault into sands of the upper section. Geopressure generally occurs at the base of the high-sand upper section; the thick, shaly sands are the geopressed geothermal target. The stratigraphic position of the transition between upper and lower sections varies from lower Frio (CC-11 or below) in the west to CC-2 in the southeast. As shown in the following discussion, this corresponds with the seaward progression of structural styles, in particular with the occurrence of high-displacement growth faulting.

The velocity structure of the sediments in the Corpus Christi area, as determined from sonic logs and velocity analyses of the seismic data, shows a similar division (fig. I-4). From the surface to about 8,000 ft, velocity increases linearly with depth from 6,500 ft/sec to about 11,000 ft/sec. Velocity decreases below 8,000 ft, reaching only 8,500 ft/sec at depths greater than 12,000 ft. This break in velocities has been interpreted to represent a response to undercompacted geopressed shale. However, no such break has been observed in other Frio study areas. It is likely that the break reflects the pronounced lithologic change from sand-rich strata in the upper section to shale-rich strata in the lower section. The lithologic change reinforces the velocity decrease owing to geopressure; this is different from conditions in the Brazoria and Blessing areas (Winker and others, 1981).

#### Structure and Structural Development

On the basis of correlation of well logs and interpretation of seismic lines, a series of structure maps on selected horizons (figs. I-5 through I-8) and a set of sequential isopach maps (figs. I-5, I-9 through I-11) were prepared, and two seismic lines (figs. I-12 and I-13) were interpreted. A sequential isopach map of the X-Y interval (Y deeper than X) represents an approximate paleostructural map of the horizon Y at the time of the horizon X (neglecting compaction) if the horizon X was deposited near sea level (which is probably true of the Frio depositional systems considered here). Thus, the structures active at a certain time are more easily recognized on these maps. The isopach maps of the Corpus Christi area mimic the structural maps in most respects, except that they do not show post-Frio regional tilting. This indicates that the intensity of structural activity decreased with time and that significant overprinting has not occurred.

Three phases of structural development can be recognized both on the maps and on the seismic sections. These phases form a sequence of waning shale mobility and intensity of faulting. The structural sequence progresses basinward so that strata of successively younger

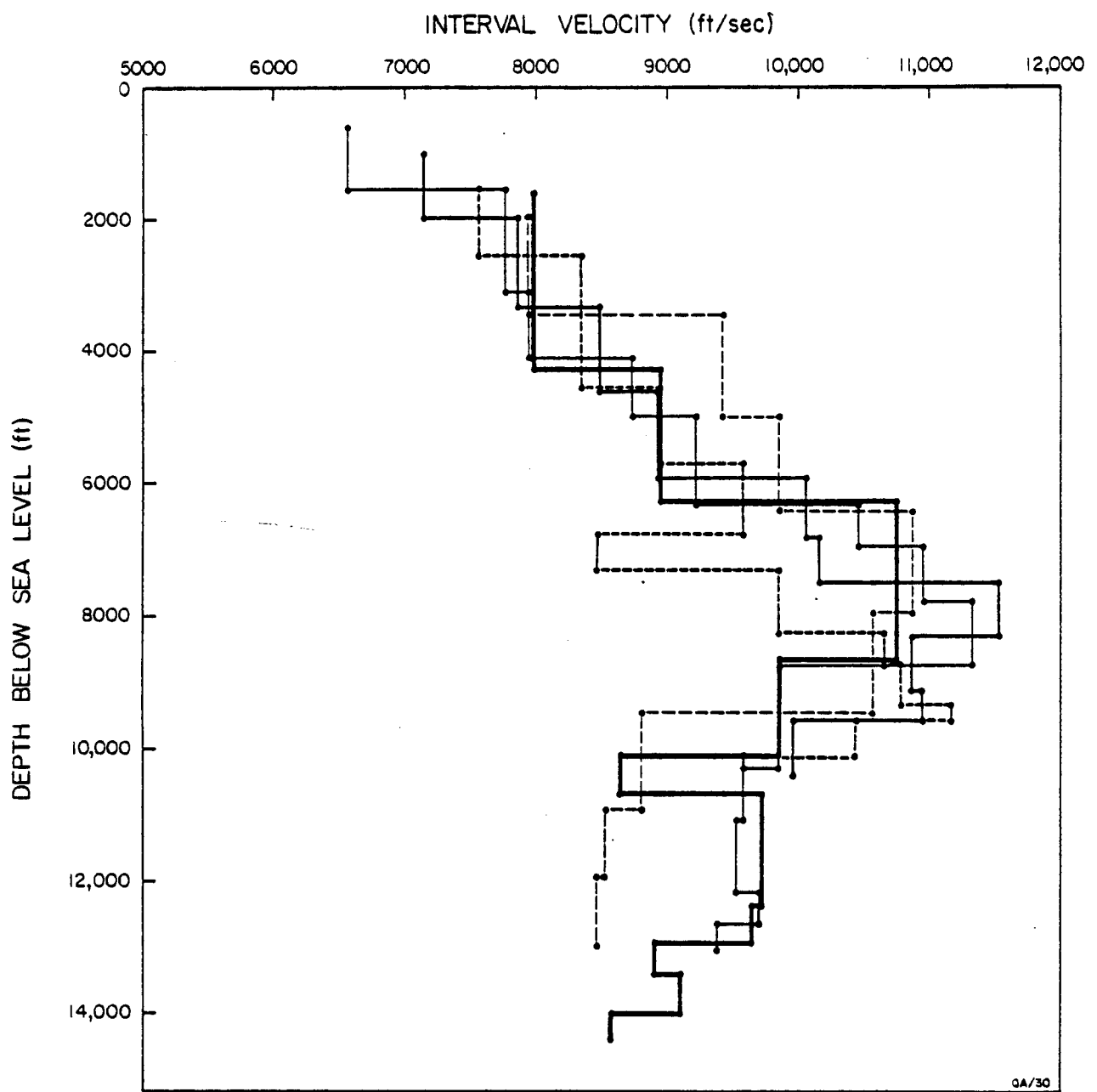


Figure I-4. Interval velocity versus depth, Corpus Christi study area.

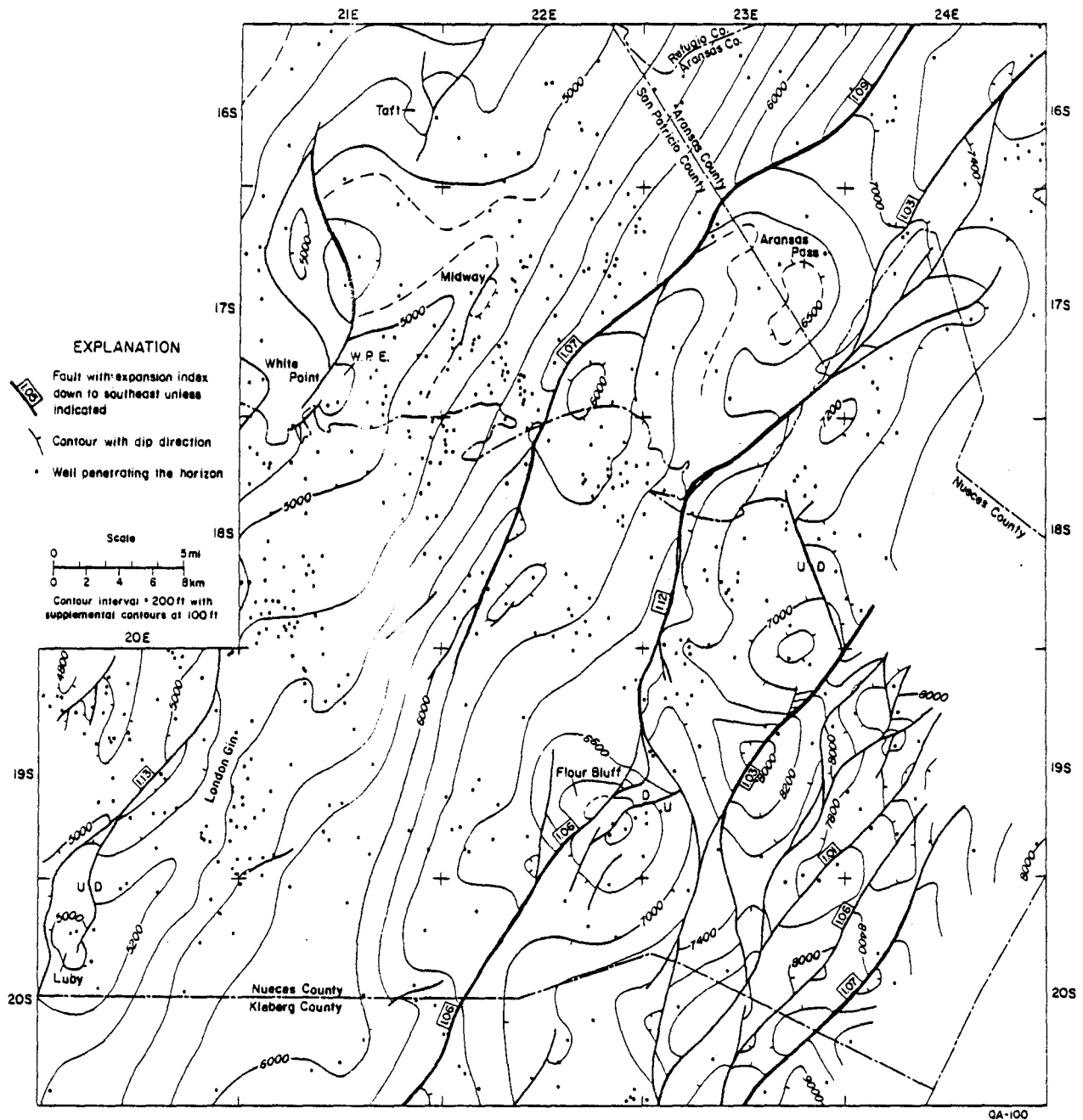


Figure I-5. Structure map on CC-1 (top of Frio). Large oil-bearing structures are named. W.P.E. = White Point East.

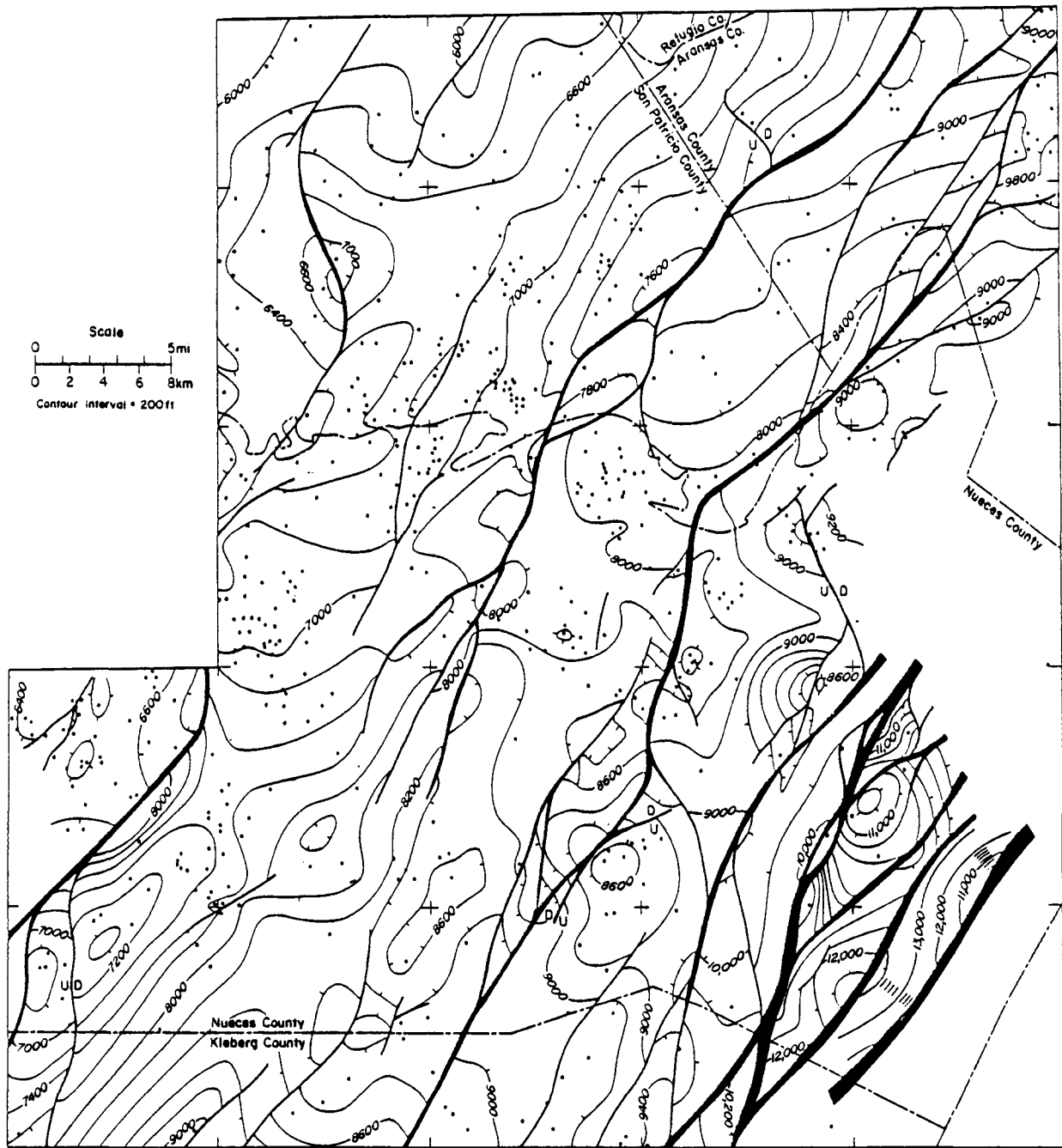


Figure I-6. Structure map on CC-4 (approximately Nonion struma).

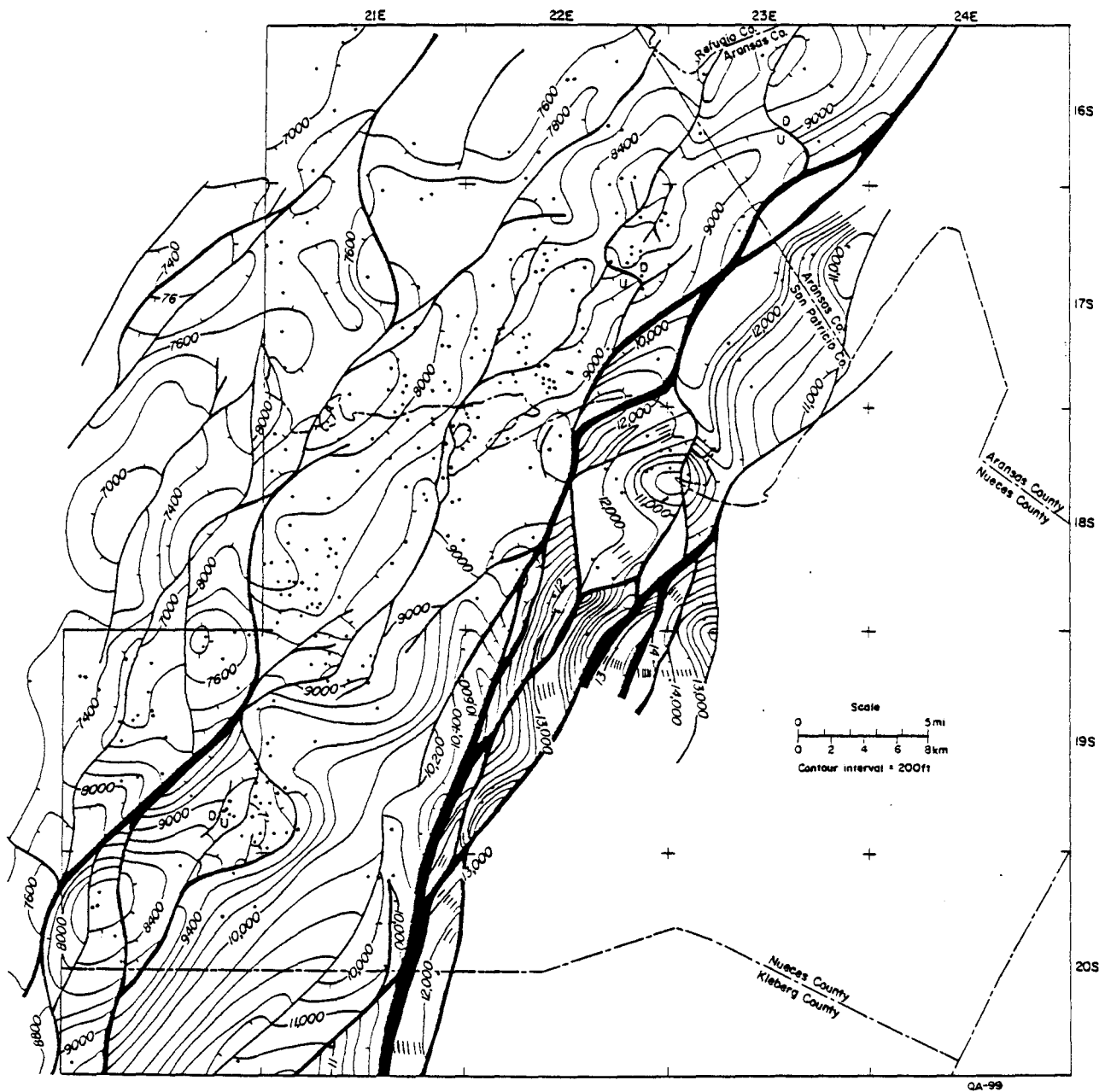


Figure I-7. Structure map on CC-9 (approximately Textularia mississippiensis).

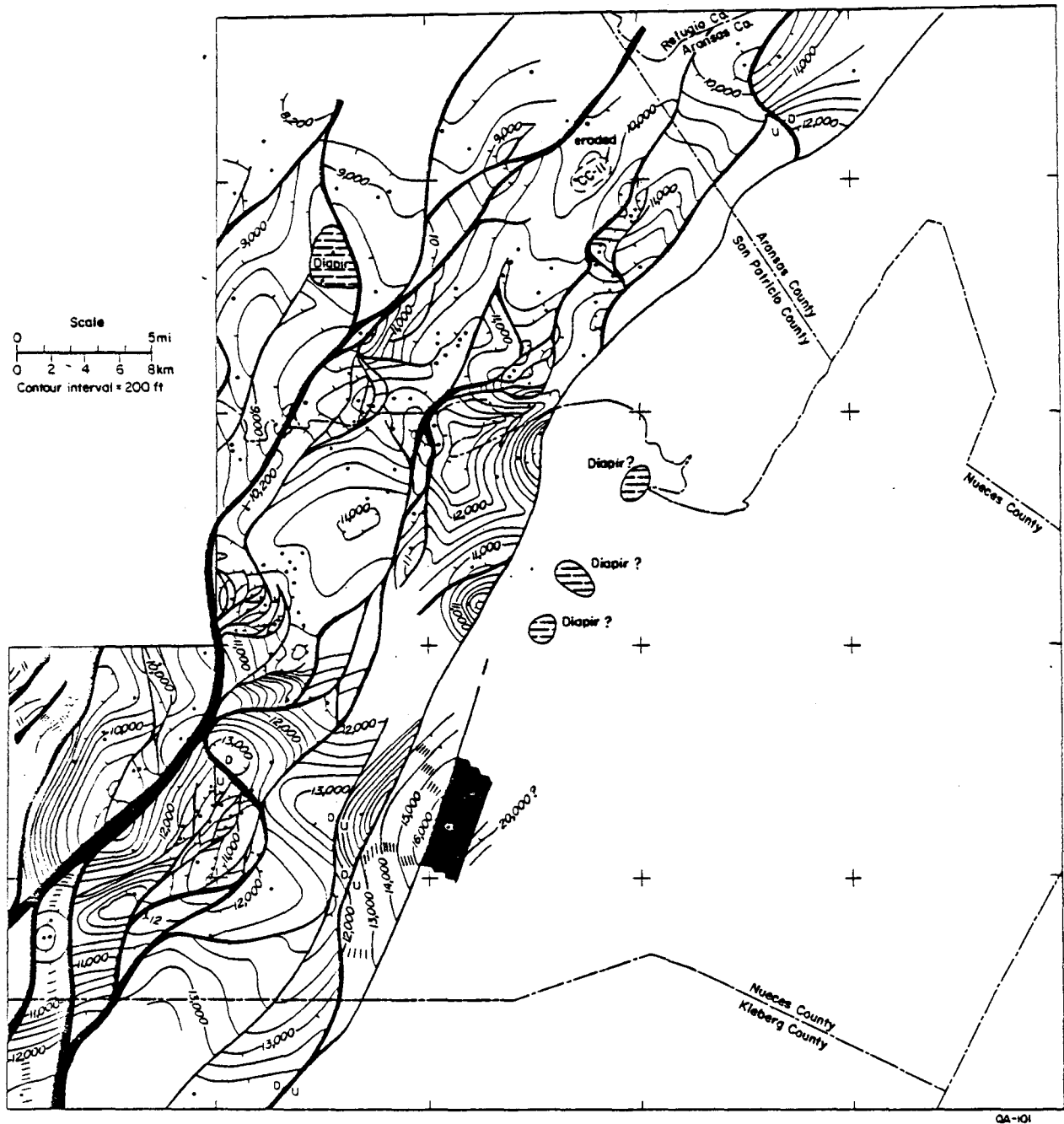


Figure I-8. Structure map on CC-11 (approximately Anomalina bilateralis).

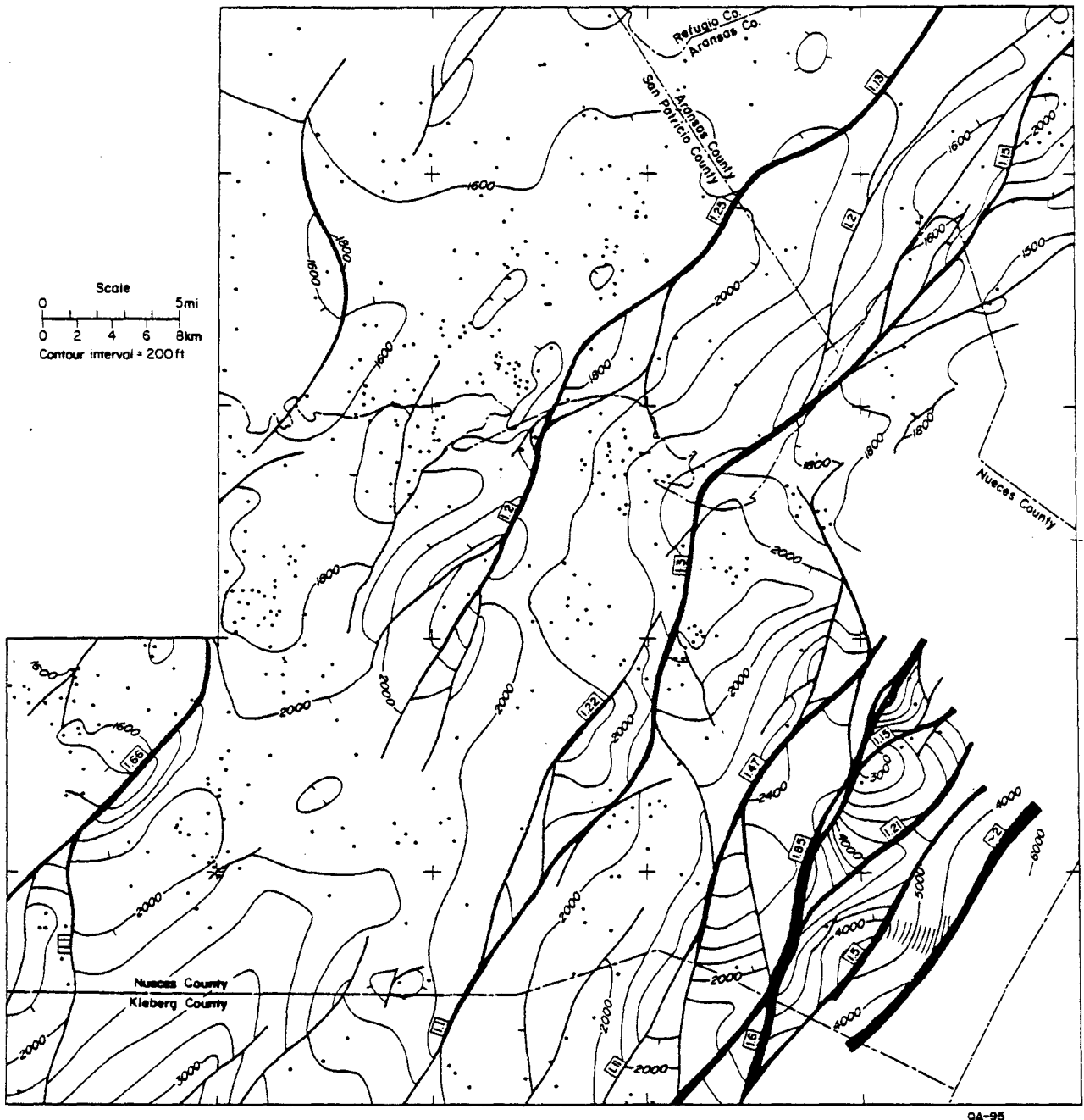


Figure I-9. Isopach map of the CC-1 to CC-4 interval (upper Frio).

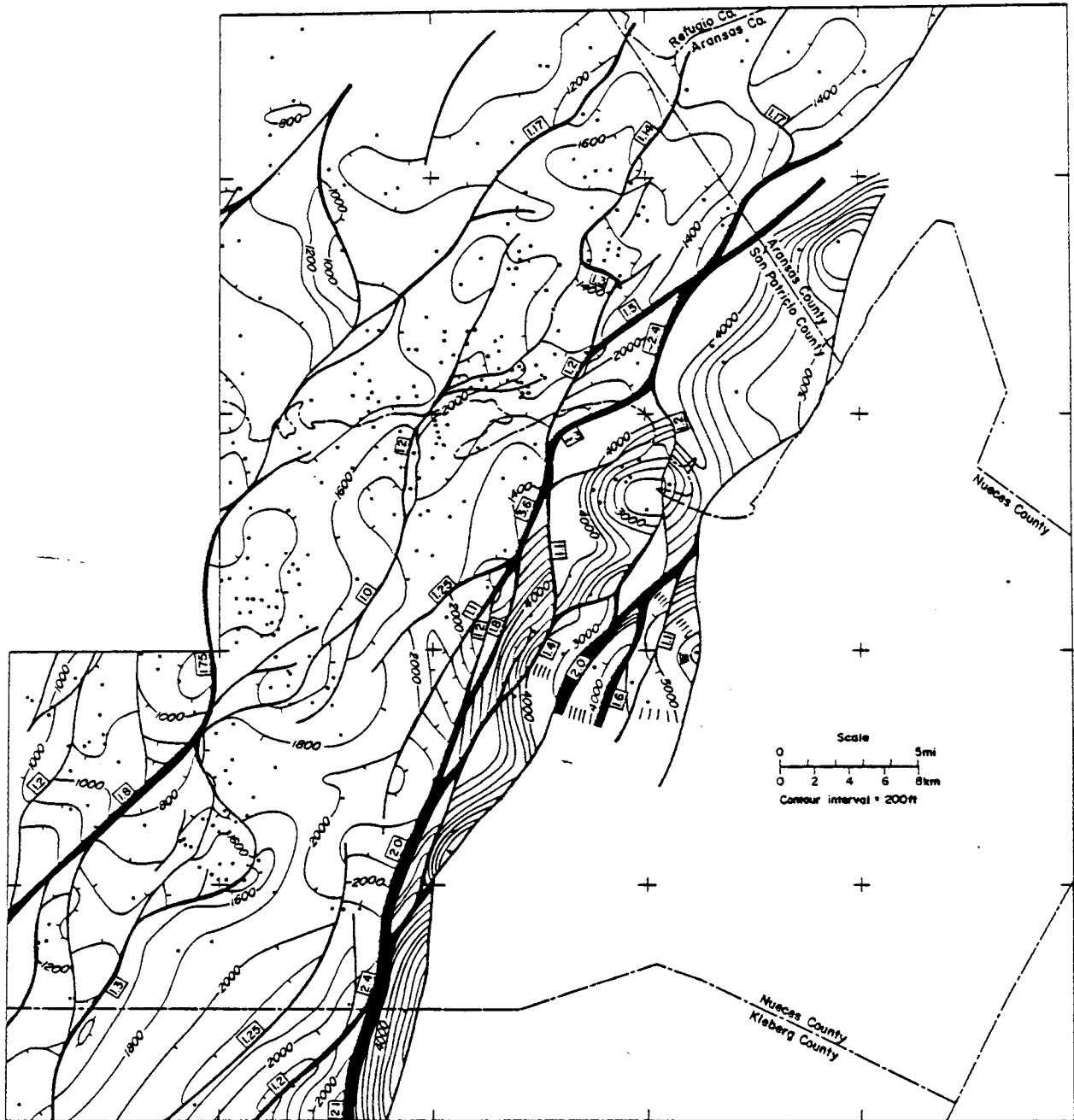
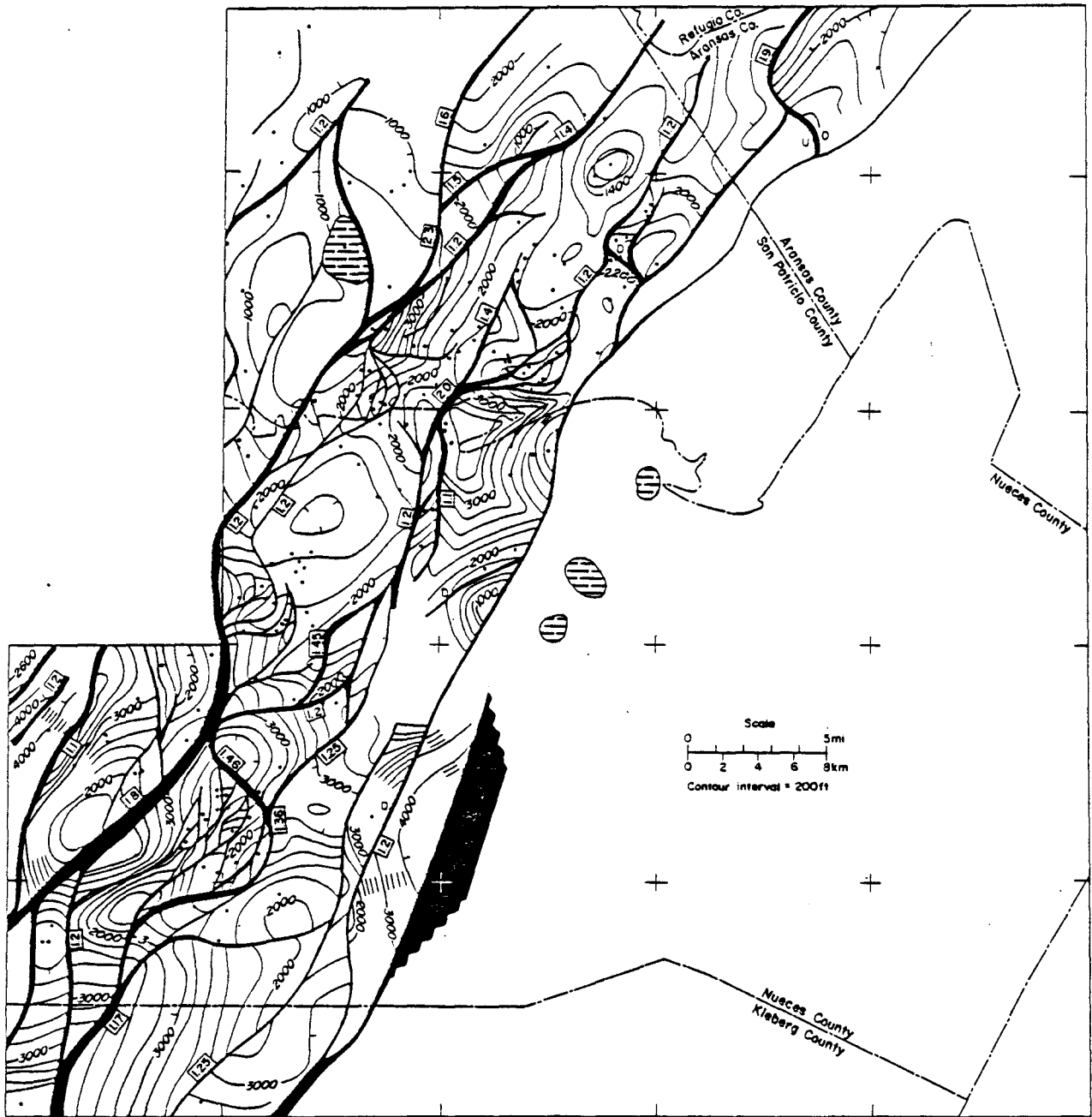


Figure I-10. Isopach map of the CC-4 to CC-9 interval (middle Frio).



QA-96

Figure I-11. Isopach map of the CC-9 to CC-11 interval (lower Frio).

age have a similar structural style toward the basin. This progression follows the progradation of the shelf margin by the bar/strandplain system.

The earliest phase on which there is adequate data is characterized by large listric (flattening-downward) growth faults and a variety of shale tectonic structures. Expansion indices of large sedimentary sequences over the growth faults in this phase are more than 1.5 and often more than 2.0 (that is, twice as large on the downthrown side as on the upthrown side). Expansion indices of up to 5.0 can be documented for individual sand bodies; large expansions such as these place the lower boundary of the larger isopach intervals below present drilling depths. Major displacement occurs on a few zones of faulting. The major growth faults consist of several strands that branch and rejoin, forming a braided pattern. Smaller growth faults cross-link the major fault zones. Strata dip landward toward the faults but are highly modified by shale mobilization. Significant antithetic faults, possibly caused by shale tectonics, are noted in the southern part of the area (fig. I-12).

Three varieties of shale tectonic features are recognizable within this phase. Discrete shale diapirs occur, especially in the northern and central part of the area. These diapirs bring prodelta/slope shale of Vicksburg (lower Oligocene) and Jackson (upper Eocene) ages into contact with lower and middle Frio strata (fig. I-14). Growth faults are often found on the basinward side of the diapir. These diapirs are similar to those to the northeast in Calhoun and Jackson Counties reported by Bishop (1977). Domes and domal anticlines that are inferred to be cored by Vicksburg shale form high-relief structures in this early structural phase. The northeast flank of the Mobil-David dome in the southwestern part of the area has nearly 2,000 ft of structural relief on the CC-11 horizon (fig. I-15). Similar domes occur at Bohemian Colony (18S-21E) and Portland (17S-22E) (figs. I-8 and I-11). Strata on the crests of these features are broken by many normal faults of 100- to 300-ft displacement (figs. I-11 and I-15). Between and around the shale-cored domes, or "growth anticlines," of Han (1982) are structural depressions that are inferred, by analogy to salt-withdrawal basins known to be associated with salt domes, to be caused by shale withdrawal (no salt structures are known to be in the Corpus Christi study area). Information on these depressions is sketchy because they are sparsely drilled. The depression northeast of Mobil-David dome is fairly well known (Morton and others, 1982; figs. I-11 and I-15). Similar withdrawal basins are inferred to be in 18S-31E, 18S-22E, and elsewhere in the area. The basins apparently are less affected by the small faults that segment reservoirs on the growth anticlines. Because the basins subsided more rapidly during deposition, they localize a greater thickness of sand in each progradational unit.

The intermediate structural phase is characterized by less intense growth faulting and systematic dip reversal of the strata. Growth faults of this phase have expansions of 1.2 to 1.8

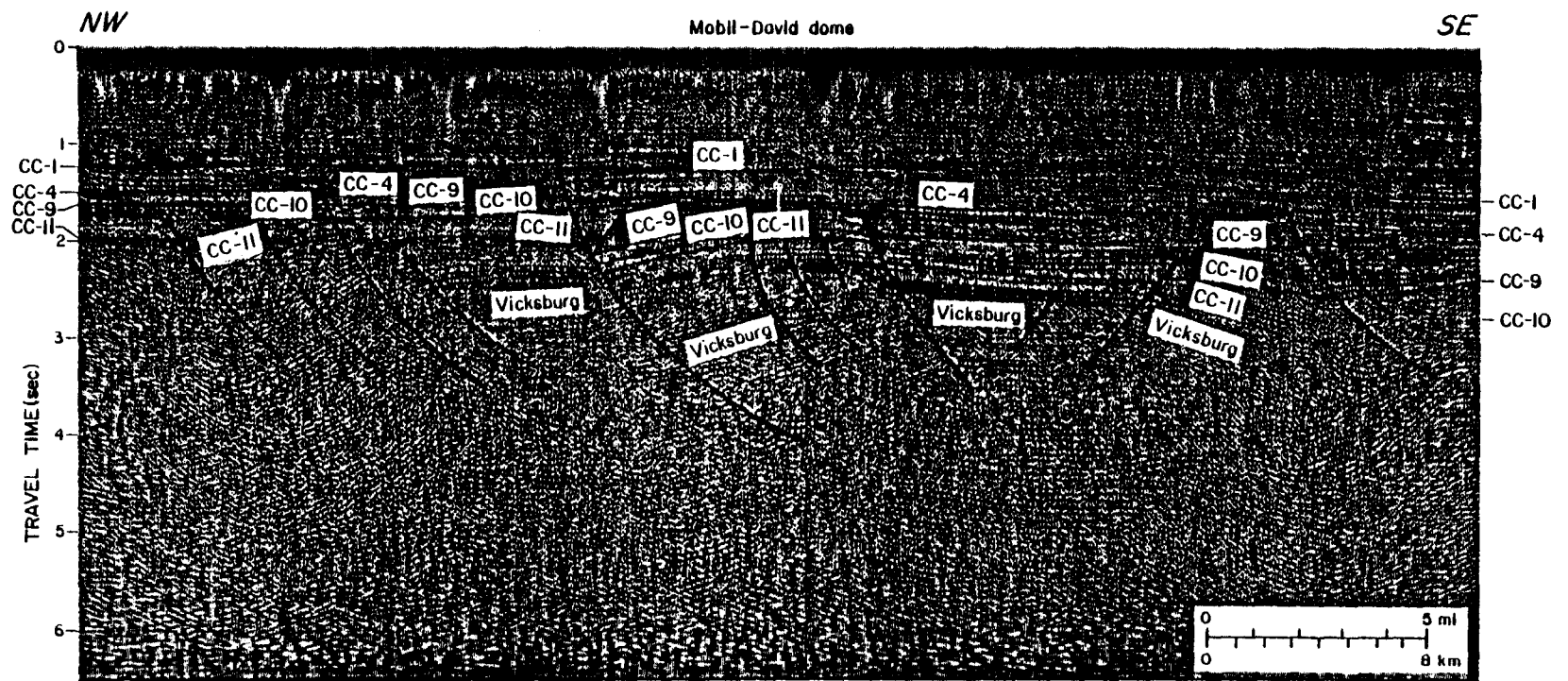


Figure I-12. Interpreted seismic section, Nueces County.

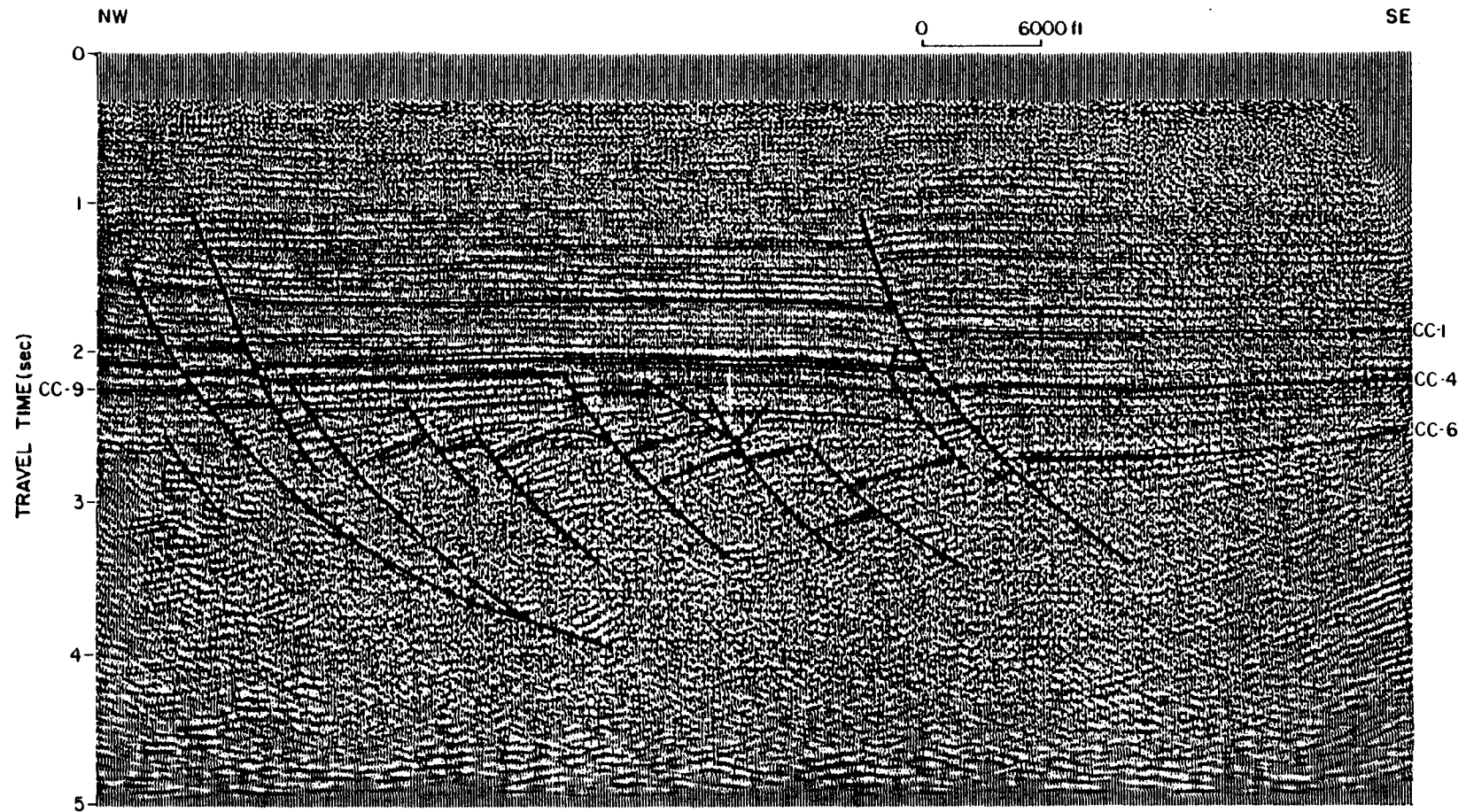


Figure I-13. Interpreted seismic section, Corpus Christi Bay, Nueces County.

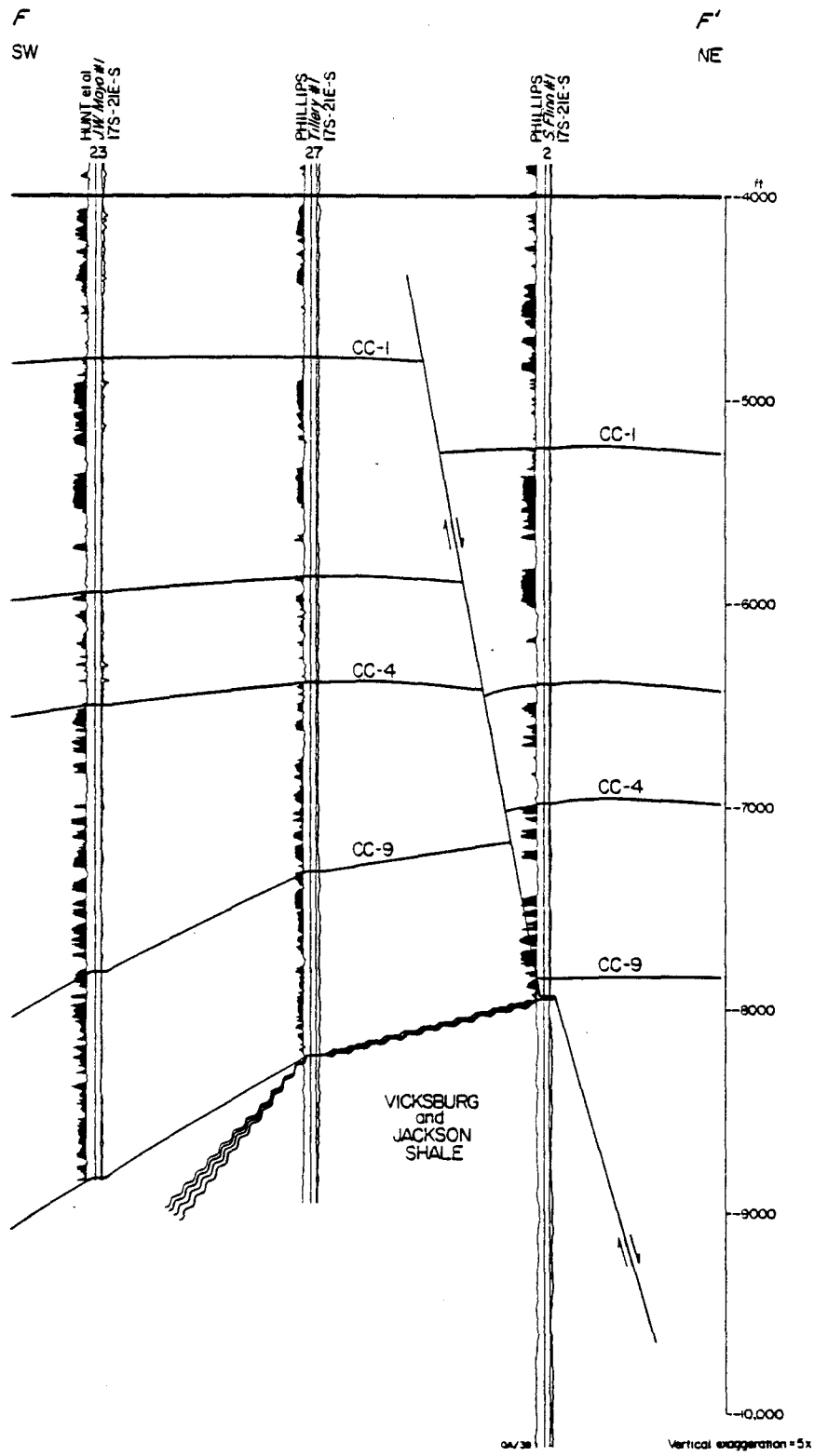


Figure I-14. Structural section across a shale diapir, San Patricio County; line of section on figure I-2.

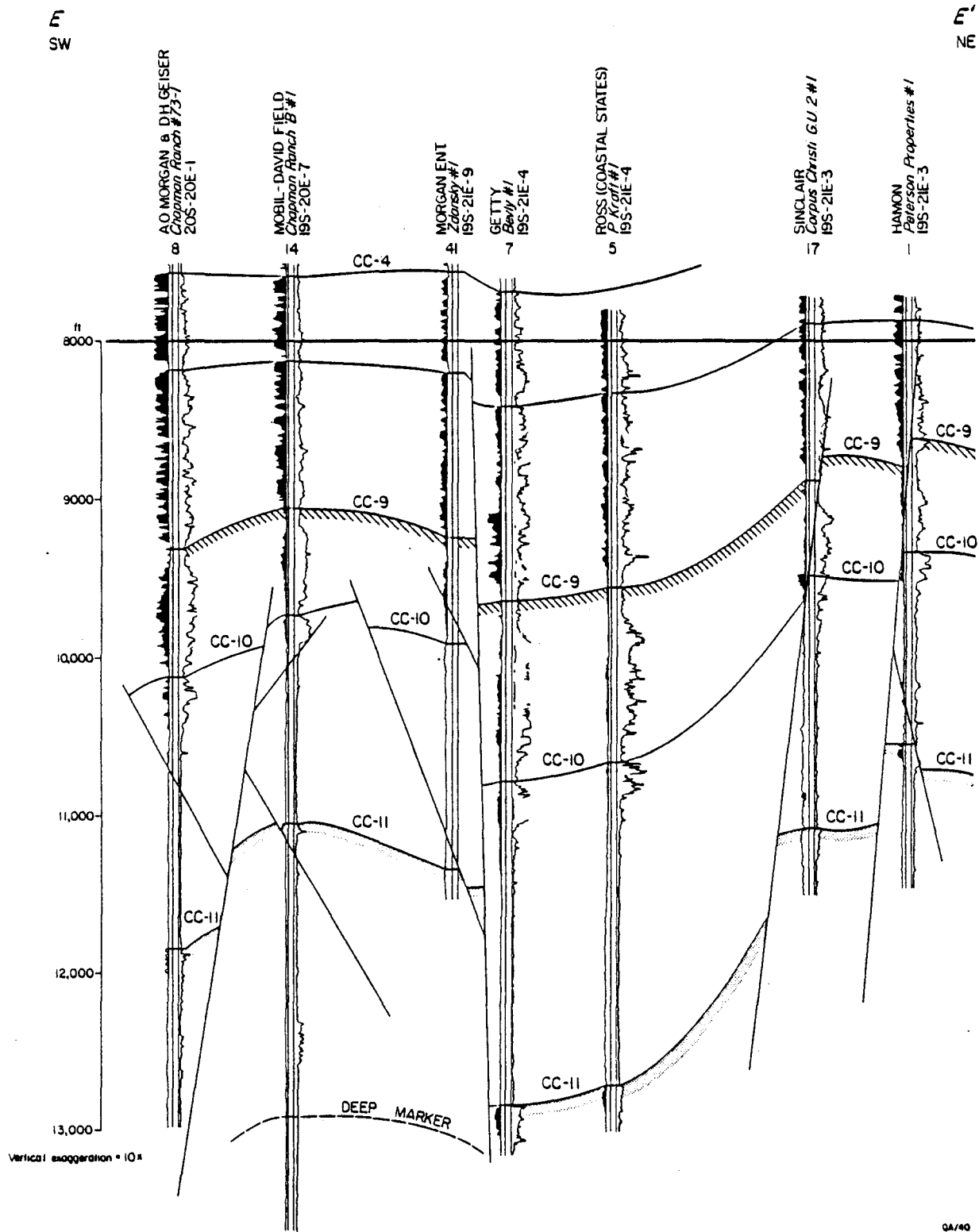


Figure I-15. Structural section across Mobil-David dome and the P. Kraft withdrawal basin; line of section on figure I-2.

on the large isopach intervals of figures I-9 through I-11. The thickest sediments are deposited on the immediate downthrown side of the major growth faults, whereas thinner sediments are deposited on the farther basinward edge of each fault compartment. Continued faulting results in complete "dip reversal," or landward dips in the overall gulfward-dipping Tertiary sequence (fig. I-13). Shale tectonism is much subdued, and the withdrawal basins are largely filled in; however, the effects of either continued mobility or compaction, or both, lead to undulations in the higher structure horizons and the long-lived, relatively positive areas over some domes.

The late structural phase consists of low-intensity growth faulting, which may be reactivated intermittently to the present time, and associated rollover anticlines. The faults have expansions of less than 1.3 in most cases, often less than 1.1. These rollover anticlines are large, gently dipping, little-faulted structures and contain many of the significant oil fields of the area (Aransas Pass, White Point East, Luby, and others; fig. I-5). Rollover anticlines have origins similar to those of the deeper dip-reversed compartments. They form closed anticlines because of the small number of faults at shallow depth and because the lesser displacements of the faults are insufficient to generate a complete reversal. The major growth faults of the earlier phases generally continue to be active but only along certain strands, which differ in places from those on which most of the early movement occurred.

Geopressure in the area is mainly restricted to sands deposited in the first structural phase. The high intensities of the growth faults and the shale tectonic disturbances have isolated most sand bodies and allowed high pressures to be maintained. Some of the deeper dip-reversed fault blocks, downdip of the larger faults of the second structural phase, are also geopressured. The sand-rich "upper" sequence was deposited during the second and third structural phases.

Three true-depth cross sections illustrate the nature and progradation of the structural phases (figs. I-16 through I-18). The first phase is well developed primarily in the CC-11 horizon, which also shows shale tectonic effects over a broader extent than any other horizon (figs. I-11 and I-16). Most of the rest of the deeper part of the section illustrates the second structural phase (dip reversal), whereas shallower strata show basinward dip having gentle rollover anticlines.

Because of the large number of wells that have been correlated, it was possible to estimate the intensity of faulting with depth by tabulating the intersections of faults with well bores; both displacement and depth encountered were listed (fig. I-19). When plotted, it is evident that a large number of faults have less than 400 ft of displacement at depths greater than about 9,000 ft. Faults of large displacement, however, continue to relatively shallow depths. To quantify this assessment, the number of faults in each 50-ft interval were counted

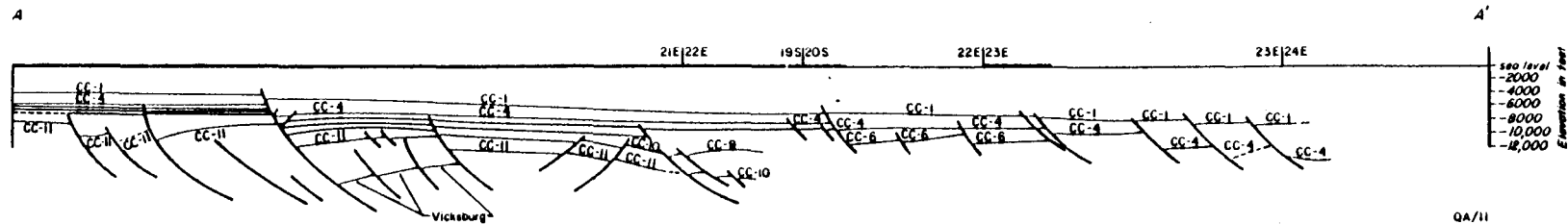


Figure I-16. Section A-A', true depth, southern Nueces County; line of section on figure I-2.

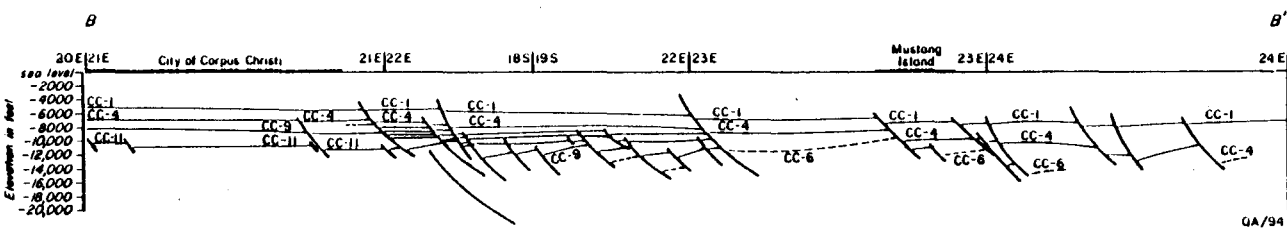


Figure I-17. Section B-B', true depth, northeastern Nueces County; line of section on figure I-2.

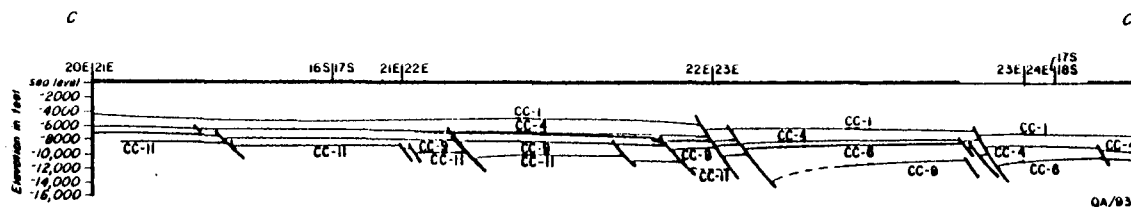


Figure I-18. Section C-C', true depth, San Patricio County; line of section on figure I-2.

and plotted against depth on a histogram. This shows a maximum number of fault-well intersections at 9,000 to 10,000 ft. It is evident, however, that the decline in fault-well intersections below 10,000 ft is owing to the smaller number of wells drilled to sufficient depth. Therefore, to estimate the geologic variable (number of faults), one must correct the fault histogram to include the projected number of fault-well intersections that would have occurred if all wells had been drilled to great depth. To perform the correction, the total depths of the 557 wells used were plotted against depth, and a cumulative frequency plot,  $F(z)$ , was made. The fault-well intersection frequency was then divided by  $F(z)$ , yielding the open-bar histogram. This was then smoothed by forward- and reverse-moving averages, yielding an estimated curve of fault intersections per 100 ft. This quantifies the original qualitative estimate of increasing faults with depth and indicates a large jump in fault density between 8,500 and 10,000 ft; below that, fault density is essentially constant. This jump corresponds to the top of geopressure, indicating a close relationship between the many small faults and geopressure occurrence. Most likely, the small faults assist in isolating the geopressed sandstones from the regional aquifer system, thereby allowing geopressure to be maintained.

One limitation of the above technique should be mentioned. Deep oil and gas exploratory wells in the study area are drilled mainly on the domes and the structural highs, not in the withdrawal basins or the areas immediately downdip of major growth faults. These areas are probably less faulted than the domes (fig. I-15); hence, the estimate of fault density at depths greater than 10,000 ft is probably too high. However, the conclusions drawn above are not substantially altered.

The sequence of structural phases can be described in terms of the sequence of events of a prograding shelf margin outlined by Winker (1981). The first phase represents the initial progradation of the shelf margin onto the upper continental slope. Uncompacted shale, which may form an irregular surface because of sediment piling in the toes of earlier growth-fault zones, is loaded by a rather thin shallow-water sequence. The shale is mobilized, producing large shale masses, diapirs, and active growth faults. The second phase represents a mature continental margin. The greater thickness of sediment overlying uncompacted shale mutes the shale's buoyant instability (Bishop, 1977), but growth faults are still active, resulting in net translation of much of the continental shelf edge seaward on deeper lying décollement surfaces, which may lie in the Vicksburg or Jackson (Ewing, 1982). The third structural phase begins when the shelf margin has migrated seaward of the area. Many of the growth faults are stabilized. As basinward tilting continues, some of the growth faults are episodically reactivated, producing rollover anticlines of large extent. Such reactivation continues to the present day, but displacements are slight.

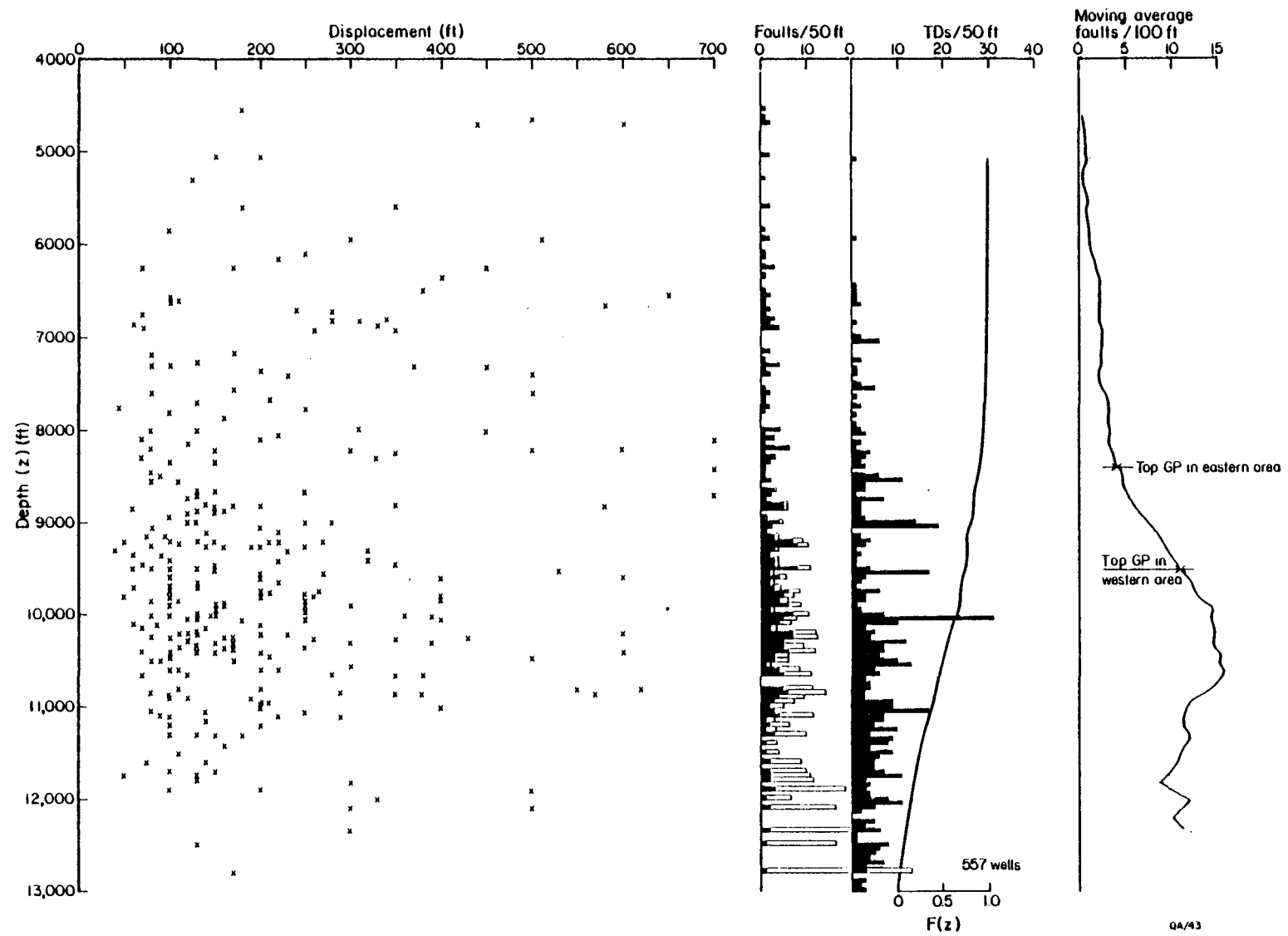


Figure I-19. Distribution of fault-well intersections with depth, Corpus Christi study area. TD = total depth of well;  $F(z)$  = cumulative frequency of wells with total depth greater than the depth given, as a fraction of the total number of wells.

## Structural Constraints on Geopressured Reservoirs at Depth

As noted previously, fault intensity in this area generally increases with depth. Fault compartments in the geopressure zone typically are rather small and poorly defined. The largest unfaulted structures in the first structural phase appear to be the shale-withdrawal basins. These can have considerable area and can localize the thicker accumulation of sand.

One of these shale-withdrawal basins was tested by the Well of Opportunity program. The Ross (Coastal States) No. 1 Pauline Kraft well was drilled to the Anderson sand CC-11 in the basin northeast of Mobil-David dome. A relatively thick, hot sand body was found, but the permeabilities were very low. Low permeability is known to be a strong deterrent to geothermal development in South Texas (Loucks and others, 1981). Enhancing porosity and permeability in deep sand bodies would be essential to the development of geothermal reservoirs in this area.

Seismic sections do not indicate any great changes in structural style below the depth of currently available well control. More diapiric or incipiently diapiric slope shale is likely to occur. The stratigraphy of the Gulf Coast Tertiary basin suggests that no shallow-water reservoirs occur below the Frio sands in this area. Deep-water sandstone reservoirs may exist in the Vicksburg or earlier units, and many of them may be relatively large, but their character is unknown.

### SARITA DIP SECTION

A dip-oriented seismic section through part of the Frio growth-fault trend in Kleberg and Kenedy Counties (fig. I-1) was purchased several years ago as a regional control line for the geopressured geothermal research program. Little work had been done on it before this study. The western half of the seismic line crosses the middle of the Sarita prospect area outlined by Weise and others (1981a) (fig. I-20).

This study did not structurally reinterpret previous work, in part because of the difficulty of correlating electric logs in the prospect area. Instead, a cross section of well logs incorporating the available paleontological data was drawn up roughly parallel to the seismic line. This cross section was correlated in tandem with the interpretation of the seismic section. The results are generally consistent with the previous correlations, although some change is indicated.

As shown on figure I-1, the Sarita dip section crosses the north-central part of the Norias delta system of the Frio Formation in South Texas (Galloway and others, 1982). The Norias

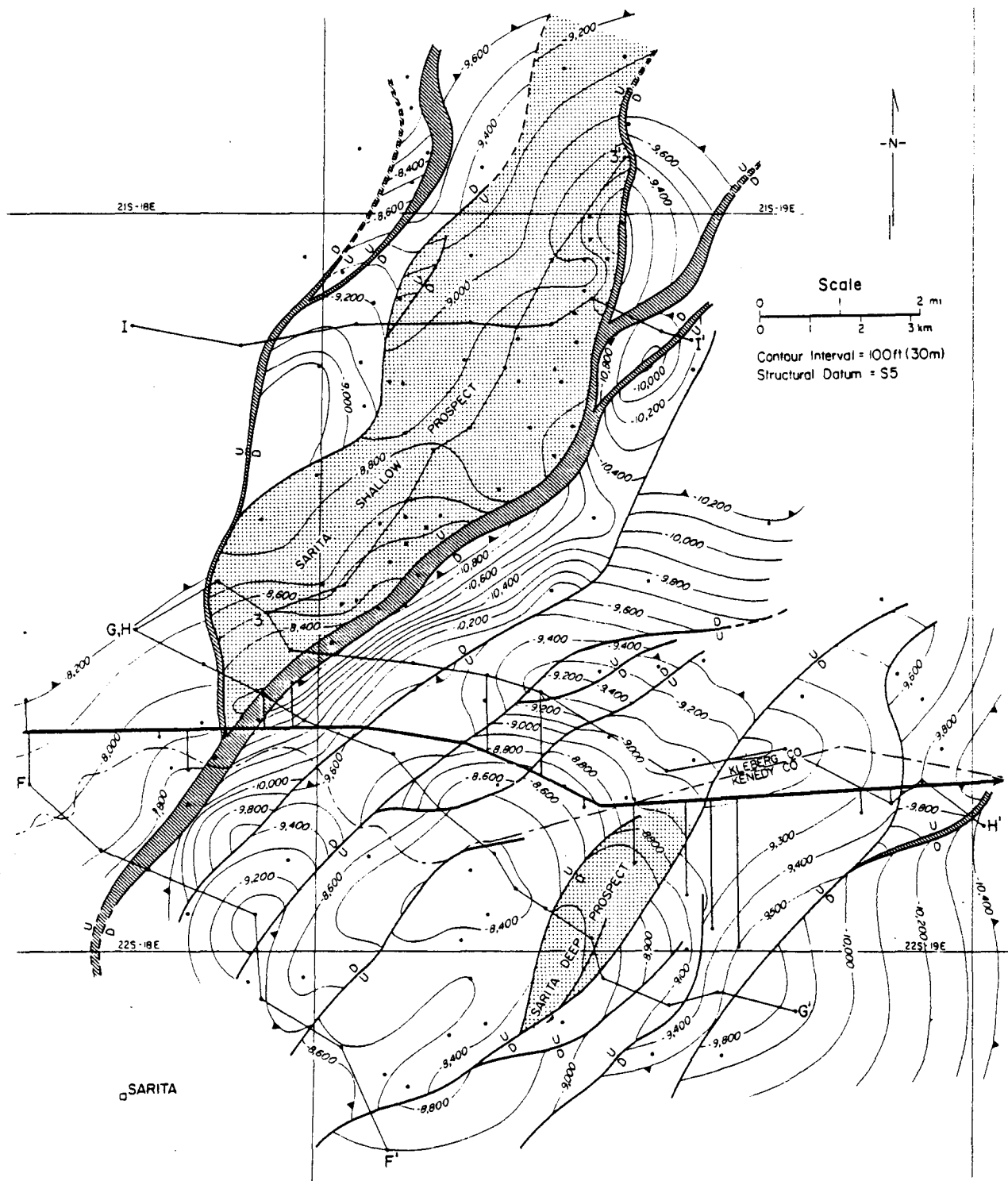


Figure I-20. Structure map contoured on S5 horizon, Sarita prospect area, showing the line of section of figures I-21 and I-22 (from Weise and others, 1981a).

delta is marked by a rapid seaward progradation throughout Frio time, which was terminated by a limited Anahuac transgression. This progradation extended the shelf margin some 40 to 60 mi seaward in South Texas; the seaward limit of the delta system has not been delineated. Faulting, shale tectonics, and possibly salt tectonics accompanied the Norias progradation.

### Stratigraphy

In studying the Sarita area, Weise and others (1981a) described the stratigraphy of the Frio Formation in terms of markers S1 through S8 (fig. I-21), ranging from the top of the Frio to basal Frio strata. They divided the section into three parts: The section below S5 is characterized by upward-coarsening sandstone and shale sequences several hundred feet thick that are interpreted to be progradational deltaic facies. Between S5 and S3 are shales and laterally discontinuous, 10- to 90-ft-thick sandstones that are interpreted to be dominantly aggradational delta-plain facies. The upper part of the section contains persistent, upward-coarsening sandstones. These may represent delta-front sandstones, relating to the transgressive episode from late Frio to Anahuac.

Weise and others (1981a) did not attempt correlation of the S horizons with benthic foraminifer markers. Because benthic foraminifera were used in the present study (fig. I-22), especially in the downdip area, it is possible to roughly correlate the S horizons with these markers. The S1 marker represents Heterostegina; it is the top of the Frio updip of the Anahuac pinch-out but lies within the Anahuac in downdip sections. The S3 marker is roughly Cibicides hazzardi (upper Frio). The S5 marker is roughly Nodosaria blanpiedi (middle Frio). The deep S7 marker correlates with the Anomalina bilateralis horizon (lower Frio). The top of Vicksburg, taken here as the first occurrence of Textularia warreni, was not included in the earlier marker scheme but lies below S8. The datum formed by the last appearance of each marker species in the Corpus Christi study area rises basinward through the section; hence, their correlations to log markers are only approximate.

Well log correlations in and downdip of the Sarita area are difficult at best. This is owing to the dominantly aggradational delta-plain nature of much of the section and to rapid, unpredictable expansions caused by growth faults. To confirm the well log correlations, seismic reflection facies were analyzed for the seismic line. This was done by noting on an overlay the faults determined from seismic data and significant reflectors. Paleontologic horizons from nearby wells were converted to travel time, plotted on the overlay, and checked with the reflector picks. The character of packages of reflectors was then noted on the overlay. The result is shown in figure I-23. Five seismic reflector facies were distinguished. High-

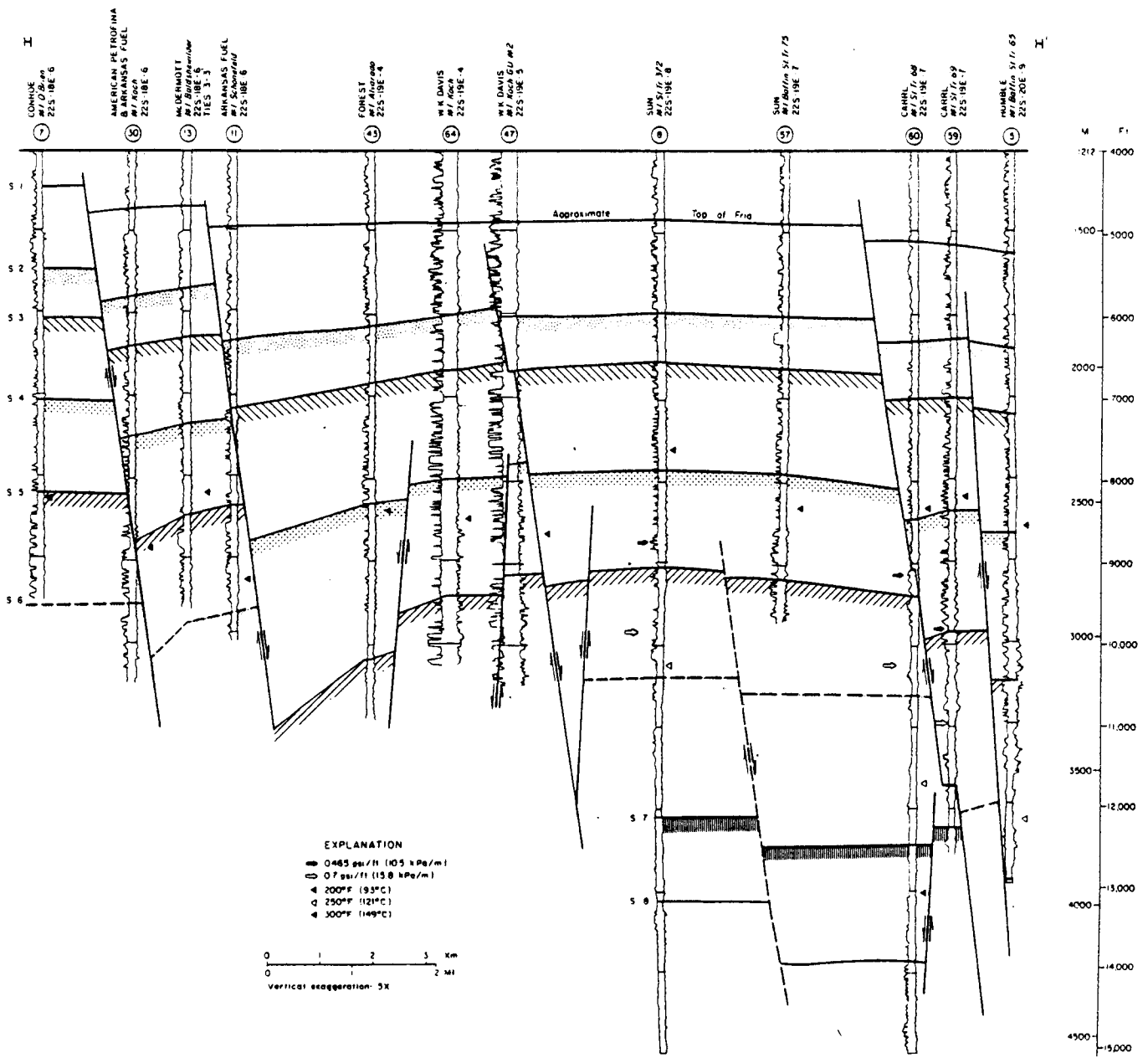


Figure I-21. Structural dip section H-H', Sarita prospect area (from Weise and others, 1981a). Compare to figures I-3 through I-5.

frequency, low-continuity reflectors of varying amplitude dominated the higher parts of the section and were locally present at depth. Reflectors of high amplitude and frequency and good continuity were found locally within the first facies and in a band below the first facies. Chaotic reflectors, including noise zones, predominated at greater depth. Local transparent zones occurred within the upper facies. Strong, low-frequency, continuous reflectors were noted at approximately 6 seconds on the section.

The reflector facies may be interpreted in terms of overall depositional environments. The upper discontinuous facies represents the aggradational delta-plain and fluvial systems in the Frio Formation and overlying strata; these environments are characterized by discontinuous sandstones in a shale matrix. The band of continuous reflectors marks the deltaic progradational environment in which sandstones are more continuous and correlatable. The chaotic facies largely represents prodelta/slope shale sequences and includes a shale mass behind the major growth fault. The deep low-frequency facies may represent Cretaceous carbonates at a depth of greater than 30,000 ft. The geometry of the facies shows the strong progradation of the shelf-margin over slope shales and of the delta-plain over the delta-front environments. The Anahuac transgression is visible at the right. The results of the reflector facies analysis were used to check the reflector correlations across major growth faults and the correlations on the well log section (fig. I-22).

Geopressure occurs at an average depth of 9,500 ft at the west end of the line to about 9,000 ft at its midpoint and eastern end (Weise and others, 1981a). This falls generally at the Nodosaria blanpiedi horizon (S5) in the Sarita area but is higher in the downdip part of the section. The top of geopressure follows the base of the delta-plain-dominated facies and the top of the shale-rich delta-front and prodelta section. The pod of sand-bearing to delta-plain facies indicated on figure I-23 is also geopressured and might be a potential geothermal prospect.

#### Structure and Structural Development

The interpreted seismic section is shown in figure I-24 and a true-depth section constructed from it in figure I-25. The section is dominated by a large, low-angle listric growth fault backed by a shale ridge of diapiric or semi-diapiric Vicksburg and pre-Vicksburg shales. Antithetic faults are moderately abundant, and substantial rollover of strata into the fault is indicated. Other growth fault systems having a generally steeper angle of dip are interpreted to lie downdip of the major fault; at least one may converge with the major fault at depth.

Shallow strata show gentle rollover anticlines downdip of growth faults. Deeper strata show pronounced landward dips into the major growth fault broken by antithetic faults. This is

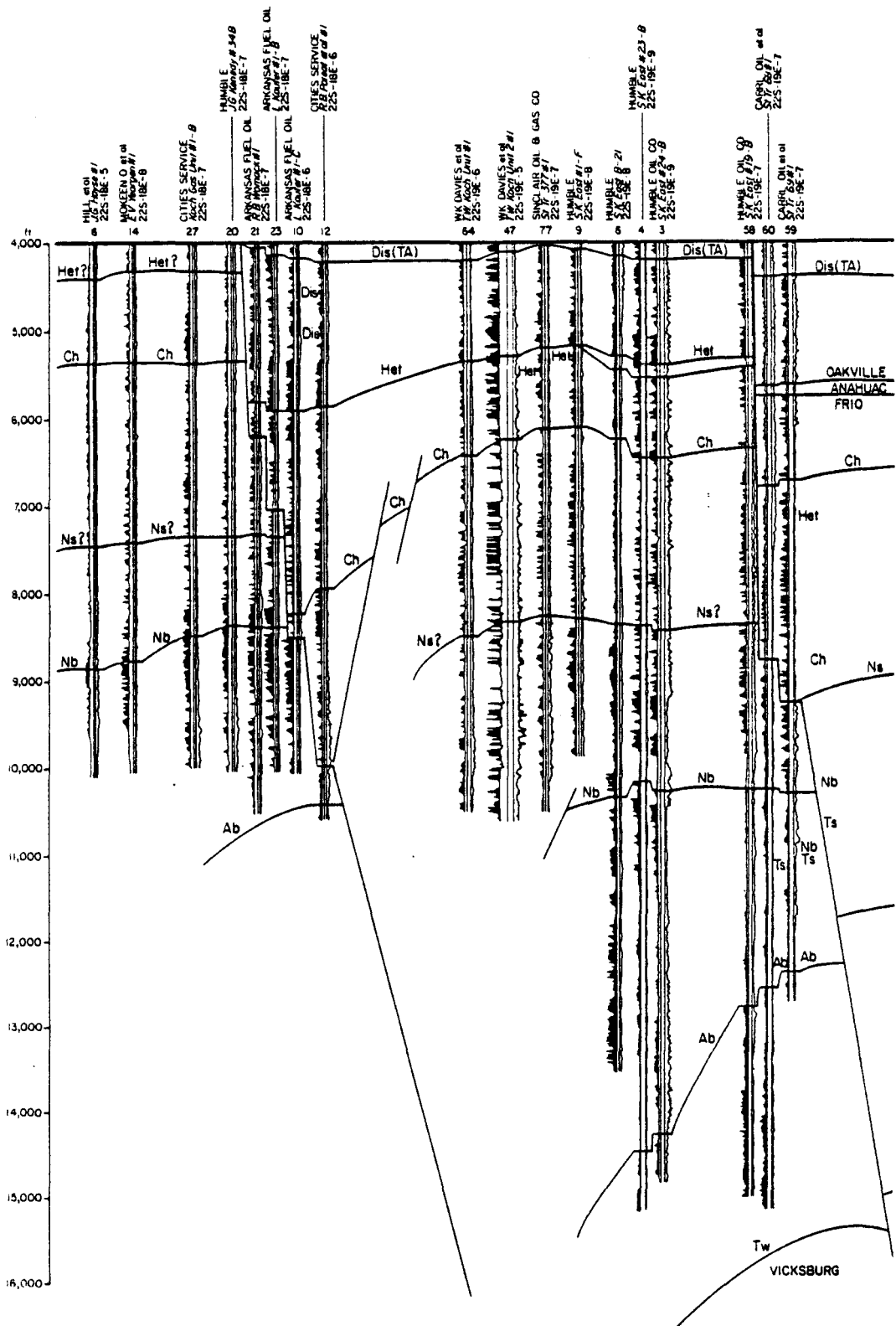


Figure I-22. Structural dip section constructed roughly along the seismic line. Line of section shown in figure I-7. The horizons shown are based on log and seismic interpretation but approximate the benthic foraminifer horizon shown.

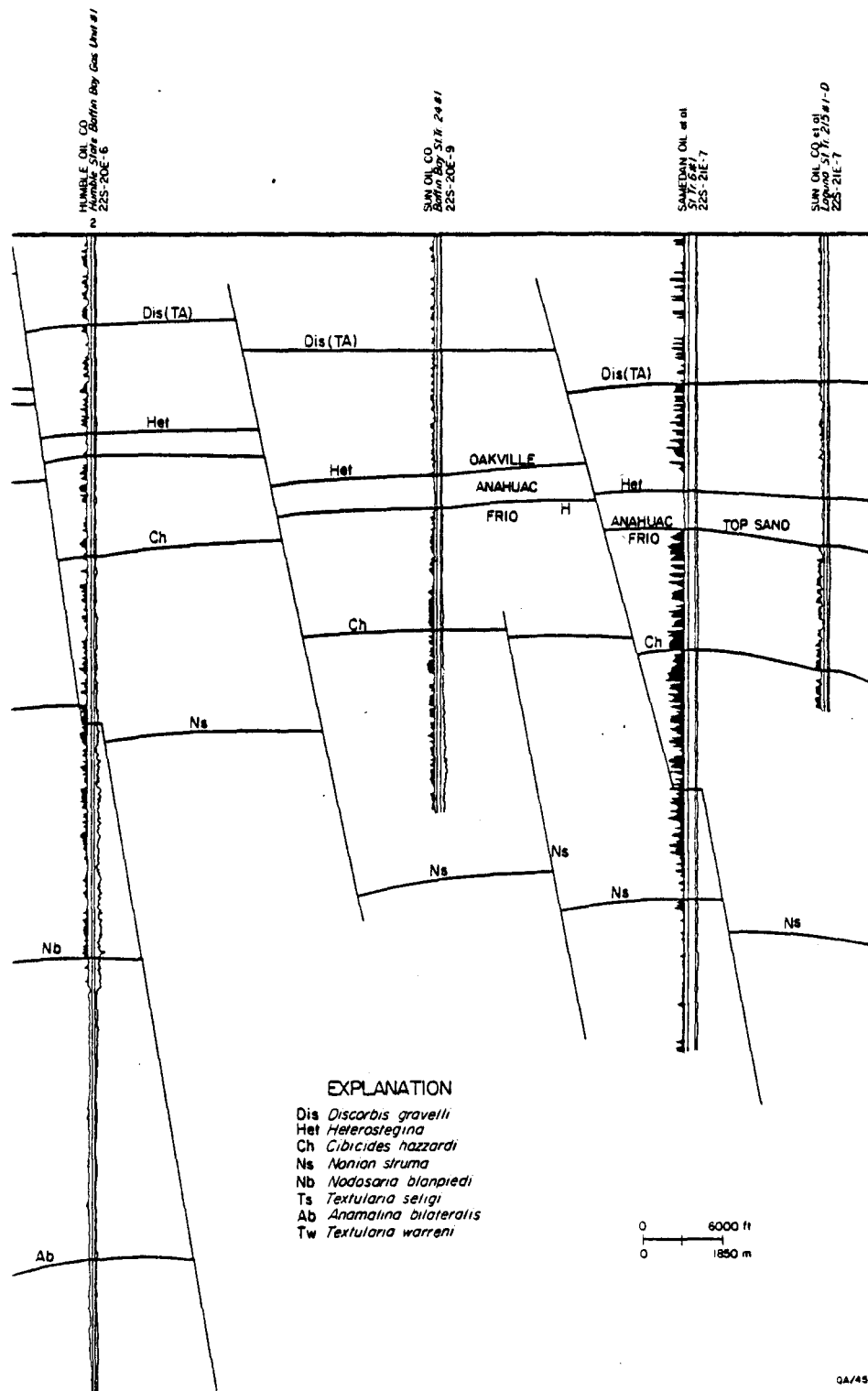


Figure I-22 (cont.)

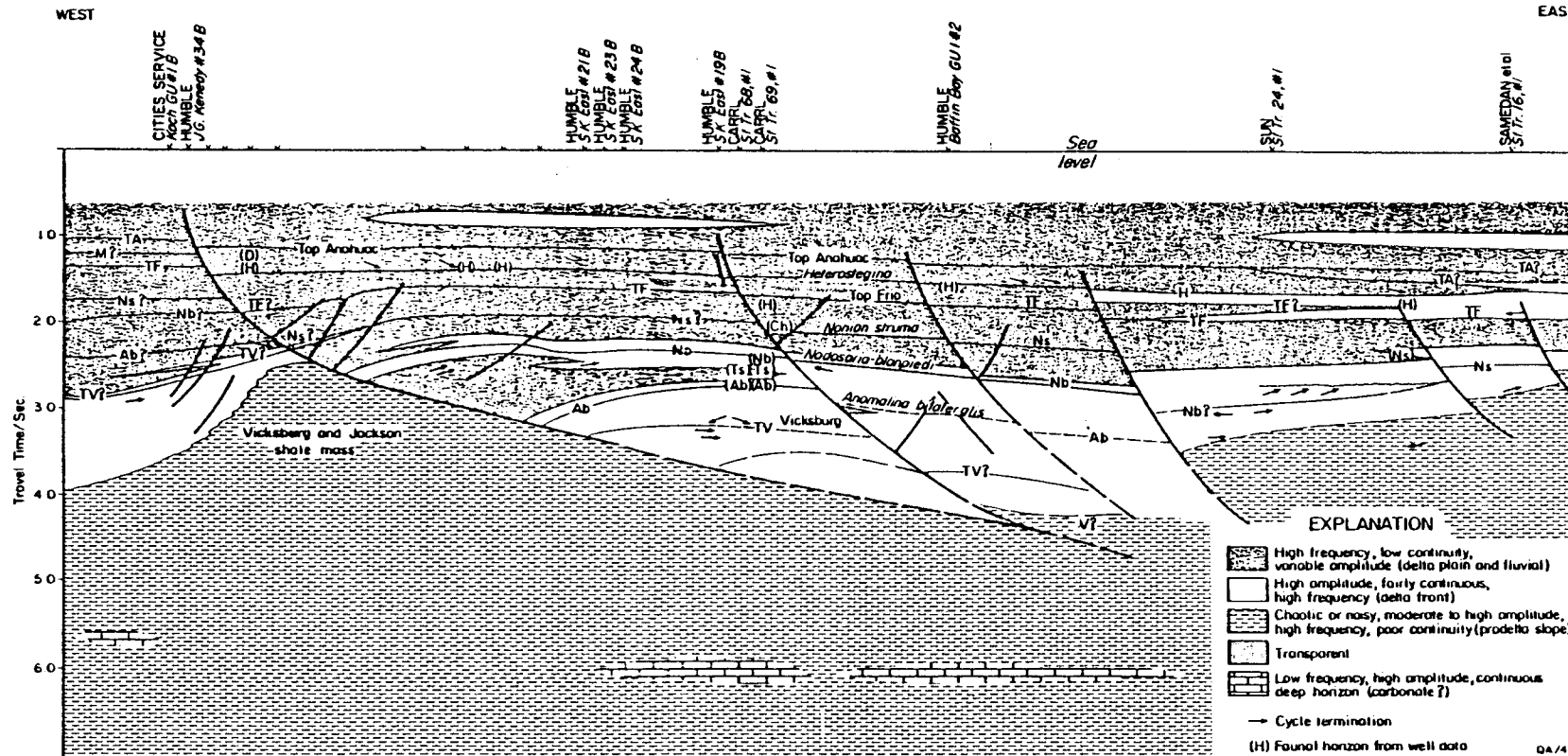


Figure I-23. Seismic reflector facies interpretation of the line. TF = top of Frio (Cibicides hazzardi on this section); TA = top of Anahuac; TV = top of Vicksburg (Textularia warreni).

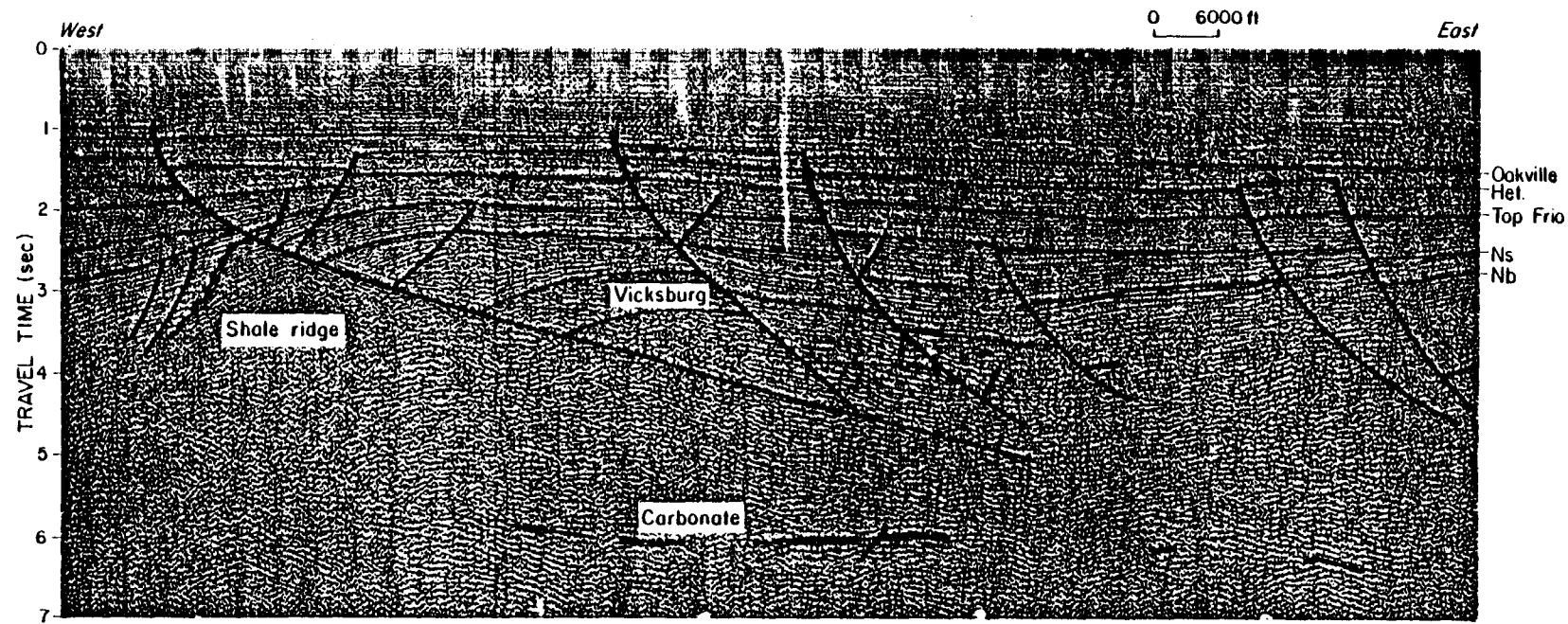


Figure I-24. Interpreted seismic section.

34

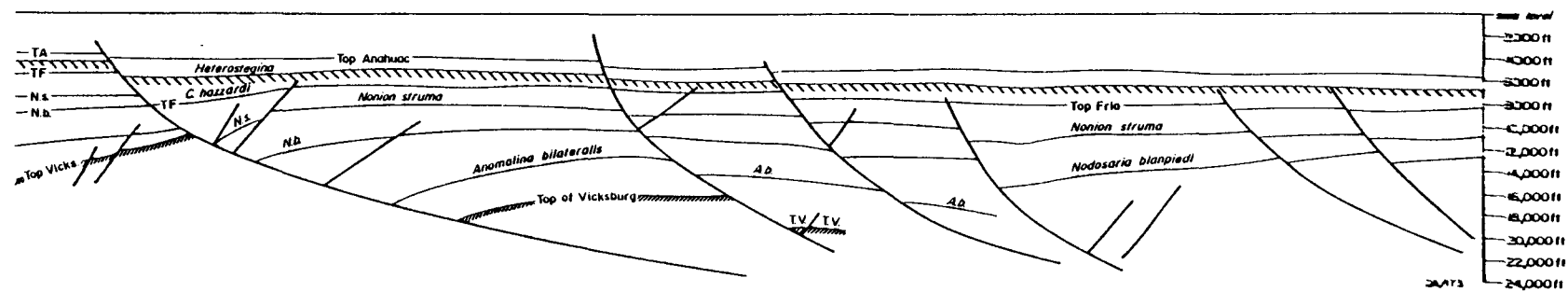


Figure I-25. True-depth structural section constructed from the line confirmed by well data.

also shown on the structure map by Weise and others (1981a) of S5 (about Nodosaria blanpiedi) (fig. I-20). The downdip growth faults seem to have caused comparatively little rollover, although some dip reversal is noted on one fault. The area on the right-hand side of the seismic section may be related to the "toe" of material moved seaward on the low-angle glide surface of the updip major growth fault.

There is little evidence of the intense faulting below the top of geopressure that was noted at Corpus Christi. This can be attributed partly to the poor well control downdip, which allows the interpreter to skip cycles and omit minor faults. If there is lack of intense faulting in the deeper section, it may reflect the relative lack of shale diapirism in the area immediately downdip of the western shale ridge. Shale tectonics appear to have been more intense at both the west and east ends of the seismic section, in the shale ridge formed behind the major fault, and in an area of reverse dips and possible local unconformities. The area between these localities is affected by growth faults but shows little other shale tectonic activity.

A large amount of basinward sliding occurred on the major low-angle growth fault. Palinspastic reconstruction of the left-hand part of the line indicates a post-Vicksburg extension of about 25,000 ft, or 50 percent (fig. I-26). Most of this extension took place before middle Frio (Nonion struma) time; later extension was only 7,000 ft. The shale ridge developed early (pre-Anomalina bilateralis), as shown by thinning of basal Frio and Vicksburg reflector packages over the ridge. Post-Anomalina bilateralis strata show little thinning over the ridge but large expansion over the growth fault. The combination of an early shale ridge backing a later growth fault has been noted elsewhere in South Texas (Bruce, 1972).

#### Structural Constraints on Geopressured Reservoirs at Depth

Geopressured reservoirs of possibly large areal extent can be found in the downdropped strata basinward of the major growth fault of the Sarita area. Many of the sand-bearing units in this area have already been drilled (fig. I-22). However, no shallow-water sand bodies are expected to occur in the Vicksburg in this downdip position, so future prospects are not encouraging. Poor reservoir quality is also a major problem in this area, as discussed previously.

#### PORT ARTHUR STUDY AREA

The Port Arthur study area is located in the Frio (or Frio-Vicksburg) growth-fault trend in far southeast Texas, including much of Jefferson and Orange Counties (fig. I-27). The area

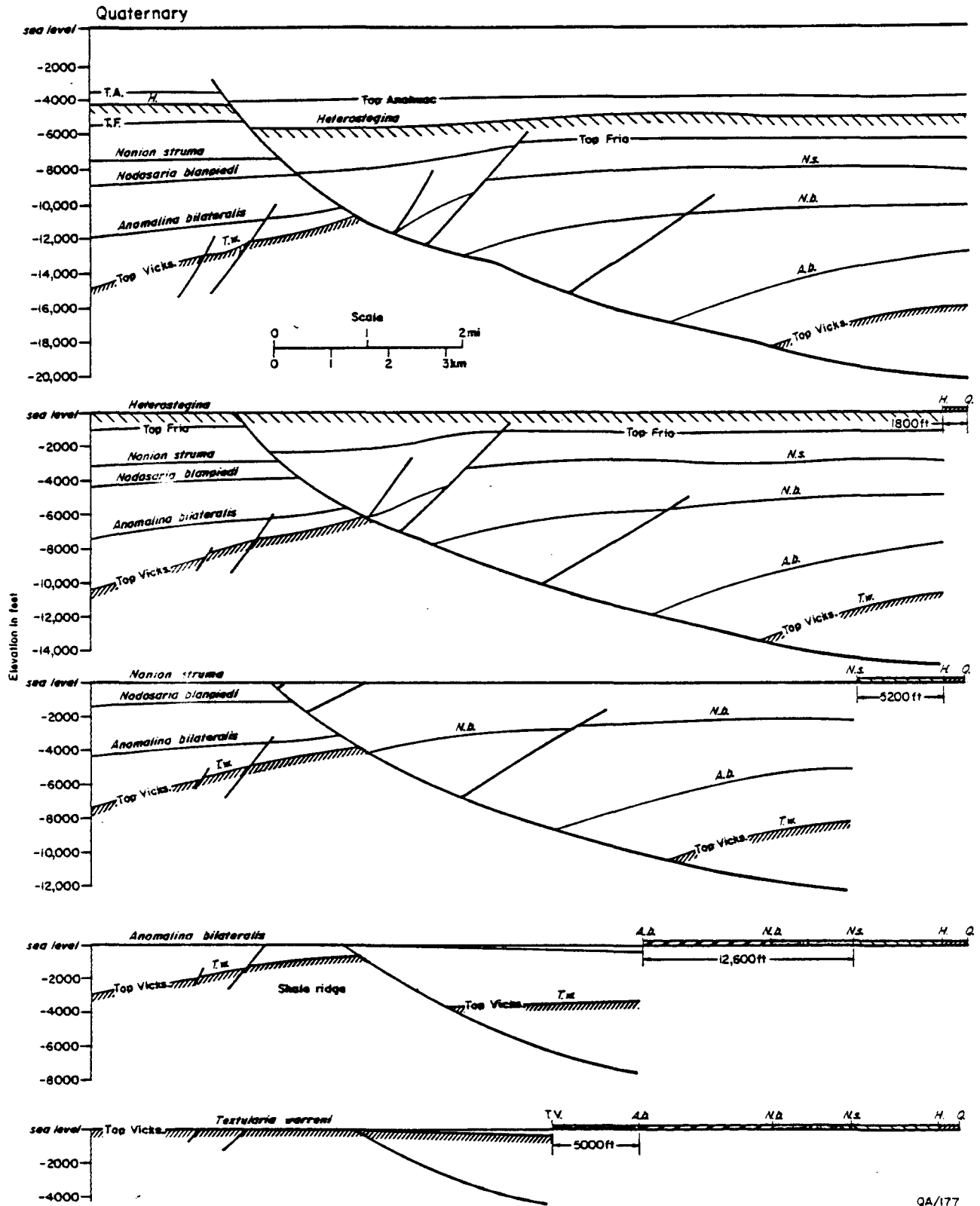
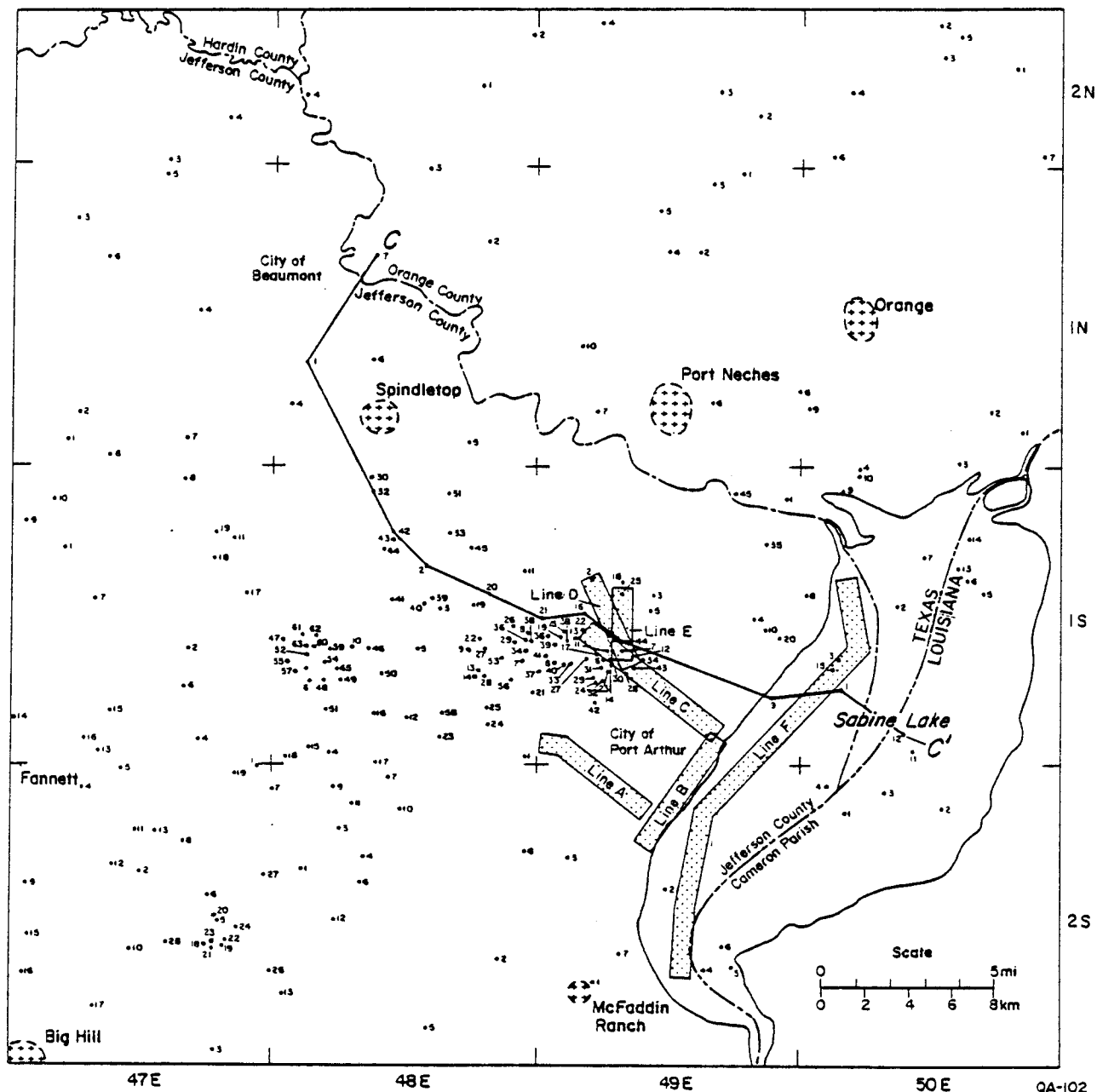


Figure I-26. Palinspastic reconstructions of the western part of the line across the Sarita prospect area. Large amounts of basinward sliding are indicated.



**EXPLANATION**

 Salt domes
  Proprietary seismic line

Figure I-27. Location map of the Port Arthur area showing well control, general locations of seismic lines, and locations of salt domes.

centers on Port Arthur and Port Acres gas-condensate fields, which are under study for possible dispersed gas production (Gregory and others, 1983). Within the area, more than 220 deep well logs have been correlated. Six seismic lines, acquired and reprocessed for the dispersed gas study, have been interpreted along with the well data.

The study area lies in the western part of the Hackberry Embayment (Paine, 1968), within which the Hackberry deep-water member of the Frio Formation was deposited (fig. I-28). The Hackberry forms a seaward-thickening wedge in southeast Texas and southwest Louisiana that is inserted into the normal Frio marine succession of the Buna strandplain/barrier-bar system and possibly the marginal parts of the Houston delta system of Galloway and others (1982) (fig. I-1). The wedge pinches out to the north along a line that Bornhauser (1960) termed the Hartburg flexure. The lower Hackberry is a sand-rich unit that fills channels eroded up to 800 ft into the pre-Hackberry sediments (fig. I-29). Studies by Paine (1968) and Berg and Powers (1980), as well as current work at the Bureau (Ewing and Reed, in preparation), indicate that these sands formed in a submarine canyon-fan environment. These lower Hackberry sands are currently the most important geopressured exploration target in the area.

Three salt domes are wholly included in the study area: Spindletop, Port Neches, and Orange. In addition, two salt domes, Fannett and Big Hill, are along the boundaries of the area, and a probable salt dome, McFaddin Ranch, is in the southern part of the area.

#### Stratigraphy

The Frio Formation in the Port Arthur area ranges from about 2,000 to more than 6,000 ft thick, increasing basinward. The updip part of the area consists of stacked barrier-bar and strandplain sandstones of the Buna barrier system. Downdip, the sands become less dominant, and the deep-water sand-shale wedge of the Hackberry is inserted.

The Frio can be divided into three units (fig. I-30). The lower unit (between the top of the Vicksburg at Textularia warreni and Nodosaria blanpiedi) is very thin and sand-poor; it is difficult to distinguish from the underlying Vicksburg. The middle unit (from Nodosaria blanpiedi to about Marginulina texana) contains abundant sand updip but only a few discontinuous sands of indeterminate origin downdip; the latter are extensively eroded at the sub-Hackberry unconformity and their original thicknesses and geometries are obscure. The Hackberry wedge lies between Nonion struma and Marginulina texana in upper-middle Frio. The upper unit consists of nearly continuous sand updip and alternating sand and shale downdip. These sands contain upward-coarsening cycles and are continuous along strike; however, they shale out fairly rapidly downdip and are inferred to be either barrier-bar or strandplain sand

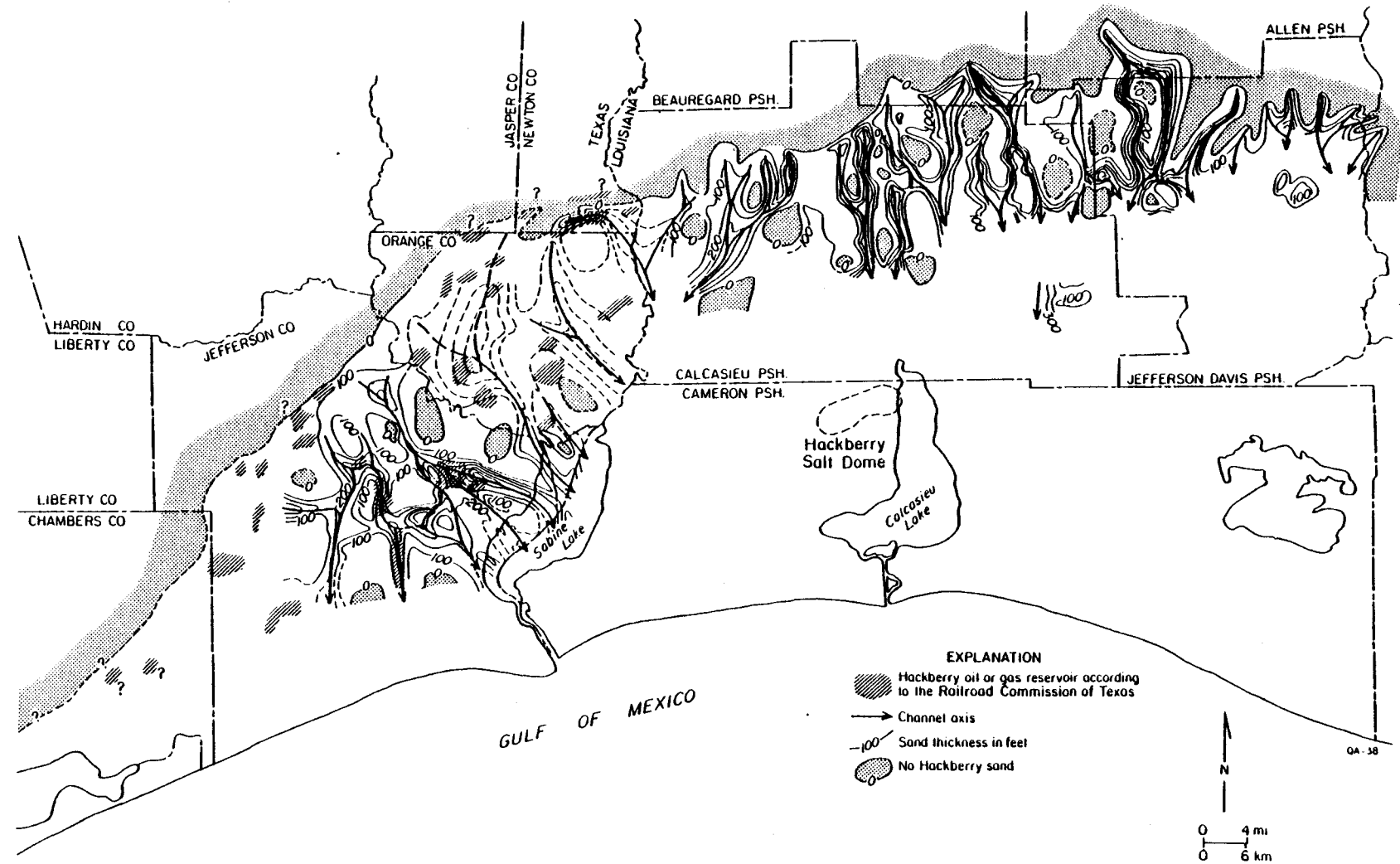


Figure I-28. Regional distribution of sand-bearing lower Hackberry channels in the Hackberry Embayment west of Acadia Parish, Louisiana. Louisiana data from Paine (1968); Texas data from Bornhauser (1960) and this study. The type locality of the Hackberry at Hackberry salt dome is also shown.

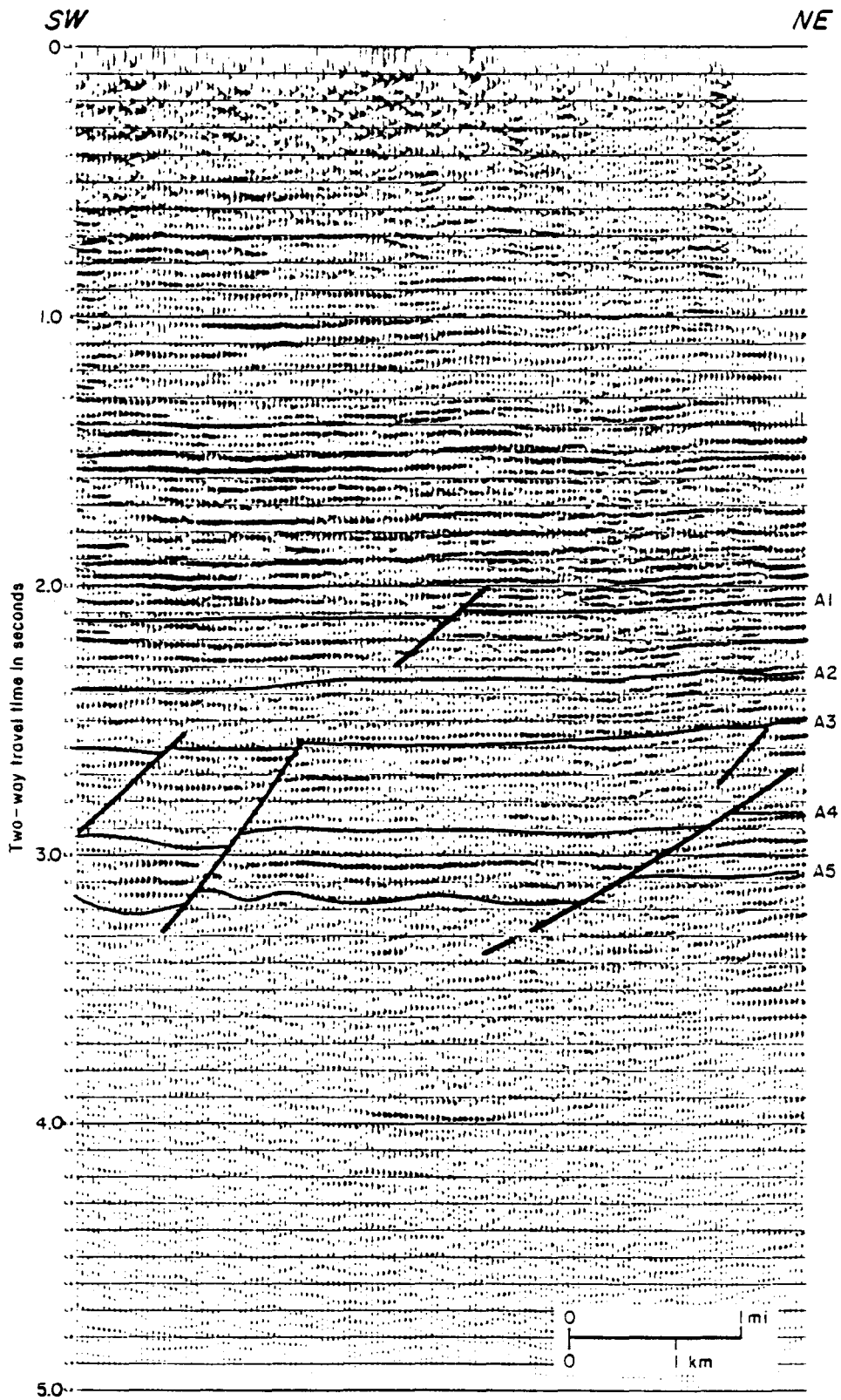


Figure I-29. Interpretation of a strike-oriented seismic line along the shore of Sabine Lake.

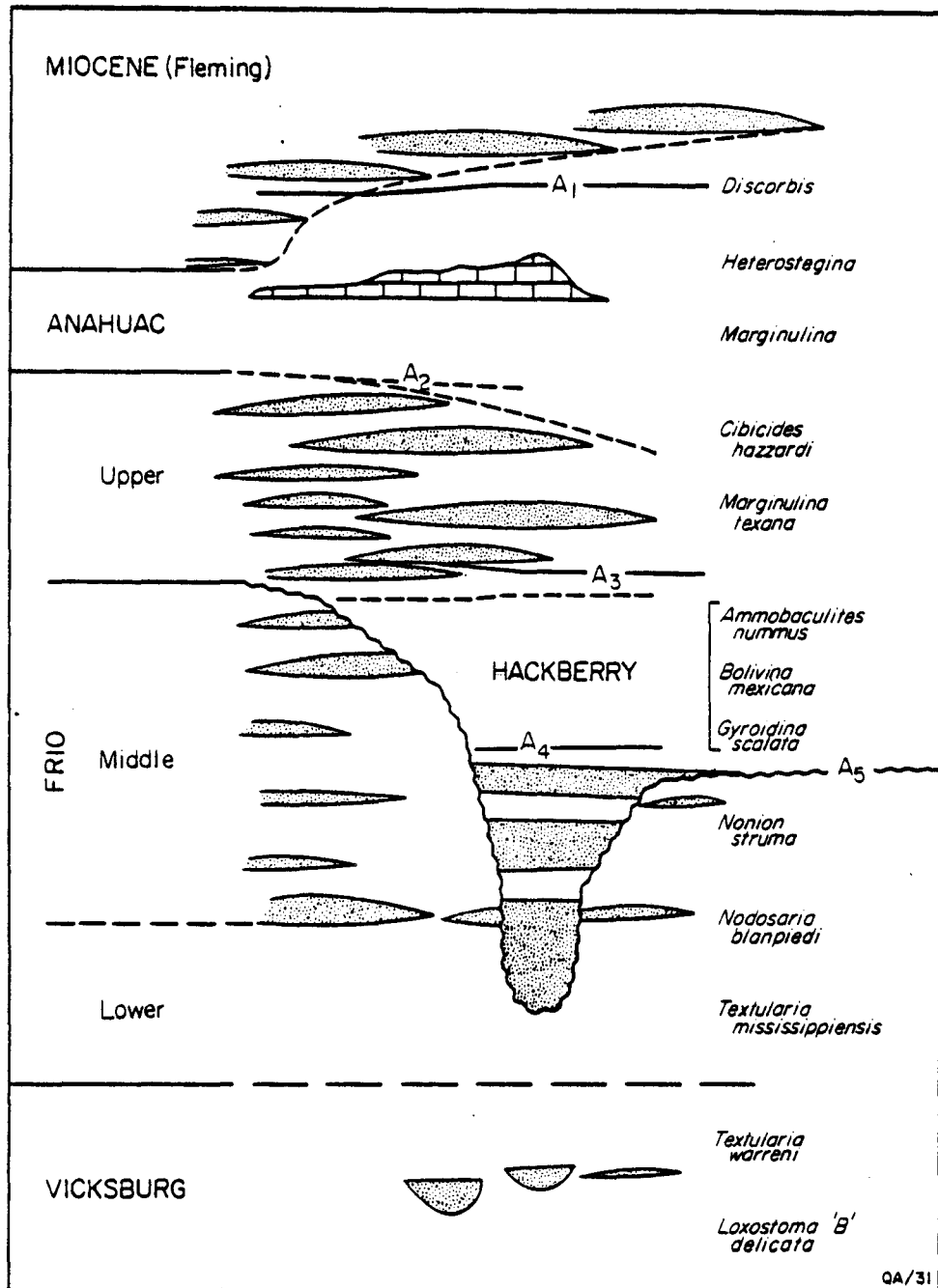


Figure I-30. Stratigraphic diagram of Frio and related strata, Jefferson County study area, showing diagnostic foraminifera, sand-body distribution (shaded), and marker horizons used in this study (A1 through A5).

bodies, or both. They are overlain by transgressive, shallow marine shales of the Anahuac Formation. Within the Anahuac Formation is a locally developed limestone member known informally as the Heterostegina limestone. Undifferentiated sandstone and shale of Miocene age overlie the Anahuac.

The Vicksburg Formation, which underlies the Frio in this area, consists largely of shale. The resistivity of the Vicksburg shale is typically higher than that of the lower Frio, but the two are otherwise very similar. Within the Vicksburg are discontinuous sand bodies having blocky spontaneous potential patterns similar to those of the Hackberry sands; this suggests that some of the Vicksburg sediments represent deeper water (slope?) deposits.

Within the downdip parts of the study area, no units below the pre-Hackberry unconformity can be correlated in enough well logs to reliably determine their structural configuration. Furthermore, the seismic data are not of good enough quality to determine the deep structure. Correlation markers were therefore set up from A1 through A5, ranging from the top of the Anahuac to the pre-Hackberry unconformity (figure I-30). Progradation of the upper Frio sand bodies and the lower Miocene sand bodies is indicated because their respective markers pass from shale to sand sequences. Markers A1 through A3 lie in shallow-water deposits, whereas markers A4 and A5 lie in deep-water strata of the Hackberry member.

In most of the study area, the top of geopressure is near A3, the base of the upper Frio sands (fig. I-31); the Hackberry and lower sands southeast of Spindletop are geopressed. In the northwestern part of the area, the top of geopressure lies below the base of the Frio sand; this was noted near the Lear No. 1 Koelemay well of opportunity (Morton and others, 1982). In extreme downdip wells where the upper Frio is sand-free, the top of geopressure rises into the upper Frio and probably to the base of the Miocene. In the Port Arthur - Sabine Lake area, the top of geopressure coincides with a sharp drop in seismic velocity (fig. I-32). However, the effects of geopressure at A3 are coincident with the lithologic transition from a sandy to a shale-dominated sequence; hence, the contribution of geopressure cannot be adequately assessed. The lower Hackberry sands show higher velocities than the Hackberry shale, although not as high as extrapolation of values from shallower sands would indicate.

#### Structure and Structural Development

By using both well log data and the available seismic sections, structure maps and sequential isopach maps (to approximate paleostructure or paleogeography) of the Port Arthur area have been made. Analysis of these maps suggests four phases of structural activity in the area.

43

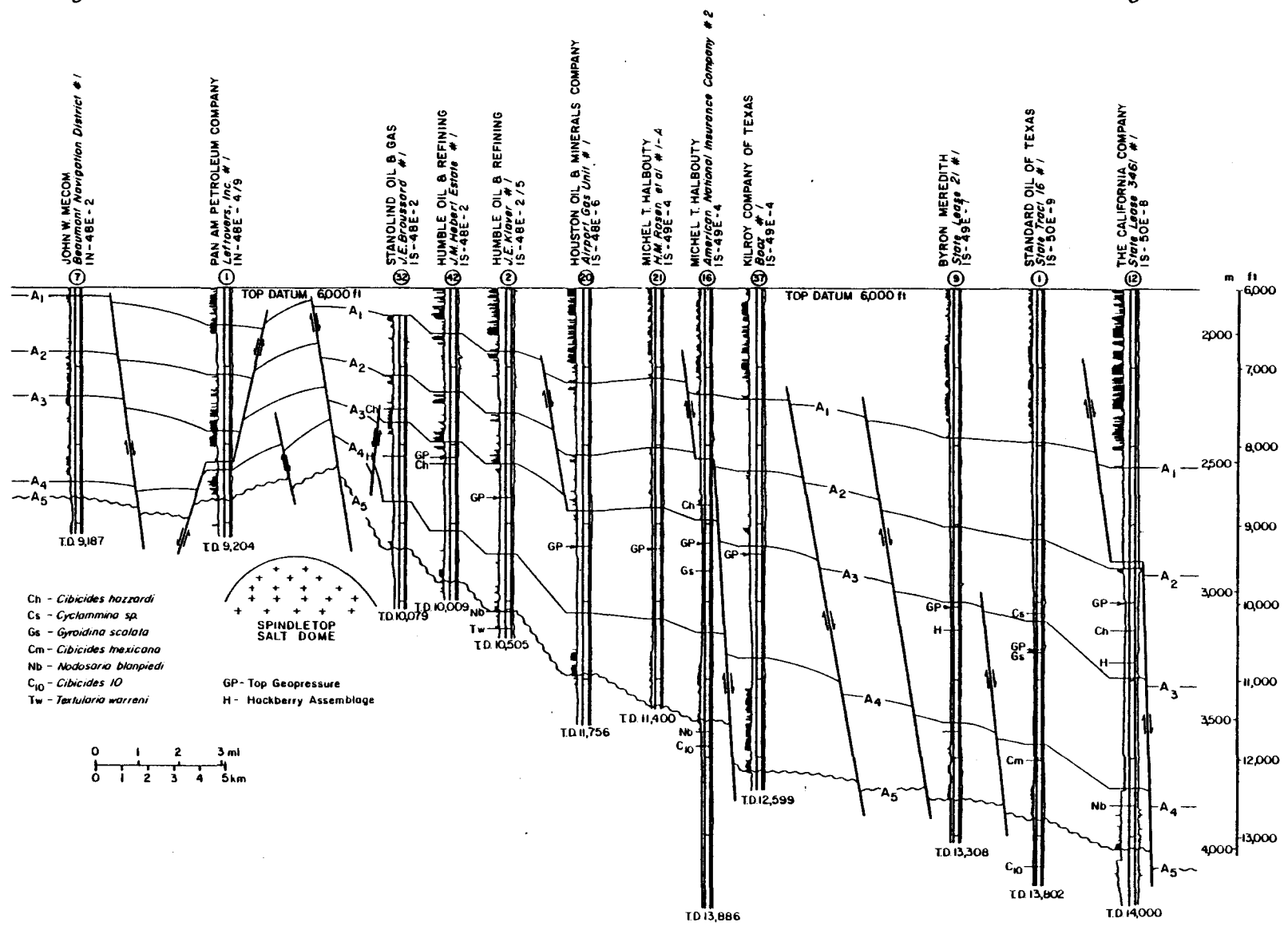


Figure I-31. Structural section C-C' passing by Port Arthur field and Spindletop salt dome.

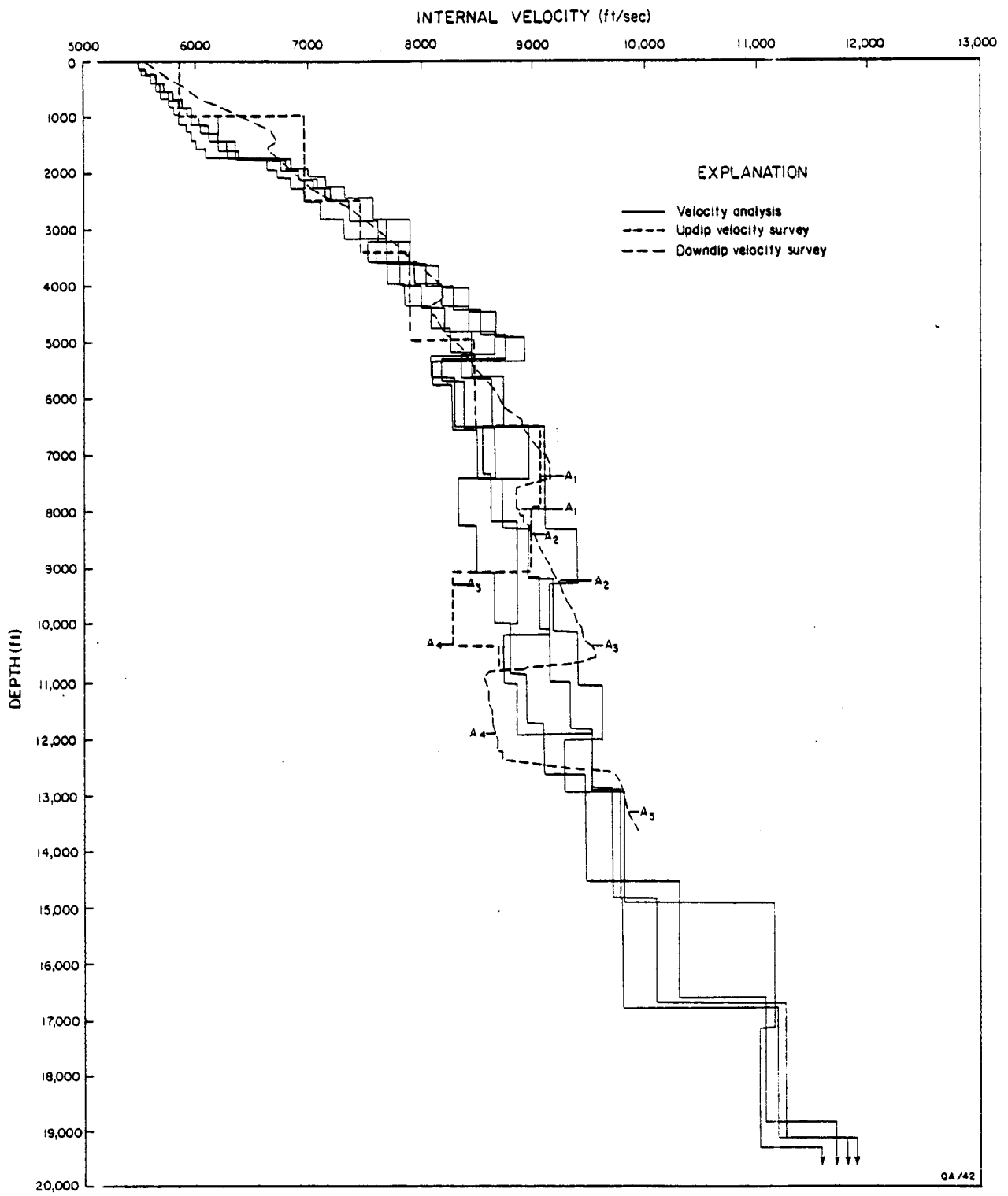


Figure I-32. Interval velocity versus depth for two velocity surveys and velocity analyses from seismic data. Stratigraphic horizons shown for the velocity surveys.

Well penetrations below the Hackberry sand sequence are sparse, and a reliable top of the Vicksburg is difficult to pick using the logs available. However, by using paleontological information and limited well log correlation, an isopach map from A3 to the top of the Vicksburg can be sketched (fig. I-33). (The A4 and A5 markers could not be used for this isopach because they are known to have been much below sea level; in addition, A5 is an irregular, unconformable surface.) Two broad uplifts, inferred to be salt-cored, underlie the northern half of the area, one under the more recent Orange and Port Neches domes and the other under Spindletop dome and farther west. A withdrawal basin north of the uplifts and a sag between the uplifts and to the south suggest salt movement into the uplifts. The large, irregular changes in thickness in the southwestern part of the area suggest a growth fault having some combination of dip-reversal and salt-generated activity. One shale diapir has been drilled that indicates Jackson shale below the Hackberry. Development of the area before deposition of the upper Frio seems owing to a combination of shale tectonic growth faulting and broad salt uplifts.

It is not certain where the lower Frio and Vicksburg shelf margins lie. Sands found in the study area within the Vicksburg lie in the southwest and central parts of the area and appear very similar to Hackberry sands. These sands were probably deposited in deep water on the continental slope. The depositional environment of the lower Frio is debatable, but faunal evidence suggests shallow-water deposition; this was shown to the west in Chambers County by Gernant and Kesling (1966), and it is generally assumed elsewhere in the Hackberry Embayment. If deposition was in shallower water, then the shelf margin prograded across the study area during upper Vicksburg and Frio time, but virtually no sand marks this progradation. This is an example of progradation of a mud-dominated shelf margin. Other examples on the Texas Gulf Coast include the Yegua-Jackson-Vicksburg progradation immediately northwest of the Port Arthur area in Jefferson and Hardin Counties (Morton and others, 1982), the Claiborne progradation of Central and South Texas in Victoria to Starr Counties, and the Claiborne progradation of South Texas in Starr to Duval Counties. In any event, some of the structural activity shown on figure I-33 occurred while the area was at or seaward of the shelf margin.

The second phase of structural development was the formation of the Hackberry Embayment and its filling by deep-water shales and channel sands (fig. I-34). A pre-Hackberry unconformity (A5) was developed over the entire area downdip of the Hartburg flexure, which is marked by a zone of growth faulting (fig. I-35). This unconformity is interpreted by most workers to reflect subsea erosion of varying intensities related to submarine fan deposition downdip and to the immediately overlying channel-fill sands. If the lower Frio was of shallow-water origin, as discussed above, then a large-scale, rapid foundering of the shelf margin must

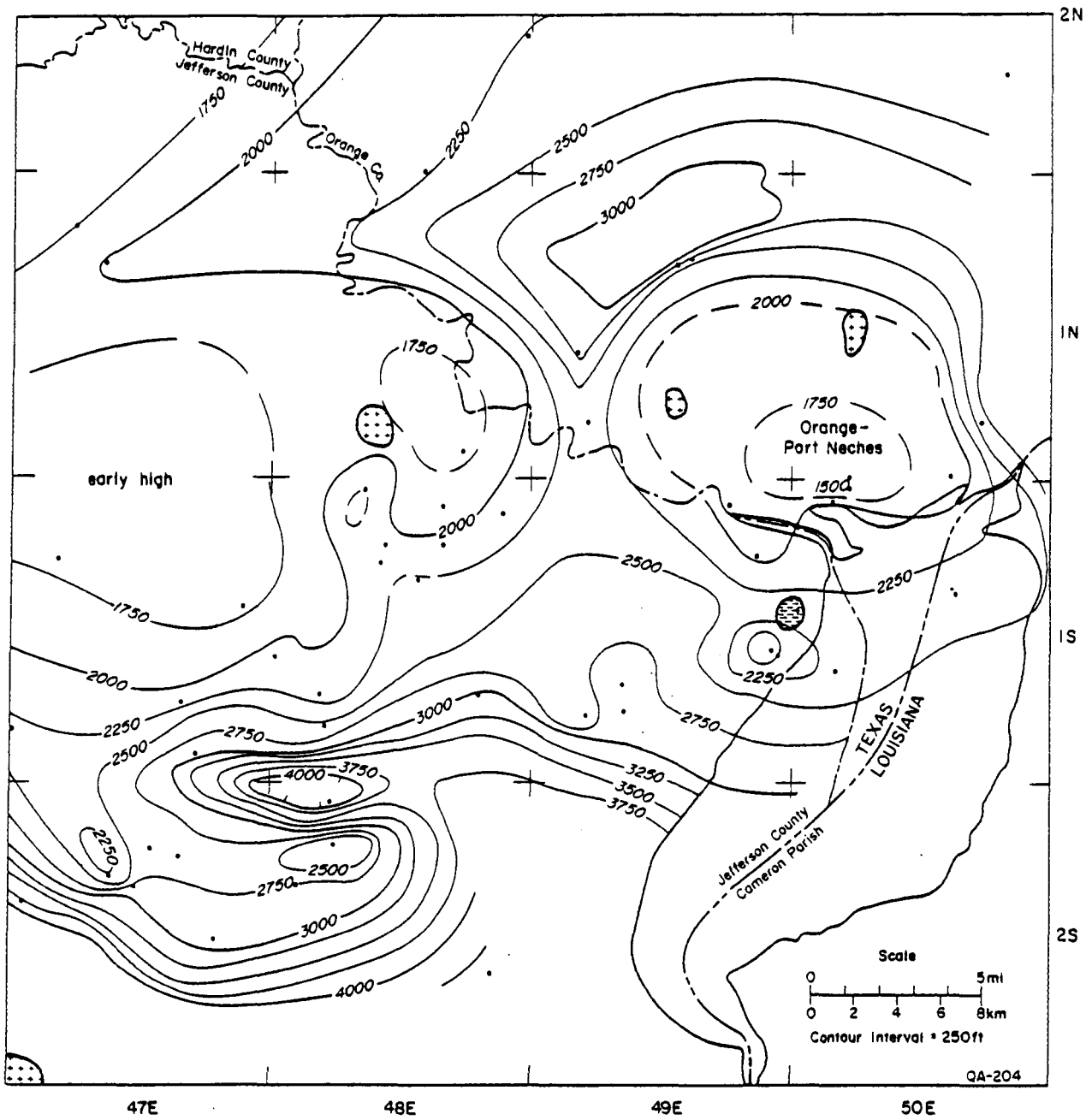


Figure I-33. Isopach map of the A3-Vicksburg interval, Port Arthur area, showing broad uplifts and depressions during lower Frio deposition.

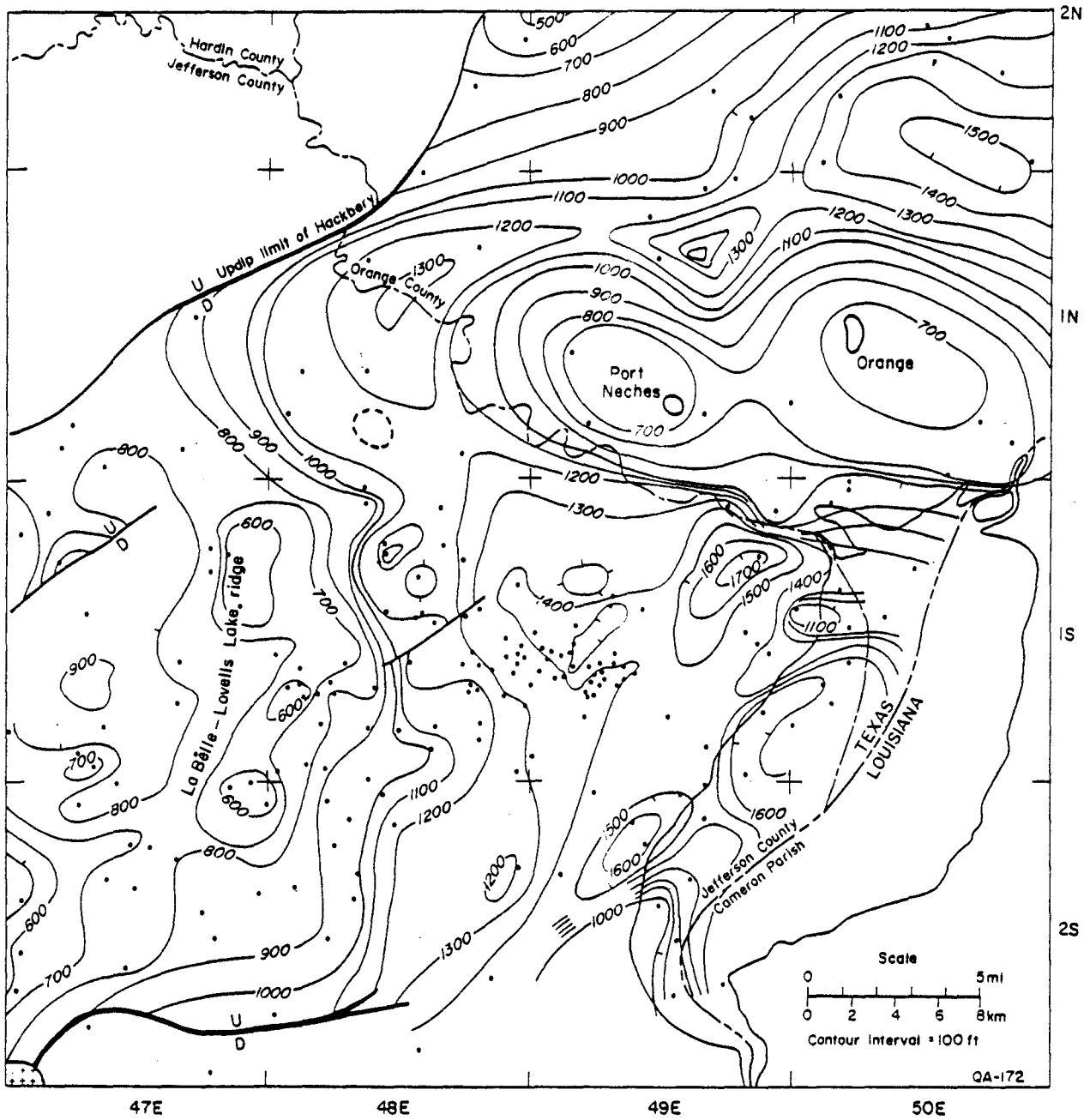


Figure I-34. Isopach map of the A3-A4 interval, Port Arthur area, showing salt uplifts and major growth faults influencing Hackberry deposition.

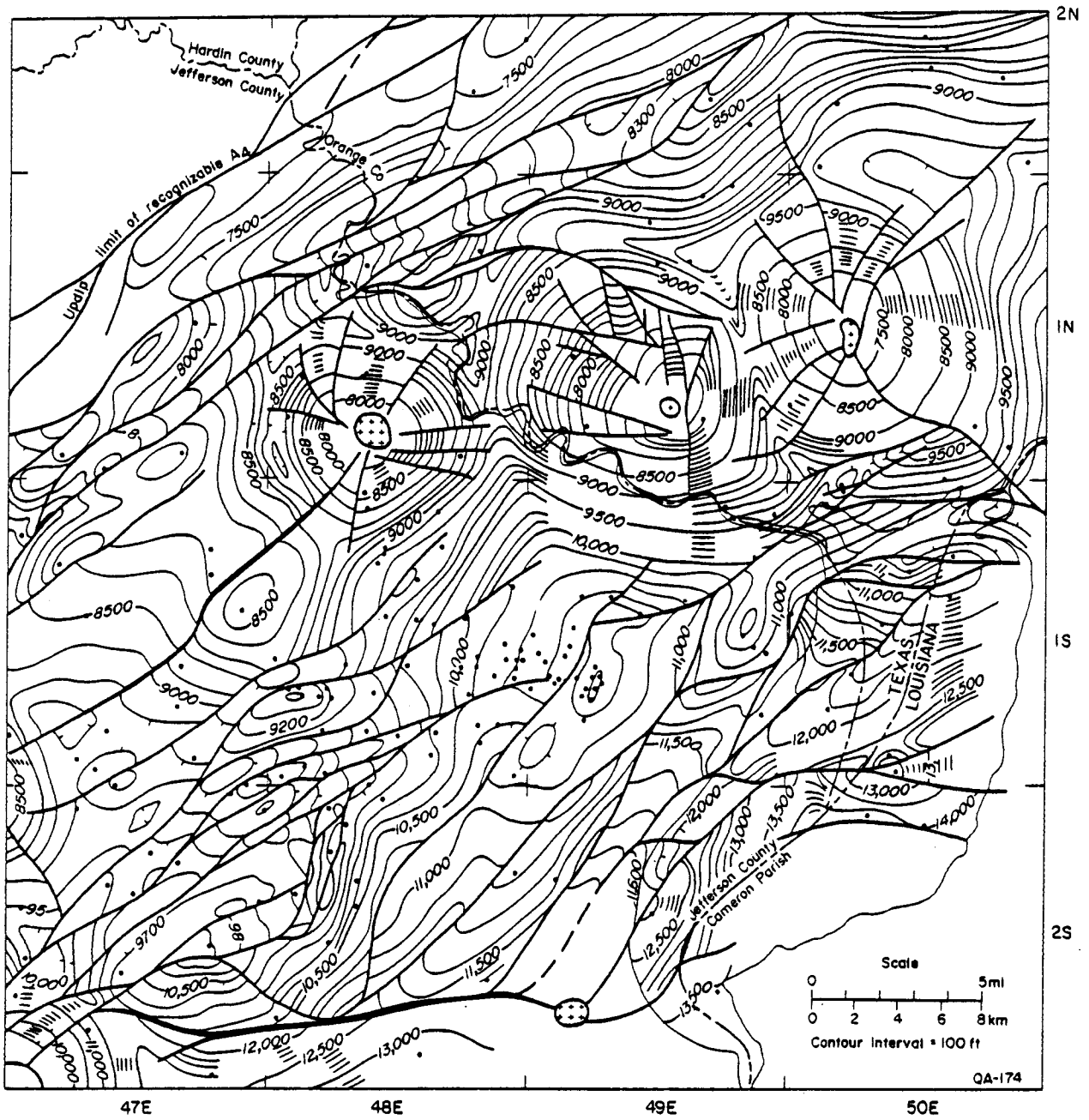


Figure I-35. Structure map contoured on A4 horizon, Port Arthur area.

account for the Hackberry. If, however, the lower Frio was deposited in deep water, the Hackberry may be related to either deltaic progradation to the west or eustatic sea-level fluctuations (which have been proposed to explain Pleistocene channels in offshore Louisiana by Coleman and Prior, 1982).

An isopach of the A3-A4 interval (fig. I-34) further reveals the structural elements active during Hackberry time. The large uplift in Orange County has now split into two broad uplifts centered on Orange and Port Neches domes. The previous uplift in Jefferson County appears as a north-south elongate high extending from Lovells Lake south to La Belle field (field locations on fig. I-36). An uplift around the McFaddin Ranch dome to the south is possible. The eastern margin of the north-south high is quite sharp and may represent a fault in some areas; however, no fault has been demonstrated from the structure data on A4 (fig. I-35). The courses of the sand-filled Hackberry channels cut across all the highs. Activity on the many small growth faults indicated in figure I-36 is likely to have occurred throughout Frio time; however, displacements are small (fig. I-31).

After the area had been infilled to sea level by Hackberry shale, the barrier-bar system of the upper Frio prograded to the shelf margin. Structures active during this time are shown on an isopach map of the A1-A3 interval (fig. I-37); A1 is used rather than A2 to increase the accuracy of the measurement. During this time, the Orange and Port Neches uplifts were less broad than before; deeper level diapirism likely occurred. The north-south high area extended northeastward past the present-day Spindletop dome; the southern part of the high area was complicated by growth faults. A rapidly thickening section in the southern and southeastern margins of the area, in part occurring along large growth faults through Big Hill and McFaddin Ranch domes, probably marks the upper Frio and Anahuac shelf margin.

The structural elements active during Anahuac time also are shown on an isolith map of the Heterostegina limestone (fig. I-38). This limestone is known to form reefs around several salt domes and salt uplifts in southeast Texas; it probably accumulated wherever uplifts raised the seafloor above the muddy bottom. In the Port Arthur area, the limestone forms an east-west band across the area lying between the updip margin of the Anahuac and the downdip limit of environments favorable for carbonate deposition. Within this band, three pinnacle reef accumulations (more than 100 ft thick) occur; these are at Hildebrandt Bayou, Port Neches, and Orange fields. A similar thick occurs around Fannett dome immediately west of the study area. These reefs correspond to the Orange and Port Neches salt uplifts and to the Lovells Lake - La Belle salt-cored ridge. No thick limestone accumulation is known to occur at Spindletop dome; the maximum true limestone thicknesses there range only up to 80 to 85 ft. The isolith

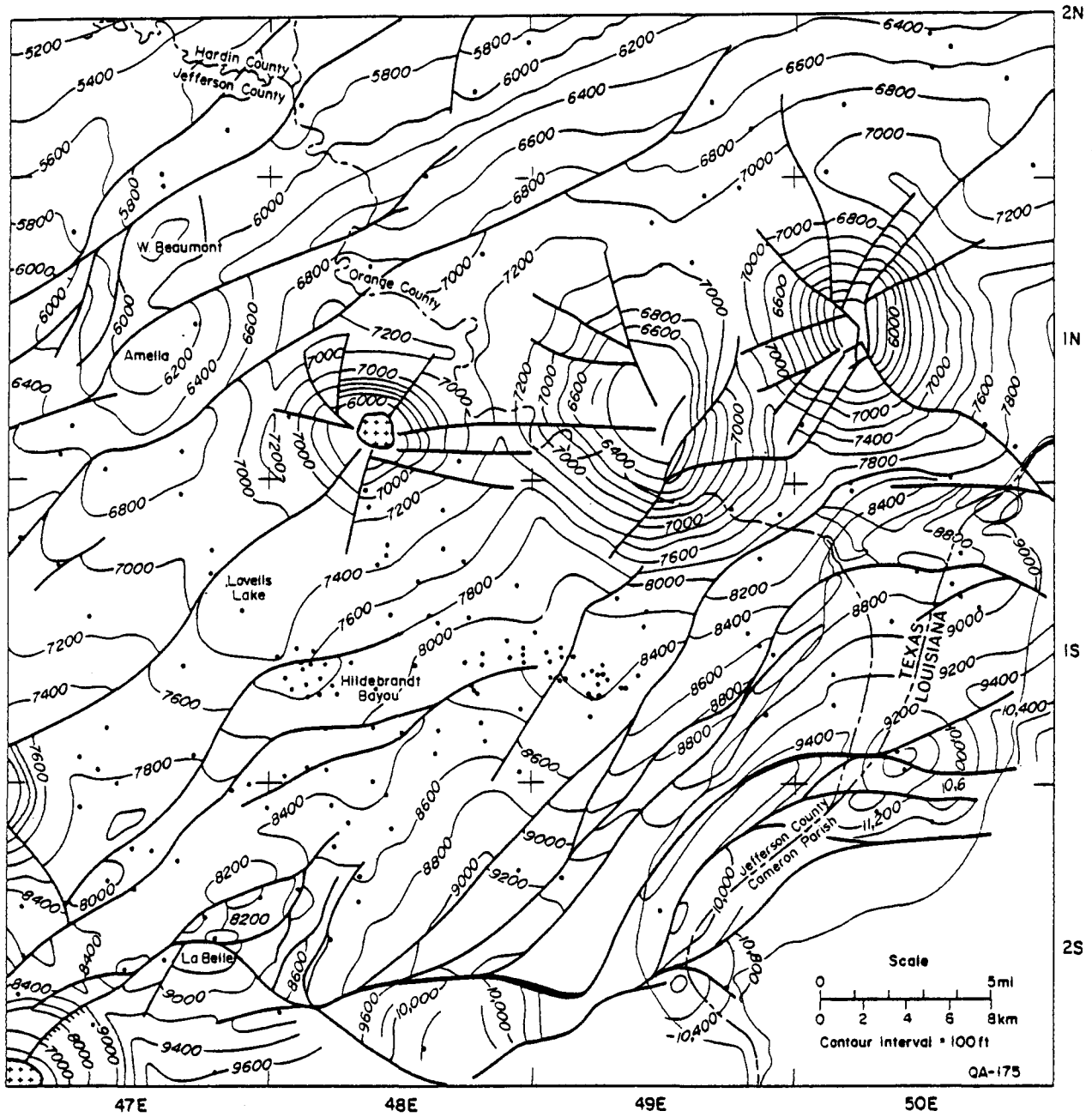


Figure I-36. Structure map contoured on A2 horizon, Port Arthur area. Structures producing oil from strata near A2 are named.

contours suggest an atoll shape to the limestone, which is centered immediately north of Hildebrandt Bayou field.

Post-Anahuac activity is best shown on the A2 structure map (fig. I-36). Uplift of the Orange and Port Neches domes continued, along with uplift of Big Hill, McFaddin Ranch, and Fannett domes. Spindletop dome grew from the earlier salt-cored high, which retained only a very subdued expression. Continued activity on the Hartburg faults and on all faults in the area created the rollover anticlines that localize many of the important oil fields in the area (Amelia, West Beaumont, Lovells Lake, and La Belle fields). The Miocene shelf margin prograded seaward beyond the southern boundary of the study area. A south-southeast regional dip was developed on all horizons.

Several significant features can be summarized. Salt and shale tectonism have been active together for a long period of time in this area. Growth faulting is generally of very low displacement; however, abundant and long-lived growth faults at the shelf margin may have experienced substantial displacement in some periods. Salt uplifts of large lateral extent existed from Vicksburg to Miocene time, becoming gradually more restricted and more diapiric in nature. Spindletop, a prolific oil-producing dome, formed very late in the tectonic sequence, having risen from an older salt-cored ridge. Port Neches and Orange domes, which show steady development through time, are important oil-producing domes but not as significant as Spindletop. The oil at Spindletop may have resulted from draining of part of the early-formed salt uplift during Miocene time. Although its nature remains elusive, the Hackberry deep-water erosional and depositional episode is superimposed on the coexisting salt and shale tectonics.

#### Structural Constraints on Geopressured Reservoirs at Depth

Currently available data are not adequate to discuss the structures that exist at depth within the Vicksburg and deeper strata. The shallower structures indicate, however, that strike-elongate, rather narrow fault compartments are to be expected, variably modified by salt withdrawal (fig. I-35). These compartments are similar in shape to those of the Wilcox fault trend in the Cuero area (Winker and others, 1981) and are unlikely to yield large reservoir volumes when they crosscut dip-oriented sand bodies such as the Hackberry sands. Some of the higher Hackberry sands, however, have more of a blanket geometry (for example, the C sand at Port Arthur; Gregory and others, 1983) and might have a more substantial aquifer volume. There is no good evidence for deep, unfaulted salt-withdrawal basins in the area; indication of domes in the northeastern part of the study area results from lack of information.

The study area lies in a sand-poor region of the Oligocene continental margin. Sand appears to have been supplied either by longshore transport from the Houston delta to the west

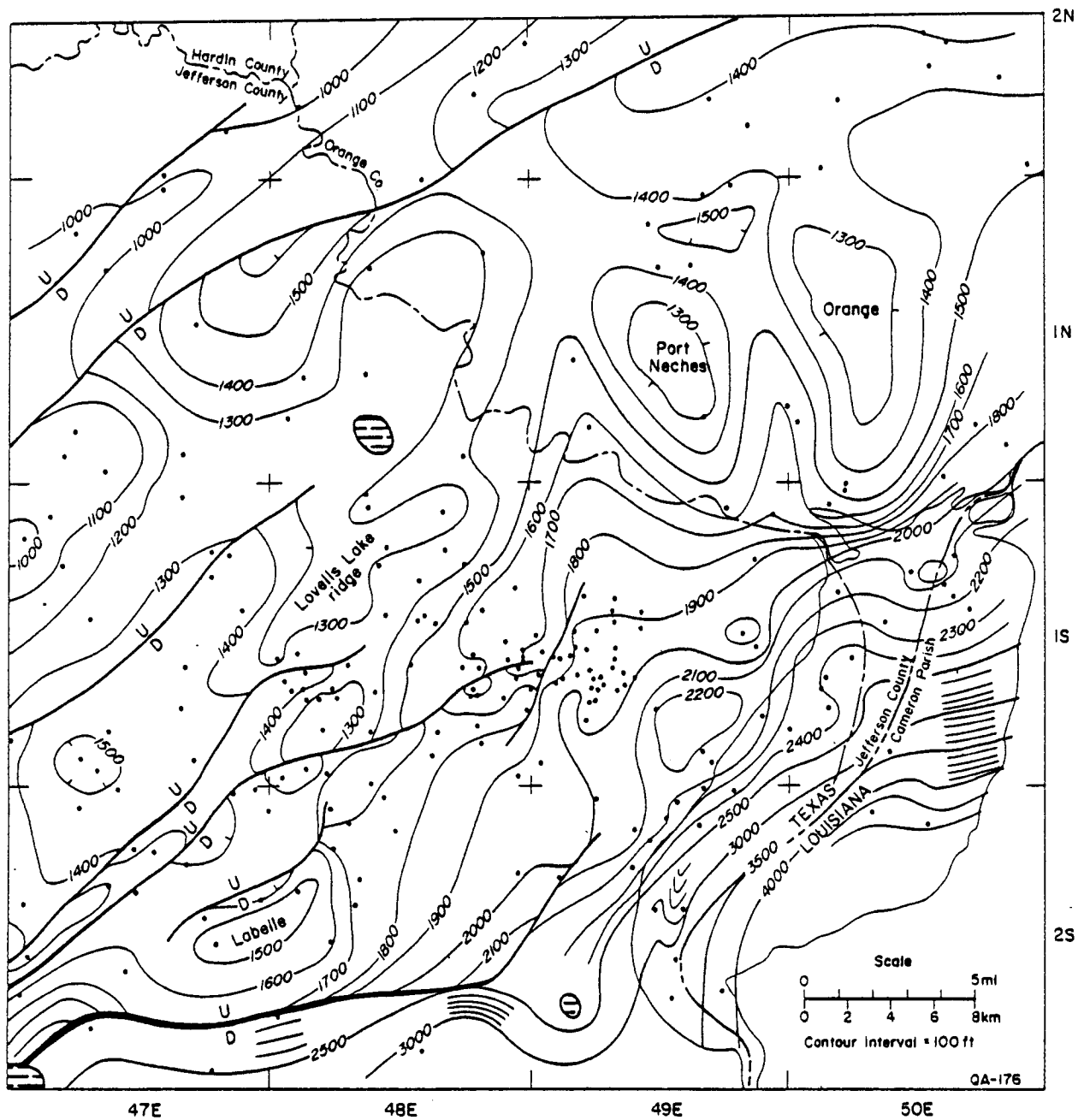


Figure I-37. Isopach map of the A1-A3 interval, Port Arthur area, showing salt uplifts and significant growth faults influencing upper Frio and Anahuac deposition. More faults were active than are shown.

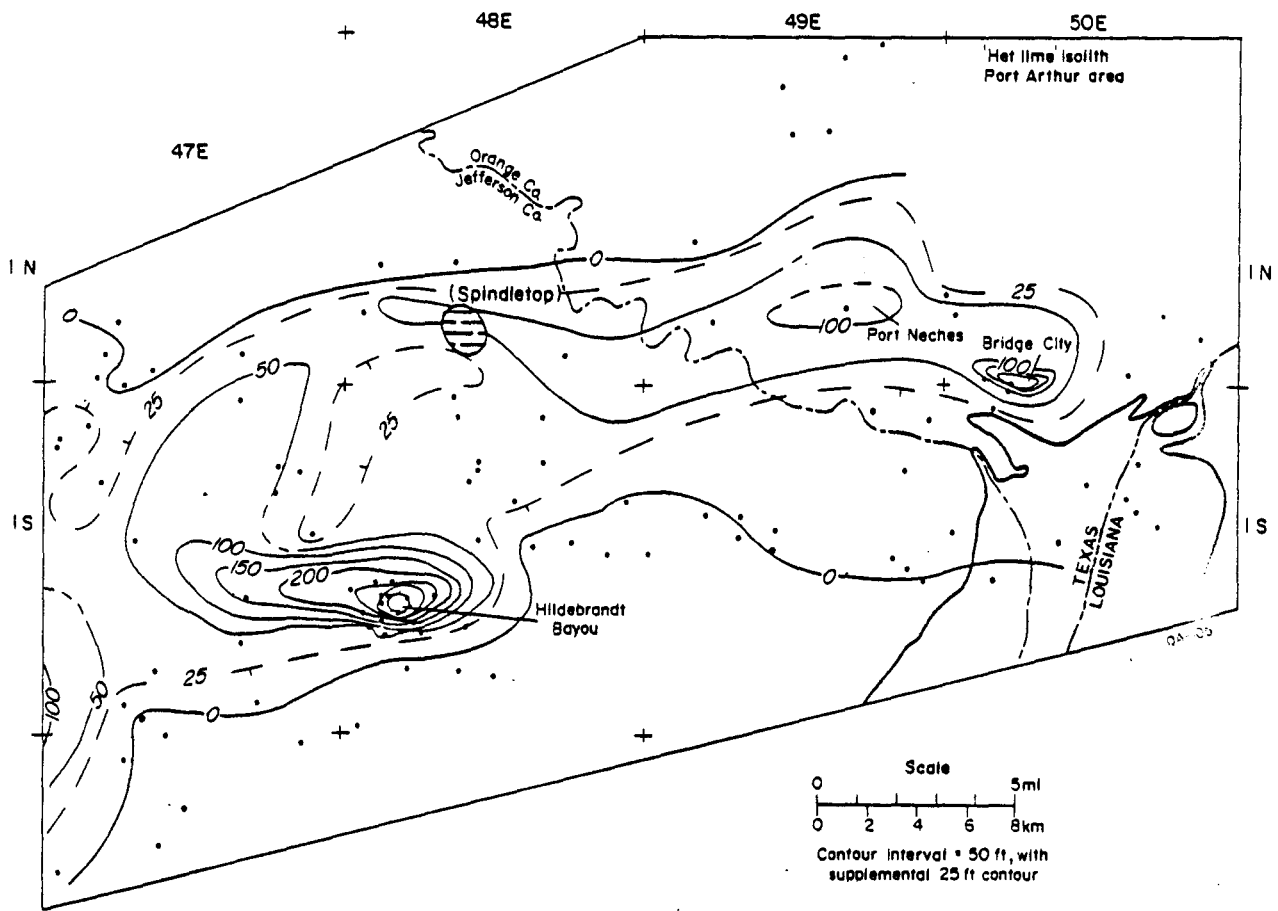


Figure I-38. Isolith map of the *Heterostegina* limestone (middle Anahuac). Within a broad belt of thin limestone, pinnacle reefs formed at Hildebrandt Bayou, Orange, and Port Neches uplifts. Reefy limestones mark topographic highs during Anahuac transgression.

or by unknown sources in Louisiana. Progradation of the shelf margin seems to have been accomplished by muddy sediments rather than by sandstones; little evidence of expansion of the Frio sandstones across growth faults can be found. A similar mud-dominated margin may have existed in the Yegua Formation in northwestern Jefferson County near the Lear No. 1 Koelemay well of opportunity (Morton and others, 1982). This margin is characterized by closely spaced growth faults of low intensity and long life and generally subdued structures. Geopressed geothermal prospects are poor in these areas.

## FRIO STRUCTURAL STYLES AND DEEP GEOTHERMAL POTENTIAL

With the completion of this report, the Bureau has studied five areas along the Frio growth-fault trend of the Texas Gulf Coast to determine their structural history and geothermal potential. From south to north, they are Sarita, Corpus Christi, Blessing, Pleasant Bayou, and Port Arthur. (Studies of Blessing and Pleasant Bayou were reported in Winker and others, 1981.) In addition, the far South Texas Frio trend in the McAllen-Pharr area has been studied by J. H. Han (section II, this report) under the salinity part of this contract. The even spacing of these study areas, which sample most of the major downdip depositional systems of the Frio Formation (fig. I-1), allows us to make significant generalizations about the entire Frio growth-fault trend.

### Comparison of Structural Styles of Five Frio Study Areas

A distinction has been made for many years between the part of the growth-fault trend east and northeast of central Matagorda County and the part to the southwest. The eastern part is dominated by conspicuous salt tectonic features: salt domes, salt-cored anticlines, and salt-withdrawal basins. In contrast, the area southwest of Matagorda County is marked by long belts of growth faults, shale diapirs, and shale ridges, which are manifestations of shale tectonics. In the past, these areas have been considered separately, and separate processes have been attributed to each. However, the studies reported in Winker and others (1981) at Pleasant Bayou indicate that at least part of what has been called the salt tectonic area had a shale tectonic phase shortly after shelf-margin progradation through the area. This shale phase was then overprinted by salt tectonism; the phase can only be recognized by careful seismic and well log interpretation, coupled with sequential isopach mapping. The first distinction to be made among the Frio study areas is between those areas in which shale tectonics and growth faulting have been overprinted by salt tectonism (Pleasant Bayou and Port Arthur) and those in which they have not (Blessing, Corpus Christi, and Sarita).

A second variation among study areas is the extent and timing of progradation of the shelf margin. In the southern study areas (Sarita and Corpus Christi), progradation began with the basal Frio and continued throughout most of Frio time. The shelf margin prograded steadily basinward and the structural styles, especially at Corpus Christi, migrated with the margin. In the Blessing study area, no significant progradation could be seen. At Blessing and at Pleasant Bayou, the sand-bearing lower Frio prograded basinward only during lower Frio time; it then cycled with the deposition of individual deltas and delta lobes but had a net slow retreat landward (Winker and others, 1981). In the Port Arthur area, the strike-fed Frio sand system prograded basinward during middle to upper Frio time over a previously established mud-dominated margin and muddy slope, which had foundered and received the deep-water sediments of the Hackberry member.

A third variation among study areas is the depositional systems in which they developed during Frio time. The Sarita area lay within the Norias delta system, Corpus Christi and Blessing lay within the Greta/Carancahua barrier-bar/strandplain system, Pleasant Bayou lay within the Houston delta system, and Port Arthur lay within the Buna strandplain and the Hackberry submarine canyon-fan system.

Because of these variations, each study area has a unique structural history. Shale tectonics at Sarita formed one or more shale ridges, one of which appears to have localized a major low-angle growth fault trapping a wedge of deltaic sediments at considerable depth. At Corpus Christi, shale tectonics resulted in large growth faults, shale-cored domal anticlines, and shale-withdrawal basins in deep structural levels, which become progressively younger basinward. Higher levels contain the more typical development of dip reversal and rollover anticline. These higher levels also typify known development at Blessing; shallow-level rollover anticlines pass downward into dip reversals and into major growth faults. Shale diapirs in the lower Frio are known to be not far to the southwest (Bishop, 1977). Lack of progradation in the Blessing area appears to have caused a narrow growth-fault zone; major Frio-age growth-fault activity was restricted to a few major faults. In the Pleasant Bayou area, a major early growth fault caused dip reversal and deposition of thick sandstone units against the fault (Winker and others, 1981); this development is similar to that at Blessing. Salt tectonics prevailed in the upper Frio and Anahuac, causing diapiric intrusion of Danbury Dome and development of a major salt-withdrawal basin. An early stage of salt movement has been interpreted to have formed the Chocolate Bayou domal anticline as a turtle structure; this movement may have taken place while the area was basinward of the shelf margin (Winker and others, 1981). In the Port Arthur area, low-displacement, long-lived faults defining narrow, strike-elongate fault compartments were formed along the mud-dominated margin. Salt tectonism was active

concurrently with growth faulting and may either have been localized by or have localized some growth faults. No progradation of structural styles can be inferred, except that general post-Yegua (Vicksburg?) sand-poor progradation built up the shelf margin. The mechanism of foundering of the area in the middle Frio is still uncertain, but it may involve megaslumping and sea-level fall.

These contrasts among study areas can be considered in a general historical framework of the Texas Gulf Coast. Frio sedimentation occurred over a preexisting clastic shelf margin established in Vicksburg time. To the south, a deltaic system in the Vicksburg had built a large platform basinward (Loucks, 1979); to the north, a mud-dominated margin persisted until the East Texas Vicksburg delta (Gregory, 1966), which prograded the shelf margin only slightly, was reached. A mud-dominated margin may also have been produced in overlying slope sediments of far southeast Texas. Landward of the entire Vicksburg progradational package is the Vicksburg Fault Zone, a major structural feature characterized by low-angle listric growth faulting, great expansion of the Vicksburg sediments, and a modified décollement surface in lower Vicksburg or Jackson (Eocene) geopressed slope shales.

In early Frio time, two deltaic systems prograded seaward over the Vicksburg shelf margin. The Norias delta in South Texas built out over one or more linear shale ridges, and at least one low-angle growth fault was formed. Initial loading of strandplain sediments marginal to the Norias delta caused intense, irregular shale tectonic activity in the Corpus Christi area; the activity may have extended farther north and east. The Houston delta in East Texas prograded to nearly its maximum extent in early Frio time, loading the Vicksburg continental slope and causing large-scale growth faulting and possibly other shale tectonism. The margin was passive in far southeast Texas, having thin mudstone accumulation. Most Frio growth faults are moderate-angle listric normal faults; some may merge downward with the Vicksburg.

In middle Frio time, the Norias delta system and its flanking strandplain system continued to prograde basinward. The early shale tectonic activity was subdued by burial with delta-plain and fluvial sediments, and new bands of intense growth faulting were established farther basinward. The barrier-bar system in Central Texas was virtually static, so that the early-formed growth faults were continually reactivated. A similar situation existed for the Houston delta system, although limited progradation may have occurred in some areas. The loading by the early Frio shelf margin of salt masses that previously had lain on the continental slope resulted in the beginning of salt remobilization and diapirism. In southeast Texas, salt continued slope-style movement in broad uplifts as a strandplain system began to prograde across the area. A large segment of the old shelf margin foundered, was eroded by submarine canyon cutting, and was filled with deep-water sandstone and shale.

In late Frio time, the Norias delta and its adjoining strandplain system reached their maximum basinward extent and began to retreat landward. The growth faulting associated with this maximum extent is largely offshore but, by analogy with Blessing and Pleasant Bayou areas, may represent a longer lived set of faults than the earlier South Texas belts. The Houston delta system and the strandplain to the south continued a slow retreat, and the shelf margin gradually stabilized. Salt tectonism became steadily more intense, and the present-day pattern of salt domes and salt-withdrawal basins began taking shape. The strandplain system in southeast Texas, however, continued to prograde over the earlier deep-water strata until the Anahuac transgression ended Frio deposition.

In Anahuac time, the Frio progradational package was transgressed by shallow marine strata. In South Texas, this progradation was limited and late; not all of the Frio growth-fault trend was transgressed. In East Texas, the transgression began earlier as the continuation of the overall Frio trend and progressed farther landward. Limestones accumulated in high grounds on the transgressed shelf because of either large-scale salt diapirism or high-standing salt anticlines. Miocene depositional systems then prograded over the submerged shelf and began the creation of a new prograding shelf margin, which now lies offshore.

#### Structural Constraints on Geopressured Reservoirs at Depth

The studies of the Blessing and Pleasant Bayou areas did not consider fault-compartment sizes and possible geopressured reservoirs at depth because they were concerned with known drilled-out geopressured reservoirs. Therefore, brief discussion of these areas is in order. The Blessing prospect lies within a fault compartment showing dip reversal of strata between rather widely spaced growth faults. Because of the strike-oriented geometry of the depositional system, reservoir volumes within this compartment were sufficient to produce a favorable geothermal prospect. Similar reservoirs could occur at depth at many points along the Greta/Carancahua barrier/strandplain system where similar conditions exist. The presence of sand is a major limiting factor. At the Pleasant Bayou test well site, the prospect was formed by a combination of an early-formed, very large dip-reversed fault compartment between growth faults and a late-formed salt-withdrawal basin. The combination of these two types of structures in such favorable areal extent may be unique to the Pleasant Bayou area. In neither Blessing nor Pleasant Bayou can a significant increase in faulting with depth be detected; however, these study areas were rather small, and sample size may not have been sufficient to allow definitive conclusions.

Production of geopressured geothermal energy requires a producing aquifer of sufficient volume to maintain the system; therefore, it is desirable that areal extent of the aquifer be as

large as possible. This, in turn, depends on the shape and orientation of the depositional sand body, the size, shape, and orientation of the fault compartment, and the sealing or nonsealing character of the faults. By applying this general outline to the study areas described above, we can compile a short list of optimum structural situations for finding large reservoirs.

Salt-withdrawal basins have large areas of nominally continuous strata, which have the added advantage of being, by definition, off-structure. Geothermal production, therefore, is unlikely to compete with conventional hydrocarbon production. However, as seen at Pleasant Bayou, a salt-withdrawal basin of simple contour may mask the deep structure formed earlier. Hence, prospects in these basins must be approached with care. Furthermore, salt-withdrawal basins are rarely drilled by exploration companies so control is sparse. Early-formed withdrawal basins may evert to turtle structures because of continued salt mobilization. These large unfaulted domal structures would be ideal for geothermal production except that they are also ideal for conventional hydrocarbon production.

In areas of intense shale tectonism such as Corpus Christi, shale-withdrawal basins may be created that are similar to but smaller than the salt-withdrawal basins of the upper coast. Like the salt basins, these tend to be equidimensional and to contain a fairly large area of unfaulted strata. Medium-sized geothermal prospects, off-structure to most hydrocarbon activity, could be found here, given appropriate reservoir quality.

Fault blocks between widely spaced growth faults offer the most opportunities for finding large prospects. Both Blessing and Pleasant Bayou prospects are of this type. The Frio fault systems tend to be widely spaced except in far southeast Texas; hence, more area is available between them than is between systems in the Wilcox growth-fault trend. Fault compartments of this shape are most efficiently utilized by strike-oriented sand bodies, such as those of the Greta/Carancahua barrier/strandplain system; however, deltaic systems having an unusually broad fault compartment or coalescing sand bodies, such as at Pleasant Bayou (Tyler and Han, 1982), also may form good prospects. The least faulted compartments may occur between the shale diapiric ridges that back some growth faults; the areas abutting or lying atop the ridges may tend to be highly faulted, as at Sarita and Corpus Christi. One disadvantage of this type of compartment is that the structurally high part of the reservoir is prospective for conventional hydrocarbons; however, as at Blessing, suitable reservoirs may be found.

#### OUTLOOK: GEOTHERMAL PROSPECTS IN THE FRIO TREND IN THE NEXT DECADE

On the basis of the foregoing analysis, we may hazard a guess of where large fault compartments having sand suitable for geothermal production might be found in the next

decade. The great unknown is the downsection and downdip distribution of sand. Sand may be found anomalously far downdip or downsection in pods displaced by growth faults, such as at Sarita, or by slumping. Exploration in many parts of the Frio trend has reached close to the downsection limit of sand, but some areas remain to be explored. The occurrence of downsection pods of sand is not yet very predictable.

Large prospective sand bodies are unlikely to be found in far southeast Texas owing to the sand-poor section and the closely spaced faults. All other parts of the Frio trend have some prospectivity. Prospects similar to those at Blessing probably occur intermittently along the Greta/Carancahua barrier system; many of these, however, will produce gas. Point Comfort is one of these prospective areas. Some prospective areas may exist in the Houston delta system, although they are unlikely to be nearly as large or attractive as the Pleasant Bayou prospect. Unraveling fault geometries in this area is an arduous undertaking, and future discoveries of large reservoirs may be slow. Prospective areas probably exist in shale-withdrawal basins in the Central and South Texas area, although the one basin tested has very low permeability. Prospective sections between growth faults within the delta front of the Norias delta may also be abundant; however, both the data and the reservoir quality are poor. If good-quality sandstones could be found, the Norias delta would become very attractive.

In summary, future geothermal prospects in the Frio trend of the Texas Gulf Coast are most likely to be in the strike-oriented systems of the central coast and the Houston delta system of the upper coast. It is unlikely that any of these will surpass the attractiveness of Pleasant Bayou, but several may equal that of Blessing.

#### ACKNOWLEDGMENTS

Thanks are extended to Teledyne Exploration, Mobil Producing, Texas and New Mexico, Kilroy Company of Texas, and Exxon Company, U.S.A., for release of seismic data essential to this study. M. B. Edwards, C. Winker, and W. E. Galloway provided important insights into Frio stratigraphy and structure. This research was funded in part by the U.S. Department of Energy, Division of Geothermal Energy, under Contract No. DE-AC08-79ET27111. The seismic data on the Port Arthur area were acquired under Gas Research Institute Contract No. 5080-321-0398. This report was typed by Dorothy C. Johnson under the direction of Lucille C. Harrell. Illustrations were drafted by John T. Ames, Mark T. Bentley, Jamie McClelland, and Richard M. Platt.

## REFERENCES

- Bebout, D. G., Loucks, R. G., and Gregory, A. R., 1978, Frio sandstone reservoirs in the deep subsurface along the Texas Gulf Coast, their potential for the production of geopressed geothermal energy: The University of Texas at Austin, Bureau of Economic Geology Report of Investigations No. 91, 92 p.
- Bebout, D. G., Weise, B. R., Gregory, A. R., and Edwards, M. B., 1982, Wilcox sandstone reservoirs in the deep subsurface along the Texas Gulf Coast, their potential for the production of geopressed geothermal energy: The University of Texas at Austin, Bureau of Economic Geology Report of Investigations No. 117, 125 p.
- Berg, R. R., and Powers, B. K., 1980, Morphology of turbidite-channel reservoirs, lower Hackberry (Oligocene), southeast Texas: Gulf Coast Association of Geological Societies Transactions, v. 30, p. 41-48.
- Bishop, R. S., 1977, Shale diapir emplacement in South Texas: Laward and Sherriff examples: Gulf Coast Association of Geological Societies Transactions, v. 27, p. 20-31.
- Bornhauser, M., 1960, Depositional and structural history of the Northwest Hartburg field, Newton County, Texas: American Association of Petroleum Geologists Bulletin, v. 44, no. 4, p. 458-470.
- Boyd, D. R., and Dyer, B. F., 1964, Frio barrier bar system of South Texas: Gulf Coast Association of Geological Societies Transactions, v. 14, p. 309-322.
- Bruce, C. H., 1972, Pressured shale and related sediment deformation: a mechanism for development of regional contemporaneous faults: Gulf Coast Association of Geological Societies Transactions, v. 22, p. 23-29.
- Coleman, J. M., and Prior, D. B., 1982, Formation of the Mississippi Canyon (abs.): Gulf Coast Association of Geological Societies Transactions, v. 32, p. 519.
- Ewing, T. E., 1982, Décollement zones for Texas Gulf Coast growth fault trends (abs.): Geological Society of America Abstracts with Programs, v. 14, no. 7, p. 486.
- Ewing, T. E., and Reed, R. S., in preparation, Hackberry oil and gas fields in southeast Texas: channel/fan depositional systems and structural controls (abs.): American Association of Petroleum Geologists Bulletin.
- Galloway, W. E., Hobday, D. K., and Magara, K., 1982, Frio Formation of the Texas Gulf Coastal Plain: depositional systems, structural framework and hydrocarbon distribution: American Association of Petroleum Geologists Bulletin, v. 66, no. 6, p. 649-688.
- Gernant, R. E., and Kesling, R. V., 1966, Foraminiferal paleoecology and paleoenvironmental reconstruction of the Oligocene middle Frio in Chambers County, Texas: Gulf Coast Association of Geological Societies Transactions, v. 16, p. 131-158.
- Gregory, A. R., Lin, Z. S., Reed, R. S., Morton, R. A., and Ewing, T. E., 1983, Exploration and production program for locating and producing prospective aquifers containing solution gas and free gas--Texas Gulf Coast: The University of Texas at Austin, Bureau of Economic Geology, final report to Gas Research Institute, Contract No. 5080-321-0398.

## Section II

### VARIATIONS IN CHEMICAL COMPOSITIONS OF TERTIARY FORMATION WATERS, TEXAS GULF COAST

*By R. A. Morton, J. H. Han, and J. S. Posey*

*Assisted by R. L. Kugler, B. R. Bracken, and J. F. O'Connell*

#### ABSTRACT

Sandstone aquifers deeply buried beneath the Texas Gulf Coastal Plain contain waters having concentrations of total dissolved solids that range from about 10,000 to more than 250,000 mg/L. The salinities of the waters, which are primarily from the Frio and Vicksburg Formations, vary systematically both at depth within a limited field area and laterally between subregional areas. The depth-dependent changes follow two trends. In most fields, salinities (1) decrease with depth above the top of geopressure (0.5 psi/ft), (2) increase with depth if the zone of intermediate pressure gradients (0.5 to 0.75 psi/ft) is more than 1,500 ft thick, and (3) decrease with depth at extremely high pressure gradients (>0.75 psi/ft). In contrast, if the zone of intermediate pressure gradients is thin (<1,500 ft), then salinities in the geopressured zone continue to decrease with depth but at a lower rate than in the hydro pressured zone.

Four hydrochemical subregions are recognized on the basis of composition and concentration of the brines. Highly concentrated sodium-chloride waters are produced from upper coast fields within the salt dome province of the Houston Embayment, whereas sodium-chloride waters of low to intermediate concentrations are produced along the structural platform of the middle coast. A unique area of highly concentrated calcium-sodium-chloride waters in Kenedy and northern Hidalgo Counties is separated by abrupt boundaries from the middle coast waters to the north and by an area of low-salinity sodium-chloride waters to the south in southern Hidalgo County.

The abrupt boundaries apparently reflect deep-seated structural discontinuities that regionally control fluid movement. The vertical patterns of dilution and concentration of brines with respect to seawater are also controlled by fluid movement. The concentrated brines contained in geopressured sandstones apparently originated deeper in the basin, where they migrated vertically along major faults and laterally within the intervals of intermediate to high sandstone percent. The intrusion of these brines into sediments normally containing water

- Gregory, J. E., 1966, A lower Oligocene delta in the subsurface of southeastern Texas: Gulf Coast Association of Geological Societies Transactions, v. 16, p. 241-277.
- Han, J. H., 1982, Genetic stratigraphy and associated growth structures of the Vicksburg Formation, South Texas: The University of Texas at Austin, Ph.D. dissertation, 162 p.
- Holcomb, C. W., 1964, Frio Formation of southern Texas: Gulf Coast Association of Geological Societies Transactions, v. 14, p. 23-33.
- Loucks, R. G., 1979, Sandstone distribution and potential for geopressed geothermal energy production in the Vicksburg Formation along the Texas Gulf Coast: The University of Texas at Austin, Bureau of Economic Geology Geological Circular 79-4, 32 p.
- Loucks, R. G., Richmann, D. L., and Milliken, K. L., 1981, Factors controlling reservoir quality in Tertiary sandstones and their significance to geopressed geothermal production: The University of Texas at Austin, Bureau of Economic Geology Report of Investigations No. 111, 41 p.
- Morton, R. A., Ewing, T. E., and Tyler, N., 1982, Continuity and internal properties of Gulf Coast sandstones and their implications for geopressed energy development: The University of Texas at Austin, Bureau of Economic Geology, annual report to U. S. Department of Energy, Contract No. DE-AC08-79ET27111 (-4), 142 p.
- Paine, W. R., 1968, Stratigraphy and sedimentation of subsurface Hackberry wedge and associated beds of southwestern Louisiana: American Association of Petroleum Geologists Bulletin, v. 52, no. 2, p. 322-342.
- Tyler, N. and Han, J. H., 1982, Elements of high constructive deltaic sedimentation, lower Frio Formation, Brazoria County, Texas: Gulf Coast Association of Geological Societies Transactions, v. 32, p. 527-540.
- Weise, B. R., Edwards, M. B., Gregory, A. R., Hamlin, H. S., Jirik, L. A., and Morton, R. A., 1981a, Geologic studies of geopressed and hydropressed zones in Texas: test-well site selection: The University of Texas at Austin, Bureau of Economic Geology, final report to Gas Research Institute, Contract No. 5011-321-0125, 308 p.
- Weise, B. R., Jirik, L. A., Hamlin, H. S., Hallam, S. L., Edwards, M. B., Schatzinger, R. A., Tyler, N., and Morton, R. A., 1981b, Geologic studies of geopressed and hydropressed zones in Texas: supplementary tasks: The University of Texas, Bureau of Economic Geology, final report to Gas Research Institute, continuance of Contract No. 5011-321-0125, 120 p.
- Winker, C. D., Morton, R. A., Ewing, T. E., and Garcia, D. D., 1981, Depositional setting, structural style, and sandstone distribution in three geopressed geothermal areas, Texas Gulf Coast: The University of Texas at Austin, Bureau of Economic Geology, annual report to U. S. Department of Energy, Contract No. DE-AC08-79ET27111 (-3), 132 p.

diluted during compaction and clay mineral diagenesis explains the depth-dependent changes in formation water salinity.

## INTRODUCTION

During 1981-82, water samples were collected from wells producing from the Frio and Vicksburg Formations in South Texas. Chemical analyses of waters from geopressed sandstones in five South Texas fields (McAllen Ranch, McAllen, Pharr, La Blanca, and South Weslaco; fig. II-1) completed the regional data base for the Texas Gulf Coast. Field techniques used to obtain the samples and laboratory techniques used to analyze the waters have been previously described (Morton and others, 1981).

In addition to the water sample analyses by the Bureau of Economic Geology (appendix II-A), chemical analyses were obtained from operators of many fields throughout the Frio trend. These analyses, which were screened for reliability, substantially increased the distribution and number of data points used to determine chemical composition and concentrations of total dissolved solids in deep geopressed sandstones.

## WATER CHEMISTRY OF INDIVIDUAL FIELDS

The effects of lithologic changes, local structure, pressure regimes, and thermal gradients on water chemistry are best illustrated by plots of ion concentrations and ionic ratios for individual fields. These fields were selected because accurate analyses are available for depth intervals of several thousand feet and the vertical distribution of data allowed delineation of depth-dependent trends. Moreover, the waters produced from these fields and the changes that occur at depth are representative of other fields in the same general area.

### Willow Slough Field

In the Willow Slough field (fig. II-1), water is produced in conjunction with hydrocarbons from middle and lower Frio sandstones (fig. II-2). The local structure is a fault-bounded anticline that extends about 4 mi along strike (northeast, southwest) and 2 mi in the dip direction. Several strike-aligned growth faults cross the field and displace the Frio sediments from 200 to 400 ft. Other normal, antithetic faults further complicate the structure.

The upper Frio sediments in the Willow Slough field contain little or no sand and are lithologically uniform with the overlying Anahuac Shale. The middle Frio, however, contains



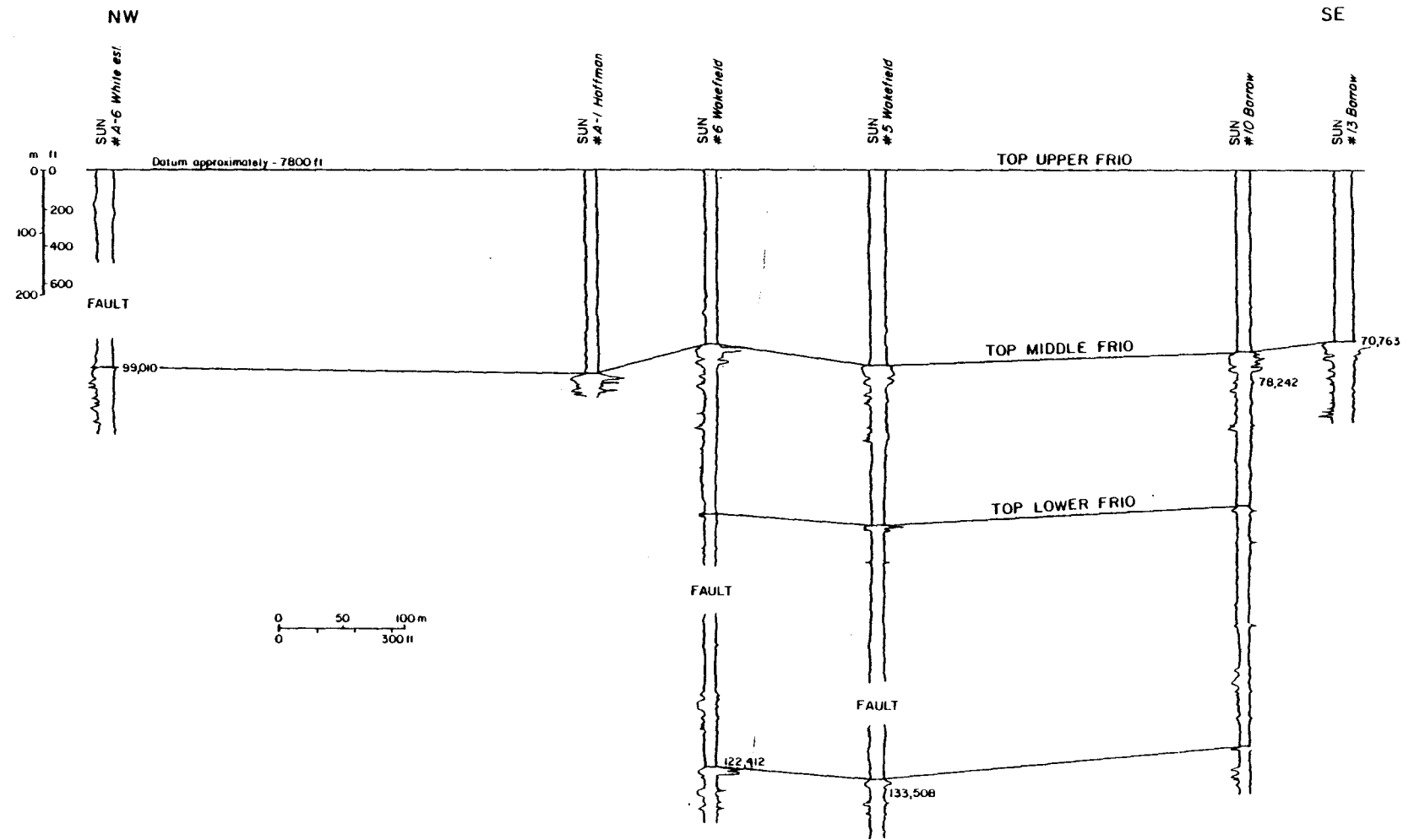


Figure II-2. Stratigraphic dip section through the Willow Slough field, showing the salinities of water produced from two sandstone intervals.

thick (70 to 100 ft) sandstones that grade downward into thinner (10 to 20 ft) sandstones and finally into massive shales. The entire progradational sequence appears to be deltaic in origin. Sandstones in the lower Frio are 50 to 60 ft thick, have blocky spontaneous potential patterns, are laterally extensive, and are separated by several hundred feet of shale. These sandstones resemble strandplain facies deposited in a broad interdeltic area (Galloway and others, 1982).

Water analyses are from reservoir depths between 8,300 and 10,700 ft. Dissolved solids at these depths range from 70,000 to more than 130,000 mg/L (fig. II-3). The trends of these salinity variations apparently correspond to pressure regimes as documented in other areas by many more chemical analyses (Morton and others, 1981). In the Willow Slough area, salinity decreases in the transition zone near the base of normally pressured sediments then increases in the zone of intermediate pressure gradients. If this trend is projected downward, then there appears to be a decrease in salinity at higher pressure gradients ( $>0.7$  psi/ft). The lack of sufficient data at intermediate depths makes interpretation of the salinity trends tentative. In fact, the chemical analyses actually show an increase in salinity between 9,000 and 11,000 ft.

Calcium, which ranges from 1,600 to 5,800 mg/L, generally exhibits trends with depth that are similar to those of total dissolved solids. Calcium decreases with depth above the top of geopressure, where temperatures are less than 200°F and the thermal gradient is about 2°F/100 ft. Calcium increases at depth, where pressure gradients exceed hydrostatic gradients (fig. II-3) and where temperatures are greater than 200°F. The increase in thermal gradient below 10,000 ft coincides with a substantial increase in sand percent.

Mole ratios of sodium to calcium also correspond to changes in temperature and pressure. The ratios increase slightly with depth and reach a maximum at the base of normally pressured sediments near 9,000 ft, where calcium concentrations are lowest. Below the top of abnormal pressure, calcium concentrations increase more rapidly than sodium concentrations; consequently, the sodium-calcium ratio decreases with depth.

Alkalinities, which are less than 250 mg/L (table II-1), and the chloride-sodium ratios, which are slightly greater than 1, are apparently independent of changes in lithology, pore pressure gradient, or thermal gradient (fig. II-3). These measures of chemical composition are fairly uniform throughout the productive interval. Together, the high concentrations of sodium, calcium, and dissolved solids and the low alkalinities are typical of Frio waters of the upper coast.

#### Red Fish Reef Field

Waters produced from Frio sandstones in the Red Fish Reef field contain high concentrations of dissolved solids and sodium and low concentrations of potassium; their sodium-calcium

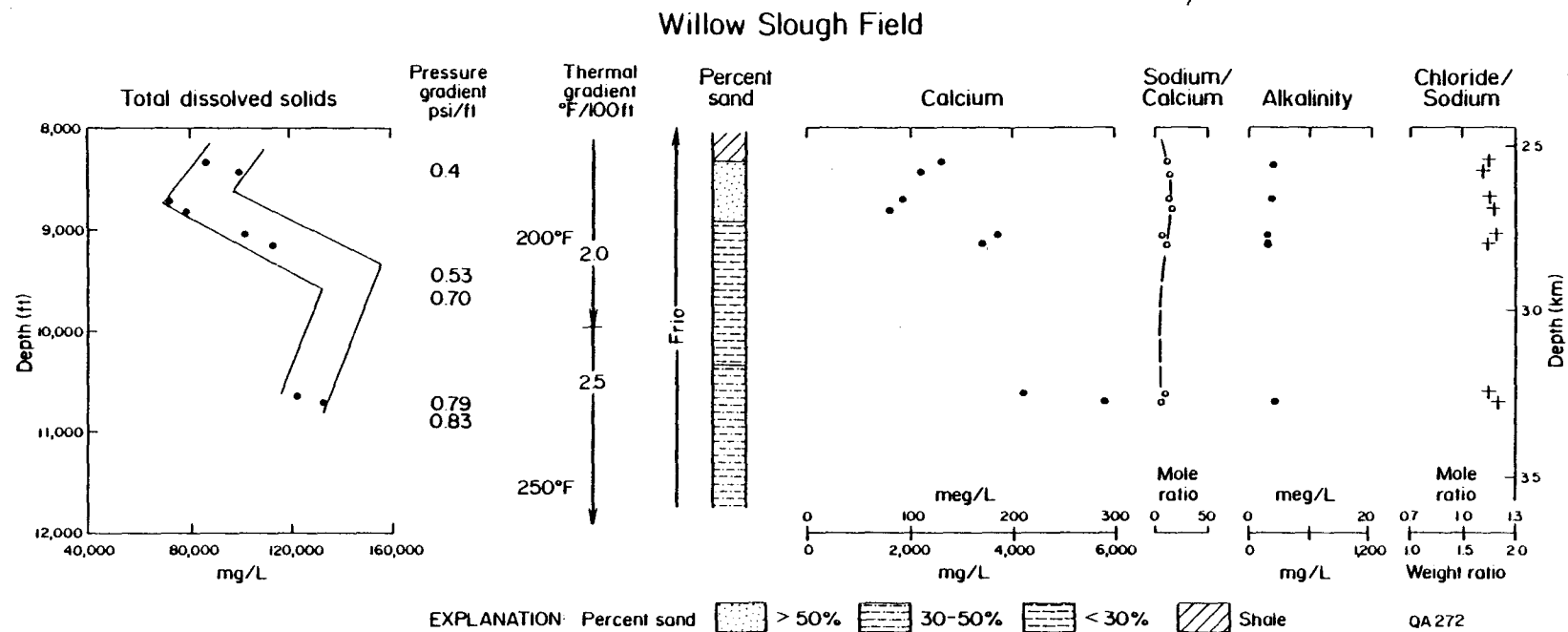


Figure II-3. Concentrations of total dissolved solids, major ions, and ion ratios in the Frio Formation, Willow Slough field. Chemical data from unpublished files of Sun Oil Company.

Table II-1. Ranges of ion concentrations and ion ratios of Tertiary formation waters, Texas Gulf Coast.

Field	Formation*	Total Dissolved Solids (mg/L)	Calcium (mg/L)	Sodium (mg/L)	Potassium (mg/L)	Chloride/Bromide mole ratio	Chloride/Sodium mole ratio	Sodium/Calcium mole ratio	Alkalinity (mg/L)
Alazan North	Frio	91,000	8,100	25,000	150	96	1.4	3	84
Algoa	Frio	133,000 - 139,000	8,300 - 8,600	42,000 - 44,000	624 - 643	442 - 452	1.25	5	88 - 94
Alta Loma	Frio	21,000 - 80,000	100 - 1,200	8,000 - 30,000	180 - 230	262 - 424	0.9 - 1.1	17 - 59	403 - 964
Alvin South	Frio	80,000 - 98,000	900 - 1,000	31,000 - 38,000	216 - 292	277 - 341	1.0 - 1.1	34 - 37	340 - 600
Arrowhead	Vckb	191,000 - 255,000	30,000 - 42,000	39,000 - 41,000	-	-	2.0 - 2.6	<1	49 - 645
Bartell Pass	Frio	28,000	400	10,000	112	84	1.1	23	490
Blackjack	Frio	16,000 - 18,000	30 - 100	7,000	49	77 - 92	0.8 - 0.9	51 - 235	2,040 - 2,950
Brannon	Frio	16,000 - 19,000	40	5,000 - 7,000	32	119 - 175	0.9	134 - 159	800 - 1,720
Cabeza Creek	Rklw, Wlcx	14,000 - 25,000	70 - 800	1,000 - 8,000	40 - 210	-	1.0 - 1.1	14 - 115	299 - 1,305
Candelaria	Frio	96,000 - 245,000	6,000 - 34,000	11,000 - 40,000	135 - 2,900	71 - 109	1.0 - 4.5	<1	47 - 173
Cedar Point	Mio, Frio	81,000 - 129,000	1,700 - 6,600	25,000 - 48,000	94 - 311	293 - 452	1.1 - 1.5	4 - 28	37 - 464
Chevron	Mio, Frio	70,000 - 100,000	1,300 - 3,400	24,000 - 35,000	150 - 285	93 - 137	1.1 - 1.2	9 - 22	36 - 561
Chocolate Bayou	Frio	18,000 - 135,000	200 - 9,000	13,000 - 42,000	90 - 1,900	172 - 464	0.9 - 1.2	5 - 120	262 - 1,635
Copano Bay	Frio	98,000	6,000	30,000	-	-	1.3	5	409
Corpus Channel	Frio	46,000 - 108,000	6,000 - 9,000	11,000 - 30,000	124 - 300	83 - 97	1.3 - 1.6	2 - 3	114 - 215
Corpus Christi	Frio	22,000 - 46,000	200 - 500	9,000 - 17,000	76 - 375	71 - 116	0.9 - 1.0	19 - 87	400 - 1,550
Danbury	Frio	74,000 - 235,000	1,500 - 22,000	28,000 - 70,000	223 - 1,218	194 - 237	1.0 - 1.4	3	30 - 220
Dickinson	Frio	44,000 - 97,000	500 - 2,900	16,000 - 34,000	-	-	1.1 - 1.2	9 - 40	458 - 885
Donna	Frio	12,000 - 32,000	100 - 3,900	4,000 - 11,000	41 - 197	70	1.0 - 1.6	2 - 61	110 - 366
Doyle	Yegua	15,000	40	5,000	61	-	0.9	120	1,900
East Runge	Wlcx	69,000	1,700	25,000	-	-	1.2	15	664
East White Point	Mio, Frio	25,000 - 85,000	200 - 3,000	9,000 - 29,000	70 - 215	87 - 165	1.0 - 1.2	7 - 46	97 - 278
Edinburg	Frio	6,000	200	2,000	55	755	1.1	10	144
El Pistle	Frio	146,000	25,000	24,000	1,250	166	2.2	<1	89
Encinal Channel	Frio	213,000 - 241,000	21,000 - 31,000	53,000 - 58,000	485	93	1.5 - 1.7	2 - 3	41 - 123
Fagan	Frio	52,000	500	19,000	177	-	1.1 - 1.2	35	753
Flowella	Frio	21,000 - 45,000	300 - 600	7,000 - 17,000	1,000	-	1.0 - 1.2	13 - 46	264 - 902
Geronimo	Frio	21,000 - 25,000	30 - 100	8,000 - 9,000	36 - 71	123 - 137	0.8 - 1.0	59 - 292	870 - 1,750
Harris	Wlcx	13,000 - 29,000	1,000 - 7,000	-	-	-	-	-	340 - 610
Harvey Deep	Frio	18,000 - 28,000	50 - 200	7,000 - 12,000	45 - 81	129 - 161	0.9 - 1.0	55 - 129	880 - 1,520
Hastings Southeast	Frio	136,000	4,000	49,000	371	385	1.1	12	219
Hildebrandt Bayou	Hkby	43,000	200	17,000	99	148	0.9	84	1,678
High Island Block 14L	Mio	136,000	4,200	49,000	371	220	1.1	47	1,130
Hinde	Frio	35,000 - 44,000	3,000 - 4,000	1,000 - 12,000	-	-	1.3 - 1.4	3 - 4	414 - 557
Hostetter	Wlcx	26,000	200	10,000	-	-	1.0	50	676
Indian Point	Frio	21,000 - 80,000	100 - 3,700	8,000 - 26,000	5 - 260	79 - 164	1.0 - 1.2	7 - 96	162 - 740
Javelina	Vckb	31,000 - 51,000	5,000 - 13,000	6,000 - 7,000	-	-	2.1 - 2.9	<1	350 - 414
Jeffress	Vckb	32,000 - 62,000	5,000 - 12,000	6,000 - 11,000	-	-	1.9 - 2.3	<1	328 - 550
La Belle	Mio, Frio	36,000 - 121,000	900 - 3,800	13,000 - 43,000	-	-	1.1 - 1.2	11 - 79	80 - 122
La Blanca	Frio	7,000 - 15,000	100 - 600	2,000 - 5,000	19 - 260	100 - 202	0.9 - 1.3	5 - 31	79 - 400
Lake Creek	Wlcx	36,000 - 171,000	600 - 1,500	13,000 - 61,000	-	-	1.1 - 1.2	23 - 41	195 - 503

\*Frio - Frio, Hkby - Hackberry, Mio - Miocene, Rklw - Reklaw, Vckb - Vicksburg, Yegua - Yegua

Table II-1 (cont.)

Field	Formation*	Total Dissolved Solids (mg/L)	Calcium (mg/L)	Sodium (mg/L)	Potassium (mg/L)	Chloride/Bromide mole ratio	Chloride/Sodium mole ratio	Sodium/Calcium mole ratio	Alkalinity (mg/L)
League City	Frio	102,000 - 127,000	2,000 - 5,000	37,000 - 43,000	-	-	1.1 - 1.2	8 - 20	450 - 885
Lyda	Vckb	36,000 - 169,000	1,600 - 20,000	12,000 - 43,000	-	-	1.2 - 2.2	1 - 7	111 - 390
Martinez	Wlcx	13,000	50	4,000	24	-	0.9	92	1,730
Maude B. Traylor	Frio	19,000 - 70,000	300 - 500	8,000 - 27,000	56 - 171	96 - 139	0.9 - 1.0	60 - 232	574 - 1,710
May-South May	Frio	21,000 - 95,000	1,800 - 13,000	5,000 - 22,000	44 - 131	87 - 108	1.1 - 1.74	2 - 11	110 - 415
McAllen	Frio	15,000 - 37,000	400 - 4,200	4,000 - 10,000	37 - 330	145 - 589	1.0 - 1.5	2 - 20	169 - 308
McAllen Ranch	Vckb	62,000 - 136,000	14,000 - 24,000	9,000 - 26,000	470 - 1,470	94 - 119	2.1 - 2.9	<1	118 - 709
McGill	Frio	58,000	2,000	20,000	264	-	1.2	10	411
Midfields	Frio	16,000 - 83,000	20 - 1,200	5,000 - 31,000	-	-	0.7 - 1.1	25 - 221	171 - 3,510
Midway	Frio	20,000 - 38,000	20 - 700	7,000 - 31,000	41 - 198	132 - 204	1.0 - 1.1	18 - 65	420 - 1,180
Mobil David	Frio	43,000	600	17,000	54	78	1.0 - 1.1	29	510
Mustang Island	Frio	48,000 - 60,000	300 - 2,000	18,000 - 22,000	-	-	1.0 - 1.1	10 - 60	354 - 1,315
Nelsonville	Wlcx	100,000 - 130,000	2,000 - 5,500	36,000 - 46,000	-	-	1.1 - 1.2	7 - 18	250 - 296
Nine Mile Point	Frio	17,000 - 23,000	60 - 300	6,000 - 8,000	122 - 130	76	0.8 - 1.0	25 - 103	580 - 2,220
North Rincon	Frio, Vckb	11 - 50	170 - 11,000	4,000 - 15,000	45	-	1.0 - 1.8	1 - 40	110 - 554
Nueces Bay	Frio	24 - 70	100 - 4,000	9,000 - 23,000	-	-	1.0 - 1.3	5 - 85	354 - 1,545
Oyster Bayou	Frio	91,000 - 138,000	3,400 - 4,800	30,000 - 47,000	-	-	1.2	8 - 9	162 - 318
Panther Reef	Frio	20 - 60	400 - 2,100	7,000 - 22,000	63 - 130	71 - 131	0.9 - 1.2	11 - 168	710 - 1,800
Pharr	Frio	13,000 - 44,000	900 - 5,200	2,000 - 11,000	94 - 267	123 - 143	1.2 - 1.6	2 - 5	114 - 191
Pheasant Southwest	Frio	15,000 - 25,000	80 - 100	6,000 - 10,000	61 - 65	66 - 92	0.9 - 1.0	58 - 118	806 - 1,790
Port Acres	Frio	82,000 - 84,000	1,900 - 2,700	28,000 - 30,000	-	-	1.0 - 1.1	11 - 15	158 - 6,751
Portland	Frio	13,000 - 106,000	50 - 4,300	6,000 - 34,000	40 - 78	97 - 213	0.8 - 1.2	6 - 153	506 - 2,760
Red Fish Bay	Frio	22,000 - 95,000	400 - 6,000	7,000 - 29,000	-	-	1.0 - 1.3	5 - 23	403 - 898
Red Fish Reef	Frio	45,000 - 160,000	200 - 10,000	17,000 - 48,000	350 - 450	346 - 391	1.0 - 1.5	5 - 40	185 - 668
Red Fish Reef North	Frio	67,000 - 120,000	0.6 - 4,900	23,000 - 35,000	-	-	1.0 - 1.9	6 - 38	179 - 366
Rita	Frio	82,000 - 171,000	14,000 - 29,000	14,000 - 33,000	145 - 1,870	81 - 109	1.6 - 2.4	<1 - 2	21 - 120
Robinson Lake	Frio	165,000	11,000	50,000	-	-	1.3	4	107
Rowan North	Frio	57,000	300	23,000	171	186	1.0	69	1,280
Sabine Lake	Mio	108,000	1,800	42,000	240	350	1.0	24	562
Sarita	Frio	79,000 - 98,000	5,000 - 7,000	23,000 - 29,000	140 - 225	102 - 116	1.3 - 1.4	3 - 4	51 - 175
Seabreeze	Frio	80,000 - 85,000	2,200 - 4,200	28,000	-	-	1.2	7 - 12	0 - 237
South Weslaco	Frio	9,000 - 15,000	100 - 800	3,000 - 5,000	33 - 49	80 - 87	0.9 - 1.2	4 - 38	230 - 527
Stowell	Mio, Frio	86,000 - 114,000	2,200 - 4,600	31,000 - 38,000	-	-	1.1 - 1.2	8 - 17	222 - 908
Sugar Valley	Frio	92,000 - 110,000	1,000 - 2,000	27,000 - 39,000	260 - 379	327 - 377	1.0 - 1.1	12 - 41	207 - 300
Tidehaven	Frio	33,000 - 51,000	90 - 4,800	12,000 - 13,000	80 - 144	180 - 388	1.0 - 1.5	3 - 131	20 - 1,310
Tijerina-Canales-									
Blucher	Frio	22,000 - 44,000	100 - 1,000	8,000 - 13,000	85 - 163	-	1.0 - 1.1	8 - 142	264 - 940
Trull	Frio	14,000	20	5,000	30	59	0.8	301	2,475
Willow Slough	Frio	70,000 - 133,000	1,600 - 5,800	25,000 - 44,000	-	-	1.1 - 1.2	7 - 17	0 - 240
Winnie North	Frio	104,000 - 107,000	2,800	38,000	-	-	1.1	14	164 - 172
Yeary	Frio	41,000	500	15,000	-	-	1.0	27 - 32	212 - 360

\*Frio - Frio, Hkby - Hackberry, Mio - Miocene, Rklw - Reklaw, Vckb - Vicksburg, Yegua - Yegua

ratios are moderate and their chloride-bromide ratios are high (table II-1). These chemical characteristics are typical of upper coast waters. Atypical characteristics include high concentrations of calcium, high alkalinities, and high chloride-sodium ratios. Within the field, dissolved solids, calcium, and sodium all generally follow the same vertical trends; they decrease with depth toward the top of geopressure and increase with depth at intermediate pressure gradients (fig. II-4). Even though the trends of calcium and sodium are similar, the trend of the sodium-calcium ratio is just the opposite; the ratio increases with depth until it reaches a maximum at the top of abnormal pressure (10,500 ft), which also coincides with the minimum concentration of calcium (fig. II-4). Below 10,500 ft, the sodium-calcium ratio decreases because calcium enrichment is greater than that of sodium. The trend of alkalinity generally parallels that of the sodium-calcium ratio (fig. II-4).

Data are sparse on potassium and the chloride-bromide ratio, but analyses of both parameters indicate increases at intermediate pressure gradients. The chloride-sodium ratio decreases with depth to the base of normally pressured sediments (10,500 ft). Below that depth, increases in the chloride-sodium ratio are minor.

#### Cedar Point Field

Fairly complete chemical analyses are available of waters produced from Miocene and Oligocene reservoirs in the Cedar Point field at depths between 2,400 and 7,200 ft (fig. II-5). The data illustrate at least three changes in water composition within this thick productive interval. Deep circulation of meteoric ground water in hydro pressured Miocene aquifers partly explains the increase in salinity at shallow depths, where sand percent also increases. The slight decrease in salinity at the top of the Frio corresponds to the transition zone near the top of abnormal pressure (6,000 ft). As sand percent in the Frio Formation decreases, the trend is reversed and salinity again increases with depth at intermediate pressure gradients. Although not shown, the depth-related trends of sodium are essentially the same as those of dissolved solids.

Calcium, which ranges from 1,700 to 6,600 mg/L, also exhibits similar changes with depth. Below 4,500 ft, calcium concentrations decrease above and then increase below the top of geopressure; however, at shallower depths, calcium trends are unlike those of salinity. For example, between 2,500 and 4,500 ft, calcium increases and then decreases with depth, whereas salinity steadily increases over the same depth interval.

The chloride-sodium ratio follows the same depth trends as calcium; however, the variations in the chloride-sodium ratio are much less pronounced (fig. II-5). The sodium-

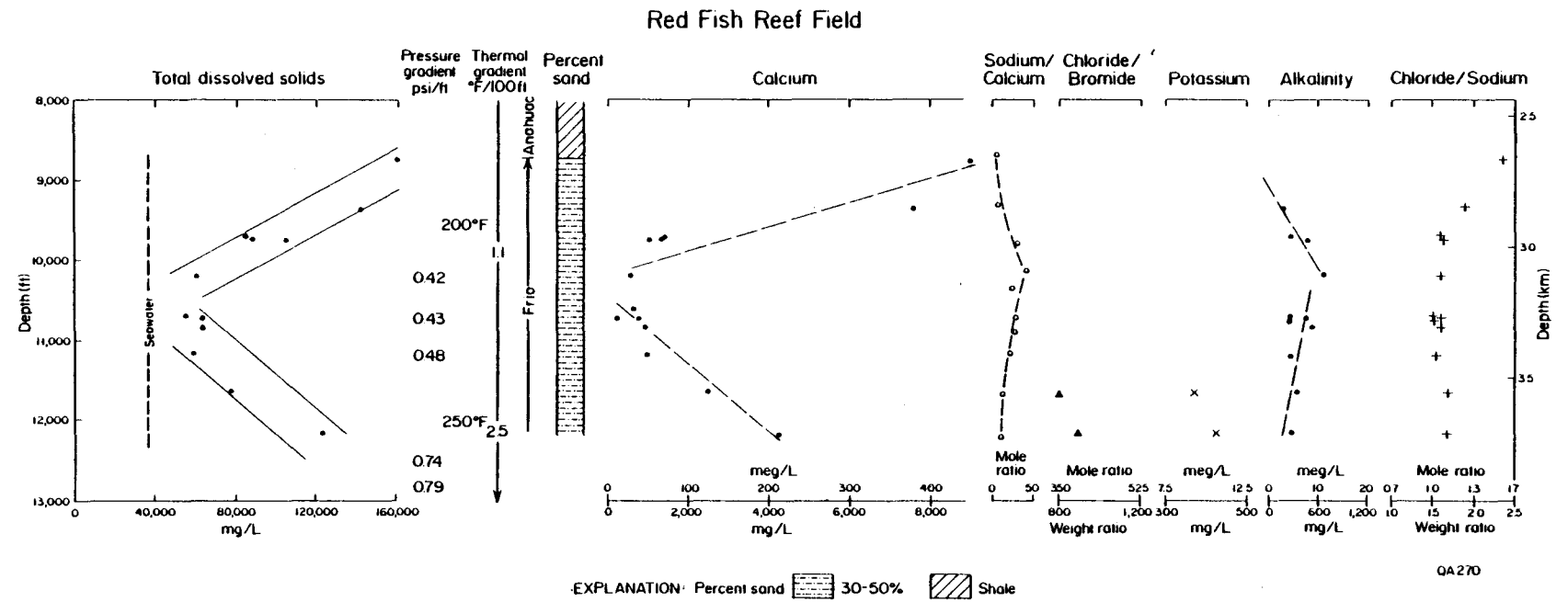


Figure II-4. Concentrations of total dissolved solids, major ions, and ion ratios in the Frio Formation, Red Fish Reef field. Chemical data from unpublished files of Sun Production Company and Morton and others (1981).

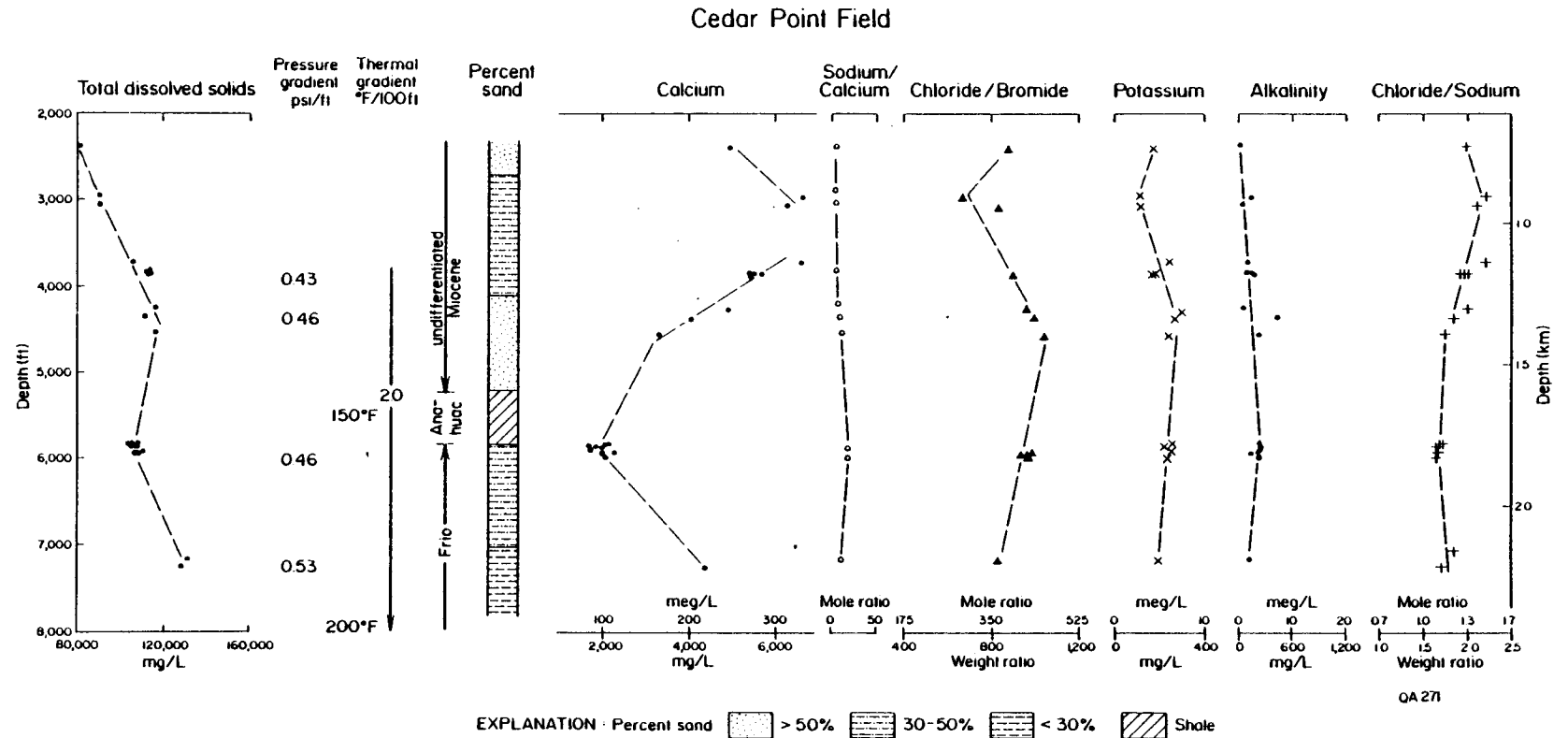


Figure II-5. Concentrations of total dissolved solids, major ions, and ion ratios in the Cedar Point field. Chemical data from unpublished files of Chevron U.S.A., Incorporated.

calcium ratio is uniform to about 4,000 ft; below that depth, it steadily increases to the top of the Frio and reaches a maximum that coincides with the calcium minimum (fig. II-5). At greater depths, the sodium-calcium ratio decreases because calcium increases more rapidly than sodium.

Modern formation waters in the Cedar Point field have low alkalinities (<500 mg/L; table II-1) that vary in a manner similar to the sodium-calcium ratio. Alkalinities gradually increase with depth to the top of geopressure and then decrease slightly at intermediate pressure gradients (fig. II-5).

For unexplained reasons, potassium concentrations and the chloride-bromide ratio undergo similar changes with depth. Both parameters decrease as sand percent decreases and vice versa. Hence, the trends of potassium and the chloride-bromide ratio with depth exhibit an increase, then a decrease, followed by another increase (fig. II-5).

### Alta Loma Field

Alta Loma field is separated from surrounding productive areas by a major growth fault that extends from southeastern Chocolate Bayou field to northwestern Alta Loma field. The major fault branches into several parallel minor faults toward the eastern part of the area and forms a steplike fault system (fig. II-6). Displacement, rollover, and expansion of the Frio Formation are less pronounced in the Alta Loma field than in the Chocolate Bayou field; however, the small branching faults make the structure more complicated. Log patterns in the Alta Loma field show overall distal deltaic or prodelta facies; an exception is the T3 sandstone, which caps a major progradational sequence and attains thicknesses of up to 300 ft.

Sandstones producing in the Alta Loma field below 10,000 ft contain water having salinities ranging from 20,000 mg/L to slightly more than 60,000 mg/L. Lithologies at these depths are dominantly shale having a few interbedded sandstones; thus, sand percent is low (fig. II-7). Although lithology and thermal gradient (2.5°F/100 ft) are essentially uniform throughout the productive interval, dissolved species vary systematically. Between 10,000 and 12,000 ft, salinities steadily increase. This trend of increasing dissolved solids at intermediate pressure gradients also occurs in the adjacent Chocolate Bayou field (Morton and others, 1981). In both fields, salinity decreases at depths having pressure gradients that exceed 0.75 psi/ft; however, these high pressure gradients are encountered at much shallower depths in the Alta Loma field. Because the Chocolate Bayou, Halls Bayou, and Alta Loma fields are separated by major growth faults, formation waters having substantially different salinities occur at comparable depths (fig. II-6). As a result of this juxtaposition, a gradient of increasing salinity

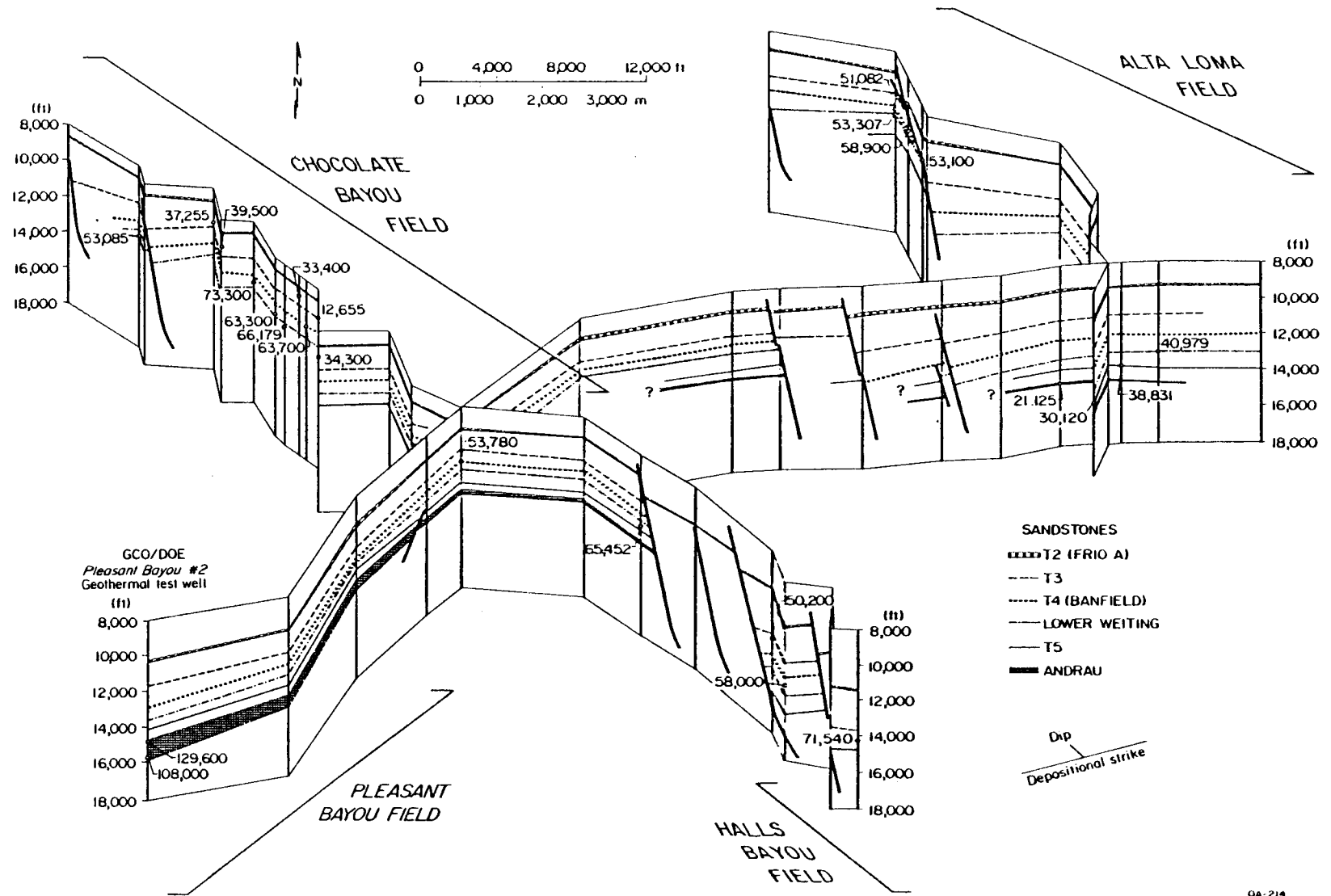


Figure II-6. Fence diagram showing structure, stratigraphic markers, and salinity data, Chocolate Bayou, Pleasant Bayou, Halls Bayou, and Alta Loma fields, Brazoria and Galveston Counties.

Alta Loma Field

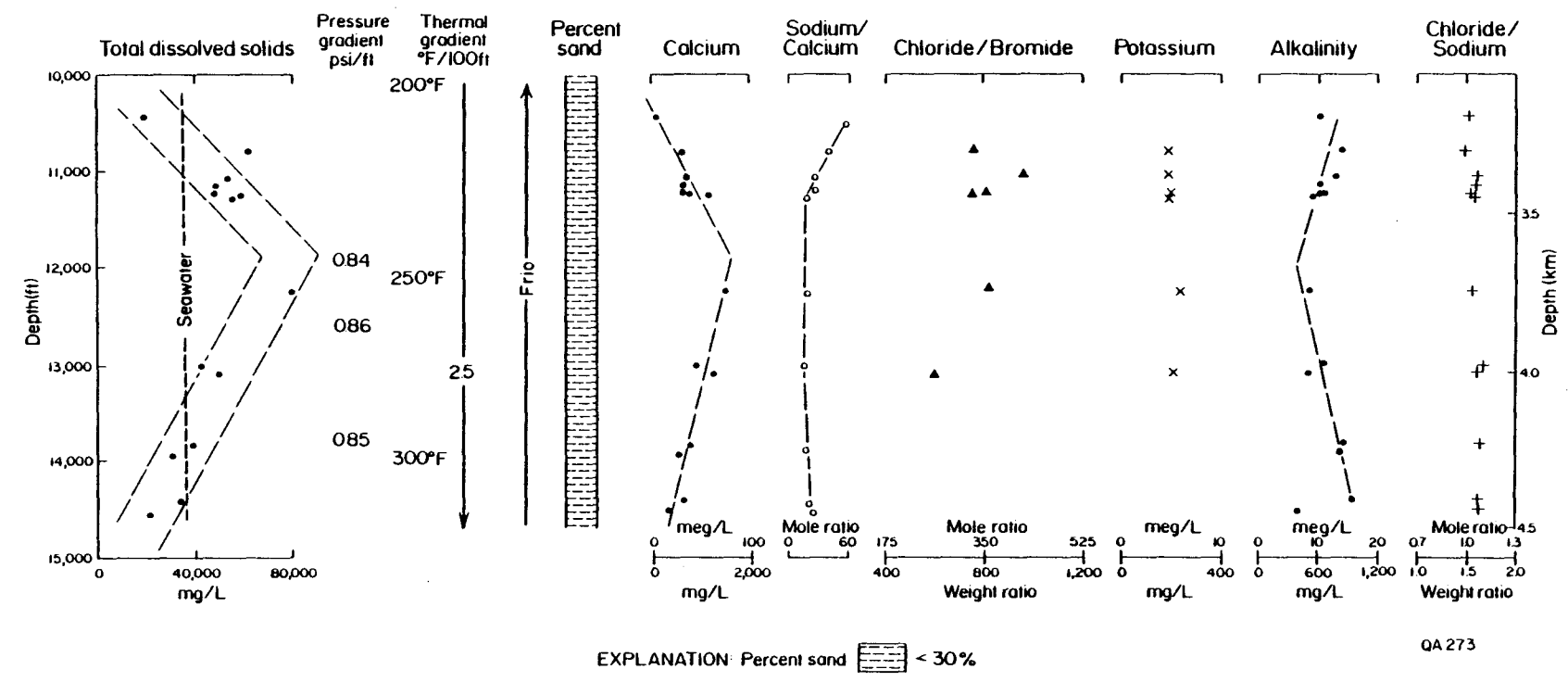


Figure II-7. Concentrations of total dissolved solids, major ions, and ion ratios in Alta Loma field. Chemical data from unpublished files of Phillips Petroleum Company, Morton and others (1981), and Kharaka and others (1977).

is established from east to west. Deep reservoirs of the lower Frio Formation have relatively low salinities in the Alta Loma field, intermediate salinities in the Halls Bayou field, and high salinities in the Chocolate Bayou field.

Calcium concentrations vary at depth in the same way as those of dissolved solids (fig. II-7). Calcium increases at intermediate pore pressure gradients above 12,000 ft but decreases at higher pressure gradients. In contrast, the sodium-calcium ratio decreases with depth and reaches a minimum near 12,000 ft, where formation temperatures approach 250°F. Below 12,000 ft and at higher pore pressure gradients, the sodium-calcium ratios increase slightly with depth primarily because sodium decreases with depth more rapidly than does calcium. Both alkalinities and the sodium-calcium ratios are inversely related to the abundance of calcium (fig. II-7). Potassium and the chloride-sodium ratio are unaffected by changes in temperature and pressure. Potassium concentrations average about 200 mg/L and are relatively uniform at depth. The chloride-sodium ratios are also nearly uniform and average about 1.0. Data on the chloride-bromide ratios are sparse but indicate a slight increase at intermediate pore pressure gradients and a decrease at high pressure gradients.

#### Sugar Valley Field

The Sugar Valley field (fig. II-1) overlies a large anticline 2 mi wide and 3 mi long that trends east-west and is cut by a strike-aligned growth fault having 200 ft of displacement and a minor fault having about 50 ft of displacement (fig. II-8). Structural closure allows production of both oil and gas from both sides of the major fault. Water samples, also from both sides of the fault, come from reservoirs within the lower part of the Frio Formation. Electric log patterns of the reservoir sandstone are blocky to spikey (fig. II-9), and sand content is high, ranging from 50 to 80 percent. Sand percent gradually diminishes upward to about 7,500 ft, where upper Frio and Anahuac shales predominate; sand percent also diminishes downward below 11,000 ft.

The chemical data are from a limited stratigraphic interval but have a broad areal extent and demonstrate that waters from the same sand body and fault block are generally within a salinity range of 10 percent (fig. II-8). Comparison of equilibrium temperatures and structure of the reservoir (figs. II-8 and II-10) shows that highest temperatures coincide with the structural highs on both sides of the major fault.

Water analyses are from the same stratigraphic interval and a limited depth range (300 ft); hence, depth-related trends are not apparent. These waters and associated hydrocarbons are trapped in the Frio sandstones in areas where changes in thermal gradient correspond



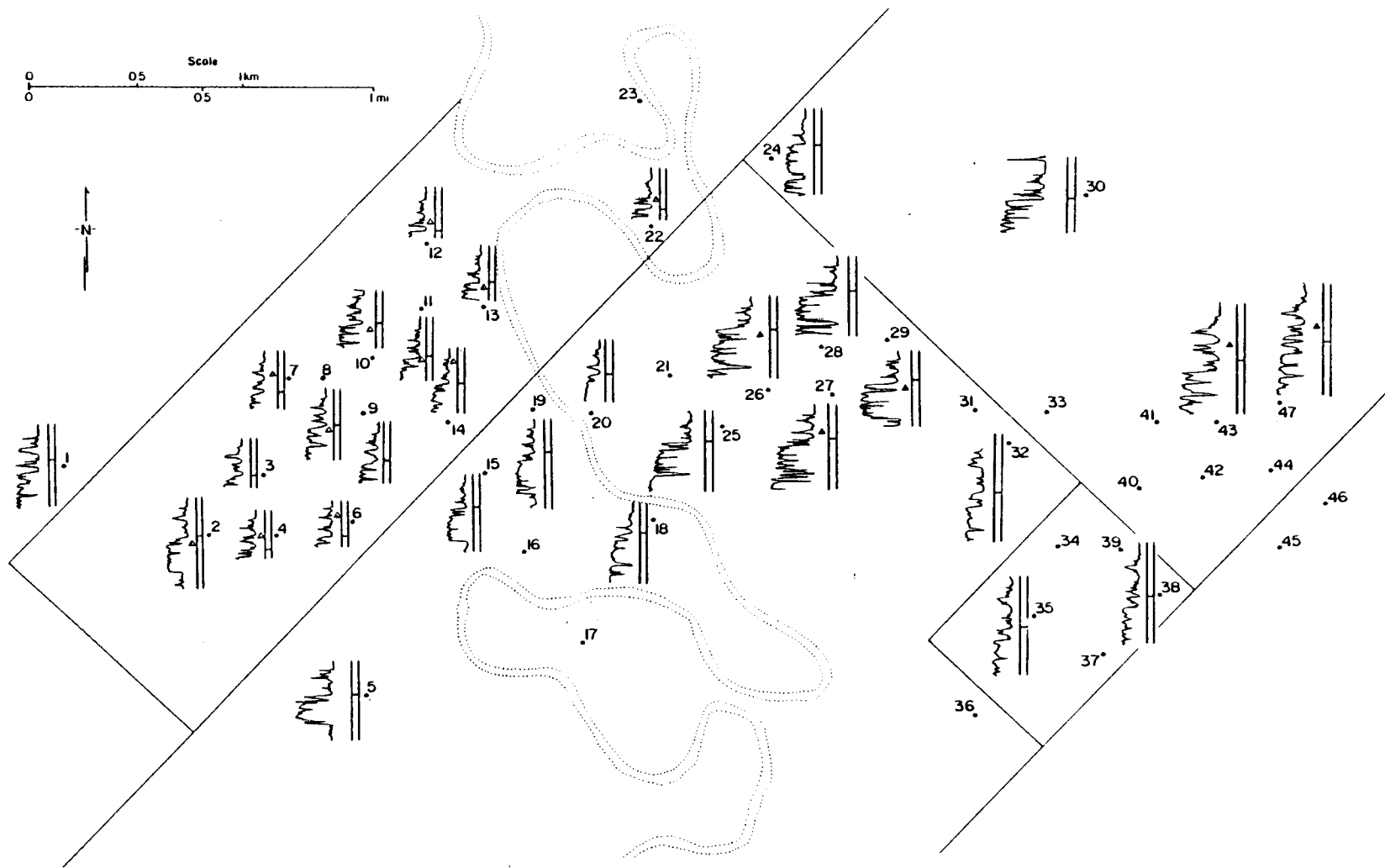


Figure II-9. Electric log patterns of the correlation marker used for figure II-8. Triangles show depths from which water analyses are available (see figure II-8 for salinities). Tick marks across log patterns are correlation markers.



to major lithologic changes. Near the productive horizon, interbedded sands and shales having intermediate sand percents grade downward into more massive sands having high sand percents (fig. II-11). This lithologic change at about 9,000 ft is accompanied by an increase in thermal gradient from 1.3°F/100 ft in the upper interbedded section to 2.0°F/100 ft in the underlying massive sand section.

Total dissolved solids range from 90,000 to 109,000 mg/L and average about 95,000 mg/L (fig. II-8). Although the depth-dependent trend of salinity is obscured by the scatter of data points, there appears to be a slight increase with depth in calcium and potassium and in the chloride-sodium ratio (fig. II-8). The high salinity and concentrations of sodium, intermediate concentrations of calcium ( $\approx 2,000$  mg/L), and high chloride-bromide ratios ( $\approx 350$ ) are typical of most upper coast waters.

#### Maude B. Traylor Field

Waters from the Maude B. Traylor field are representative of middle coast waters. Total dissolved solids, calcium, and potassium in these formations are low, but sodium and alkalinity are relatively high (table II-1). Furthermore, chloride-sodium ratios and chloride-bromide ratios are low, whereas sodium-calcium ratios are high (table II-1).

Concentrations of dissolved solids, sodium, calcium, and potassium all systematically increase with depth in the Maude B. Traylor field (fig. II-12). Salinities vary from about 20,000 to 70,000 mg/L over a vertical distance of about 1,700 ft; over the same distance, pore pressure gradients increase from 0.46 to 0.71 psi/ft. The increase in salinity at intermediate pressure gradients is similar to trends described for the Willow Slough, Red Fish Reef, Chocolate Bayou, and Alta Loma fields, as well as for other fields where the interval of intermediate pressure gradients is several thousand feet thick.

The chloride-bromide ratios and chloride-sodium ratios also increase with depth, whereas the sodium-calcium ratios and alkalinities decrease with depth (fig. II-12). The inverse relationship between sodium and calcium and the sodium-calcium ratio occurs because calcium increases with depth more rapidly than does sodium.

Sand percent of the Frio sediments is intermediate to high throughout the productive interval, and a geothermal gradient of 2.25°F/100 ft is uniform at the depths of interest. Neither temperature gradient nor lithology appears to significantly influence the changes in water chemistry.

### Sugar Valley Field

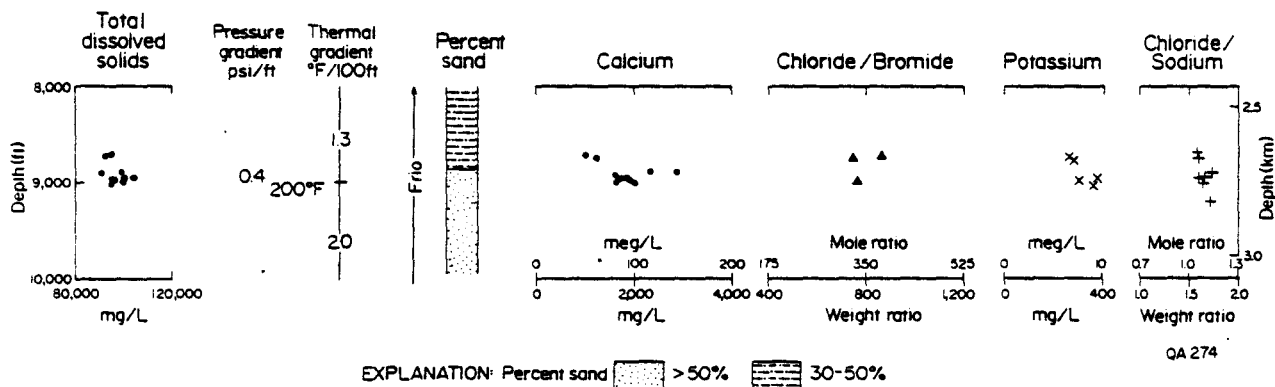


Figure II-11. Concentrations of total dissolved solids, major ions, and ion ratios in Sugar Valley field. Chemical data from unpublished files of Sun Production Company and Superior Oil Company and Morton and others (1981).

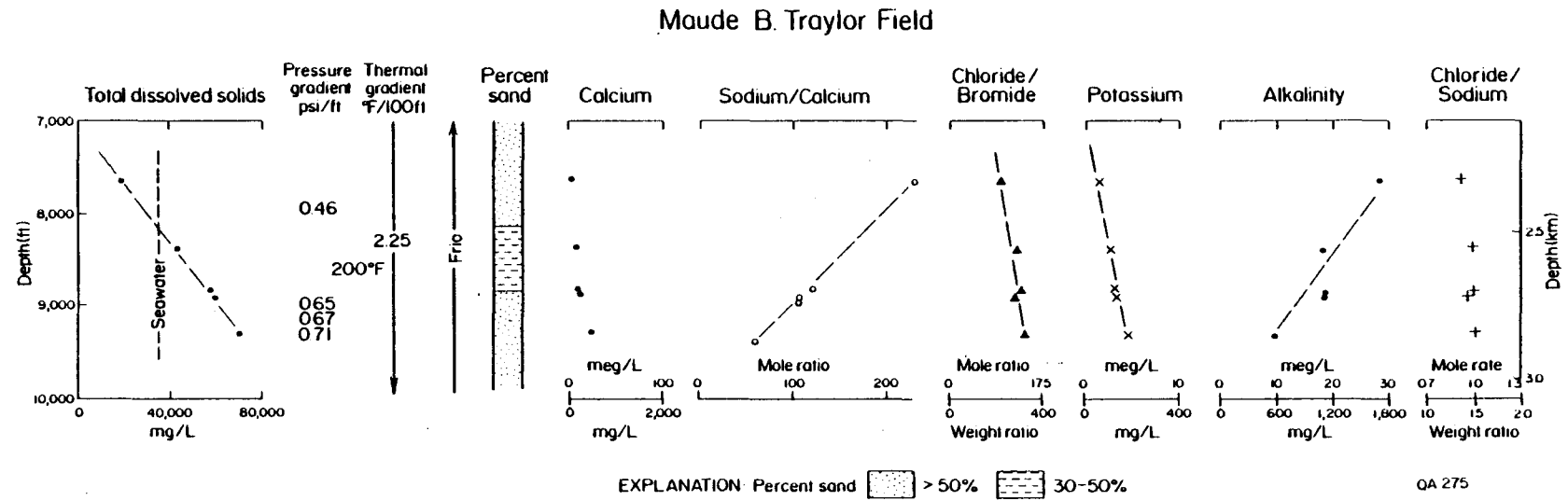


Figure II-12. Concentrations of total dissolved solids, major ions, and ion ratios in Maude B. Traylor field. Chemical data from Morton and others (1981).

## Red Fish Bay Field

Chemical analyses of formation water produced from the Red Fish Bay field show that salinity decreases with depth and that the rates of decrease mainly depend on pressure gradients. For example, salinity declines rapidly above the top of geopressure and at extremely high pressure gradients (fig. II-13). Between these zones, the salinity decrease with depth is minor. Apparently, the thin zone of intermediate pressure gradients (0.5 to 0.75 psi/ft) inhibits development of the high salinity zone seen elsewhere (figs. II-3 through II-5, II-7, and II-12).

Unlike changes in salinity, changes in the major ions and ion ratios correspond closely to changes in thermal gradient that occur at about 9,000 ft and near the top of geopressure. The abundance of calcium and the chloride-sodium ratio both decrease down to 9,000 ft and then increase at greater depths (fig. II-13). In contrast, the sodium-calcium ratio and alkalinity both increase down to 9,000 ft and then decrease at greater depths.

## May - South May Field

Salinities in the May - South May field waters range from 20,000 to 95,000 mg/L. Highest salinities occur at depths near 8,000 ft, whereas lowest salinities occur between 9,000 and 10,000 ft (fig. II-14). The decrease in salinity with depth corresponds to the transition zone near the top of geopressure, where pressures are equal to or slightly greater than hydrostatic. The salinity decrease is fairly uniform despite a change in lithology and corresponding change in thermal gradient. At about 9,000 ft, the massive lower Frio sands give way to underlying interbedded sands and shales. The downward decrease in sand percent is accompanied by an increase in thermal gradient from 1.0°F/100 ft in the shallow section to 2.5°F/100 ft below the massive sands (fig. II-14).

Variations in calcium with depth are more closely related to the thermal gradient than they are to the general salinity trend (fig. II-14). Calcium decreases with depth if formation temperatures are less than 200°F but increases with depth if temperatures and the thermal gradient are higher. Apparently, the increase in calcium with depth occurs at a lower rate than that of the overlying decrease with depth.

Changes in the sodium-calcium ratio and the chloride-sodium ratio also reflect the depth-dependent changes in lithology and thermal gradient. Alkalinity and the sodium-calcium ratio both increase with depth above 9,000 ft, but the trends reverse below that depth. Maximum values of the sodium-calcium ratio and maximum alkalinities occur at 9,000 ft, a point that coincides with the lowest concentrations of calcium and with the inflection point of thermal gradients. The general trend for the chloride-sodium ratio is opposite to that of the sodium-

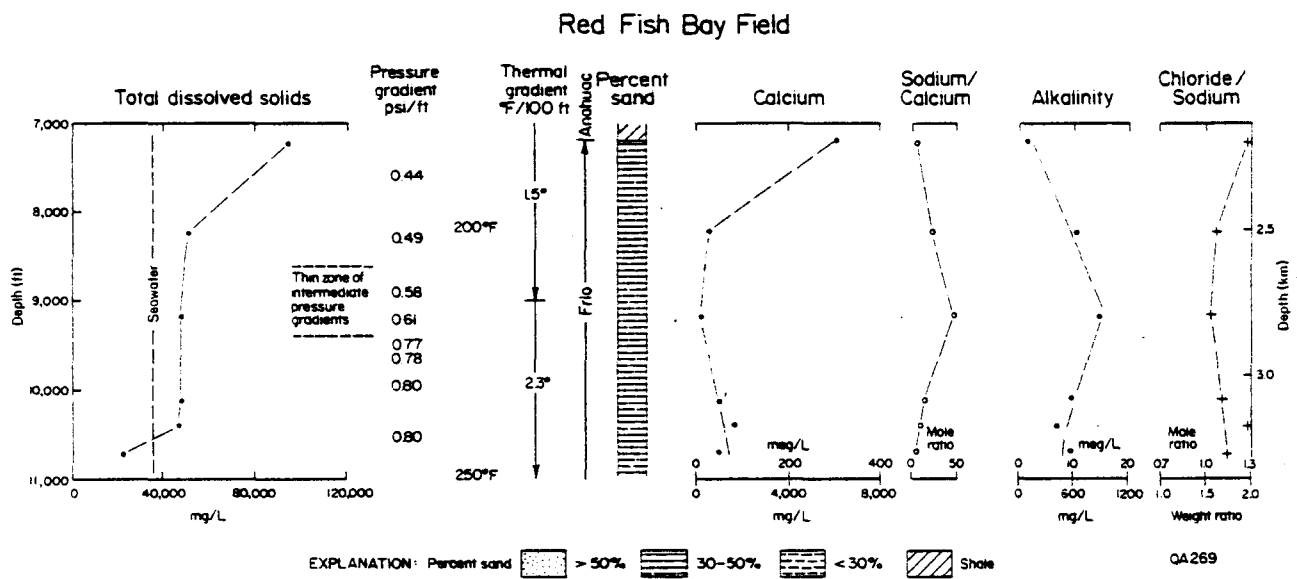


Figure II-13. Concentrations of total dissolved solids, major ions, and ion ratios in Red Fish Bay field. Chemical data from unpublished files of Sun Production Company.

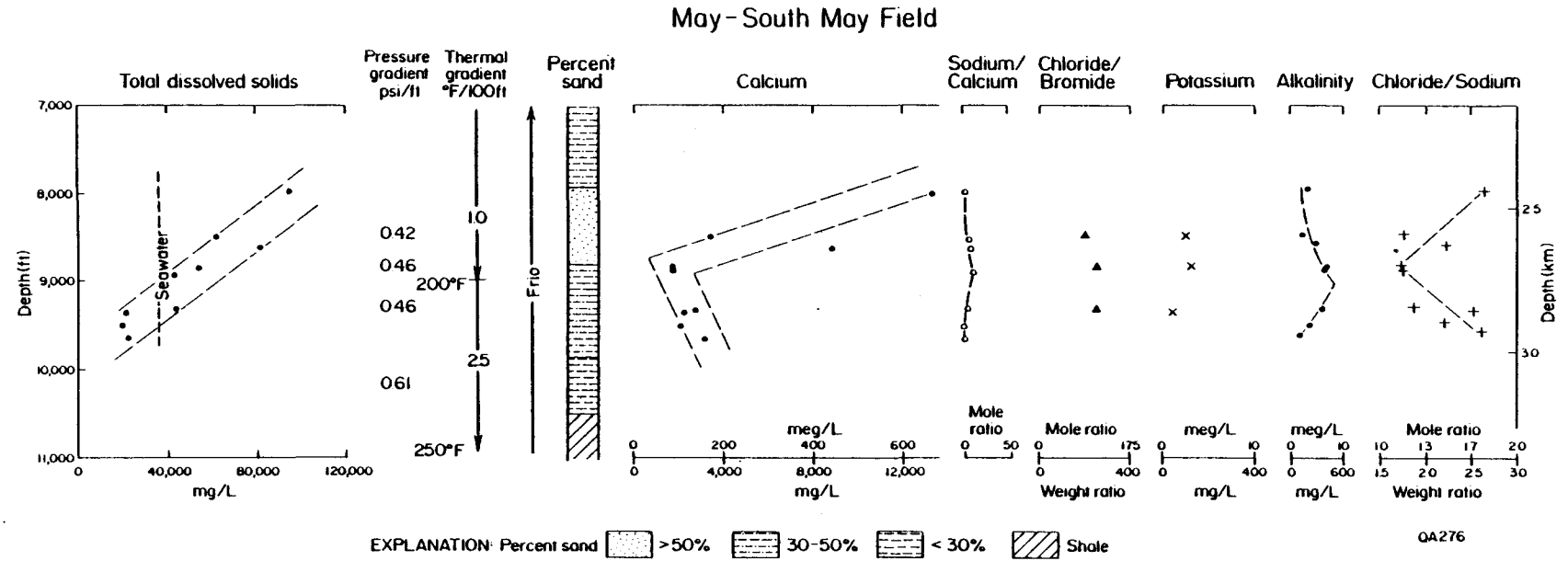


Figure II-14. Concentrations of total dissolved solids, major ions, and ion ratios in May - South May field. Chemical data from unpublished files of Cities Service Company and Morton and others (1981).

calcium ratio. The chloride-sodium ratio decreases to a minimum near 9,000 ft (fig. II-14) and increases below that depth. The relatively high values of this ratio indicate that chloride is enriched with respect to sodium. A mole ratio of 1.0 is normal for waters having equal concentrations of sodium and chloride, but all waters from the May field exceed this ratio.

The few data points on potassium and the chloride-bromide ratio are inadequate for an accurate interpretation of depth-related changes. The chloride-bromide ratios are all less than 110 and fairly uniform with respect to depth of water production (fig. II-14). Potassium concentrations are also low (130 mg/L or less), but the data suggest a decrease in potassium if temperatures exceed 200°F, the thermal gradient increases, and pressures approach abnormal gradients.

#### Tijerina-Canales-Blucher Field

Salinities in the Tijerina-Canales-Blucher field range from 22,000 to 45,000 mg/L; most values are less than 36,000 mg/L. Salinities generally increase with depth at intermediate pressure gradients (0.5 to 0.75 psi/ft) and decrease if pore pressure gradients are higher (fig. II-15). Apparently, salinity variations are not directly controlled by thermal gradient or lithology. A thermal gradient of 2.0°F/100 ft is uniform over the interval if sand percent decreases. The decrease in sand corresponds to the top of the Vicksburg, which occurs about 1,000 ft above the zone of highly overpressured sediments.

Above 7,500 ft, calcium decreases with depth; but below 7,500 ft in the zone of intermediate pressure gradients, calcium increases. The trend reverses and calcium decreases with depth if pore pressure gradients are extremely high. The trends of alkalinity and the sodium-calcium ratio are essentially opposite to the pattern described for calcium. Both parameters (1) increase with depth through the hydro pressured section, (2) decrease with depth if intermediate pressure gradients are present, and (3) increase with depth if pressure gradients are extremely high (fig. II-15).

#### McAllen Ranch Field

Brines produced from the McAllen Ranch field contain high concentrations of sodium (table II-1) and even higher concentrations of calcium on a milliequivalent basis. Therefore, the sodium-calcium ratio is less than 1.0. These calcium-sodium-chloride-type waters, which are present in Kenedy and northern Hidalgo Counties, are moderately alkaline and contain substantial amounts of potassium and strontium; in most of the samples, strontium is more abundant than potassium (appendix II-A).

### Tijerina - Canales - Blucher Field

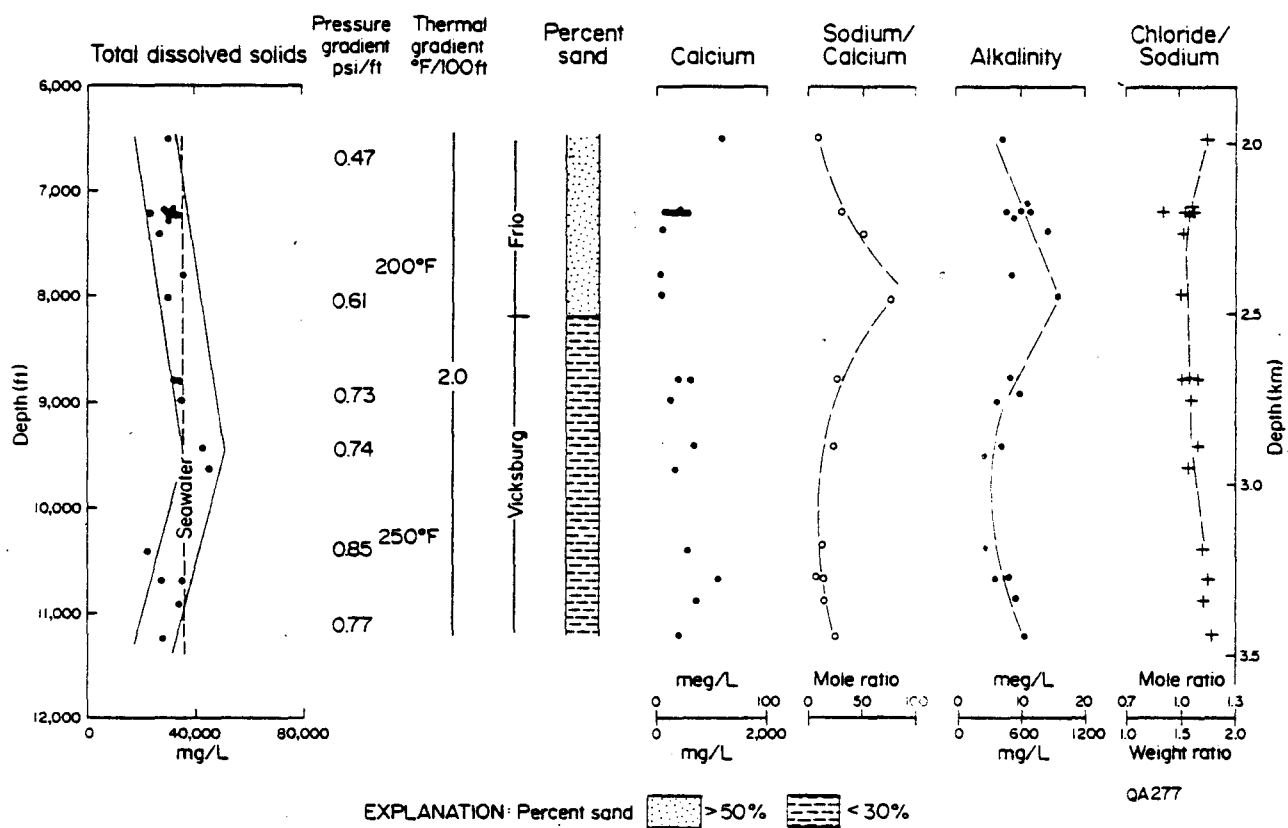


Figure II-15. Concentrations of total dissolved solids, major ions, and ion ratios in Tijerina-Canales-Blucher field. Chemical data from unpublished files of Sun Production Company.

Perforated intervals in the low-permeability Vicksburg sands are a few hundred feet thick. These unusually large and sometimes overlapping intervals of gas production make interpretation of water chemistry difficult because the actual depth of water production is uncertain. Nevertheless, trends of the commingled waters can be delineated by determining midpoints of perforated intervals and averages of several analyses for each well (fig. II-16).

The analyses show that dissolved solids range from approximately 62,000 to 136,000 mg/L (table II-1) and vary with depth. Salinities increase between 12,000 and 13,000 ft and decrease below 13,000 ft (fig. II-16). Trends of calcium concentrations and alkalinity are similar to the trend of salinity, whereas the chloride-sodium ratio is just the opposite; that is, it decreases with depth to just below 13,000 ft and then increases at greater depths. Potassium and the chloride-bromide ratio increase with depth throughout the productive interval.

The variations in water chemistry are not easily explained because the gross geological and physical conditions are fairly constant at depth. All the Vicksburg reservoirs produce from a stratigraphic interval having uniformly high sand content, the reservoirs have extremely high pressure gradients (0.84 to 0.9 psi/ft), and thermal gradient is uniformly high (2.5°F/100 ft). Thus, the depth-related changes in composition are unclear if viewed in a site-specific context.

#### North Rincon Field

Chemical analyses of water from the North Rincon field indicate that formation water salinities in Frio and Vicksburg sandstones range from 10,000 to 65,000 mg/L. Maximum salinities occur in both hydro pressured and geopressured sediments, whereas minimum salinities occur at 6,500 ft near the top of geopressure (fig. II-17). As in other areas, salinities decrease with depth above the geopressure zone and increase with depth at intermediate pressure gradients. In the North Rincon field, sediments between 4,000 and 8,000 ft deep are interbedded sandstones and shales having intermediate sand percents. The most prominent shale, which is about 300 ft thick, occurs around 5,700 ft and corresponds locally to the top of geopressure. Thermal gradient across the productive interval is uniform (2.5°F/100 ft) and unaffected by changes in lithology or pressure gradient.

Calcium and sodium trends are similar to the salinity trends; however, the rates of decrease and increase with depth are dissimilar, especially in the geopressure zone. There, calcium increases with depth more rapidly than does sodium. Consequently, the sodium-calcium ratio reaches a maximum at the top of geopressure and decreases above and below about 5,000 ft. Alkalinity and the sodium-calcium ratio have similar trends (fig. II-17).

The chloride-sodium ratios are fairly uniform at depth in the hydro pressured section and average slightly greater than 1.0. These ratios increase substantially in the geopressured section and also increase with depth (fig. II-17).

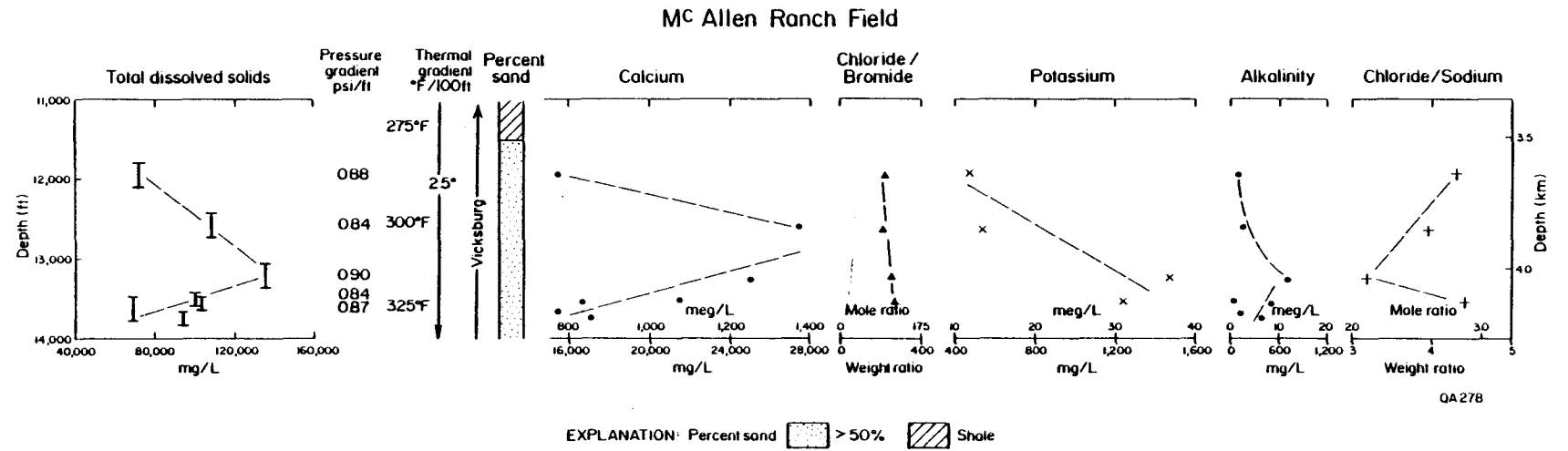


Figure II-16. Concentrations of total dissolved solids, major ions, and ion ratios in McAllen Ranch field. Chemical data from unpublished files of Forest Oil Corporation and appendix II-A.

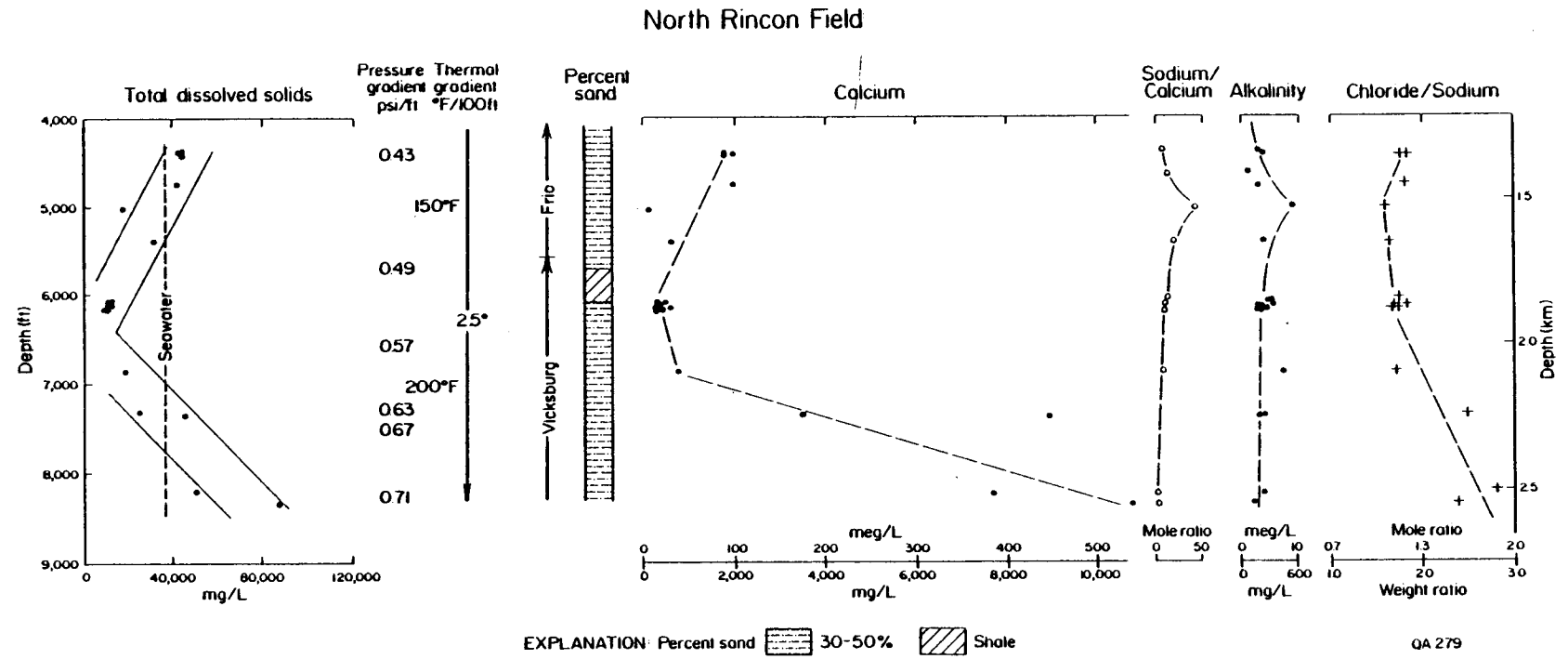


Figure II-17. Concentrations of total dissolved solids, major ions, and ion ratios in North Rincon field. Chemical data from unpublished files of Sun Production Company.

## South Texas Fields

### Structure

The main structural features of the Frio Formation in Hidalgo County, South Texas, are controlled by syndepositional growth structures such as the McAllen and Donna faults (fig. II-18). These major bounding faults had a dominant influence on the structural and stratigraphic history of the area. Several large hydrocarbon-producing fields are aligned along and formed within the structural closure on the downthrown side of the major faults. Relatively minor growth faults tend to separate broad structures into smaller closures at greater depths, resulting in deeper structures that are more complicated.

The Shepherd fault, which branches out of the McAllen fault and converges downdip with the Donna fault (Collins, 1968), has a maximum displacement of 1,000 ft on the top of the lower Frio. Structural data indicate that a drastic change in sediment source direction was responsible for development of the Shepherd fault zone.

Structures at the top of the Frio Formation are several broadly elongate, round anticlines formed on the downthrown side of major bounding faults and separated by dip-oriented synclines (fig. II-19). Syndepositional displacement and associated expansion of the upper Frio sediments are not significant except across the McAllen and Donna faults. A maximum throw of 300 ft on the McAllen fault is shown in cross section (fig. II-20); however, displacement generally tends to increase with depth. Maximum growth occurred during deposition of the lower Frio. Structures of the middle Frio include several small oval-shaped closures that form traps for the Whitted, Donna, and McAllen fields (fig. II-21). A narrow syncline having steep limbs is recognizable between growth anticlines of the Whitted and McAllen fields. A direct relationship between growth faulting and this abrupt structural low was not demonstrated by the log correlations (fig. II-22). A structural map of the top of the lower Frio can be drawn only in the deepest parts of McAllen, Pharr, and Shepherd fields (fig. II-23). The structure of the lower Frio is characterized by a large, elongate anticline parallel to the Shepherd fault. At depth, the crest of the anticline migrates downdip toward the Donna fault.

Rollover is the major recognizable growth feature in the lower Frio sediments, especially along the McAllen fault (fig. II-20); distinctive shale ridges or shale diapirs are hard to recognize on the cross sections. An exceptionally thick shale section that correlates with sandstones in equivalent stratigraphic intervals reflects intrusion of Vicksburg shale during deposition of the lower Frio. The shale section can be seen in cross section on the upthrown block of the Donna fault (fig. II-24).

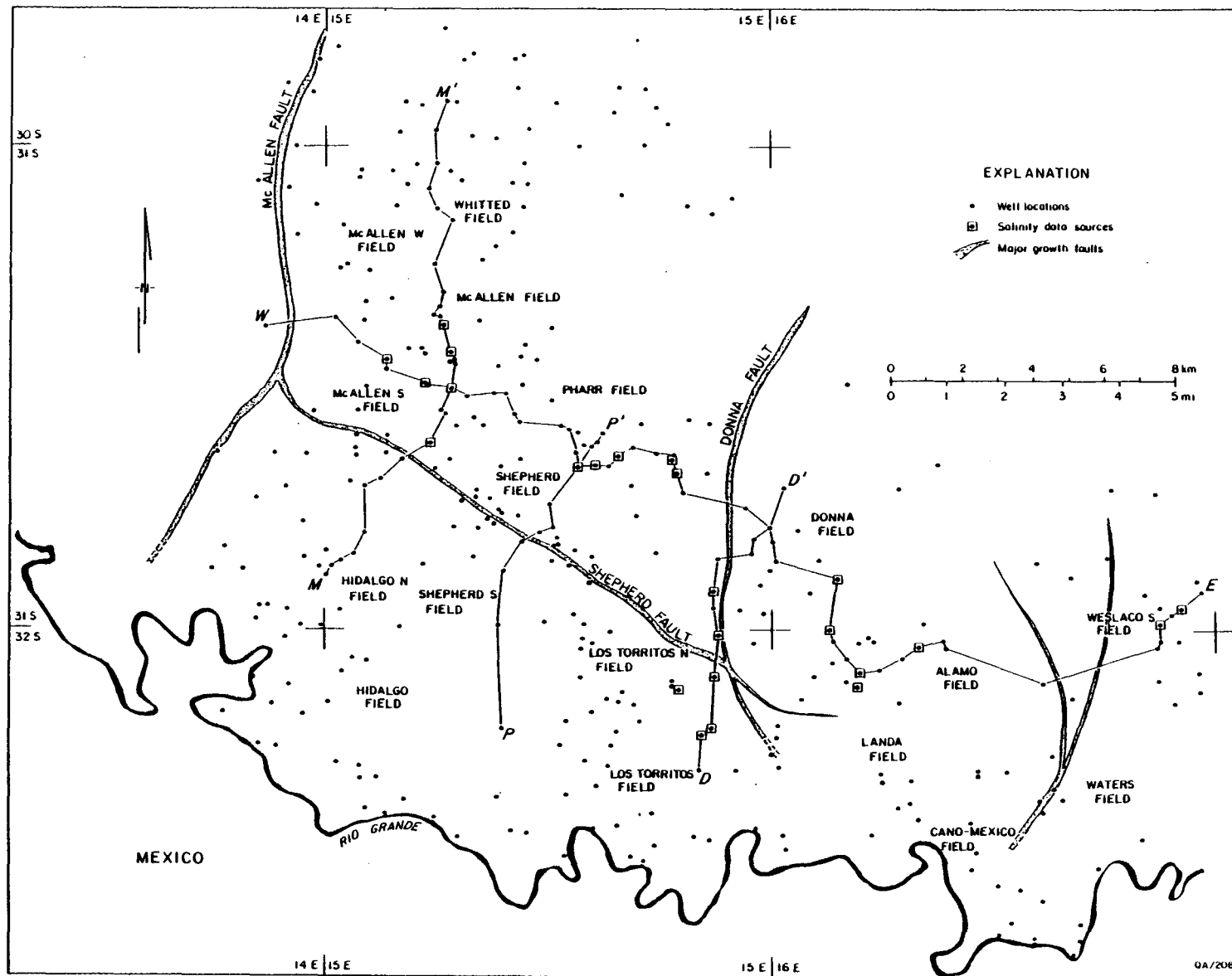


Figure II-18. Location map of wells, cross sections, and salinity data in the South Texas field area.



W  
West

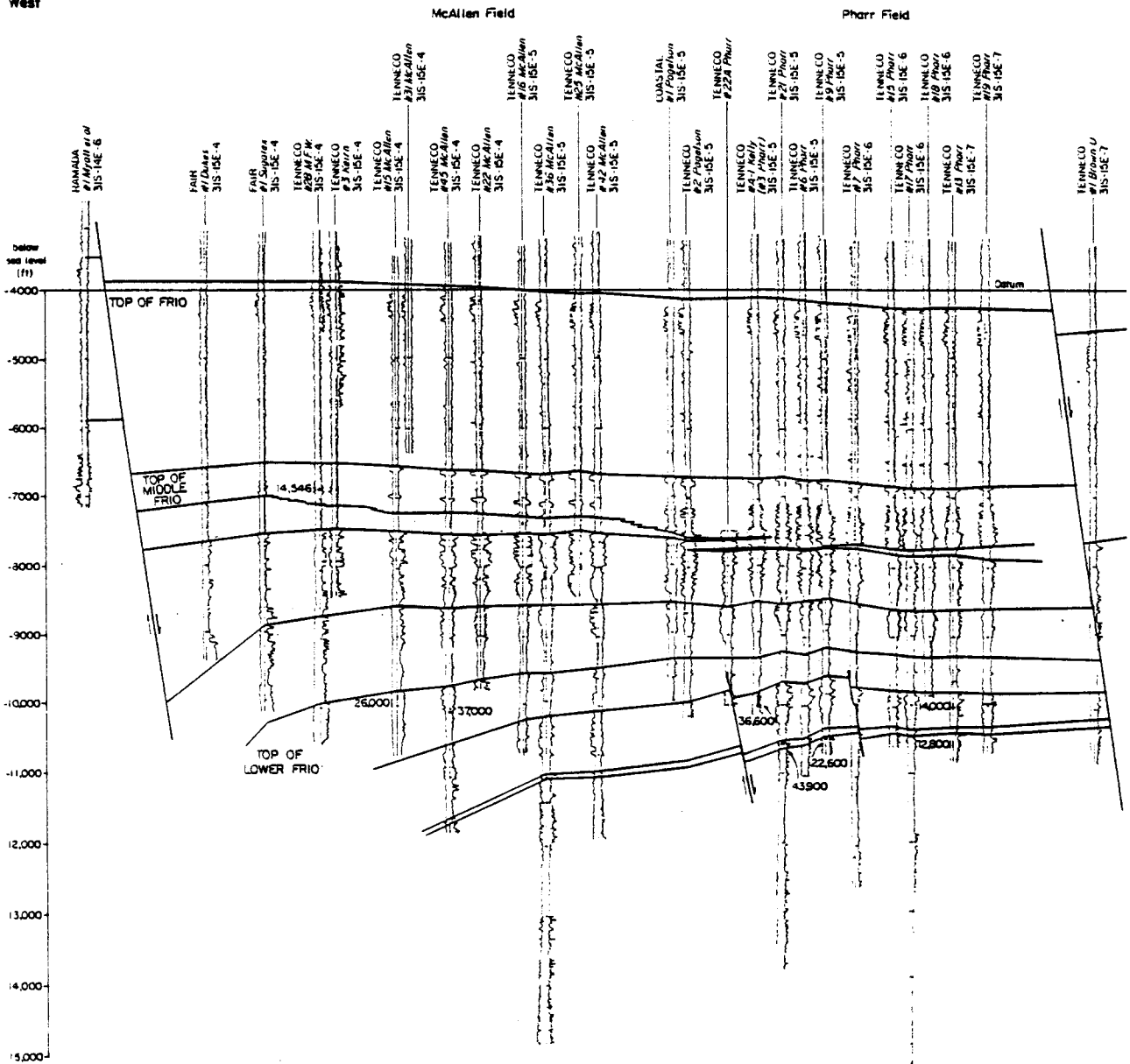


Figure II-20. Structural dip cross section through the South Texas field area; line of section on figure II-18.

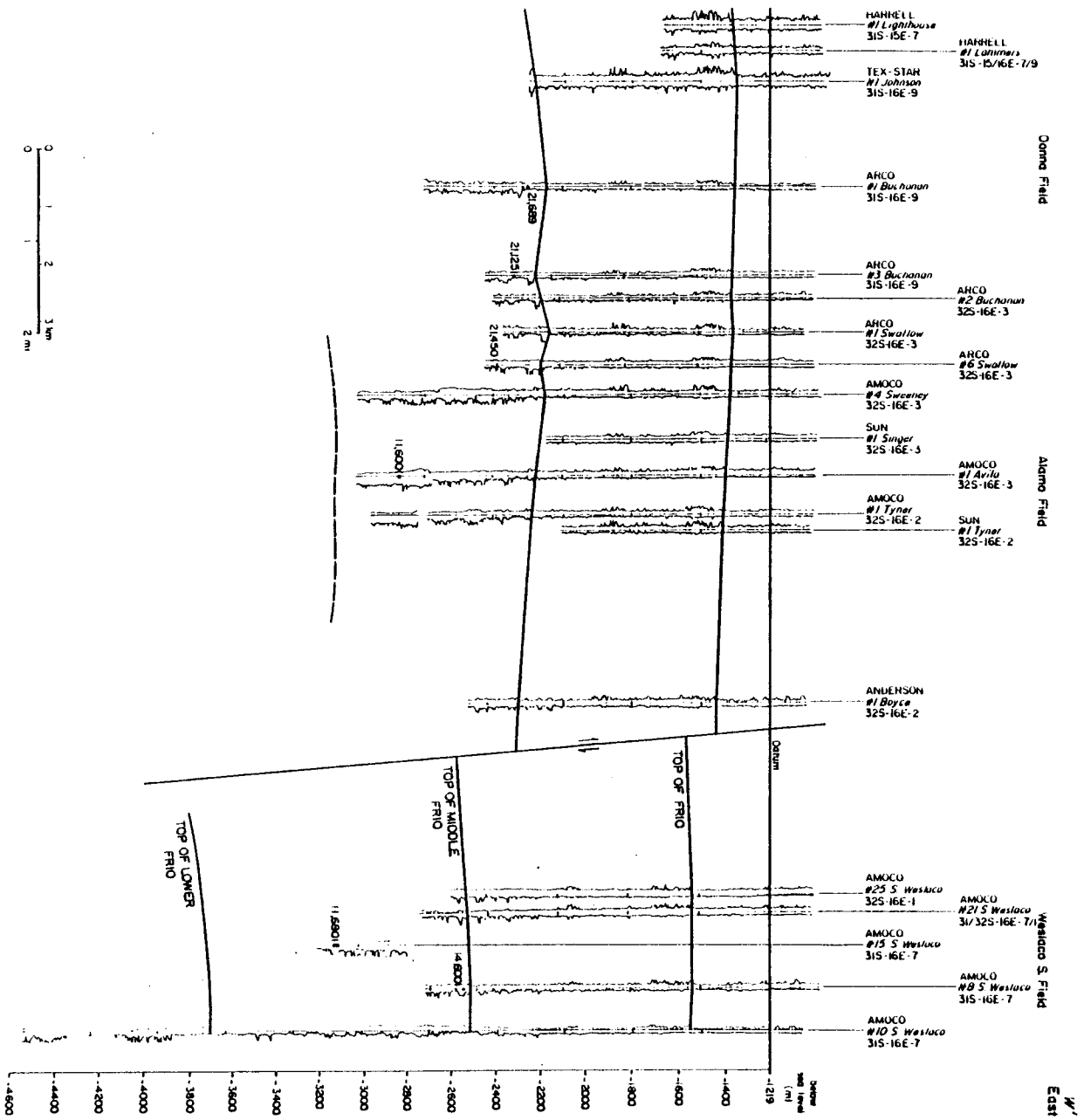


Figure II-20 (cont.)

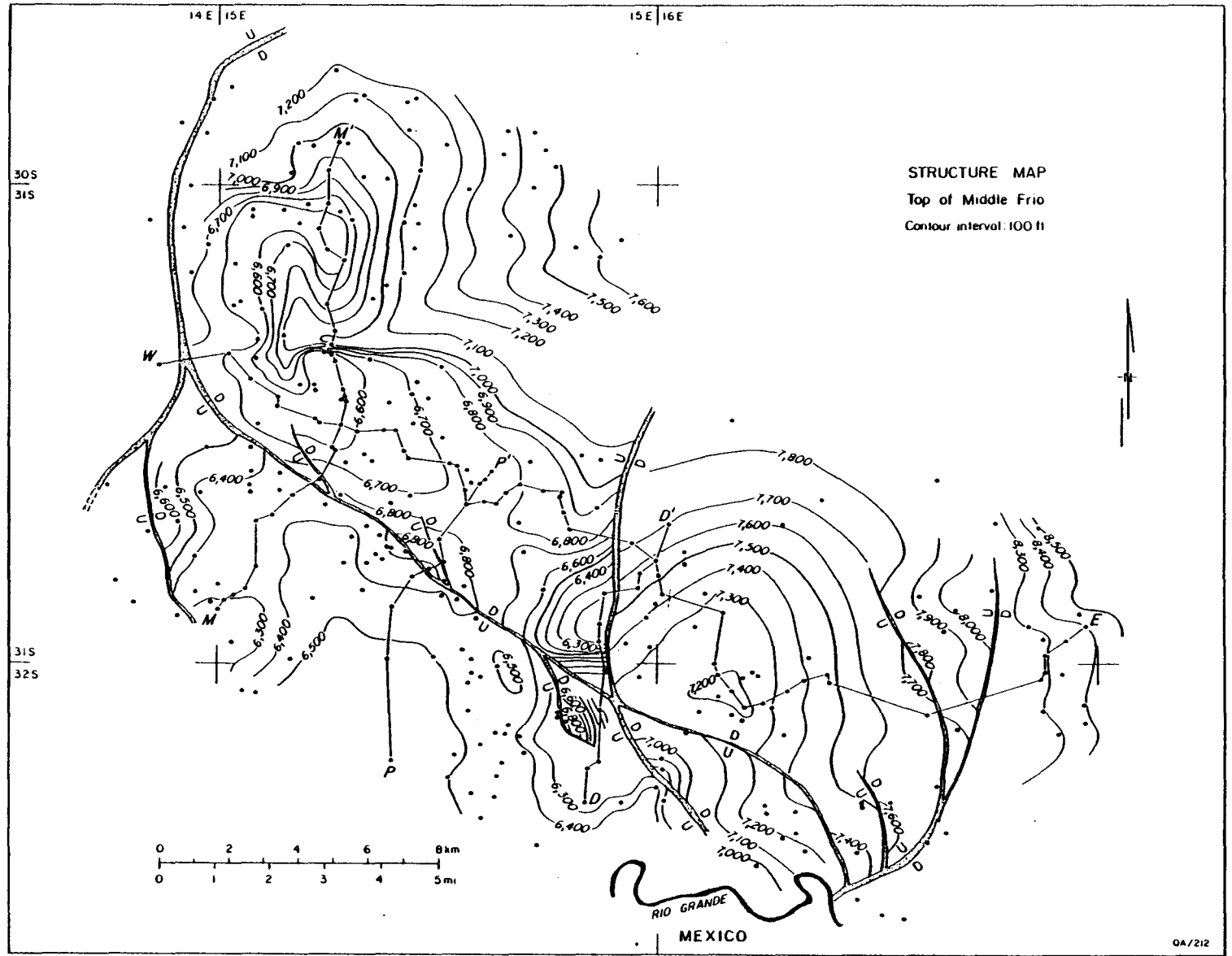
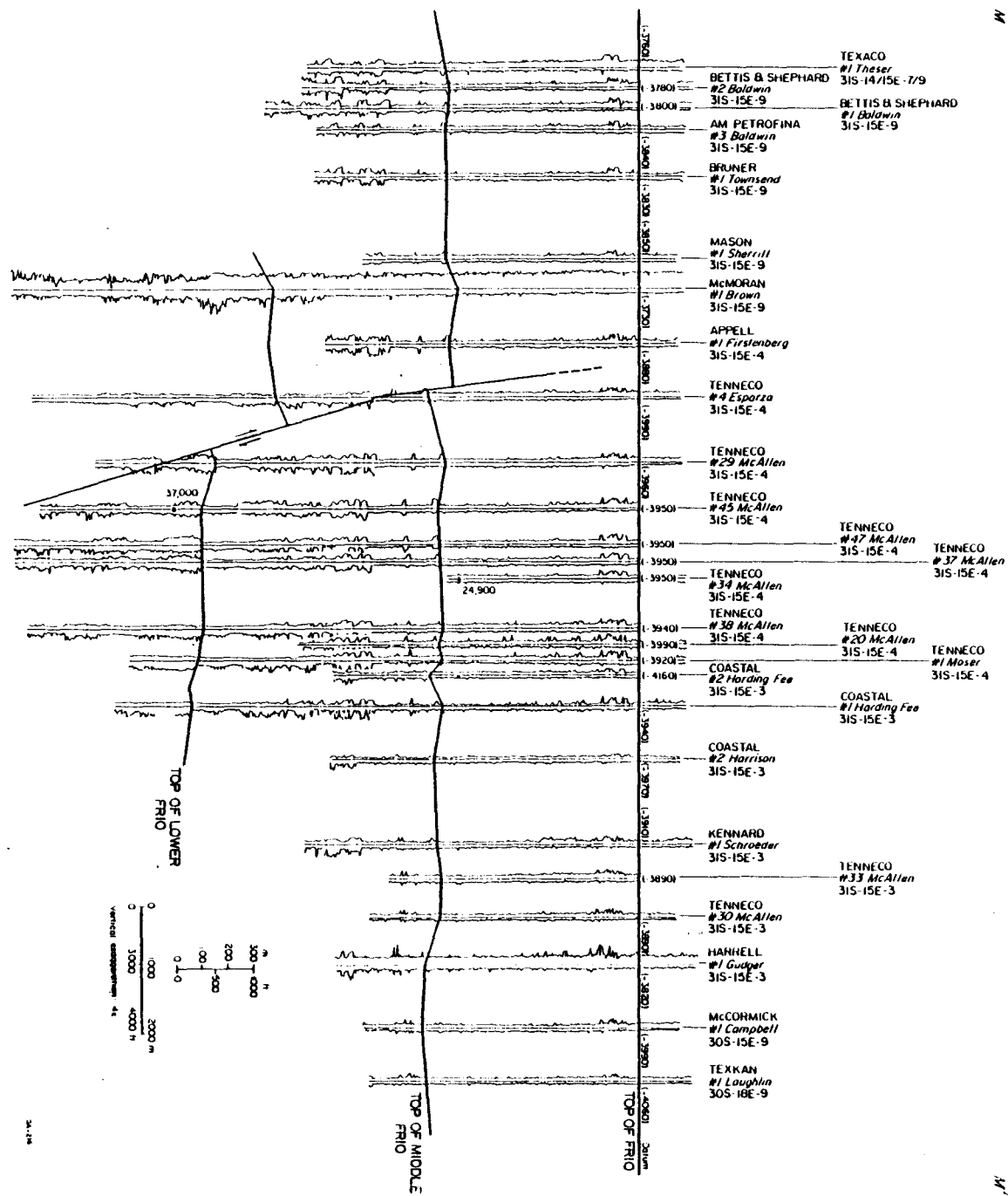


Figure II-21. Structure map of the top of the middle Frio Formation.

Figure II-22. Stratigraphic cross section through the McAllen field area; line of section on figure II-18.



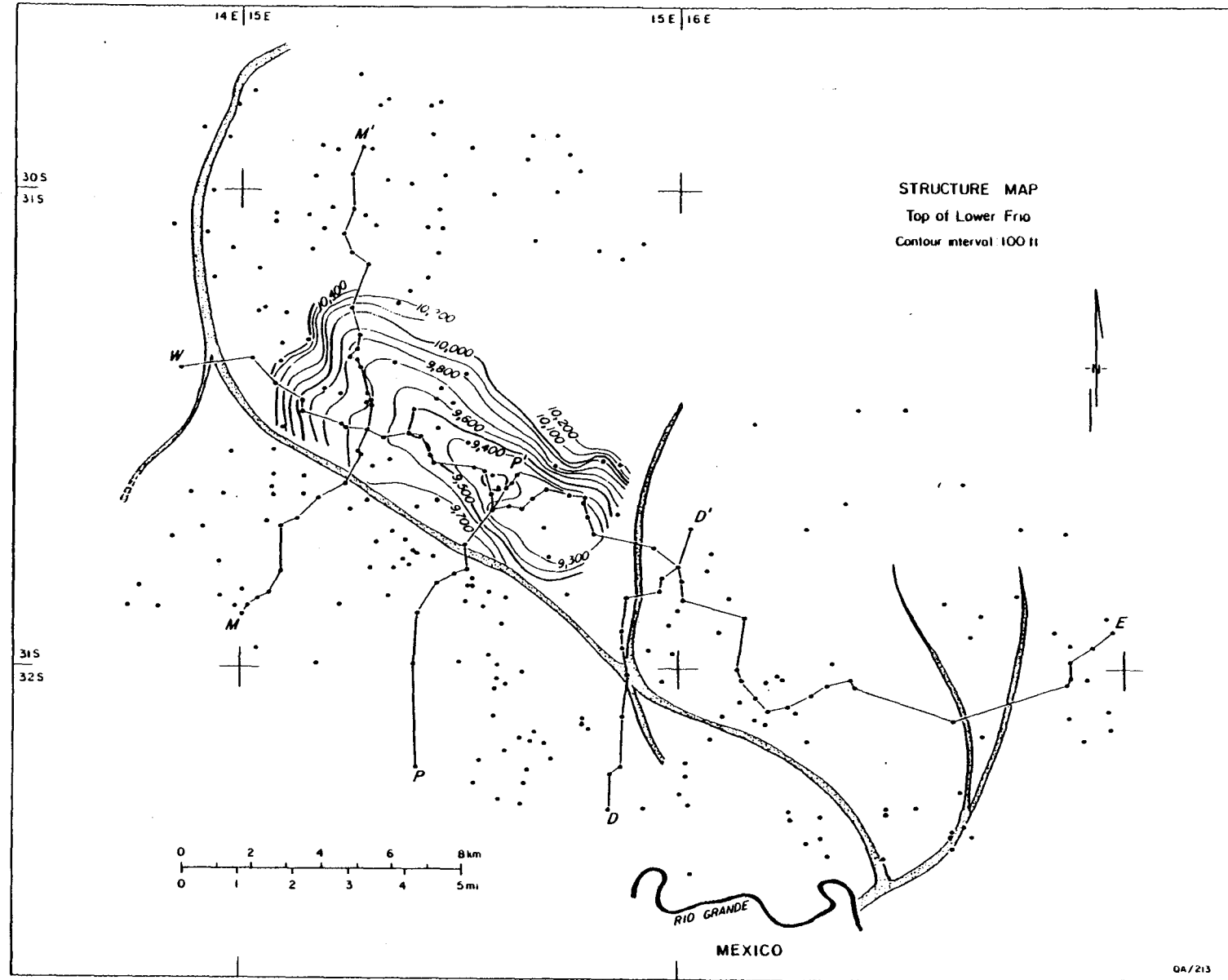


Figure II-23. Structure map of the top of the lower Frio Formation.

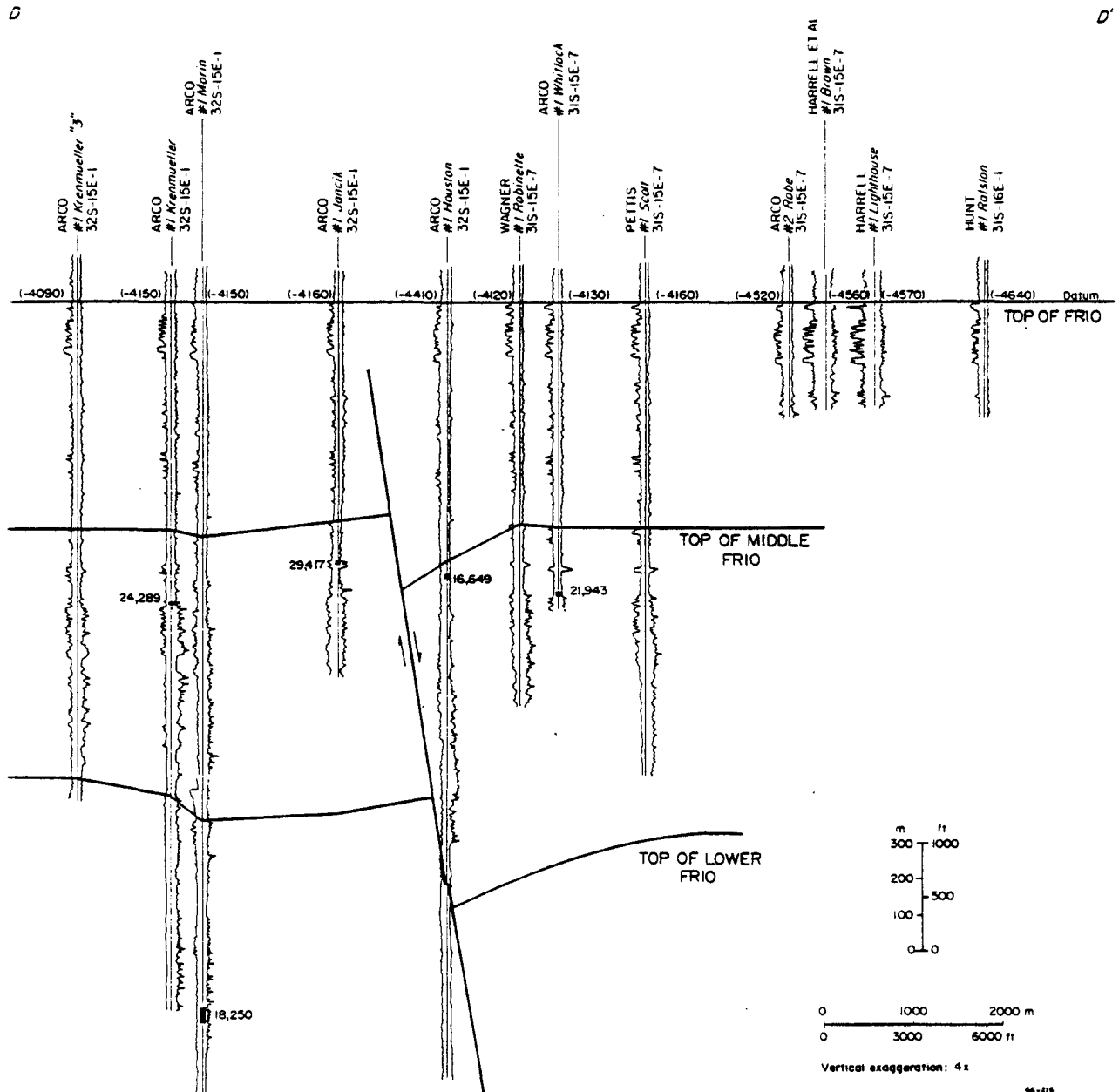


Figure II-24. Stratigraphic cross section through Donna field; line of section on figure II-18.

## Stratigraphy

The Frio Formation in the South Texas field area was deposited by the Norias delta system, a progradational sequence of sand-rich sediments located in the Rio Grande Embayment (Galloway and others, 1982). A type log (fig. II-20; Tenneco No. 36 McAllen well) shows three subdivisions made on the basis of the characteristic log patterns. Within the subunits, sandstone packages and intervening thick shale sections generally represent stacked deltaic sequences.

Mobilization of older shales and fluctuation of sediment sources greatly influenced the emplacement and development of depocenters and growth faults in the Frio delta system. The lower Frio sandstones were mainly deposited in the fault block between the McAllen and Donna faults. The few logs available from the downthrown side of the Donna fault show alternation of thin sandy and thick shaly sediments, which indicates distal delta-front or prodeltaic facies.

The middle Frio unit is characterized by several exceptionally thick progradational sequences and an offlapping pattern of several upward-coarsening cycles. The depocenter near Pharr and Shepherd fields is mainly composed of delta-front and distributary-mouth-bar sandstones. The sandstones are strongly strike-oriented in McAllen, Pharr, and Whitted fields (fig. II-25), suggesting redistribution of sediments by wave activity above former deltaic platforms. Upward and basinward migration of the depocenter indicates that the rate of deposition significantly exceeded the rate of subsidence, which resulted in continuous progradation of the shelf edge. Intercalated, wedge-like shale sections between thick sandstone sequences represent a delta-abandonment facies resulting from avulsion and diversion of major sediment sources (fig. II-20). The uppermost sandstone in the middle Frio has a primarily blocky or upward-fining sequence. The 100-ft-thick sandstone is overlain by a thick basal shale of the upper unit and is interpreted to be large-scale frontal splay deposits.

In the upper Frio, a major sand axis formed parallel to the Shepherd fault (fig. II-26) and extended downdip beyond the Donna fault. Other thick upper Frio sandstones were deposited along the upthrown side of the Shepherd fault. Either counterclockwise switching of sediment source direction or sediment input from several sources was responsible for the trend of the Shepherd fault and location of depocenters in the area. The upper Frio sandstones typically have upward-coarsening deltaic sequences in the McAllen and Pharr fields (fig. II-27) and gradually change basinward into stacked sand-rich facies. The downdip section includes thin upward-coarsening sequences overlain by thick blocky sandstone facies. The entire section is greatly expanded across the major growth faults, and thickest sandstones are developed in the Alamo field (fig. II-20).



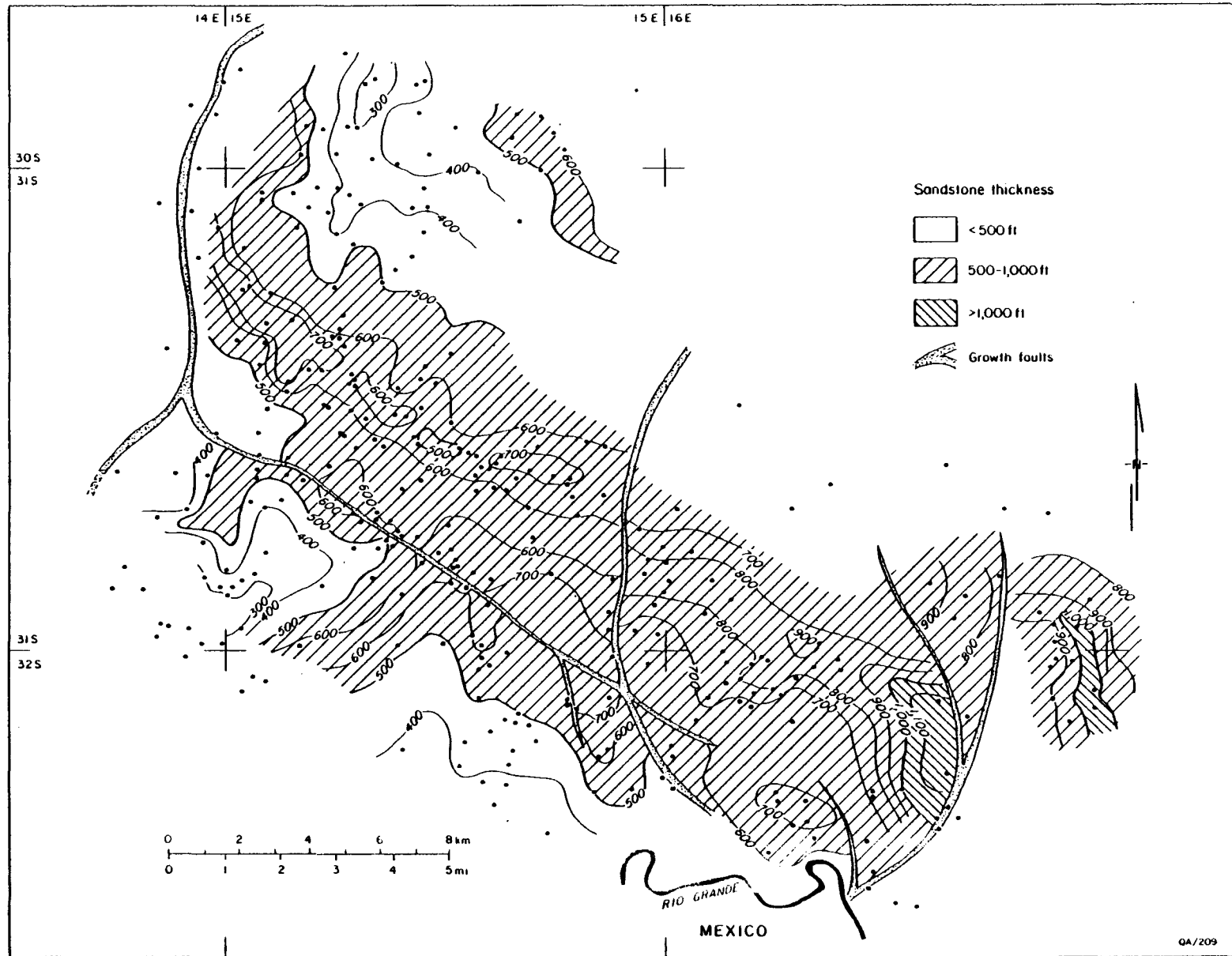


Figure II-26. Net-sandstone-thickness map of the upper Frio, South Texas field area.

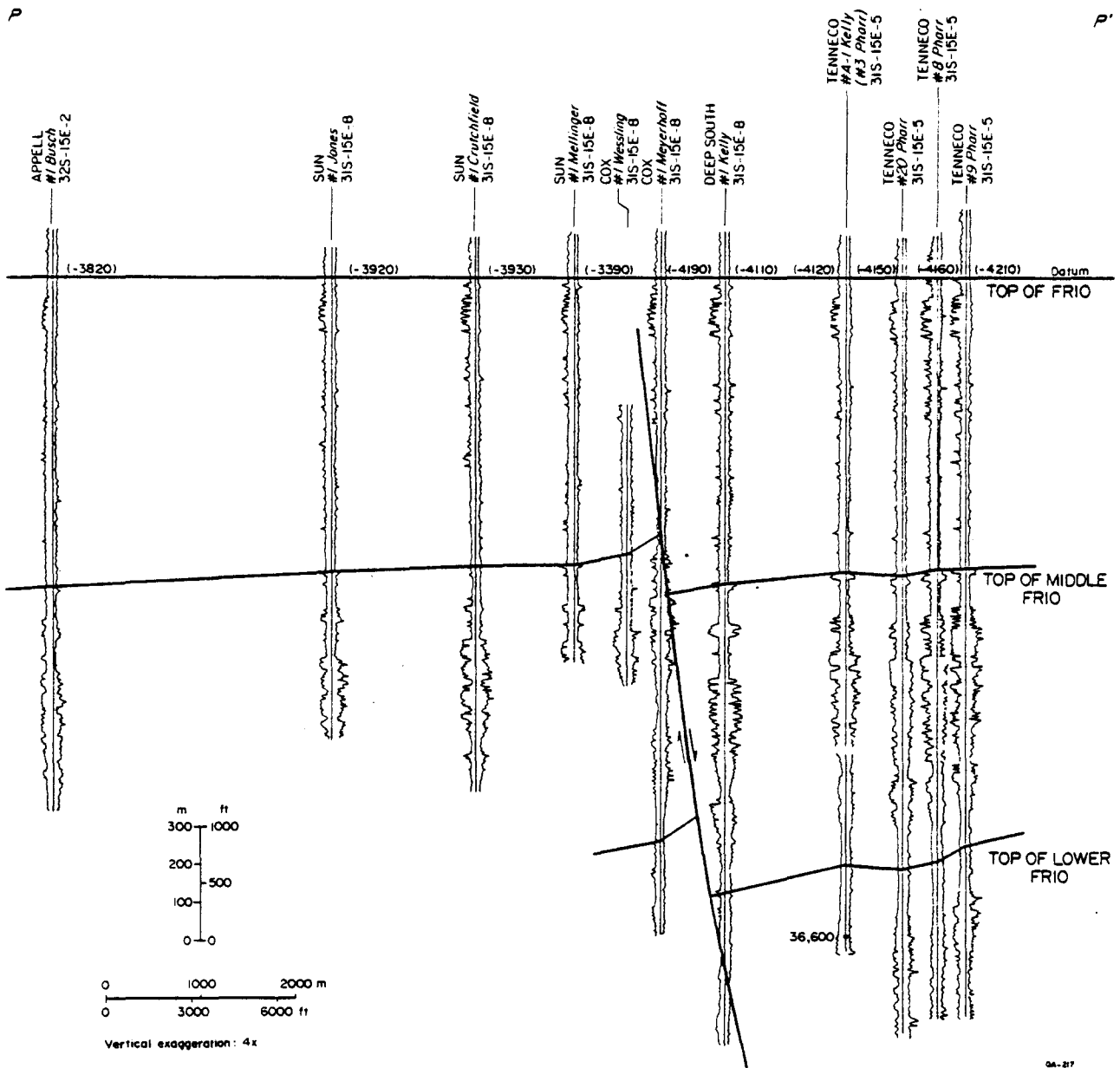


Figure II-27. Stratigraphic cross section through Pharr field; line of section on figure II-18.

## Water Chemistry

Compositions of waters produced from Donna field are similar to those of waters produced from other Frio fields in southern Hidalgo County. These sodium-chloride waters are low in total dissolved solids and therefore are low in calcium, sodium, potassium, and alkalinity and have moderately high sodium-calcium and chloride-sodium ratios.

Dissolved solids in the Donna field range from about 12,000 to 32,000 mg/L. Most of this variability can be explained by a downward decrease in salinity to a depth of approximately 9,500 ft (fig. II-28); below this depth salinity apparently increases, possibly in response to an increase in shale. Both the alkalinity and the sodium-calcium ratio have trends that are nearly identical to that of total dissolved solids. Unlike the other three parameters, the amount of calcium and the chloride-sodium ratio both increase downward to about 8,000 ft and then uniformly decrease below that depth (fig. II-28). Three potassium measurements from Donna field suggest low concentrations (<200 mg/L; table II-1) that increase slightly with depth.

## REGIONAL COMPARISON OF HYDROCHEMISTRY

Maps of total dissolved solids, ionic concentrations, and ionic ratios (figs. II-29 through II-35) illustrate the regional differences in hydrochemistry within the Tertiary sediments. The isochemical maps also assist in delineating geographic subregions where compositional differences are minor and where produced formation waters exhibit similar chemical characteristics. Because of the chemical similarities, ranges in hydrochemical constituents within the subregions generally can be predicted. Concentrations of sodium and calcium in the water vary greatly, whereas the ranges of potassium and magnesium are considerably less than those of the other two major cations (table II-1). Chloride is consistently the dominant anion in all the waters, but alkalinity is also important in distinguishing hydrochemical facies in some subregions (fig. II-34). The sulfate ion is only a minor component in most of the waters.

Because water chemistry differs at depth, maximum reported values of (1) total dissolved solids, (2) certain major ions, and (3) selected ionic ratios were used to map hydrochemical facies. By using maximum values, the maps are essentially unbiased with respect to geopressed or hydropressed sediments. This lack of bias can be demonstrated by comparing plots of Cedar Point, Alta Loma, McAllen Ranch, and North Rincon fields (figs. II-5, II-7, II-16, and II-17) and other fields where reversals in salinity trends are fully developed. Such comparison shows that the salinity maximums and minimums are similar in both hydropressed and geopressed sediments.

### Donna Field

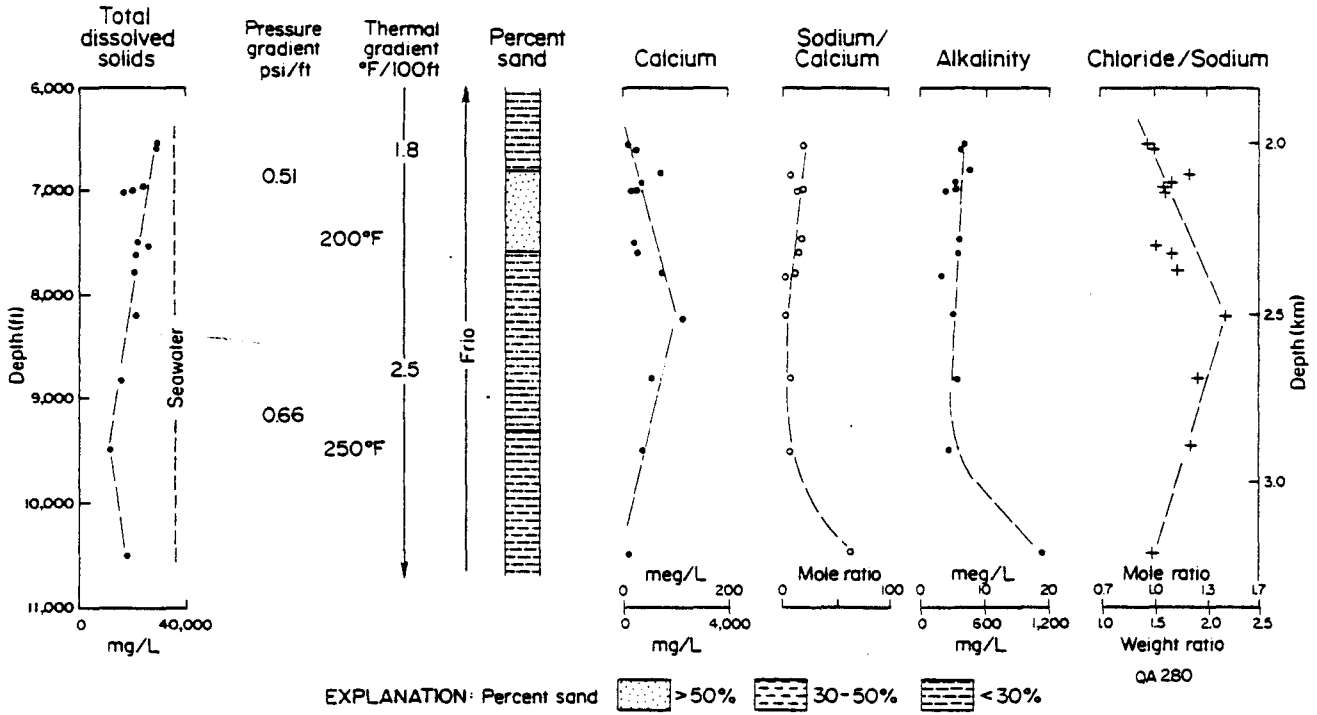


Figure II-28. Concentrations of total dissolved solids, major ions, and ion ratios in Donna field. Chemical data from unpublished files of Arco Oil & Gas Company.

## Total Dissolved Solids

Chemical reactions between the interstitial waters and the host rocks and differing diagenetic histories give rise to a wide range of water compositions and salinities. This can be demonstrated indirectly by comparing the abundance of total dissolved solids in various waters. Salinity of some waters in South Texas is about half that of normal seawater, whereas waters from the upper and lower coast are nearly seven times more saline than seawater (fig. II-29).

The salt dome province of the Houston Embayment encompasses the largest area of highly saline waters; another area having equally saline waters is in Kenedy County, northern Hidalgo County, and northeastern Starr County. Brines in the latter two counties are produced from the Vicksburg Formation, whereas those in Kenedy County are from the Frio Formation. Areas that have salinities less than 35,000 mg/L are found along the central coast in Aransas and San Patricio Counties, in some of Nueces County, in eastern Hidalgo County, and at isolated spots.

Waters having intermediate concentrations separate the areas of highest and lowest salinities; the separating boundaries can be either gradational or abrupt. The steep salinity gradient in eastern Matagorda County (fig. II-29) coincides with the western limit of salt domes; however, the abrupt boundary in northern Hidalgo and northeastern Starr Counties is not as easily explained. In both areas, the abrupt boundaries are oblique or nearly perpendicular to the regional trend of growth faults, suggesting that vertical migration of water from deeply buried sources controls the chemistry of formation waters. Water analyses from deep Wilcox reservoirs are too few to allow adequate mapping of contiguous areas. Despite this limitation, data suggest that upper coast Wilcox waters are as saline as Frio waters, whereas Wilcox waters southwest of De Witt County are uniformly low.

## Calcium

All the Tertiary formation waters contain some calcium but usually in concentrations of 5,000 mg/L or less (fig. II-30). The distribution of calcium follows a pattern consistent with that of total dissolved solids. Waters are consistently low in calcium between Brazoria and Nueces Counties and along the updip part of the Frio trend in South Texas; other areas of low calcium are found in Jefferson County and near the Rio Grande in far South Texas.

Calcium-rich waters are found in South Texas and on the upper coast near Galveston Bay (fig. II-30). In the latter area, calcium abundance in Frio waters varies between 10,000 and 12,000 mg/L. Frio waters in Kenedy County and Vicksburg waters in Hidalgo and Starr Counties contain between 20,000 and 40,000 mg/L calcium. These calcium-sodium-chloride waters typically occur where the host rocks have abundant carbonate rock fragments and carbonate

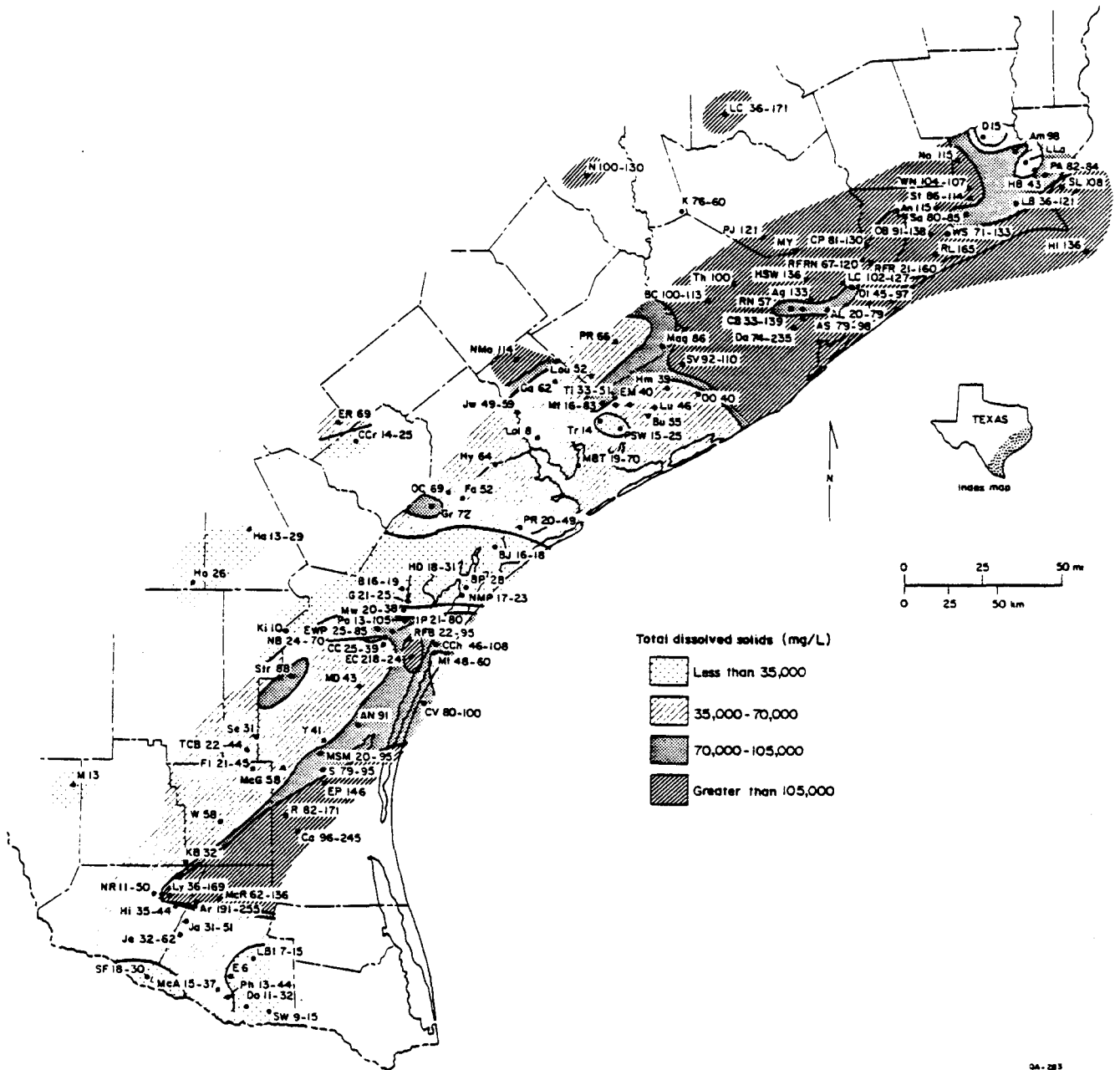


Figure II-29. Maximum concentrations of total dissolved solids in Tertiary formation waters. Chemical data from unpublished company files, Morton and others (1981), Kharaka and others (1977 and 1978), Jessen and Rolshausen (1944), and appendix II-A.



cements (Loucks and others, in press). However, the waters are deficient in bicarbonate and sulfate, making dissolution of carbonates or gypsum unlikely sources of the calcium. Possible sources of calcium include membrane filtration, conversion of smectite to illite, albitization, and decomposition of volcanic rock fragments and calcic plagioclase that are abundant in the rocks (Loucks and others, in press).

### Sodium

Large areas along the seaward margin of the coastal plain are underlain by waters having high concentrations of sodium (fig. II-31). The greatest concentrations of sodium (40,000 mg/L or more) are found in Vicksburg waters from Starr and Hidalgo Counties and in Frio waters from Brazoria, Galveston, Chambers, and Jefferson Counties. Sodium is noticeably less abundant in far South Texas (Hidalgo County), along the central coast (San Patricio and Aransas Counties), and in Matagorda County.

Sodium abundance is directly dependent on total dissolved solids in the formation water. Apart from that dependency, possible sources of sodium include cation exchange with clay minerals, conversion of smectite to illite, and dissolution of salt. Waters could be depleted in sodium if albitization was a dominant diagenetic reaction.

### Sodium-Calcium Ratio

When the molecular concentrations of sodium and calcium are compared, a pattern emerges that is similar to individual patterns of sodium and calcium (figs. II-30 and II-31) but is different in detail (fig. II-32). Most of the pore waters contain sodium and calcium in proportions between 10:1 and 100:1.

Exceptions to this are found mainly in three areas. In South Texas (Kenedy and Hidalgo Counties and adjacent areas), mole ratios are exceptionally low because the amount of calcium equals or exceeds sodium. Ratios are also low in waters along the updip Frio trend in Jackson and Wharton Counties (fig. II-32). Along the central coast between Brazoria and Nueces Counties, Frio waters are enriched in sodium with respect to calcium. The absence of salt domes and the presence of shale diapirs in this same area (fig. II-33) may partly explain the high sodium-calcium ratios. Preferential exchange of calcium for sodium in the smectite-rich shales could cause high sodium-calcium ratios in associated formation waters.

### Alkalinity

Measurements in the field of total alkalinity undoubtedly overestimate bicarbonate concentrations because weak organic (aliphatic) acid anions are present in these waters

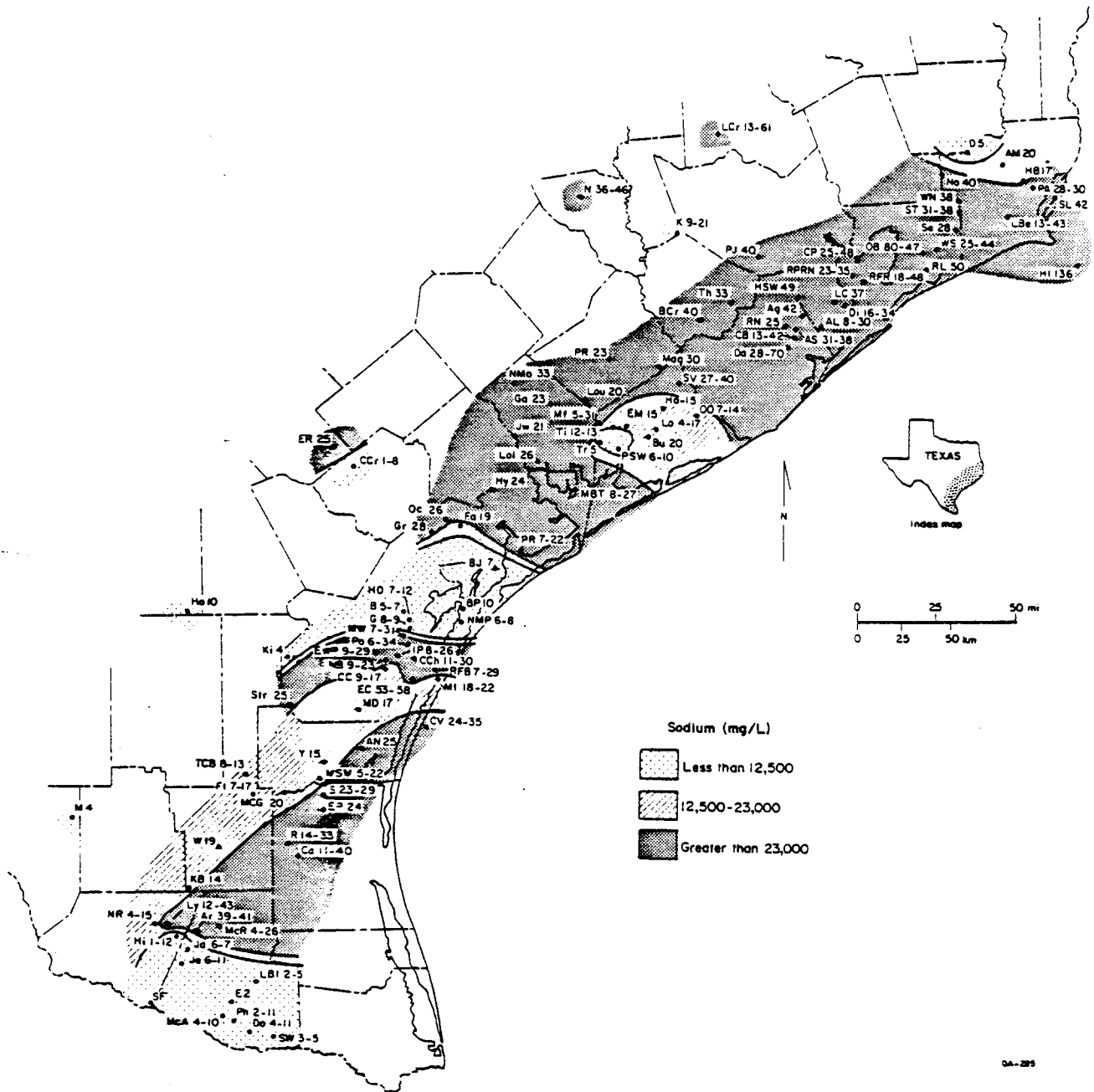
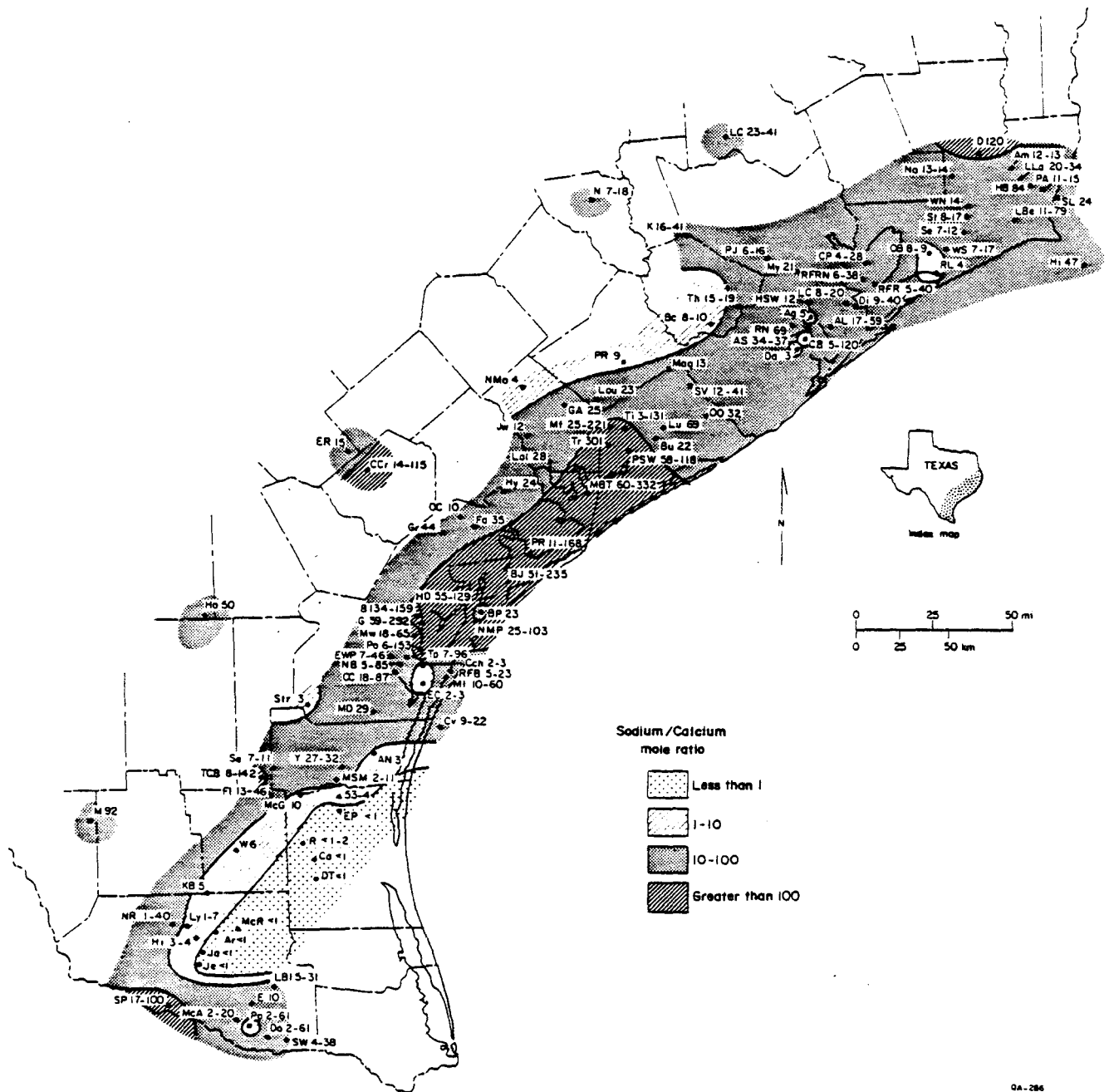


Figure II-31. Maximum concentrations of sodium in Tertiary formation waters. Chemical data from unpublished company files, Morton and others (1981), Kharaka and others (1977 and 1978), Jessen and Rolshausen (1944), and appendix II-A.



9A-286

Figure II-32. Maximum values of the sodium-calcium ratio in Tertiary formation waters. Chemical data from unpublished files, Morton and others (1981), Kharaka and others (1977 and 1978), Jessen and Rolshausen (1944), and appendix II-A.

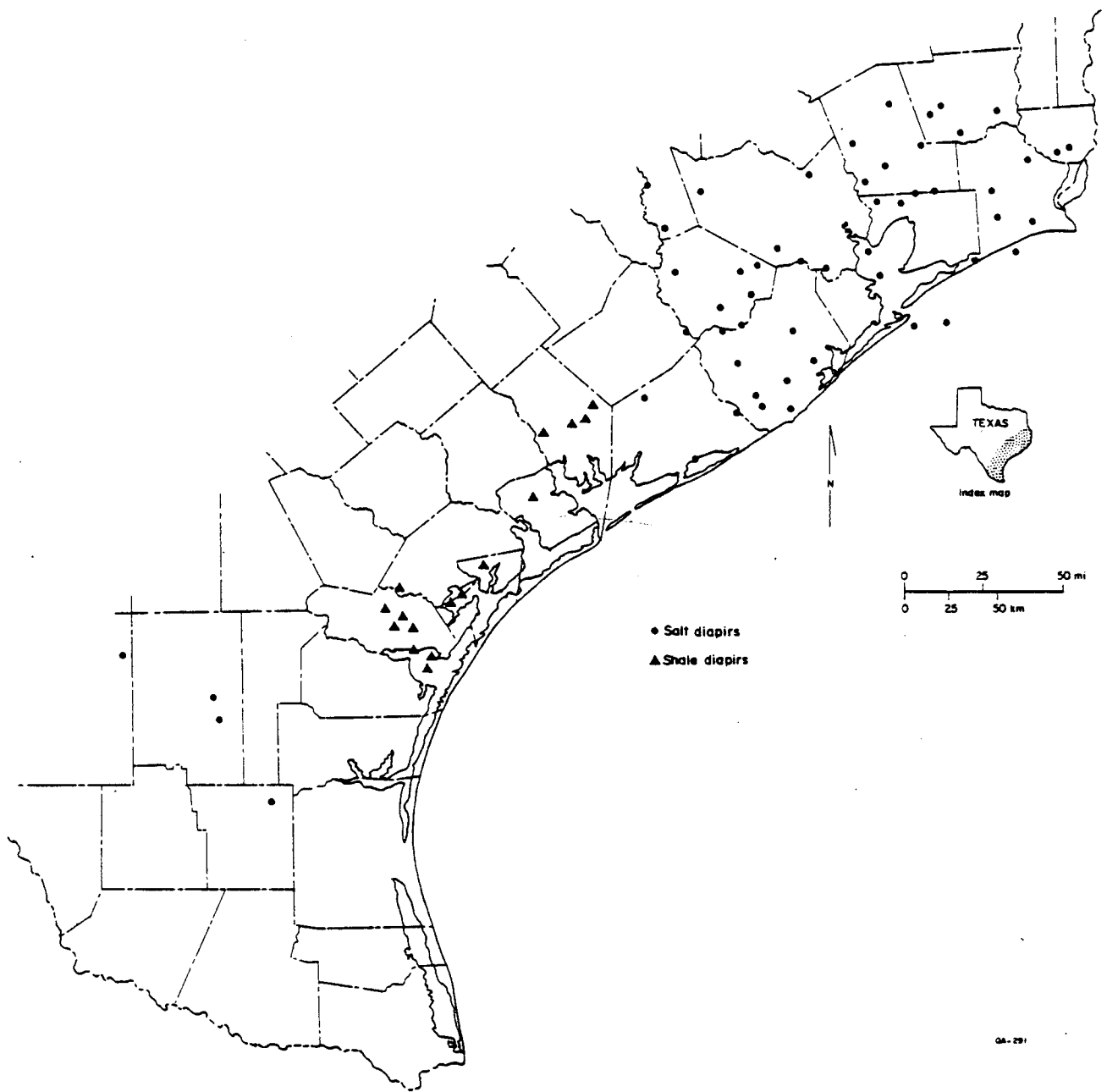


Figure II-33. Locations of known salt domes and shale diapirs beneath the Texas Coastal Plain.

(Carothers and Kharaka, 1978). Although chemically imprecise, total alkalinity and bicarbonate are used interchangeably to facilitate discussion and mapping.

Alkalinity concentrations range from 20 mg/L to nearly 3,000 mg/L and vary markedly over relatively short distances (fig. II-34). Such high variability is perhaps best explained by the many samples having low alkalinity and by the difficulty of obtaining accurate measurements. Despite these uncertainties, we can conclude that alkalinity abundance tends to cluster geographically in patterns that resemble some of the other ions. For example, it is inversely related to calcium. Alkalinity is only a minor constituent in South Texas waters, especially in Kenedy County where concentrations are extremely low. Frio waters mainly from hydro-pressured reservoirs of the upper coast also typically have low alkalinities (fig. II-34).

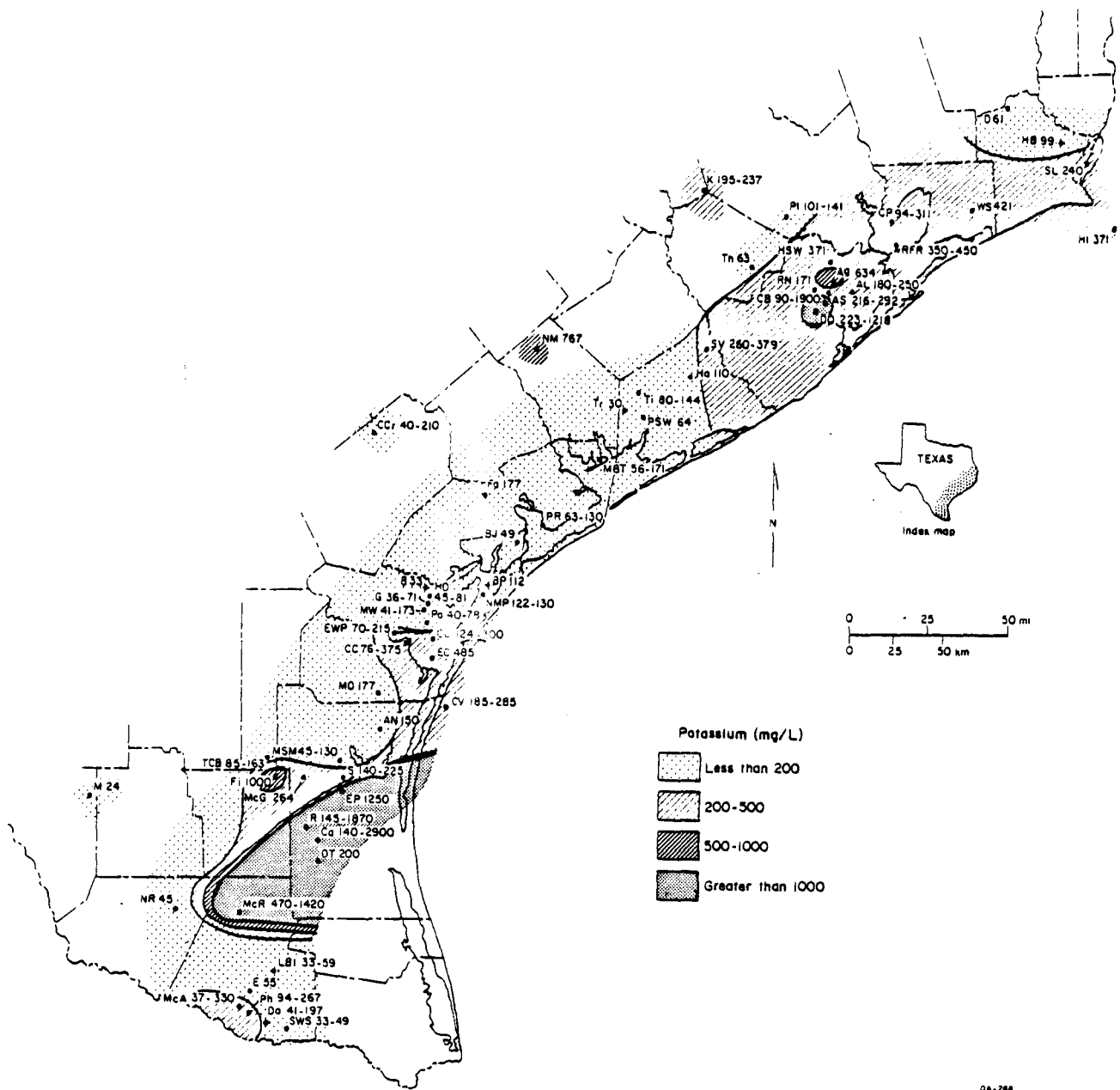
The areas of highest alkalinity are found in Jefferson County and along the central coast between Brazoria and Nueces Counties. In the latter area, sodium-calcium ratios are also high and shale diapirs are common (fig. II-33). Bicarbonate, commonly the dominant anion in interstitial waters of Gulf Coast shales (Weaver and Beck, 1971), is formed as organic material in the shale decomposes; pore waters from modern shale diapirs contain unusually high concentrations of bicarbonate (Hanor, 1981). The greater mobility of sodium and bicarbonate ions released during membrane filtration (White, 1965) may also contribute to the enrichment of these ions in formation waters. Furthermore, bicarbonate can be released within an aquifer if calcium substitutes for sodium in matrix clays (Kreitler, 1979).

Some waters containing substantial quantities of carbon dioxide are also alkaline enriched. Geopressured aquifers in the Martinez, Pleasant Bayou, and Doyle fields (fig. II-1) all produce waters having more than 6 mole percent dissolved carbon dioxide. These same waters also have alkalinities greater than 1,600 mg/L (table II-1).

#### Potassium

Potassium is a minor component in these formation waters, usually accounting for 500 mg/L or less (table II-1). Areas in which it is more abundant are limited to Kenedy and northern Hidalgo Counties in South Texas and Brazoria County along the upper coast (fig. II-35). These sites and surrounding areas are characterized by highly saline waters, which partly explains the greater potassium concentrations. Potassium feldspars in deeply buried sandstones in these areas have been leached (Loucks and others, 1981) and surrounding shales have been largely converted from smectite to illite (Freed, 1981 and 1982). These diagenetic reactions have opposite effects on abundance of dissolved potassium; the former reaction is a source, whereas the latter reaction removes substantial quantities of potassium in solution. However, potassium





QA-288

Figure II-35. Maximum concentrations of potassium in Tertiary formation waters. Chemical data from unpublished files, Morton and others (1981), Kharaka and others (1977 and 1978), and appendix II-A.

for the smectite-illite transition is provided largely by the breakdown of detrital mica and feldspars in the shales (Perry and Hower, 1972). These reactions most likely explain the increases with depth in overpressured sediments of (1) potassium in formation waters regardless of salinity changes (figs. II-4, II-12, and II-16; Morton and others, 1981) and (2) potassium oxide in sediments (Loucks and others, 1981).

#### Bromide, Chloride-Bromide Ratio, and Chloride-Sodium Ratio

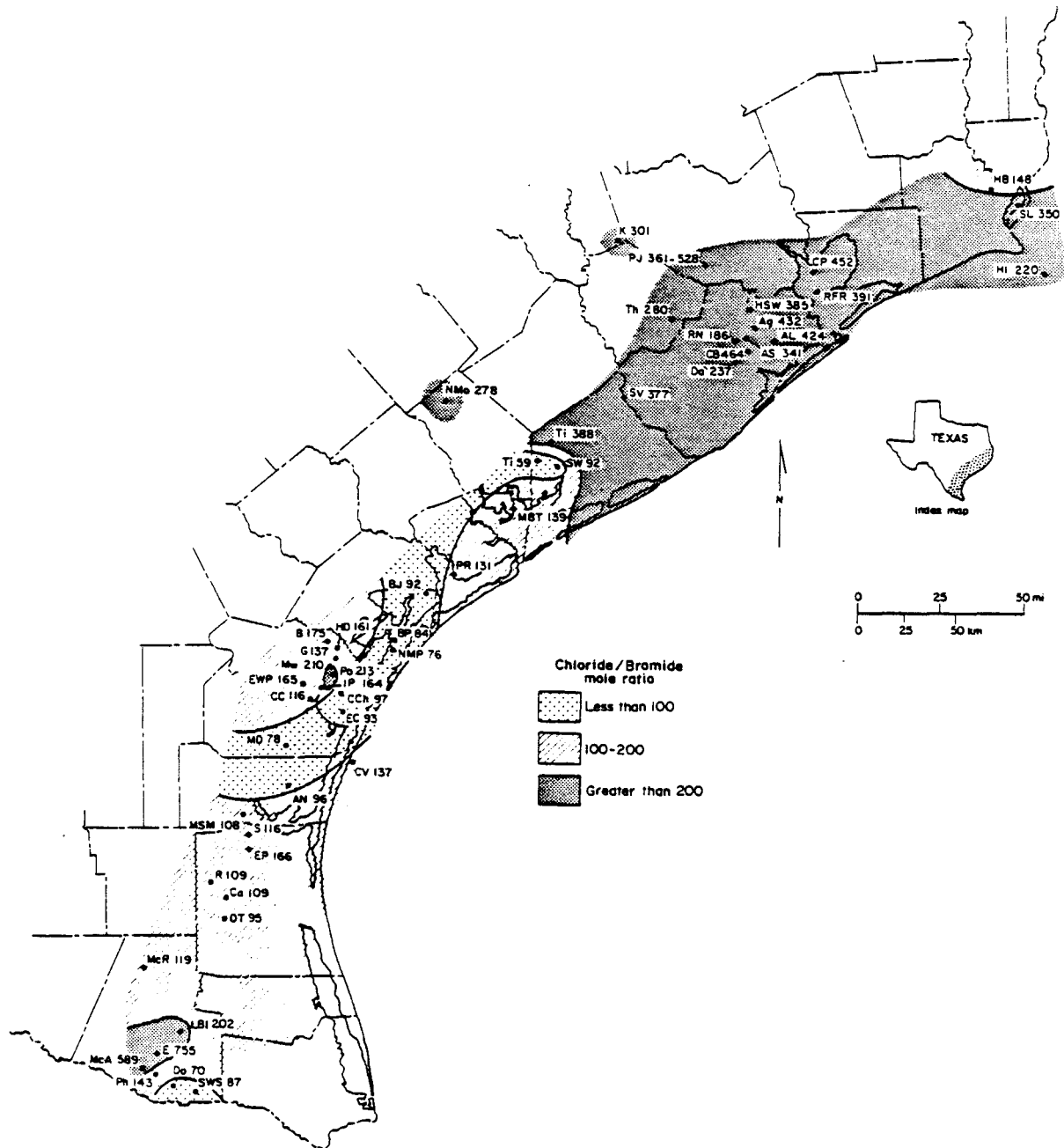
Geochemical criteria based on bromide concentrations have been used to interpret the origins of interstitial waters (White, 1965; Rittenhouse, 1967; Kharaka and others, 1978). These methods rely on the fact that bromine is rapidly concentrated in solution as seawater evaporates and salt crystals form. The precipitates, primarily halite, contain less bromine than seawater; therefore, interstitial brines that are deficient in bromine with respect to seawater are thought to be products of salt dissolution.

According to Rittenhouse (1967), five groups of waters can be identified and explained by comparing concentrations of bromide to total dissolved solids. Many of the waters analyzed for the present study have up to twice as much bromide as expected for their salinities. Rittenhouse (1967) suggested that bromide was added to such waters (group II) during early diagenesis. Almost as many Tertiary formation waters would be classified in group I as waters that have bromide in proportion to that expected for seawater.

Nearly all the waters south of Brazoria County are classified in either group I or group II. Essentially all the fields south of Nueces County produce group II waters, as do many of the fields between Matagorda and Nueces Counties. The fields producing group I waters are clustered along the central coastal region (Southwest Pheasant, Tidehaven, Headquarters, Brannon, Midway, Geronimo) or along the updip Frio trend near Corpus Christi (Harvey Deep, Portland, Indian Point, Corpus Christi).

Group III waters of Rittenhouse (1967) are produced from fields northeast of Matagorda County. These waters are characterized by total dissolved solids greater than those of seawater but bromide concentrations less than those expected by their high salinities, which are attributed to dissolved halite. The close agreement between the locations of group III waters and the presence of salt domes (fig. II-33) supports this interpretation.

When plotted geographically, the chloride-bromide ratios of formation waters (fig. II-36) provide results that are similar to those obtained from plots of bromide and total dissolved solids. Waters deficient in bromide with respect to chloride are located mainly northeast of Brazoria County, although a few fields in South Texas have high chloride-bromide ratios.



04-287

Figure II-36. Maximum values of the chloride-bromide ratio in Tertiary formation waters. Chemical data from unpublished files, Morton and others (1981), and Kharaka and others (1977 and 1978).

Waters having low chloride-bromide ratios are generally located along the central coast and in far South Texas (fig. II-36); elsewhere, calculated ratios are intermediate in value.

Kharaka and others (1978) graphically illustrated the proportions of chloride and bromide in Gulf Coast waters. Using this technique, they were able to distinguish the upper coast from the middle coast waters and explain their differences by the presence and absence of salt dissolution, respectively. The molecular ratio of chloride to sodium is also an indirect measure of the influence of salt dissolution on the salinity of formation waters. Chloride is the least reactive of the major ions; therefore, it serves as a reasonably stable basis for comparison with other dissolved species.

Subsurface waters that have been in contact with halite and that later had not been altered by chemical reactions should have chloride-sodium ratios of about 1.0. Except for the waters from a few scattered fields and from a large area in South Texas, the Tertiary formation waters do contain nearly equal amounts of sodium and chloride (table II-1; fig. II-37); chloride-sodium ratios are commonly 1.3 or less. Ratios greater than 1.3 and up to 4.5 occur in Kenedy, Hidalgo, and Starr Counties where waters are enriched in chloride with respect to sodium. However, if these waters are depleted in sodium because of albitization and enriched in calcium by the same reaction as well as by leaching of plagioclase, then the chloride-sodium ratio may not accurately reflect the processes responsible for the high chloride concentrations.

The methods used to test the hypothesis of salt solution are not totally satisfactory because the calculated ratios and cross plots represent a continuum rather than clearly segregated fields. Furthermore, they do not adequately explain the origin of the saline waters in South Texas (fig. II-29). This area of brine production is located downdip of the South Texas salt domes (fig. II-33); although evaporites may underlie the area of saline waters (Garrison and Martin, 1973), there is no supporting evidence of salt dissolution. For example, (1) salt structures have not been reported in the immediate area (Kenedy, northern Hidalgo, and Starr Counties), (2) the high-salinity trend does not extend into areas of known salt (Flowella field is near the Gyp Hill Dome), and (3) the geochemical indicators do not prove conclusively that salt dissolution caused the high chloride concentrations. Thus, the South Texas brines remain an enigma. Either the brines are salt solutions that migrated upward from great depths or other rock-water interactions, such as membrane filtration, leaching, and clay mineral diagenesis, are responsible for the ionic concentrations.

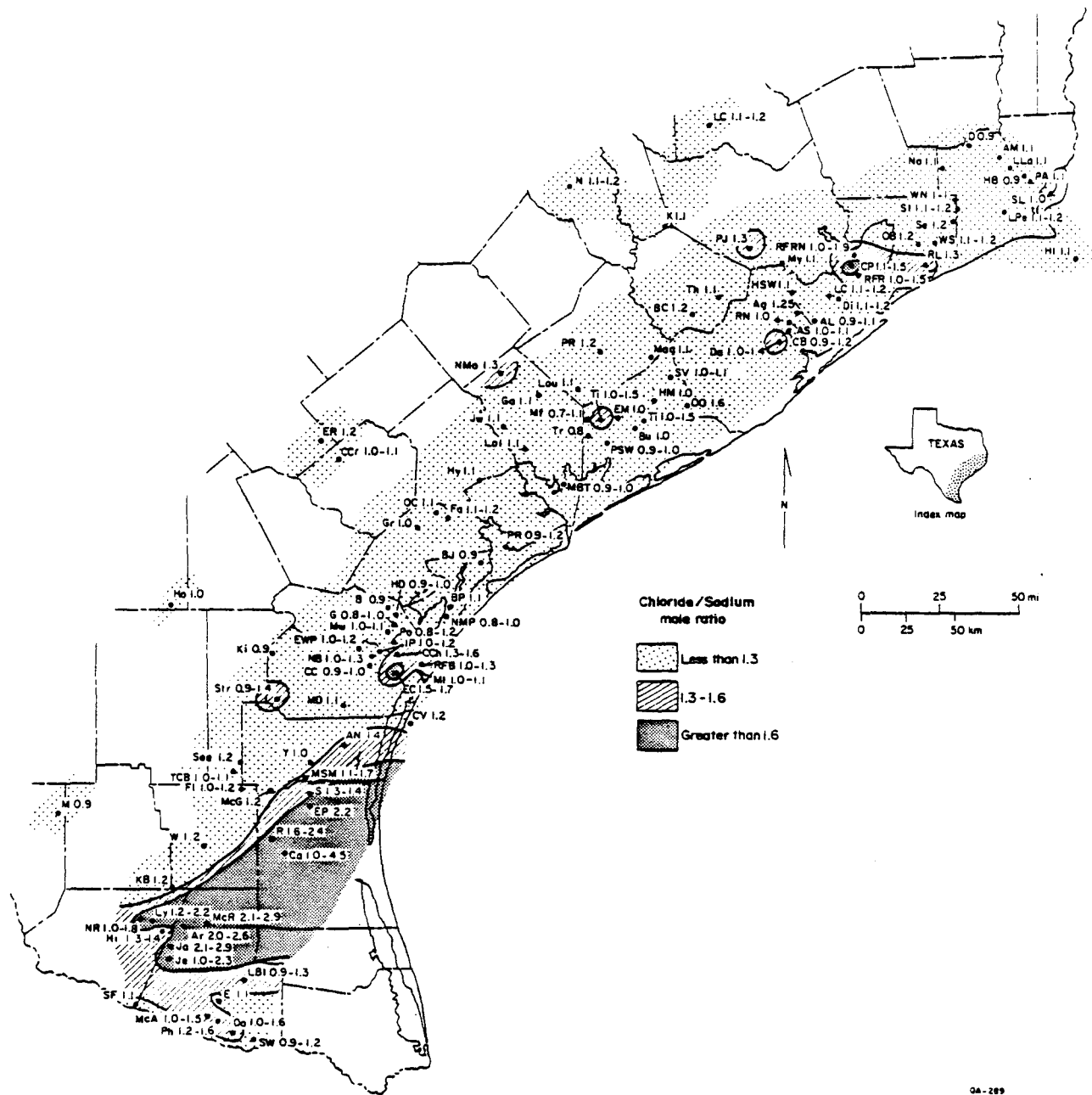


Figure II-37. Maximum values of the chloride-sodium ratio in Tertiary formation waters. Chemical data from unpublished files, Morton and others (1981), Kharaka and others (1977 and 1978), Jessen and Rolshausen (1944), and appendix II-A.

## SALINITY VARIATIONS AND FLUID FLOW

The availability of physical and chemical data on several fields within a hydrochemical subregion permits spatial comparison of temperatures, pore pressure gradients, and salinities and interpretation of possible paths of fluid movement. A more thorough analysis would require a three-dimensional synthesis that places all the thermal, kinetic, and chemical information in the proper geological setting. Although in progress, such an analysis is incomplete. In lieu of the comprehensive three-dimensional model, a simple two-dimensional analysis is presented for the Frio fields near Corpus Christi and Galveston County.

### Corpus Christi Area

Because of the depositional setting, gulfward dip, and down-to-the-basin growth faults in the Corpus Christi area, younger sediments having greater shale content are progressively encountered in a downdip direction at uniform depths of between 9,000 and 11,000 ft (Weise and others, 1981). The Frio sandstones are mainly barrier and strandplain deposits that grade downward and downdip into shelf sandstones interbedded with marine shale (Boyd and Dyer, 1964; Galloway and others, 1982). Most of the water analyses are from reservoirs within the sequence of interbedded sandstone and shale. Temperatures and pressure gradients generally increase downward and downdip (fig. II-38), accompanying the decrease in net-sandstone thickness and the stratigraphic displacement across major faults.

At all three depths (9,000, 10,000, and 11,000 ft) salinity reaches a maximum near the center of Corpus Christi Bay. This area of high average temperatures and concentrated brines occurs at the basinward limit of maximum thickness of Frio sandstones. The salinity high also overlies several shale diapirs formed by the emplacement of Vicksburg shales into overlying lower Frio sediments (Bishop, 1977). Salinities are considerably lower and interstitial pressure gradients are slightly higher in surrounding sediments at comparable depths (fig. II-38). Most of the sediments peripheral to the area of upwelling and below 10,000 ft have diluted formation waters and apparently were not intruded by the plume of ascending brines.

The variations in temperature, pressure, and salinity suggest that hot, highly concentrated brines ascended along the shale tectonic trend beneath Corpus Christi Bay and mixed with low-salinity waters in the adjacent interval of interbedded sand and shale. Waters in the overlying massive sand section are concentrated with respect to seawater, suggesting a mixture of original pore water and upwelling brines. The greater hydraulic conductivity of the thick high-permeability sandstones allowed extensive fluid movement and lateral migration of the invading

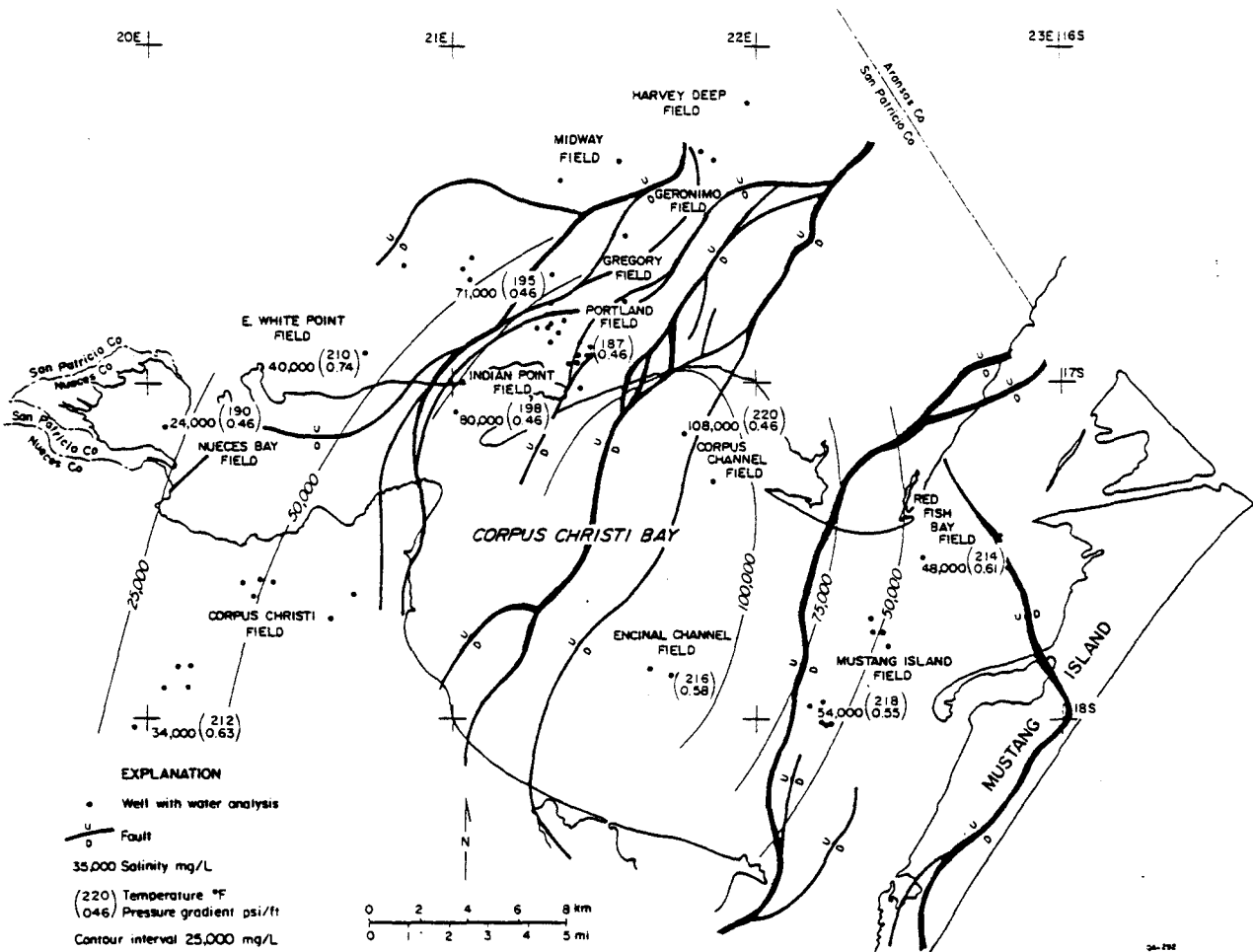


Figure II-38. Average salinities, equilibrium temperatures, and pressure gradients at 9,000 ft near Corpus Christi Bay.

water masses. The slightly lower pressure gradients in the area of possible upwelling may reflect the reduction of pore pressure accompanying fluid migration.

#### Galveston Area

Most of the water analyzed from Galveston and Brazoria Counties was produced from perforated intervals between 9,000 and 12,000 ft. At these and intermediate depths, salinity systematically decreases basinward (fig. II-39).

In the Galveston area, as in the Corpus Christi area, progressively younger sediments having increased shale content are encountered in a basinward direction as a result of regional growth faults and the environmental setting during Frio deposition. The area of interest coincides with the downdip progradational limit of the Houston delta system (Galloway and others, 1982). Thus, the basinward decrease in salinity and corresponding greater marine influence agrees with the general observation made by Timm and Maricelli (1953); however, the mass transfer of mobile ions and the chemical reactions responsible for the changes in salinity are undoubtedly more complex than this simple relationship suggests.

Nearly all of the formation waters in the Galveston area have dissolved solids greater than seawater. The landward increase in salinity coupled with the depth-related changes (figs. II-7 and II-40) suggest that concentrated brines have migrated out of the deeper parts of the basin and have contaminated the shallower formation waters. The deep high-density brines in Chocolate Bayou field occur off-structure in a salt-withdrawal basin; they also reside at the top of a sand-rich interval that marks the basinward progradation of lower Frio deltaic deposits. As in the Corpus Christi area, the higher salinities and lower pressure gradients may signify the preferred paths of lateral fluid migration through permeable beds and vertical migration along regional faults.

#### GEOCHEMICAL REACTIONS AND HYDROLOGICAL PROCESSES

The depth-dependent changes in water chemistry within an area and the regional variations in composition may be (1) responses to the current host rock formation-water system or (2) relict features introduced by fluid movement that postdates the major diagenetic events in the rock record. It is possible that both internal and external processes have influenced water composition, but if both processes were operative, one likely dominated the other. If interactions between the pore fluids and host rocks were predominant, then water chemistry should agree reasonably well with burial diagenesis of the sandstones and enclosing shales.

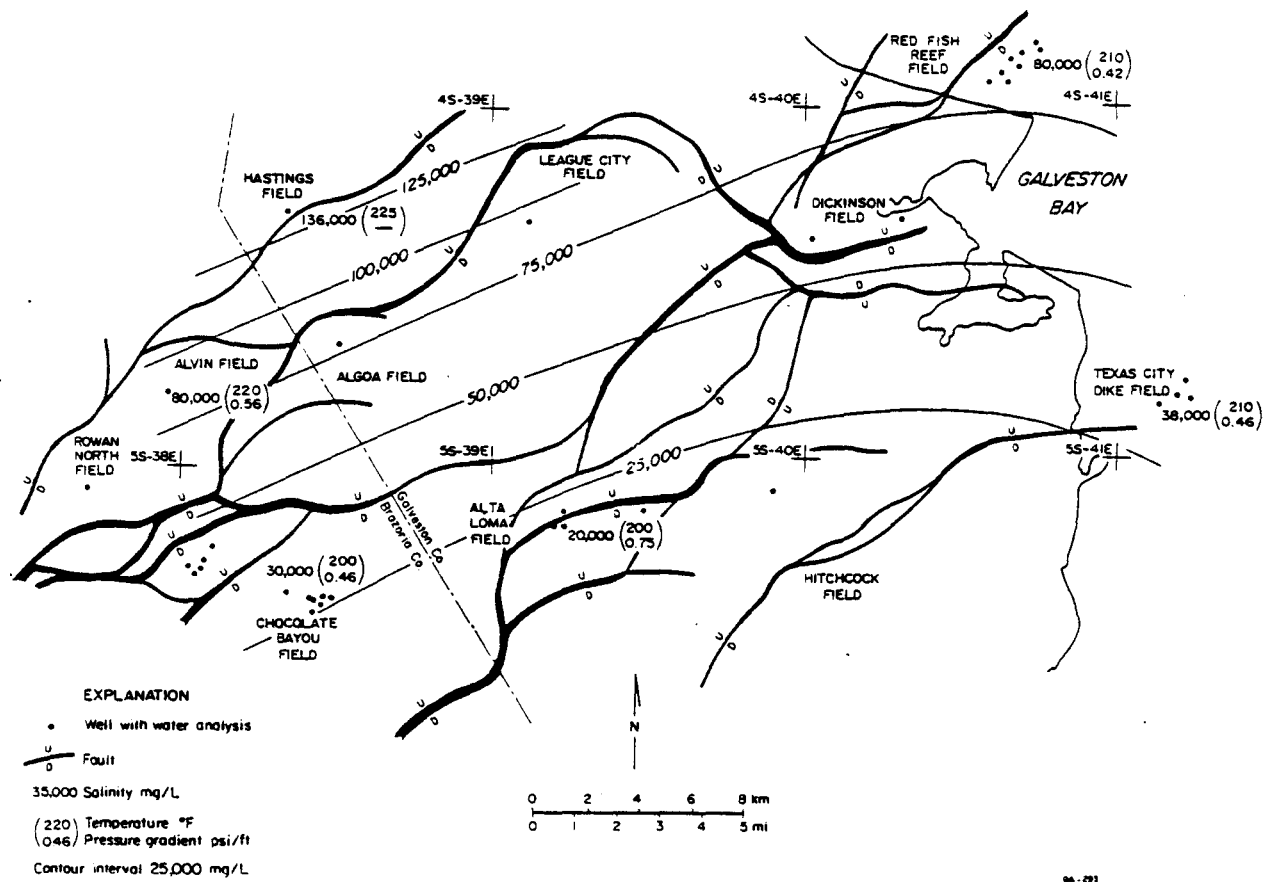


Figure II-39. Average salinities, equilibrium temperatures, and pressure gradients at 10,000 ft in western Galveston County.

However, if the waters present during burial diagenesis have been flushed from the pores and replaced by water originating elsewhere, then there might be little agreement between water chemistry and rock composition.

#### Water-Rock Interactions

Qualitative assessments of diagenetic reactions and their combined effect on adjacent pore fluids may partly explain the observed changes in water chemistry along the Texas coast. This analysis assumes (1) an open system when the reactions occurred, possibly as long as 21 mya (Morton and Long, 1982), (2) a long residence time for pore fluids, (3) little if any movement of fluids from the pores they occupied during burial diagenesis, and (4) exchange of mobile constituents regardless of nonequilibrium conditions at current depths. Such an analysis, if valid, is only a first approximation of actual conditions. More thorough explanations would require rigorous tests, including mass balance calculations and isotopic analyses of waters and specific minerals.

The abundance and source of chloride ions are fundamental keys to understanding the origins and histories of interstitial waters. Chloride is the least reactive of the dissolved species, and only a limited number of mechanisms can adequately explain concentrations or dilutions of chloride that differ greatly from those of seawater. Low chloride concentrations have been attributed to dilution by (1) deep circulation of meteoric water, (2) membrane-filtered water (White, 1965), and (3) pore water freed from clay mineral structures as a result of dehydration (Powers, 1967; Burst, 1969; Perry and Hower, 1972). Significantly greater amounts of chloride than are found in seawater are commonly attributed to either membrane concentrations or salt dissolution.

Mechanisms that dilute or concentrate connate waters, such as ion filtration and salt dissolution, are obvious causes for the major differences in total dissolved solids and individual ions of Tertiary formation waters. However, other chemical reactions may also be responsible for the specific chemical composition of formation waters. Comparison of observed hydrochemical changes at depth in the Chocolate Bayou field (Morton and others, 1981) and McAllen Ranch field (fig. II-16) with burial history and diagenetic reactions in the same areas (Milliken and others, 1981; Loucks and others, 1981) provide a basis for discussing possible water chemistry evolution.

#### Chocolate Bayou Field

Nearly all the waters produced from the Chocolate Bayou field are more concentrated than seawater (fig. II-40), and vertical changes in dissolved solids reflect greater or lesser

degrees of concentration. Furthermore, the gradual rather than abrupt changes with depth suggest fluid movement and mixing of waters rather than isolated and static hydrologic conditions.

The available literature suggests that water expelled during compaction and dehydration and subsequently filtered by semipermeable membranes causes a decrease in salinity such as was seen above the top of geopressure (10,000 ft; fig. II-38). At comparable depths, precipitation of carbonates (Milliken and others, 1981) might further deplete the waters with respect to calcium and bicarbonate.

Diffusion of brines retained in adjacent shales as compaction and ion filtration approach completion (White, 1965) may explain the increases in total dissolved solids at intermediate pressure gradients (10,000 to 14,500 ft; fig. II-38). However, diffusion is limited in scale to a few centimeters (Wood and Hewett, 1982) and therefore is an unlikely mechanism for mass transfer of dissolved constituents.

The increase in calcium relative to sodium as salinity increases over this depth interval, and the resultant decrease in the sodium-calcium ratio, could also be related to ion filtration and to the greater mobility of sodium and chloride ions because of their relatively small molecular size and monovalence (White, 1965). Additional increases in calcium below 10,000 ft, and consequent decreases in the sodium-calcium ratio with depth, could be related to albitization that occurs over the same depth interval below the 200°F isotherm (Milliken and others, 1981). Other sources of calcium include the conversion of smectite to illite (Boles, 1980; Freed, 1982), another temperature-sensitive reaction, and the leaching of carbonates at intermediate depths (Milliken and others, 1981).

Reductions in total dissolved solids, as well as calcium and sodium, at relatively high pressure gradients and temperatures (below 14,500 ft; fig. II-40) might be caused by late-stage dehydration (Burst, 1969; Perry and Hower, 1972) and the expulsion of low-salinity shale pore water that would mix with and dilute the formation waters in adjacent sandstones.

Potassium concentrations in the Chocolate Bayou field increase with depth regardless of major fluctuations in total dissolved solids (fig. II-40). Leaching of potassium feldspars (Loucks and others, 1981) and albitization (Milliken and others, 1981) within the sandstones are possible sources of the excess potassium; however, other sources include the breakdown of detrital feldspar and mica in surrounding shales (Perry and Hower, 1970).

Depth-related increases in chloride with respect to both bromide and sodium suggest dissolution of halite from adjacent salt domes or from underlying bedded salt. The increase in the chloride-sodium ratio with depth may also reflect the greater mobility of sodium and its replacement of calcium to form albite.

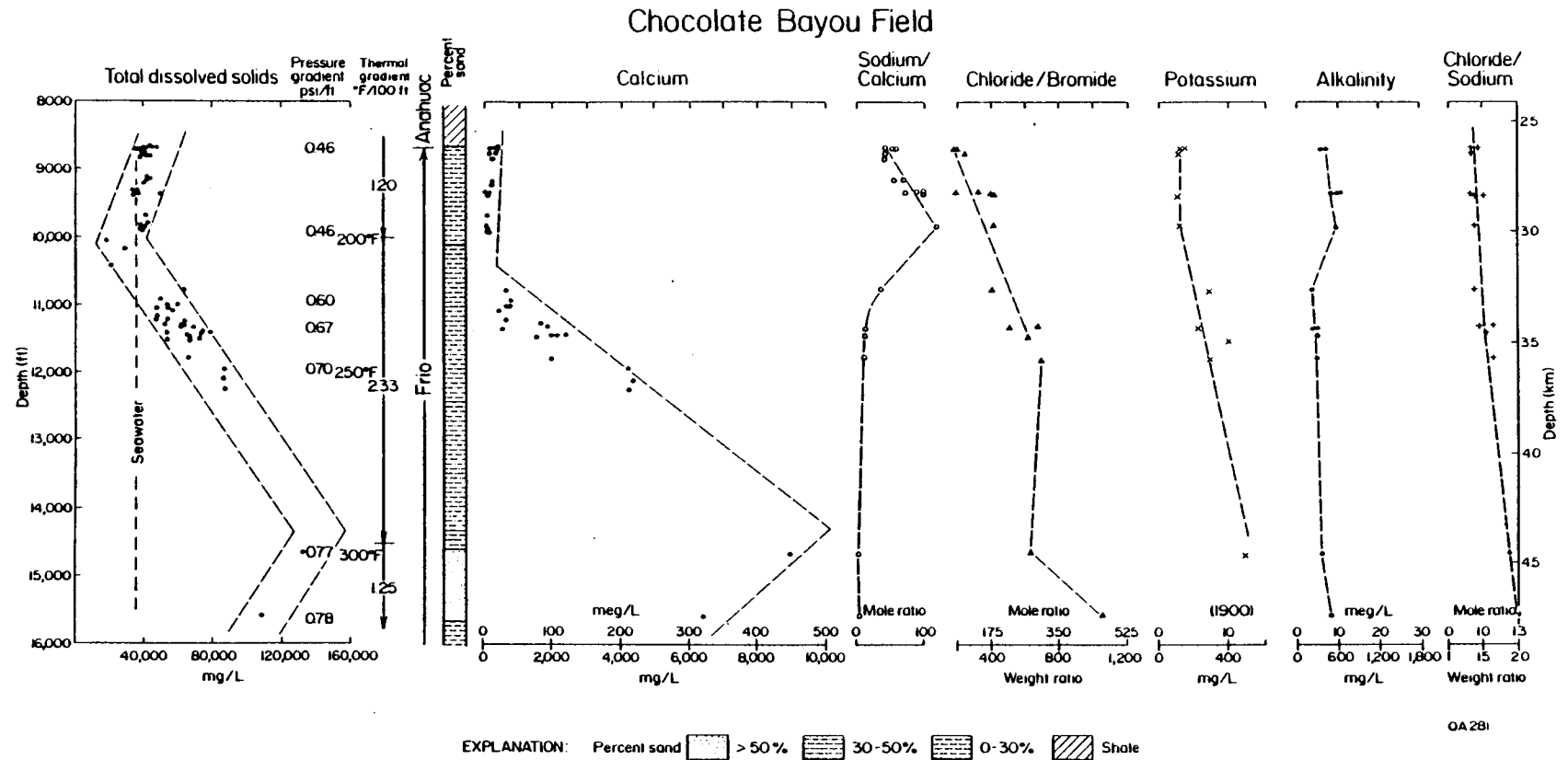


Figure II-40. Concentrations of total dissolved solids, major ions, and ion ratios in the Frio Formation, Chocolate Bayou field. Chemical data from unpublished files, Phillips Petroleum Company, Kharaka and others (1977 and 1980), and Morton and others (1981).

Despite the apparent agreement between water composition and diagenetic reactions, the evidence is not conclusive and many questions remain unanswered by this simple comparison. For example, what causes the salinity maximum in hydro pressured reservoirs near the top of the Frio sandstones and why does salinity decrease below 14,000 ft (fig. II-38)? Considering the great salinity differences in both the geopressed and hydro pressured zones and the uniform mineralogy of sediments within which some of these changes occur, it seems unlikely that any single mechanism, especially membrane filtration, can adequately explain the reversals seen at depth.

#### McAllen Ranch Field

Brines produced from the McAllen Ranch field are two to four times more concentrated than normal seawater; hence, concentrating mechanisms are responsible for the hydrochemical changes that are found at extremely high pressure gradients and high temperatures below 12,000 ft (fig. II-16). In situ membrane filtration seems an unlikely explanation because shales interbedded with sandstone and shales separating depositional sequences constitute less than one-third of the entire productive interval (fig. II-16). Flushing of concentrated brines from the underlying Jackson shales is possible, but there is no evidence to support this conclusion.

The variations in calcium with depth in the McAllen Ranch field (fig. II-16) are equally difficult to explain on the basis of diagenetic history. According to Loucks and others (1981), albitization occurs at relatively shallow depths (4,000 to 6,000 ft) and only ferroan calcite forms at depths below 12,000 ft. They also showed that calcium oxide is highly variable at depth and has no systematic trend. Furthermore, the 80-percent conversion of smectite to illite in mixed-layer structures is reached at about 9,000 ft. Therefore, neither alteration of plagioclase nor transformation of clay minerals would be likely causes of the increase and decrease in calcium between 12,000 and 14,000 ft.

Interactions of pore waters with adjacent sediments also fail to explain the general increase in potassium or the uniformity of the chloride-bromide ratio with depth (fig. II-16). Potassium feldspar is uniform through the depth of interest (Freed, 1981), whereas the potassium oxide trend (Loucks and others, 1981) resembles the trend of dissolved solids but not that of potassium. The chloride-bromide ratio also fails to explain the origin of these brines.

#### Alternative Interpretations

If the modern formation waters acquired their chemical characteristics largely from external sources and were only marginally influenced by the precipitation and dissolution of adjacent minerals, then large-scale mass transport of fluids is required. Wood and Hewett

(1982) described a theoretical model that predicts fluid circulation when porous sedimentary layers cross thermal gradients. Postdepositional temperatures and bed attitudes in the Gulf Coast Basin are theoretically sufficient to cause thermal convection, but the isotropic properties and plane-parallel boundaries of the simple model (Wood and Hewett, 1982) are unrealistic and do not approximate actual boundaries and flow paths (faults, microfractures, facies changes, thickness variations and aquifer heterogeneities) that exist in the subsurface.

Despite the model's simplicity, large-scale convection can be interpreted using the chemical data. For example, the common correspondence of salinity changes with significant lithologic changes (figs. II-5, II-7, II-14 through II-17, II-28, and II-40) suggests that thick (thousands of feet) sedimentary sequences control the flow paths and consequently the mixing of water masses. Salinity maxima usually coincide with the thick sand-rich intervals bounded above and below by shale or sediments having low percent sand. The influence of shale diagenesis that may have preceded migration is seen in the decreases in salinity at high temperatures and pressures. Dilution processes are probably associated with the smectite-illite conversion and multiple-stage dehydration widely reported for these rocks (Burst, 1969; Freed, 1981 and 1982; Perry and Hower, 1970 and 1972).

In summary, the modern formation waters probably originated deeper in the basin, where they came in contact with adjacent or underlying salt. The concentrated brines migrated vertically along faults and entered the more porous sediments (thick sandstone sequences), where they mixed with other water masses to produce the current compositions. Dilution of ascending waters occurred along the stratal boundaries of the flow paths, where shale percents increase and clay mineral reactions are of greater importance.

Exceptions to this generalized history are found in southern Hidalgo County (McAllen, Donna, South Weslaco, and La Blanca fields) and northeast of Corpus Christi (Geronimo, Brannon, Harvey Deep, Nine Mile Point, and Blackjack fields), where modern geopressured waters have salinities less than that of seawater. Apparently these areas were never influenced by salt-enriched brines; therefore, shale diagenesis has diluted the waters from their original compositions. The dominant driving forces of fluid migration are uncertain and both pressure-dependent and temperature-dependent processes may have operated in sequence.

## CONCLUSIONS

The chemistry of modern waters produced from sandstones of Frio and Vicksburg age varies areally as well as with depth. Water compositions and concentrations of dissolved species typically change according to associated pressure regimes and sometimes according to

depth-related changes in lithology and thermal gradients. Within a field area and below the interval of greatest meteoric mixing, salinities decrease with depth down to the top of geopressure (0.5 psi/ft). Below that depth, essentially two trends occur.

The most common trend occurs where intermediate pressure gradients (0.5 to 0.75 psi/ft) occupy a thick (several thousand feet), usually sand-rich sedimentary sequence. In those areas (Willow Slough, Cedar Point, Red Fish Reef, Chocolate Bayou, Alta Loma, Maude B. Traylor, Tijerina-Canales-Blucher, and North Rincon fields), salinities increase with depth below the top of geopressure and then decrease where pore pressure gradients are even higher (>0.75 psi/ft). Maximum and minimum salinities in both hydro pressured and geopressed aquifers are comparable if these trends are present. The second and least common trend occurs where intermediate pressure gradients are absent or poorly developed and high pressure gradients (>0.75 psi/ft) are encountered less than 1,500 ft below the top of geopressure. In these areas (Portland, Corpus Christi, and Red Fish Bay fields), salinities continue to decrease below the top of geopressure, albeit at a slower rate than in the overlying hydro pressured sediments.

Even though compositional differences are great on a regional scale, specific ions and ionic ratios behave similarly in most areas. For example, the sodium-calcium ratio is most sensitive to changes in calcium. The ratio reaches a maximum near the top of geopressure, where calcium is least abundant, and decreases with depth because calcium increases more rapidly than does sodium. Changes in alkalinity also correspond closely to the sodium-calcium ratio and are inversely related to the trend of calcium. Potassium concentrations, the chloride-bromide ratio, and the chloride-sodium ratio of geopressed brines commonly increase with depth.

Areal changes in water chemistry are controlled by the regional geology. Upper coast waters typically contain abundant dissolved solids and sodium, moderate amounts of calcium, and minor amounts of potassium; alkalinity varies considerably, probably because of aliphatic acid anions. These waters, which occur within the Houston Embayment, are dominantly influenced by dissolution of adjacent salt diapirs or of underlying salt deposits buried at great depths. Middle coast waters have low to intermediate dissolved solids and sodium, low calcium and potassium, and high alkalinities. These waters generally coincide with the area of shale diapirs, and some apparently have never been intruded by halite-enriched brines. Frio and Vicksburg sandstones in Kenedy County and surrounding areas contain calcium-sodium-chloride waters having high dissolved solids, calcium, sodium, and potassium but low alkalinity. In far South Texas, waters are generally depleted in dissolved solids, calcium, sodium, and potassium and have low to moderate alkalinities.

Boundaries that separate the hydrochemical subregions are both gradual and abrupt. Sharp boundaries may coincide with deep-seated structural discontinuities that form the margins of the Houston and Rio Grande Embayments; another discontinuity is located in the vicinity of northern Starr and Hidalgo Counties.

Most of the waters produced from deep Tertiary sandstones are concentrated in comparison to seawater and thus appear to have been influenced by the vertical migration of salt-enriched brines. The waters undoubtedly have been buffered by the diagenetic reactions of adjacent host rocks, but the mass transfer of brines probably postdated burial diagenesis in the sandstones and shales. Compositions of waters diluted with respect to seawater probably result from either meteoric mixing or alteration of enclosing shales, or both. Ion filtration and base exchange of ions during compaction, as well as dehydration associated with clay mineral transformations (mixed-layer smectite to illite), may have played a dominant role in the evolution of low-salinity waters.

#### ACKNOWLEDGMENTS

This study was made possible by many individuals and companies that furnished chemical analyses and water samples, provided field assistance, and arranged for sampling of the selected wells. The cooperation of the following companies is gratefully acknowledged.

Amoco Production Company	Hunt Oil Company
Andover Oil Company	Lawbar Petroleum Company
Anschutz Corporation	Maynard Oil Company
Arco Oil & Gas Company	Mitchell Energy Corporation
Chevron U.S.A., Incorporated	Mobil Producing, Texas and New Mexico
Cities Service Company	Patrick Petroleum Company
Coastal Corporation	Phillips Petroleum Company
Conoco, Incorporated	Prudential Drilling Company
Edwin L. Cox	Reading and Bates Petroleum Company
Exxon Company, U.S.A.	Royal Oil and Gas Corporation
Forest Oil Corporation	Shell Oil Company
Fort Worth Oil & Gas Company	Sun Production Company
Galaxy Oil Company	Superior Oil Company
Getty Oil Company	Tenneco Oil Company
Goldston Oil Corporation	Texaco, Incorporated
Michel T. Halbouty	Texas Oil and Gas Company
Jake L. Hamon Company	Texas International Petroleum Company
Houston Natural Gas Company	Union Texas Petroleum Corporation
Houston Oil and Minerals	Wainoco Oil and Gas Company

Water samples for this study were collected by James F. O'Connell, and chemical analyses were performed by Dorothy Gower under the supervision of Clara Ho, Mineral Studies Laboratory of the Bureau of Economic Geology. The text was typed by Jana McFarland under the direction of Lucille C. Harrell, and illustrations were prepared by Jamie McClelland, Barbara Hartmann, and Mark Bentley under the direction of Dan F. Scranton. Funding for this research was provided by the U.S. Department of Energy, Division of Geothermal Energy, under Contract No. DE-AC08-79ET27111.

#### REFERENCES

- Bishop, R. S., 1977, Shale diapir emplacement in South Texas, Laward and Sherriff examples: Gulf Coast Association of Geological Societies Transactions, v. 27, p. 20-31.
- Boles, J. R., 1980, Calcium budget in Frio sandstones, southwest Texas (abs.): American Association of Petroleum Geologists Bulletin, v. 64, p. 678.
- Boyd, D. R., and Dyer, B. F., 1964, Frio barrier bar system of South Texas: Gulf Coast Association of Geological Societies Transactions, v. 14, p. 309-322.
- Burst, J. F., 1969, Diagenesis of Gulf Coast clayey sediments and its possible relation to petroleum migration: American Association of Petroleum Geologists Bulletin, v. 53, p. 73-93.
- Carothers, W. W., and Kharaka, Y. K., 1978, Aliphatic acid anions in oil-field waters--implications for origin of natural gas: American Association of Petroleum Geologists Bulletin, v. 62, p. 2441-2453.
- \_\_\_\_\_, 1980, Stable carbon isotopes of  $\text{HCO}_3^-$  in oil field waters, implications for the origin of  $\text{CO}_2$ : Geochimica et Cosmochimica Acta, v. 44, p. 323-332.
- Collins, J. W., 1968, The geology of the McAllen-Pharr field area, Hidalgo County, Texas: Gulf Coast Association of Geological Societies Transactions, v. 18, p. 81-97.
- Freed, R. L., 1981, Shale mineralogy and burial diagenesis of Frio and Vicksburg Formations in two geopressed wells, McAllen Ranch area, Hidalgo County, Texas: Gulf Coast Association of Geological Societies Transactions, v. 31, p. 289-293.
- \_\_\_\_\_, 1982, Clay mineralogy and depositional history of the Frio Formation in two geopressed wells, Brazoria County, Texas: Gulf Coast Association of Geological Societies Transactions, v. 32, p. 459-463.
- Galloway, W. E., Hobday, D. K., and Magara, Kinji, 1982, Frio Formation of the Texas Gulf Coast Basin--depositional systems, structural framework, and hydrocarbon origin, migration, distribution, and exploration potential: The University of Texas at Austin, Bureau of Economic Geology Report of Investigations No. 122, 78 p.
- Garrison, L. E., and Martin, R. G., 1973, Geologic structures in the Gulf of Mexico Basin: U.S. Geological Survey Professional Paper 773, p. 1-29.

- Hanor, J. S., 1981, Composition of fluids expelled during compaction of Mississippi delta sediments: *Geo Marine Letters*, v. 1, p. 169-172.
- Jessen, F. W., and Rolshausen, F. W., 1944, Waters from the Frio Formation, Texas Gulf Coast: *American Institute of Mining and Metallurgical Engineers Transactions*, v. 155, p. 23-38.
- Kharaka, Y. K., Callender, E., and Carothers, W. W., 1977, Geochemistry of geopressured geothermal waters from the Texas Gulf Coast: *Proceedings, Third Geopressured-Geothermal Energy Conference, Lafayette, Louisiana*, v. 2, p. GI-121 - GI-164.
- Kharaka, Y. K., Carothers, W. W., and Brown, P. M., 1978, Origins of water and solutes in the geopressured zones of the northern Gulf of Mexico Basin: *Society of Petroleum Engineers of AIME Proceedings, 53rd Annual Conference, SPE 7505*, 8 p.
- Kharaka, Y. K., Lico, M. S., Wright, V. A., and Carothers, W. W., 1980, Geochemistry of formation waters from Pleasant Bayou No. 2 well and adjacent areas in coastal Texas: *Proceedings, Fourth Geopressured-Geothermal Energy Conference*, v. 1, p. 168-193.
- Kreitler, C. W., 1979, Ground-water hydrology of depositional systems, in Galloway, W. E., and others, *Depositional and ground-water flow systems in the exploration for uranium: The University of Texas at Austin, Bureau of Economic Geology*, p. 118-176.
- Loucks, R. G., Dodge, M. M., and Galloway, W. E., in press, Factors controlling porosity and permeability of hydrocarbon reservoirs in lower Tertiary sandstones along the Texas Gulf Coast: *The University of Texas at Austin, Bureau of Economic Geology Report of Investigations*.
- Loucks, R. G., Richmann, D. L., and Milliken, K. L., 1981, Factors controlling reservoir quality in Tertiary sandstones and their significance to geopressured geothermal production: *The University of Texas at Austin, Bureau of Economic Geology Report of Investigations No. 111*, 41 p.
- Milliken, K. L., Land, L. S., and Loucks, R. G., 1981, History of burial diagenesis determined from isotopic geochemistry, Frio Formation, Brazoria County, Texas: *American Association of Petroleum Geologists Bulletin*, v. 65, p. 1397-1413.
- Morton, J. P., and Long, L. E., 1982, Rb-Sr dating of illite diagenesis (abs.): *American Association of Petroleum Geologists Bulletin*, v. 66, p. 610-611.
- Morton, R. A., Garrett, C. M., Jr., Posey, J. S., Han, J. H., and Jirik, L. A., 1981, Salinity variations and chemical compositions of waters in the Frio Formation, Texas Gulf Coast: *The University of Texas at Austin, Bureau of Economic Geology, report to the U.S. Department of Energy, Contract No. DE-AC08-79ET27111*, 96 p.
- Perry, E. A., and Hower, J., 1970, Burial diagenesis in Gulf Coast pelitic sediments: *Clays and Clay Minerals*, v. 18, p. 165-177.
- \_\_\_\_\_, 1972, Late-stage dehydration in deeply buried pelitic sediments: *American Association of Petroleum Geologists Bulletin*, v. 56, p. 2013-2021.
- Powers, M. C., 1967, Fluid-release mechanisms in compacting marine mudrocks and their importance in oil exploration: *American Association of Petroleum Geologists Bulletin*, v. 51, p. 1240-1254.

- Rittenhouse, G., 1967, Bromine in oil field waters and its use in determining possibilities of origin of these waters: American Association of Petroleum Geologists Bulletin, v. 51, p. 2340-2440.
- Timm, B. C., and Maricelli, J. J., 1953, Formation waters in southwest Louisiana: American Association of Petroleum Geologists Bulletin, v. 57, p. 321-337.
- Weaver, C. E., and Beck, K. C., 1971, Clay water diagenesis during burial: how mud becomes gneiss: Geological Society of America Special Paper 134, 96 p.
- Weise, B. R., Edwards, M. B., Gregory, A. R., Hamlin, H. S., Jirik, L. A., and Morton, R. A., 1981, Geologic studies of geopressed and hydro pressured zones in Texas: The University of Texas at Austin, Bureau of Economic Geology, report to the Gas Research Institute, Contract No. 5011-321-0125, 308 p.
- White, D. E., 1965, Saline waters of sedimentary rocks: American Association of Petroleum Geologists Memoir 4, p. 342-366.
- Wood, J. R., and Hewett, T. A., 1982, Fluid convection and mass transfer in porous sandstones-- a theoretical model: Geochimica et Cosmochimica Acta, v. 46, p. 1707-1713.

Appendix II-A

Chemical analyses of water samples collected from the deep Frio Formation in Texas.  
Analyses by Mineral Studies Laboratory, Bureau of Economic Geology,  
Clara Ho, Chemist-in-Charge.

County:	Hidalgo	Hidalgo	Hidalgo	Hidalgo	Hidalgo	Hidalgo	Hidalgo
Field:	La Blanca	La Blanca	La Blanca	La Blanca	S. Weslaco	S. Weslaco	Pharr
Operator:	Amoco	Amoco	Amoco	Amoco	Amoco	Amoco	Tenneco
Well-Lease:	Gas Unit #12	Gas Unit #34	Gas Unit #19	Gas Unit #7	Gas Unit #20	Gas Unit #16	FWU #18
Depth (ft):	9,514-9,532	9,326-9,404	9,405-9,428	6,610-6,620	7,908-7,914	8,738-8,750	9,678-9,782
Gas-Water Ratio (Mcf/bbl):	5.8	34.3	2.3	93.7	16.5	16.5	0.3

Parameters

134

TDS mg/L	7,980	9,960	7,837*	6,950	13,200	8,568*	13,644*
Na mg/L	2,630	2,920	2,530	2,050	4,940	3,510	4,100
K mg/L	45.0	260	46.0	19.0	33.0	31.0	97.0
Mg mg/L	2.9	6.8	1.7	14.0	6.3	3.0	6.2
Ca mg/L	150	430	430	380	130	110	910
Fe mg/L	0.2	4.2	0.99	120	5.3	17.0	11.0
Al mg/L	<0.1	<0.1	<0.1	<0.1	<0.1	<0.1	1.6
Mn mg/L	0.13	0.34	0.19	3.1	0.25	0.48	0.56
Sr mg/L	10.0	19.0	19.0	6.6	4.9	7.7	46.0
Ti mg/L	<0.025	<0.025	<0.025	<0.025	<0.025	<0.025	<0.05
B mg/L	200	140	150	15	120	100	170
P mg/L	<0.3	<0.3	<0.3	<0.3	0.3	0.3	0.5
SiO <sub>2</sub> mg/L	100	73.0	85.0	5.1	69.0	56.0	105
HCO <sub>3</sub> mg/L	200	100	nm	79.0	230	nm	nm
Field alkalinity mg/L	nm						
Cl mg/L	4,130	5,250	4,588	4,000	6,570	4,723	8,190
NH <sub>3</sub> mg/L	46.0	44.0	nm	86.0	40.0	nm	nm
SO <sub>4</sub> mg/L	59.0	150	20.0	230	1,880	750	40.0
F mg/L	6.1	4.0	6.4	0.3	3.0	6.6	6.4
Br mg/L	18.0	17.0	nm	10.0	34.0	nm	nm
pH	7.2	5.4	nm	6.9	7.7	nm	nm
Field pH	7.8	7.3	nm	6.2	7.1	7.3	nm
Temperature °F	247	243	244	193	216	235	270
Cations meq/L	122	155	nm	114	222	nm	nm
Anions meq/L	122	154	nm	120	130	nm	nm

\*TDS by addition  
nm = not measured

Appendix II-A (cont.)

County:	Hidalgo	Hidalgo	Hidalgo	Hidalgo	Hidalgo
Field:	McAllen	McAllen Ranch	McAllen Ranch	McAllen Ranch	McAllen Ranch
Operator:	Tenneco	Forest	Forest	Forest	Forest
Well-Lease:	FWU #28	A.A. McAllen #6	A.A. McAllen #8	A.A. McAllen #9	A.A. McAllen #19
Depth (ft):	6,838-6,844	12,525-12,705	11,811-12,106	13,486-13,617	13,085-13,353
Gas-Water Ratio (Mcf/bbl):	75.7	8.3	5.9	15.2	10.9

Parameters

135

TDS mg/L	14,546*	75,165*	65,047*	68,334*	136,313*
Na mg/L	4,400	11,500	9,270	9,360	25,700
K mg/L	92.0	580	470	1,230	1,470
Mg mg/L	12.0	19.0	16.0	18.0	79.0
Ca mg/L	1,110	15,900	14,000	15,200	23,600
Fe mg/L	35.0	7.3	10.0	35.0	27.0
Al mg/L	4.6	<0.2	<0.2	<0.2	<0.2
Mn mg/L	0.77	3.4	2.5	2.6	13.0
Sr mg/L	60.0	1,070	990	1,060	1,700
Ti mg/L	<0.05	<0.05	<0.05	<0.05	<0.05
B mg/L	160	96.0	92.0	87.0	76.0
P mg/L	0.5	<0.5	<0.5	1.1	<0.5
SiO <sub>2</sub> mg/L	120	102	95.0	53.0	49.0
HCO <sub>3</sub> mg/L	nm	nm	nm	nm	nm
Field alkalinity mg/L	nm	nm	nm	nm	nm
Cl mg/L	8,570	45,400	39,600	40,900	81,600
NH <sub>3</sub> mg/L	nm	nm	nm	nm	nm
SO <sub>4</sub> mg/L	60.0	55.0	60.0	90.0	68.0
F mg/L	0.5	2.5	2.7	2.3	3.4
Br mg/L	nm	210	180	15.0	330
pH	nm	nm	nm	nm	nm
Field pH	nm	nm	nm	nm	nm
Temperature °F	190	305	292	322	317
Cations meq/L	nm	nm	nm	nm	nm
Anions meq/L	nm	nm	nm	nm	nm

\*TDS by addition  
nm = not measured

Section III

PREDICTING RESERVOIR QUALITY AND DIAGENETIC HISTORY  
IN THE FRIO FORMATION (OLIGOCENE) OF TEXAS

By *W. R. Kaiser*

*Assisted by B. D. Legett and J. F. O'Connell*

ABSTRACT

The use of equilibrium thermodynamics or solution-mineral equilibria as a predictor of reservoir quality was evaluated by thermodynamically comparing waters from regions of good and poor reservoir quality, the upper and lower Texas coast, respectively. Comparison among waters from these regions was made on activity diagrams of 16 diagenetic reactions, such as calcite = ferroan calcite, kaolinite = chlorite, and Ca-montmorillonite = Na-montmorillonite. Relative position of tested waters, with respect to the stability field of authigenic minerals occluding permeability and porosity, was used to predict reservoir quality. Solution-mineral equilibria in hydro pressured waters best reflect reservoir quality. Activity indices favoring chlorite and ferroan calcite stability and large  $\log[\text{Ca}^{2+}]^{.16}/[\text{Na}^{+}]^{.33}$  ratios are the best indicators of reservoir quality in deep Frio sandstones. A correlation of uncertain geochemical significance exists between activity indices, analytical molality, ionic strength, and geopres-suring. Variation in activity indices and mole ratios with depth is largest between 8,000 and 11,000 ft (2,440 and 3,355 m), the transition zone between the hydro pressured and geopressed intervals. The variation is attributed to either more active water-rock interaction or diagenesis in the transition zone. Diagenesis is mainly a function of temperature, pH, and pressure, and only secondarily of mineral solubilities. Predictions made from solution-mineral equilibria add new insight into relative mineral stabilities and in situ pH and are consistent with the diagenetic sequence developed from petrographic data. Carbonate equilibrium requires early precipitation of calcite in diagenesis. Two stages of chlorite formation are postulated, one early in the hydro pressured interval at the expense of clay coats and another late in the geopressed interval at the expense of kaolinite cement. Chlorite and illite are the stable layer silicates in deep Frio sandstones. Albitization of feldspar is initiated in the hydro pres-sured interval at less than 100°C.

## INTRODUCTION

Diagenetic studies of Gulf Coast Tertiary rocks (Lindquist, 1977; Bebout and others, 1978; Loucks and others, 1979a and 1981) have produced much data on the regional variations in detrital and authigenic mineralogy. They have progressed from broad regional assessment of reservoir quality, stressing sandstone petrography, to detailed comparison of sandstone mineralogy and elemental composition of calcite from selected areas (Loucks and others, 1979b; Richmann and others, 1980). These studies have advanced our understanding of the occurrence and quality of deep subsurface reservoirs. Factors responsible for the variation in reservoir quality were identified through comparison of detrital and authigenic mineralogies and petrophysical properties. A diagenetic sequence was established by Loucks and others (1981) relating diagenesis to depth of burial.

The role of brine chemistry in diagenesis is poorly understood and heretofore had not been an integral part of diagenetic studies. Logically, then, the next step in the effort to better understand diagenesis and to predict reservoir quality was to investigate the role of pore fluids (formation waters) or aspects of water-rock interaction. The objective was to relate water-rock interaction to sandstone diagenesis, using equilibrium thermodynamics or solution-mineral equilibria, by thermodynamically testing the relative stability of authigenic and detrital minerals with respect to formation waters. The prediction of reservoir quality remains an elusive goal. The use of solution-mineral equilibria as a predictor of reservoir quality was evaluated by thermodynamically comparing waters from regions of good and poor reservoir quality.

Analyzed formation waters came from 51 Frio oil and gas fields located in 13 coastal counties, stretching across Texas from the Rio Grande to the Sabine River, divided here into upper, middle, and lower coast (South Texas) (fig. III-1). They are Na<sup>+</sup>-Cl<sup>-</sup> waters having total dissolved solids content ranging from 6,903 to 248,454 mg/L; they represent a depth range of 3,349 ft (1,021 m) to 15,778 ft (4,810 m) and a temperature range of 46°C (115°F) to 172°C (342°F). A total of 138 waters were thermodynamically tested, 102 from the geopressured interval (>0.465 psi/ft [10.5 kPa/m] pore pressure gradient) and 36 from the hydro pressured interval (Morton and others, 1981; Kharaka and others, 1977 and 1979).



Figure III-1. Map of upper, middle, and lower Texas coast and Frio oil and gas fields having analyzed waters.

## RESERVOIR QUALITY

### Authigenic Minerals

Authigenic minerals reflect the chemical environment and are the key to reservoir quality because they reduce permeability and occlude porosity. Predicting their behavior is the key to the prediction of reservoir quality. The presence or absence of these minerals is controlled by bulk composition, temperature, and pore fluid composition. Authigenic minerals of major importance in Frio sandstones are calcite, quartz, kaolinite, and chlorite. Minor phases are albite cement, laumontite, sphene, and smectite clay coats. Key minerals were selected from the work of Loucks and others (1979a and 1981). Ferroan calcite and plagioclase compositions are based on their work. Lacking analyses of layer silicates, generalized formulas for chlorite, montmorillonite, and illite were chosen from the work of Carroll (1970) and Galloway and Kaiser (1980) (table III-1).

### Thermodynamic Data

Thermodynamic functions were estimated because of the fragmentary nature and general absence of thermodynamic data at elevated temperatures and pressures. Such estimates are uncertain to the extent of approximately 2 to 5 kcal/mol. However, close agreement between estimated and experimentally derived values is common, sometimes to within 2 percent of each other. Moreover, it is well to remember that there are no "correct" thermodynamic functions of minerals. For example, the free energy of formation ( $\Delta G_f$ ) of anorthite at 25°C and 1 bar pressure differs by 5.8 kcal/mol, -960.1 versus -954.3, as reported in Robie and others (1978) and Helgeson and others (1978), respectively. Estimated values are not sufficiently accurate to predict equilibrium temperatures of univariant reactions. Nevertheless, they offer, in the absence of experimental data, a means of approximating chemical reality in geologic systems.

Thermodynamic functions for members of solid solutions, layer silicates, and ionic species were estimated in 25° or 50°C increments over the temperature range of 25° to 350°C. Methods of estimation differ depending on mineral class and availability of published data. The calculation of  $\Delta G_f$  for ferroan calcite and plagioclase is essentially the estimation of  $\Delta G_f$  for solid solutions, assuming ideal behavior (Saxena, 1973; Kerrick and Darken, 1975). The contribution of nonideality can be estimated, but the improved accuracy is small (<2 kcal/mol) and seldom worth the effort (Wood and Fraser, 1976).

Free energies at elevated temperatures can be computed for layer silicates, zeolites, and ionic species if average standard heat capacity ( $C_p^T$ ), standard enthalpy of formation ( $\Delta H_f^\circ$ ),

and log K of formation ( $\log K_f$ ) at 298°K or 25°C are known. The log K of formation at the desired temperature ( $\log K_{f,T}$ ) can be estimated by using an equation modified from Helgeson (1969):

$$\log K_{f,T} = \log K_f - \frac{\Delta H_f^\circ}{2.303R} \left( \frac{1}{T} - \frac{1}{298} \right) - \frac{C_p^\circ \int_{298}^T (T-298)}{2.303RT} + \frac{C_p^\circ \int_{298}^T \ln(T/298)}{2.303R}$$

A free energy value can then be calculated from:

$$\Delta G_{f,T} = -\log K_{f,T} (2.303RT).$$

Calculating values of thermodynamic functions for layer silicates presents special problems. Few thermodynamic data are available at elevated temperatures because of compositional and structural complexity. By necessity, thermodynamic functions must be estimated for an idealized mineral composition.

Heat capacity was calculated using a structural algorithm after Helgeson and others (1978). The assumption is that the standard heat capacity of reaction ( $C_{p,r}^\circ$ ) among oxides and silicates of the same or similar structural class equals zero at 25°C and 1 bar ( $\Delta C_{p,r}^\circ = 0$ ). This assumption accounts at least in part for the temperature dependence of bond energies within the mineral. To estimate Maier-Kelley heat capacity power functions, end member values were chosen from Helgeson and others (1978) for chlorite, montmorillonite, and illite. Kaolinite's power function is well established. In most cases, the structural algorithm affords estimates of heat capacity at higher temperatures that are within 2 percent of experimentally determined values.

Standard enthalpies of formation were estimated using a graphical method of Helgeson (personal communication, 1971) and described in Eugster and Chou (1973). Enthalpies ( $\Delta H_f^\circ$ ) of layer silicates divided by the number of tetrahedrally coordinated Si and Al ions ( $Si_{tet} + Al_{tet}$ ) plotted against  $\Sigma \Delta H_f^\circ$  of octahedral, exchange, and hydroxyl ions (as aqueous species) divided by ( $Si_{tet} + Al_{tet}$ ) yields a straight line having a slope of approximately 1. Plotting of estimated and experimentally determined values also yields a line slope of 1, indicating close agreement between values. The method provides acceptable estimates and in some cases generates values within the limits of experimental uncertainty.

Free energies of formation were estimated using the method of Tardy and Garrels (1974), on the assumption that oxide and hydroxide components of layer silicates have fixed free energies of formation within the silicate. The general rule is that all components are treated as oxides with the exception of Mg, which is treated as  $Mg(OH)_2$  in all silicates. There is close agreement between estimated and experimentally determined values.

Activities of ionic species were calculated by computer using an updated version of SOLMNEQ (solution-mineral equilibrium computations) (Kharaka and Barnes, 1973). SOLMNEQ

uses the extended Debye-Huckel equation, designed for aqueous solutions having ionic strengths of up to 3.0 in which more than 80 percent of the solute is  $\text{Na}^+$  and  $\text{Cl}^-$ , to estimate activity coefficients. The range of temperatures covered is 25° to 300°C, at pressures of the liquid-vapor equilibrium for water; best results are achieved at temperatures of up to 200°C. These chemical constraints correspond to the bulk of Frio waters. The equilibrium distribution of inorganic species commonly present in natural waters is computed from chemical analyses, temperature, and pH. Values of ion activity coefficients have the smallest uncertainty (less than an order of magnitude), whereas  $\log K_r$ ,  $\log K_f$ , or gas fugacities may be uncertain to a few orders of magnitude.

## Stability Relations

### Reaction Pairs

Carbonate equilibrium, chloritization, kaolinitization, cation exchange, and albitization reactions were written to test relative mineral stability in Frio Formation waters. Twelve key reaction pairs are given in table III-2. The Na-montmorillonite and K-spar analogs of equations 3, 6, 7, and 10 are not shown, but they were considered in this study and yielded similar results. Reactions were written with Al immobile because dissolved Al was not determined and thus could not appear as an ionic species. Furthermore, Al is relatively immobile in diagenesis.

Equation 1 speaks to the sequencing of calcite and ferroan calcite during diagenesis. In effect, this sequencing governs reservoir quality in the Frio Formation, because calcite is the major inhibitor of porosity and permeability, and helps explain variations in calcite composition with depth.

Equations 2, 3, and 4 are chloritization reactions. In equation 2, the relative stability of kaolinite and chlorite is tested, whereas equations 3 and 4 are important to the diagenesis of clay coats or the relative stability of Ca-montmorillonite and illite. Equations 5, 6, 7, and 8 are kaolinitization reactions; equation 5, kaolinitization of plagioclase, is perhaps the most important among these as a generator of voids and as a source of Al. Chloritization frees  $\text{H}^+$ , whereas kaolinitization consumes  $\text{H}^+$ , perhaps playing a role in pH control by acting as buffers. Both sets of reactions free  $\text{H}_4\text{SiO}_4^0$  as well as cations ( $\text{K}^+$ ,  $\text{Na}^+$ , and  $\text{Ca}^{2+}$ ) important in diagenesis. Of course, chloritization consumes  $\text{Fe}^{2+}$  and  $\text{Mg}^{2+}$ , whereas kaolinitization frees  $\text{Fe}^{2+}$  and  $\text{Mg}^{2+}$ .

Equation 9 is a cation-exchange reaction exchanging two  $\text{Na}^+$  for one  $\text{Ca}^{2+}$  ion. Equation 10 represents the smectite/illite transformation whose role in diagenesis is well known and will not be discussed here (Hower and others, 1976; Boles and Franks, 1979). Finally, two

Table III-1. Mineral composition.

**Authigenic minerals**

Quartz	$\text{SiO}_2$
Calcite	$\text{CaCO}_3$
Ferroan calcite	$\text{Ca}_{.95}\text{Fe}_{.05}\text{CO}_3$
Kaolinite	$\text{Al}_2\text{Si}_2\text{O}_5(\text{OH})_4$
Albite	$\text{NaAlSi}_3\text{O}_8$
Chlorite	$\text{Mg}_{2.3}\text{Fe}_{2.3}\text{Al}_{2.8}\text{Si}_{2.6}\text{O}_{10}(\text{OH})_8$
Illite	$\text{K}_{.6}\text{Mg}_{.25}\text{Al}_{2.3}\text{Si}_{3.5}\text{O}_{10}(\text{OH})_2$

**Detrital minerals**

Plagioclase (An30)	$\text{Na}_{.7}\text{Ca}_{.3}\text{Al}_{1.3}\text{Si}_{2.7}\text{O}_8$
Microcline	$\text{KAlSi}_3\text{O}_8$

**Clay coats**

Ca-montmorillonite	$\text{Ca}_{.16}(\text{Al}_{1.56}\text{Mg}_{.25}\text{Fe}_{.25})\text{Si}_4\text{O}_{10}(\text{OH})_2$
--------------------	--

Table III-2. Reaction pairs\*.

1.  $\text{CaCO}_3 + 0.05\text{Fe}^{2+} = \text{Ca}_{.95}\text{Fe}_{.05}\text{CO}_3 + 0.05\text{Ca}^{2+}$
2.  $1.4\text{Kao} + 2.3\text{Mg}^{2+} + 2.3\text{Fe}^{2+} + 6.2\text{H}_2\text{O} = \text{Chl} + 0.2\text{H}_4\text{SiO}_4^{\circ} + 9.2\text{H}^+$
3.  $1.8\text{Ca-mont} + 1.85\text{Mg}^{2+} + 1.85\text{Fe}^{2+} + 14.8\text{H}_2\text{O} =$   
 $\text{Chl} + 0.29\text{Ca}^{2+} + 4.6\text{H}_4\text{SiO}_4^{\circ} + 6.8\text{H}^+$
4.  $\text{Illite} + 1.64\text{Mg}^{2+} + 1.89\text{Fe}^{2+} + 8.24\text{H}_2\text{O} = 0.82\text{Chl} + 0.6\text{K}^+ + 1.37\text{H}_4\text{SiO}_4^{\circ} + 6.46\text{H}^+$
5.  $\text{Plagio} + 1.3\text{H}^+ + 3.45\text{H}_2\text{O} = 0.65\text{Kao} + 0.3\text{Ca}^{2+} + 0.7\text{Na}^+ + 1.4\text{H}_4\text{SiO}_4^{\circ}$
6.  $2\text{Ab} + 2\text{H}^+ + 9\text{H}_2\text{O} = \text{Kao} + 2\text{Na}^+ + 4\text{H}_4\text{SiO}_4^{\circ}$
7.  $\text{Ca-mont} + 1.32\text{H}^+ + 4.78\text{H}_2\text{O} =$   
 $0.78\text{Kao} + 0.25\text{Mg}^{2+} + 0.25\text{Fe}^{2+} + 0.16\text{Ca}^{2+} + 2.44\text{H}_4\text{SiO}_4^{\circ}$
8.  $\text{Illite} + 1.1\text{H}^+ + 3.15\text{H}_2\text{O} = 1.15\text{Kao} + 0.6\text{K}^+ + 1.2\text{H}_4\text{SiO}_4^{\circ} + 0.25\text{Mg}^{2+}$
9.  $\text{Ca-mont} + 0.33\text{Na}^+ = \text{Na-mont} + 0.16\text{Ca}^{2+}$
10.  $\text{Ca-mont} + 0.41\text{K}^+ + 0.57\text{H}^+ + 2.64\text{H}_2\text{O} =$   
 $0.68\text{Illite} + 0.08\text{Mg}^{2+} + 0.25\text{Fe}^{2+} + 0.16\text{Ca}^{2+} + 1.62\text{H}_4\text{SiO}_4^{\circ}$
11.  $\text{Plagio (An}_{30}) + 0.6\text{Na}^+ + 1.2\text{H}_4\text{SiO}_4^{\circ} = 1.3\text{Ab} + 0.3\text{Ca}^{2+} + 2.4\text{H}_2\text{O}$
12.  $\text{K-spar} + \text{Na}^+ = \text{Ab} + \text{K}^+$

\*Reactions written with Al immobile.

albitization reactions, equations 11 and 12, are considered. Note that albitization of plagioclase and K-spar frees  $\text{Ca}^{2+}$  and  $\text{K}^+$  and consumes  $\text{Na}^+$  and  $\text{H}_4\text{SiO}_4^0$ .

### Activity Diagrams

Frio waters were thermodynamically tested by plotting activity indices (log activity ratios and products) of each water on activity diagrams for 16 reaction pairs (table III-2). All waters were plotted assuming a water activity of 1. Nine diagrams are presented (figs. III-2, III-3, and III-5 through III-11). Stability relations are shown at subsurface temperatures and 1 bar pressure to represent hydro pressured conditions and 600 bars to represent geopressed conditions. The role of increased pressure in mineral stability is manifest in a more positive free energy of water (Fisher and Zen, 1971) causing the stability field of the product mineral to expand (for example, figs. III-8 and III-10). Because values of molal ionic volumes are sparse and scattered, the effect of pressure on ionic species is ignored in this study; the change in molal volume of solids is essentially constant (Garrels and Christ, 1965).

Relative position of tested waters on the activity diagrams, with respect to the stability field of authigenic minerals occluding permeability and porosity, was used to predict reservoir quality. Waters from regions of good and poor reservoir quality, the upper and lower Texas coast, respectively, were compared. Sandstone reservoirs having permeabilities greater than 20 md and abundant deep secondary porosity exist on the upper Texas coast, whereas permeability in sandstones of the lower coast or South Texas is less than 1 md.

Carbonate equilibrium--Calcite stability is the key to reservoir quality in the Frio Formation; its stability or precipitation is favored by higher pH, temperature, and  $[\text{Fe}^{2+}]$ . Therefore, the inverse of these are indicators of calcite instability or dissolution--in effect, good reservoir quality. Inferences about these indicators are drawn from the calcite/ferroan calcite activity diagram, geothermal gradients, and available petrographic data.

Middle and upper coast waters at subsurface temperatures plot in the calcite and ferroan calcite stability fields. Almost all lower coast or South Texas waters fall in the ferroan calcite field (fig. III-2). All South Texas and upper coast hydro pressured waters fall in the ferroan calcite field. These two areas are on opposite ends of the reservoir-quality spectrum because of the presence and absence, respectively, of late-stage ferroan calcite cement. The critical parameter is pH; calcite precipitation is difficult, if not impossible, at low pH. Using a mass-balance approach, Kharaka and others (1979) calculated an in situ pH of 4.1 for two upper coast geopressed waters (Pleasant Bayou geothermal test well, Brazoria County). At an equilibrium pH of 4, a concentration of total dissolved carbonate species of approximately 60,000 mg/L is required for calcite precipitation in Pleasant Bayou waters, a concentration that seems

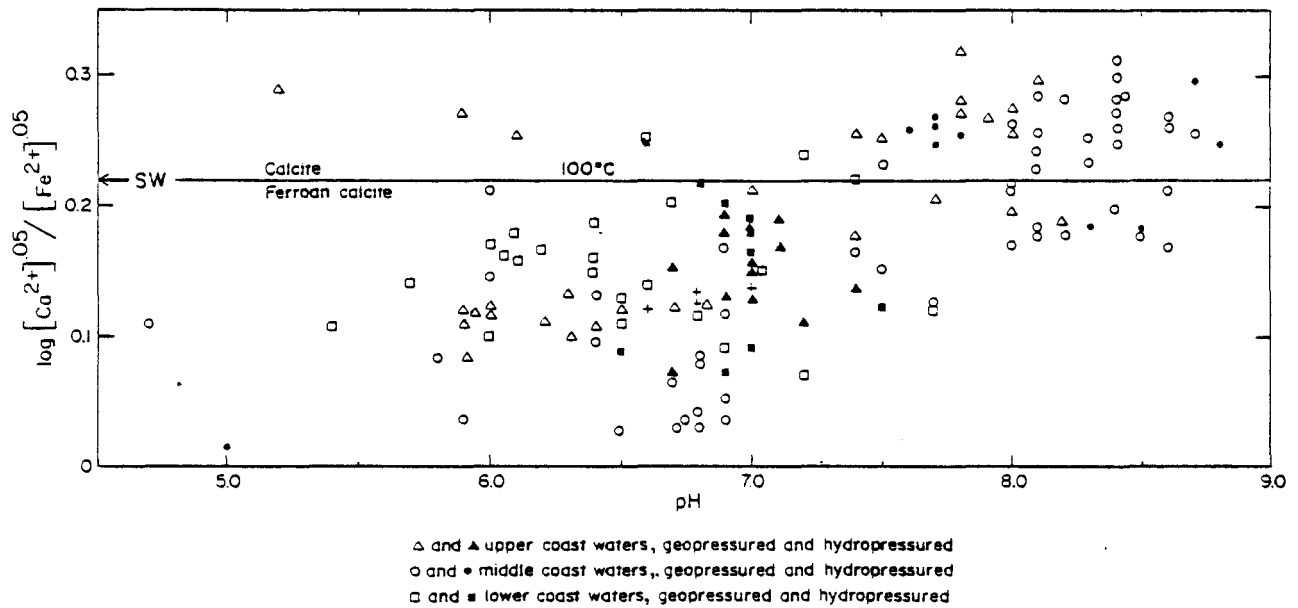


Figure III-2. Activity diagram of the reaction calcite = ferroan calcite (equation 1, table III-2). Open symbols designate geopressured waters, solid symbols designate hydro pressured waters, crosses designate East White Point field hydro pressured waters. On the ordinate, for reference, SW =  $\log [Ca^{2+}]^{.05} / [Fe^{2+}]^{.05}$  ratio in seawater.

unrealistically high for natural waters. The point is that high pH favors calcite precipitation or stability. The absence of late-stage, porosity-occluding ferroan calcite in upper coast Frio sandstones is attributed to low in situ pH, whereas its presence in South Texas is attributed to postulated higher pH and secondarily to higher temperature and  $[Fe^{2+}]$ . Overall, calcite becomes more stable at higher temperature, and in the presence of  $Fe^{2+}$ , ferroan calcite is more stable than non-ferroan calcite.

Early prediction was that South Texas hydro pressured waters would plot more deeply into the ferroan calcite stability field (Kaiser and Richmann, 1981; Kaiser, 1982); that is, into the stability field of the mineral mainly responsible for occluding permeability and porosity. This prediction was half right. The position of four waters confirms the prediction, whereas two contradict it; others cluster with upper coast waters (fig. III-2). All but three middle coast hydro pressured waters plot in the calcite stability field. If wellhead pH's actually reflect higher in situ pH, then one might predict late-stage, non-ferroan calcite cement and poor reservoir quality in the middle coast deep Frio. These waters at wellhead pH's are supersaturated with respect to calcite.

Knowledge of in situ pH is critical to the prediction of reservoir quality. Hydro pressured waters of the East White Point field in San Patricio County (crosses, fig. III-2) illustrate the uncertainty by plotting in the ferroan calcite stability field amid South Texas and upper coast waters, indicating in the absence of pH data either poor or good reservoir quality.

Chloritization--Three activity diagrams are presented to evaluate chlorite stability (figs. III-3, III-5, and III-6). The relative stability of chlorite and kaolinite is discussed first. Equation 3 (table III-2) is evaluated with reference to the fate of Ca-montmorillonite clay coats or cutans, coatings on framework grains formed during pedogenesis (Brewer, 1964), and leads to consideration of chlorite/illite stability (equation 4).

All Frio waters plot in the chlorite stability field under geopressed conditions represented by 100°C and 600 bars pressure, which both contradicts and supports petrographic evidence (fig. III-3). Chlorite is generally absent in upper coast sandstones and abundant in South Texas sandstones. Factors controlling chlorite stability relative to kaolinite are pH, temperature, and  $\log Mg^{2+} - Fe^{2+}$  activity product. Note that  $[H^+]$ , or pH, is to the 9.2 power. The role of pH in two upper coast waters is illustrated in figure III-4. At a wellhead pH of 6.35 they plot in the chlorite stability field, whereas at an in situ pH of 4 they are shifted into the kaolinite field. At pH values of 4 to 6, not unreasonable in situ values for subsurface waters, all tested upper coast waters plot in the kaolinite stability field, consistent with petrographic evidence. The general absence of chlorite in upper coast sandstones is explained by temperatures too low for chlorite stability. For example, Pleasant Bayou waters fall in the chlorite field as temperatures rise above 150°C to approximately 175°C (fig. III-4).

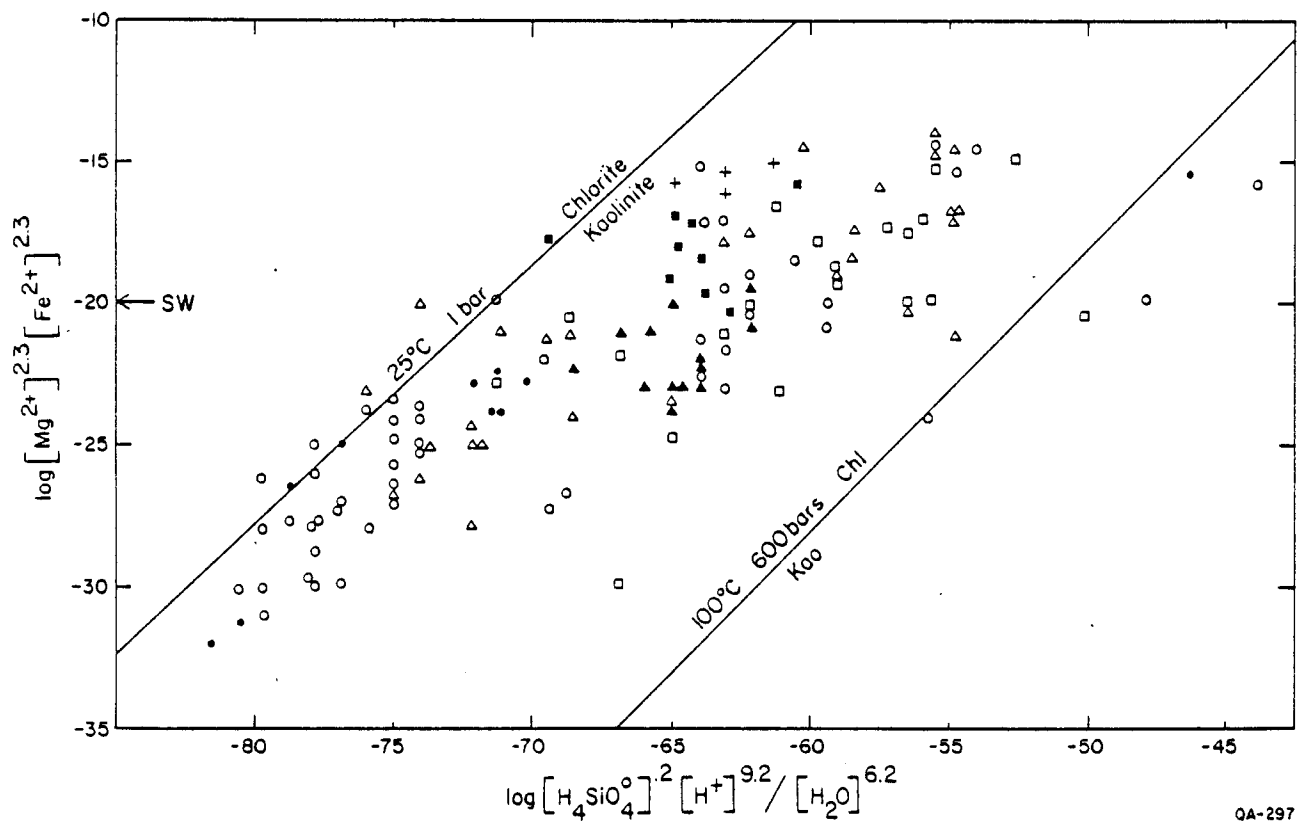


Figure III-3. Activity diagram of the reaction kaolinite = chlorite (equation 2, table III-2). SW = log activity product in seawater.

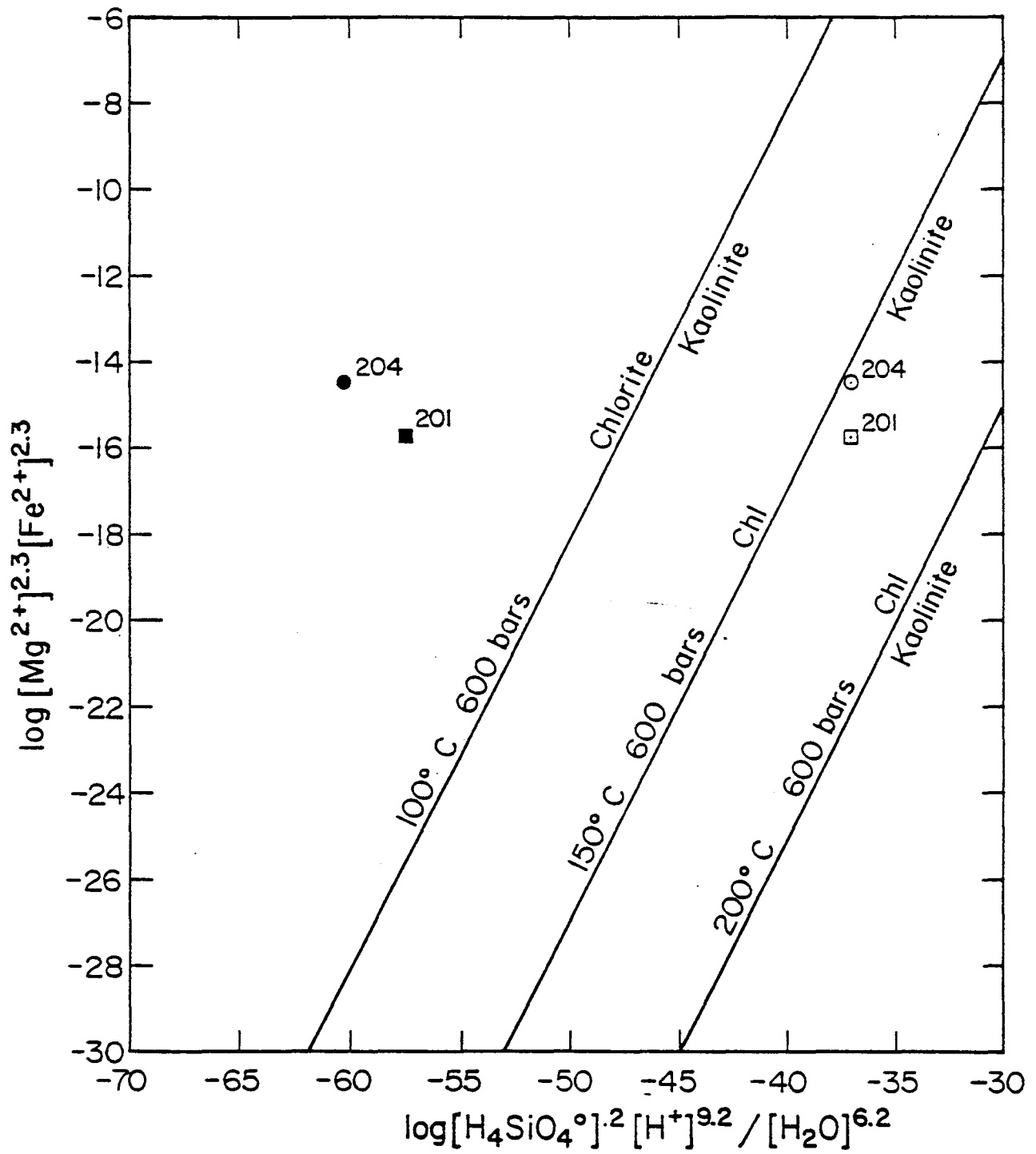


Figure III-4. Activity diagram of the reaction kaolinite = chlorite. Upper Texas coast, Brazoria County, Pleasant Bayou geothermal test well waters at wellhead pH (solid symbols) and in situ pH (open) (from Kaiser and Richmann, 1981).

Apparently, chloritization can be initiated at low temperatures (50° to 75°C) if pH is high, approximately 8. Note in particular that at these temperatures and pH, hydro pressured waters of the middle coast fall in the chlorite stability field (fig. III-3). However, at more realistic in situ pH values of 5 to 7, these waters are shifted right, deep into the kaolinite field at 50° to 75°C. At the same pH values, South Texas hydro pressured waters remain in the chlorite stability field because of larger  $\log[\text{Mg}^{2+}]^{2.3}[\text{Fe}^{2+}]^{2.3}$  products, in excess of -20, or that for seawater. Clearly, higher temperature, pH,  $[\text{Mg}^{2+}]$  and  $[\text{Fe}^{2+}]$ , and volcanic-rich detritus promote chlorite formation in South Texas (Kaiser, 1982).

Prior prediction was that South Texas hydro pressured waters would plot more deeply into the chlorite stability field (Kaiser and Richmann, 1981; Kaiser, 1982), and thereby serve as a direct indicator of poor reservoir quality, because chlorite is an important inhibitor of permeability and porosity in the deep Frio of South Texas. Indeed, this turned out to be the case. Consequently, poor reservoir quality is predicted in the deep Frio of the East White Point field (fig. III-3). Insofar as kaolinite is an indicator of acidic waters and of possible undersaturation with respect to calcite, then hydro pressured waters clustering in or toward the kaolinite stability field might be an indirect indicator of deep secondary porosity.

Ca-montmorillonite is stable with respect to chlorite at 25°C in all tested waters (fig. III-5). At temperatures between 50° and 75°C, chloritization is promoted in hydro pressured waters by high pH and small  $\log[\text{Ca}^{2+}]^{.29}/[\text{Fe}^{2+}]^{1.85}[\text{Mg}^{2+}]^{1.85}$  ratios of less than 15.4, or that for seawater. Again, because chloritization is favored in South Texas hydro pressured waters, it is postulated that clay coats underwent chloritization to chlorite rims in South Texas. Clay coats may also undergo transformation to mixed layer smectite/illite (S/I). Thermodynamic data developed in this study indicate the S/I transformation begins, in the presence of  $\text{K}^+$ , between 50° and 75°C. All Frio waters with respect to the montmorillonite/illite reaction pair plot deeply into the illite stability field. Illite in turn becomes unstable relative to chlorite as diagenesis proceeds. Illite is stable at low temperature and pressure; however, as temperature and pressure increase, the chlorite stability field expands to include most of the Frio waters (fig. III-6). Thus, chlorite is the layer silicate ultimately stable in deep Frio sandstones. Low pH favors illite stability, as illustrated by middle coast waters. Even at the rather high in situ pH of 7, they are shifted left into the illite stability field at 100°C. Again, South Texas hydro pressured waters plot more deeply into the chlorite field, separated from upper and middle coast waters at the log activity ratio for seawater. Petrographic and SEM (scanning electron microscopy) analysis of deep Frio sandstones in South Texas shows chlorite is abundant relative to illite, which is consistent with prediction here from solution-mineral equilibria data.

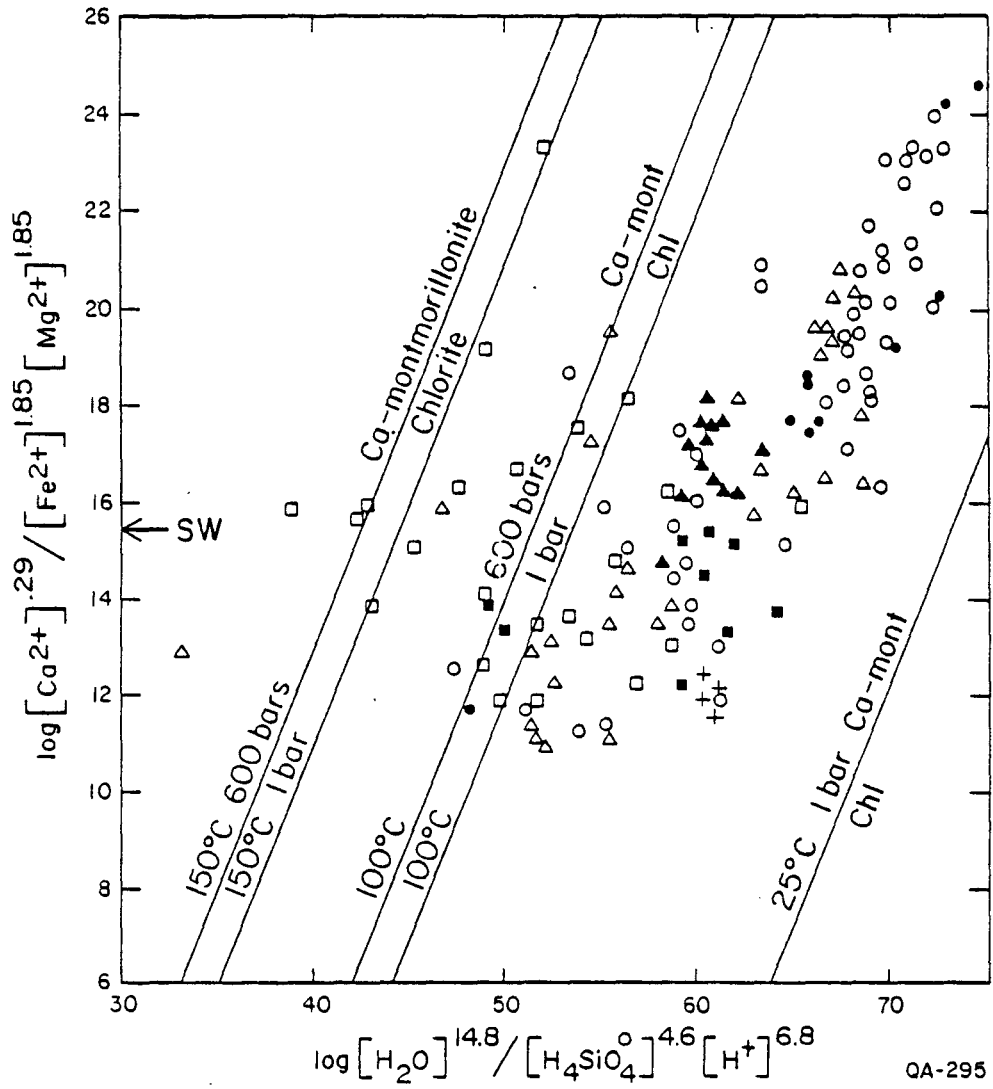


Figure III-5. Activity diagram of the reaction Ca-montmorillonite = chlorite (equation 3, table III-2).

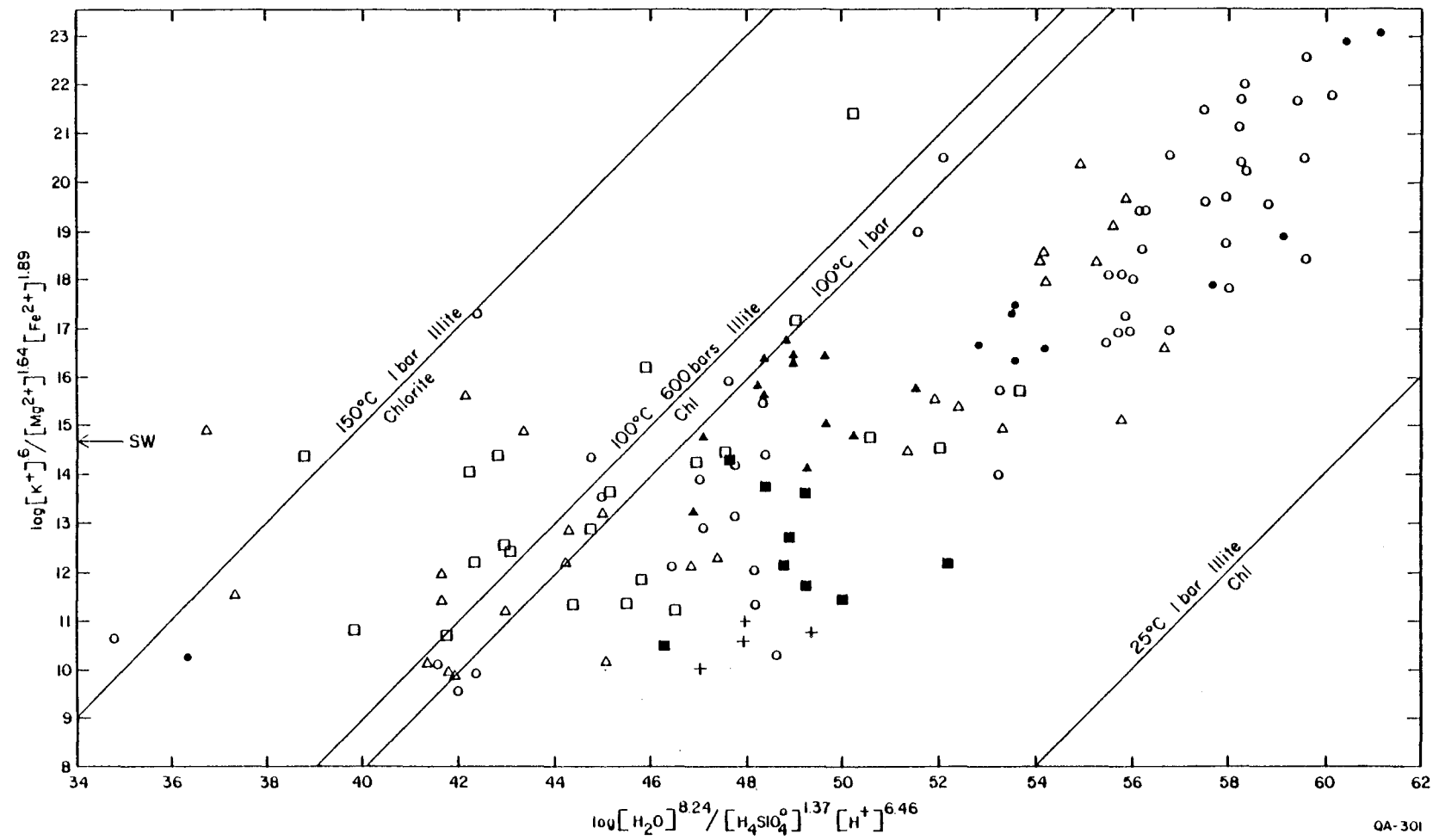


Figure III-6. Activity diagram of the reaction illite = chlorite (equation 4, table III-2).

Kaolinitization—Reactions of major importance in the Frio are equations 5 and 7 (table III-2). Petrographic evidence is unequivocal on kaolinite replacement of plagioclase; however, there is no clear evidence that kaolinitization of albite and K-spar occurred during Frio diagenesis. Conversion of montmorillonite to kaolinite is probably most important early in the shallow diagenetic environment, perhaps in low-pH meteoric water and later at the top of geopressure in low-pH compactional water. Relative to illite (equation 8), kaolinite is highly unstable in Frio waters. Their activity indices fall deep into the illite stability field, indicating that illite is one of two stable layer silicates in the Frio; the other is chlorite.

In high-pH hydro pressured waters, at 100°C and 1 bar, plagioclase is stable. Under geopressed conditions and lowered pH, the kaolinite field expands (fig. III-7). Predictably, kaolinite begins forming as a grain replacement of plagioclase, consuming the whole grain as diagenesis proceeds, and eventually growing outward to fill surrounding pore space. This sequence has been confirmed petrographically by Loucks and others (1981) and means that replaced plagioclase nucleates kaolinite cement. In passing from hydro pressured to geopressed conditions, the kaolinite field has its maximum expansion. Because most dissolved grains are either plagioclase or volcanic rock fragments, kaolinitization's effect on reservoir quality should be most evident at the top of geopressure. The absence of K-spar and albite alteration to kaolinite is predictable from thermodynamics. K-spar is stable with respect to kaolinite, and albite's stability field is large in Frio waters; therefore, K-spar and albite are less subject to kaolinitization than is plagioclase.

Ca-montmorillonite is stable with respect to kaolinite in Frio waters up to approximately 100°C; as temperature and pressure increase and with appropriately low pH, kaolinite becomes stable (fig. III-8). Prediction is that Ca-montmorillonite would persist relative to kaolinite in hydro pressured waters at pH greater than 6 or 7. The activity index for seawater once again divides South Texas hydro pressured waters from upper and middle coast hydro pressured waters. Waters from the latter regions favor kaolinite stability and indirectly indicate superior reservoir quality. Kaolinitization of montmorillonite is favored over chloritization in upper and middle coast waters because, as discussed above, temperature,  $[Mg^{2+}]$  and  $[Fe^{2+}]$ , and in situ pH are lower. Furthermore, thermodynamically it is easier to make kaolinite and illite from montmorillonite than from chlorite.

Cation exchange—Relative abundance of Ca- or Na-montmorillonite is controlled primarily by temperature and secondarily by the  $\log[Ca^{2+}].16/[Na^{+}].33$  ratio. All Frio waters at 25°C fall in the Ca-montmorillonite stability field; as temperature increases, the Na-montmorillonite field expands (fig. III-9). At approximately 100°C, most hydro pressured waters fall in the Na-montmorillonite field. In most geopressed waters, Na-montmorillonite and

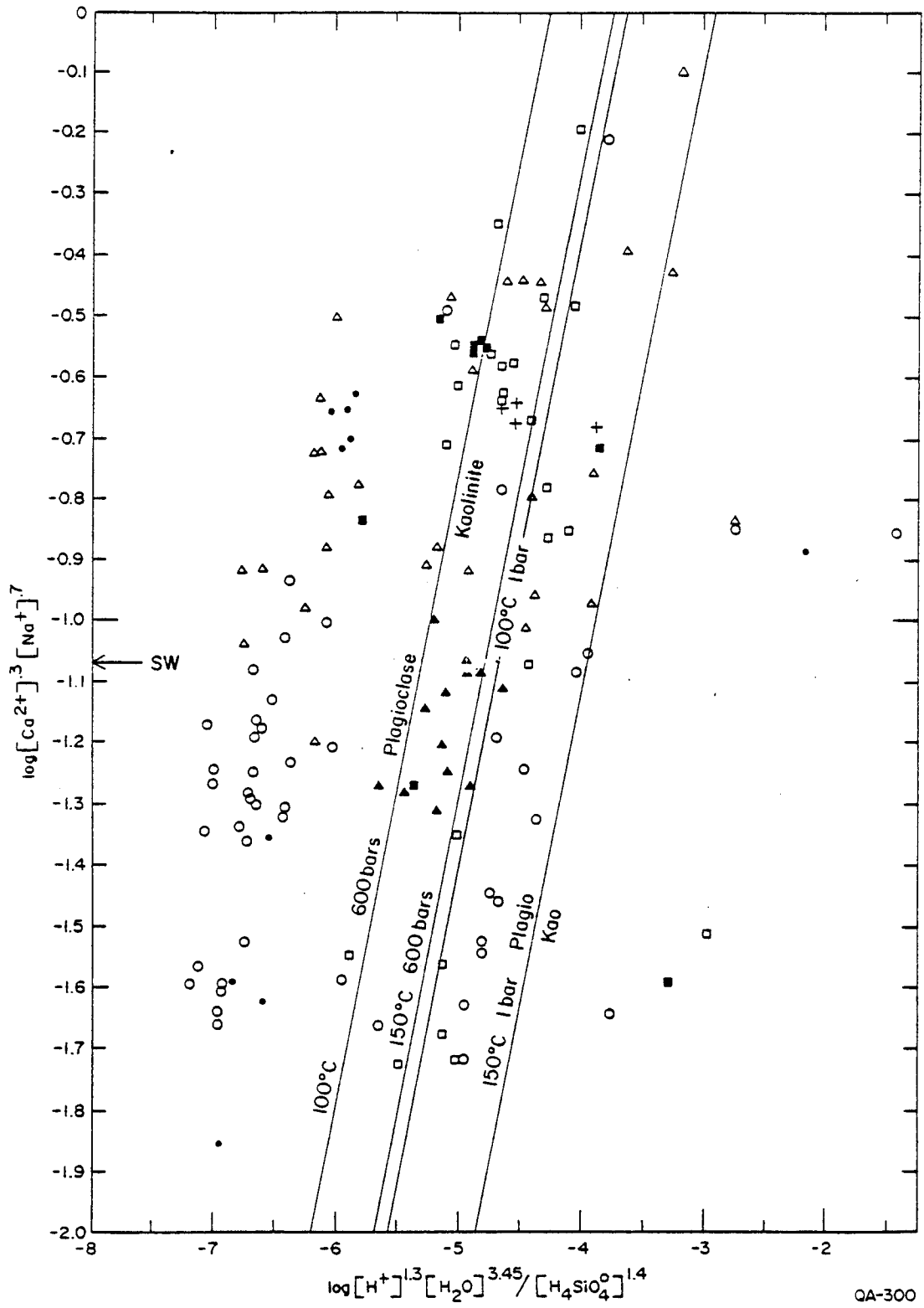


Figure III-7. Activity diagram of the reaction plagioclase (An30) = kaolinite (equation 5, table III-2).

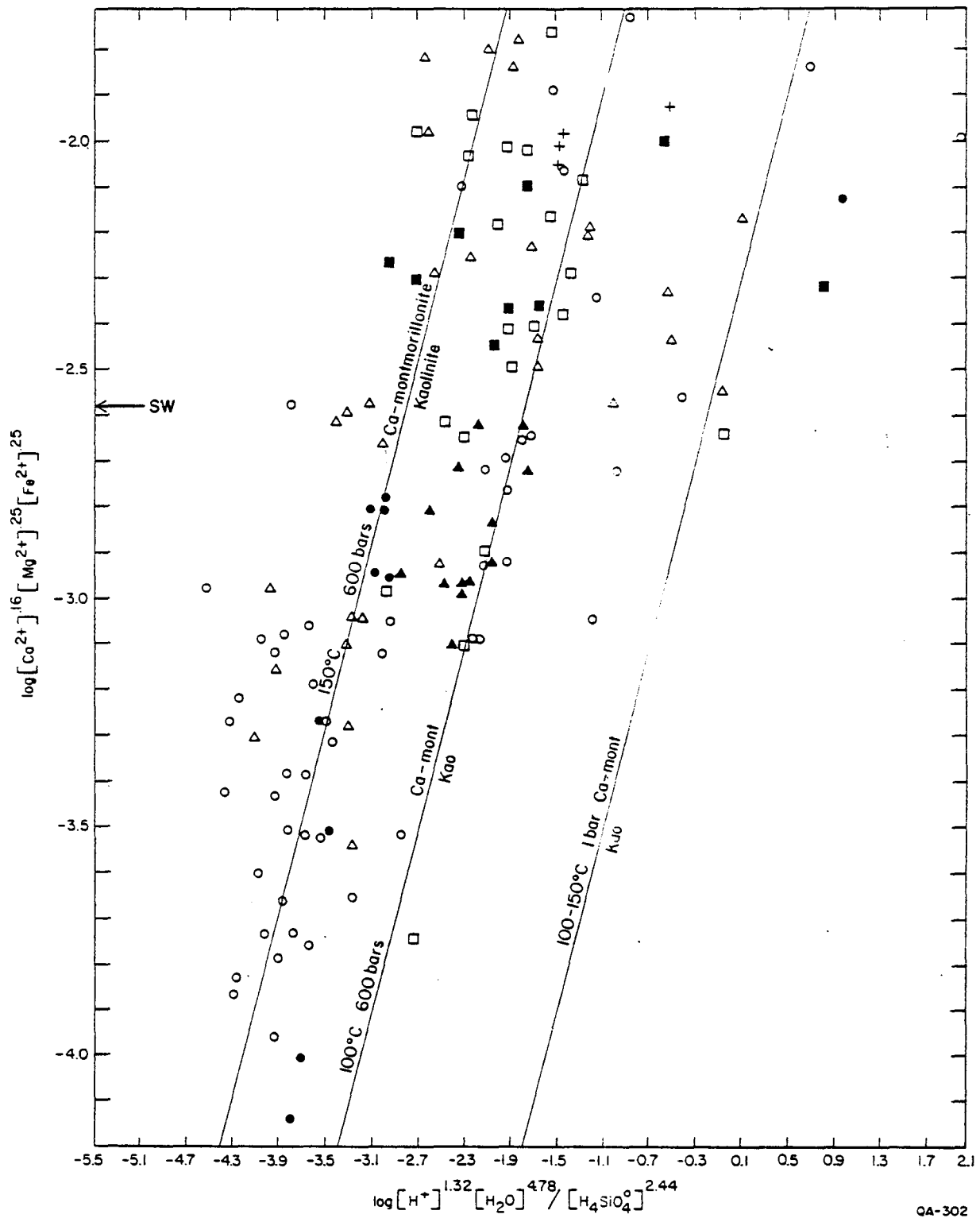


Figure III-8. Activity diagram of the reaction Ca-montmorillonite = kaolinite (equation 7, table III-2).

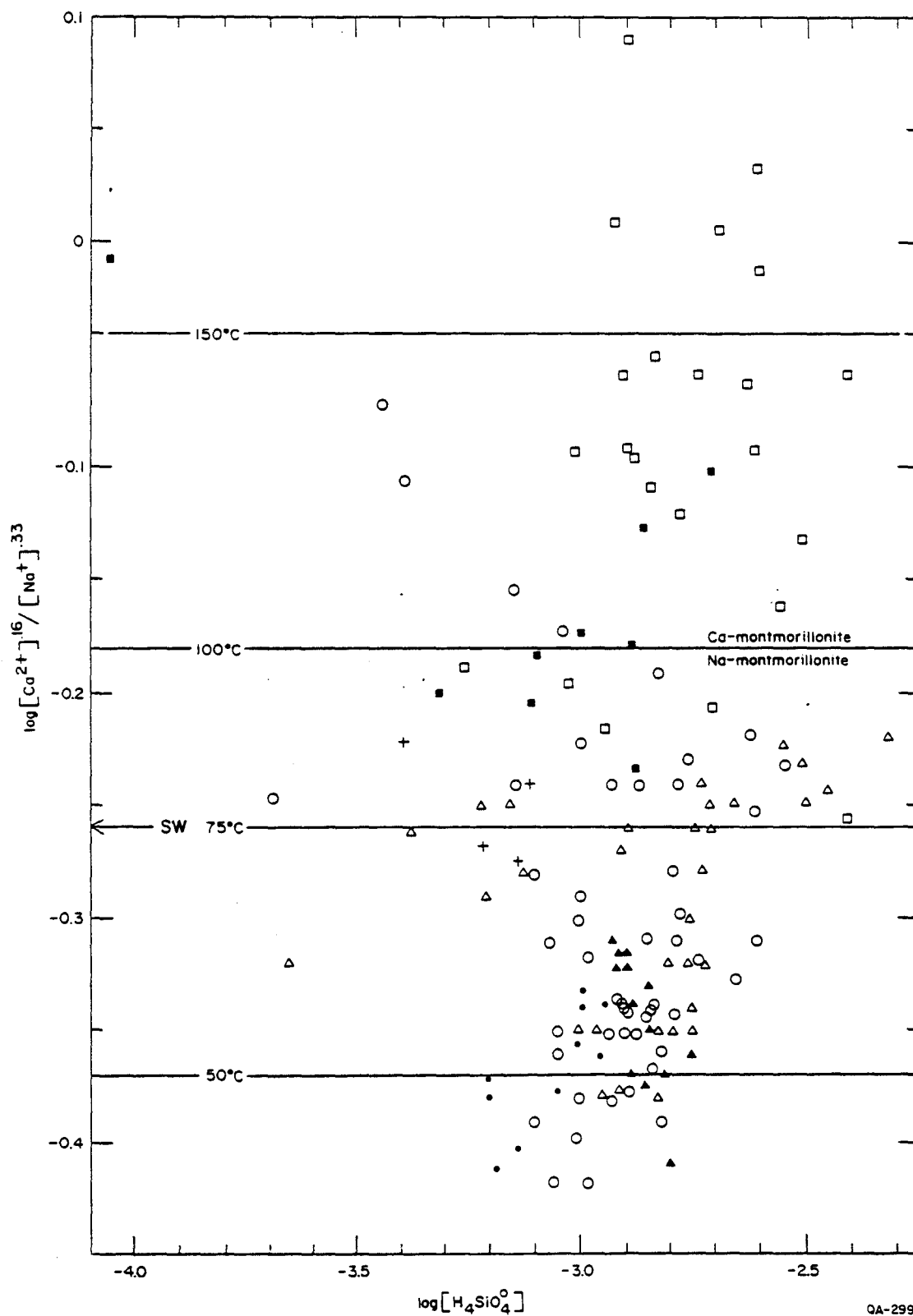


Figure III-9. Activity diagram of the reaction Ca-montmorillonite = Na-montmorillonite (equation 9, table III-2).

kaolinite or Na-montmorillonite and chlorite would likely coexist in upper/middle coast and South Texas sandstones, respectively. Geographic clustering of data points on the montmorillonite activity diagram is excellent. All South Texas waters have large  $\log[\text{Ca}^{2+}]^{.16}/[\text{Na}^{+}]^{.33}$  ratios, whereas the smallest ratios occur in middle and lower coast waters. Small ratios are postulated to be indicators of good reservoir quality at depth and large ratios to be indicators of poor quality.

Albitization—Two reactions were considered: albitization of plagioclase and of K-spar (equations 11 and 12, table III-2). Under hydro pressured conditions, represented by 1 bar pressure and temperatures of 100°C or less, all Frio waters relative to the plagioclase/albite reaction pair plot well into the albite stability field (fig. III-10). This implies that albitization is initiated in the hydro pressured interval at less than 100°C, probably between 50° and 75°C. Under geopressed conditions, represented by 600 bars pressure, the plagioclase stability field expands because of higher temperature and pressure. In effect, albitization becomes more difficult with depth. At 125°C, plagioclase is stable in Frio waters, suggesting that albitization is essentially completed at approximately 125°C and certainly before 150°C. Figure III-10 indicates a temperature of approximately 100°C in South Texas. Indeed, petrography shows that albitization is completed earlier in South Texas than on the upper coast.

Thermodynamically, K-spar is stable relative to albite but less so at increased temperatures, whereas albite is stable relative to plagioclase. This means that plagioclase is albitized before K-spar in the Frio (Kaiser and Richmann, 1981). Albitization or Na-metasomatism of K-spar (microcline) requires a  $\log[\text{K}^{+}]/[\text{Na}^{+}]$  ratio appropriate for the temperature. As temperature and  $\log[\text{K}^{+}]/[\text{Na}^{+}]$  ratio increase, the albite stability field expands to include all but one Frio hydro pressured water at 100°C (fig. III-11). Albitization is initiated between 50° and 75°C in Frio formation waters. In effect, less  $\text{Na}^{+}$  is required for albite stability at higher temperatures; K-spar is favored in fresher waters at lower relative temperatures. K-spar and albite cements or overgrowths would be stable in Frio low-temperature hydro pressured waters; they are minor, volumetrically insignificant, near-surface cements in Frio sandstones.

#### Geopressuring

There is a correlation of uncertain geochemical significance between ionic strength, analytical molality, activity indices, and geopressuring. Because the specific electrical effects of interactions among the variously charged ions are taken into consideration, ionic strength is superior to concentration in comparing waters of diverse compositions. Ionic strength (I) in the Frio ranges from 0.12 to 4.8. The correlation between I and the pressure regime is obvious:

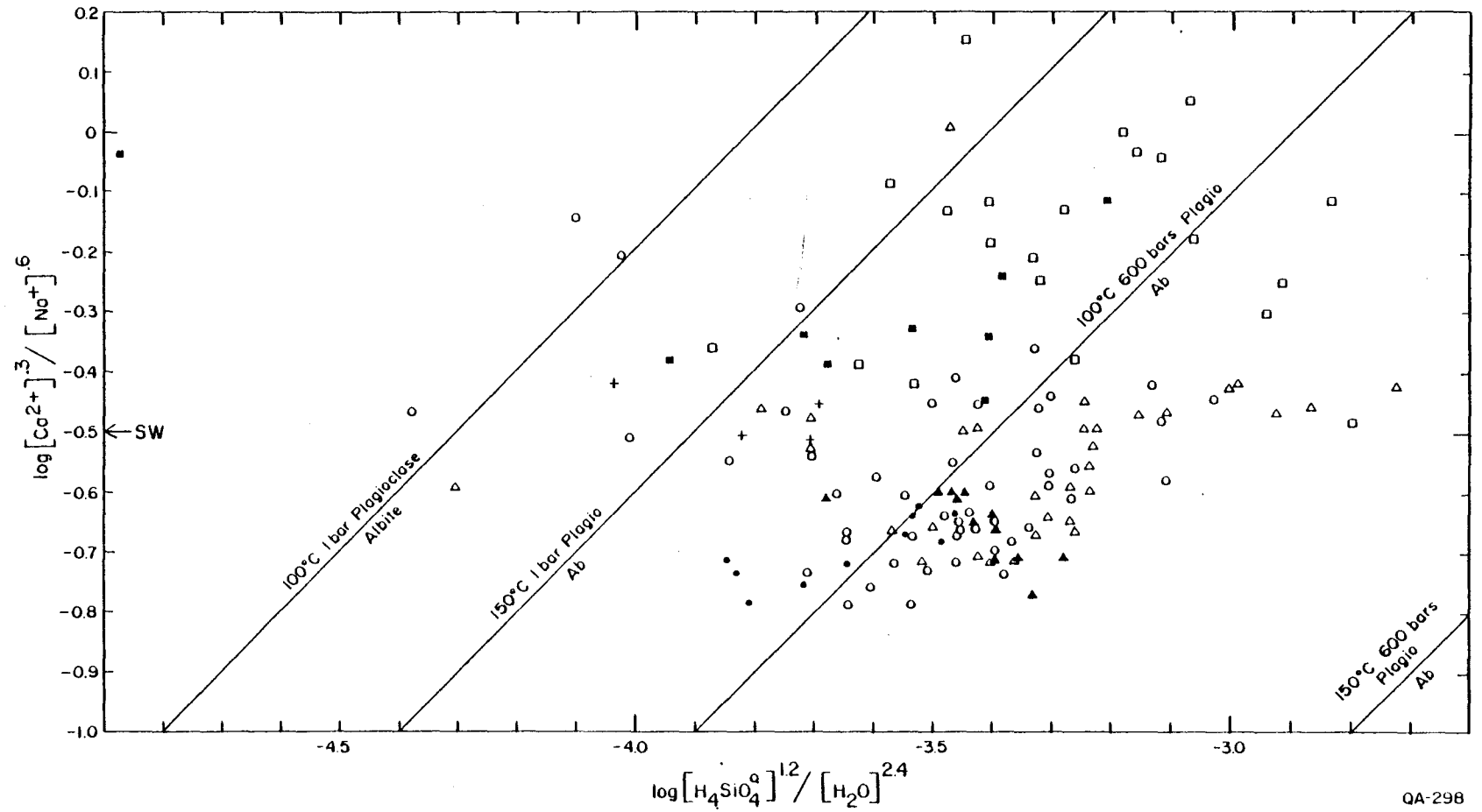


Figure III-10. Activity diagram of the reaction plagioclase (An30) = albite (equation 11, table III-2).

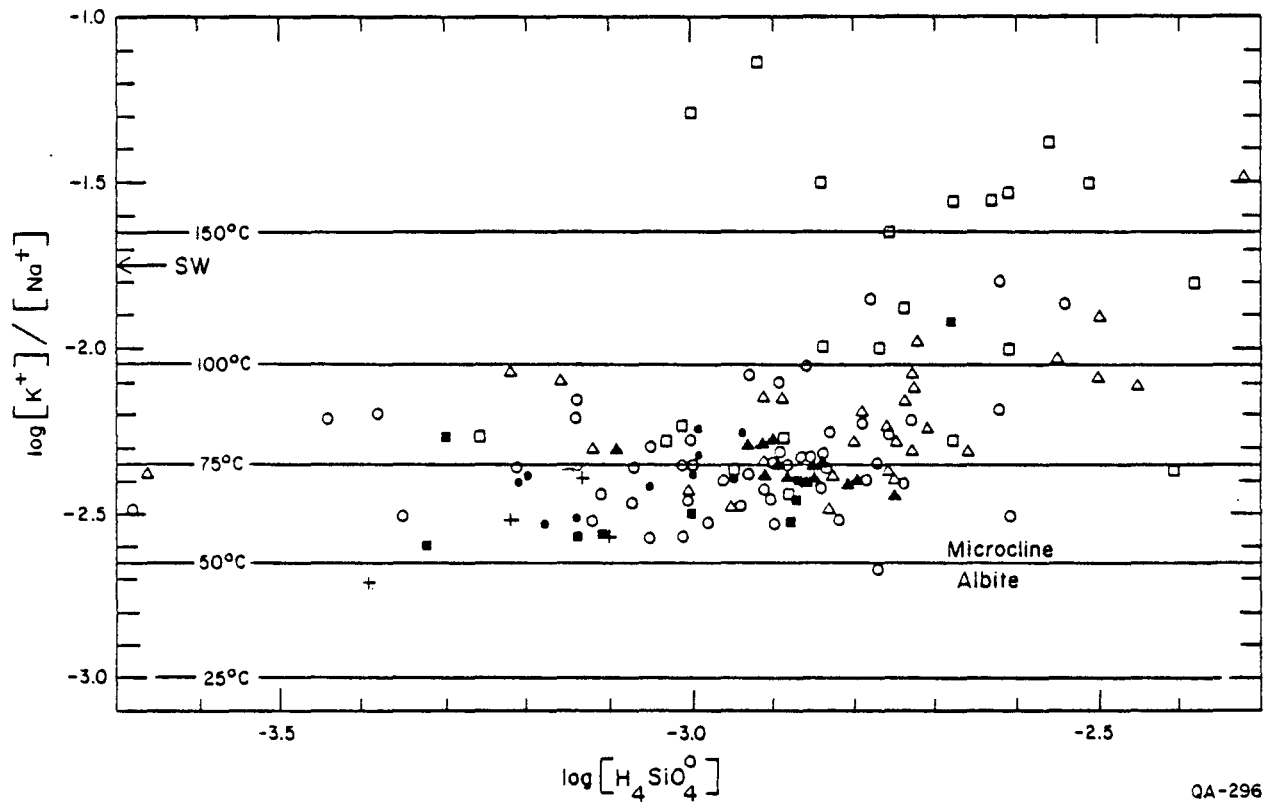


Figure III-11. Activity diagram of the reaction microcline = albite (equation 12, table III-2).

Hydropressured waters decrease or show no strong trend in I with depth to approximately 10,000 ft (3,050 m) or the top of geopressure (fig. III-12). In geopressured waters, I uniformly increases with depth to approximately 14,000 ft (4,270 m), then apparently begins to decrease.

Several mole ratios ( $\text{Ca}^{2+}/\text{Na}^+$ ,  $\text{Cl}^-/\text{Ca}^{2+}$ ,  $\text{Cl}^-/\text{Mg}^{2+}$ ,  $\text{Cl}^-/\text{K}^+$ ,  $\text{Mg}^{2+}/\text{Ca}^{2+}$ ,  $\text{K}^+/\text{Na}^+$ ,  $\text{Cl}^-/\text{Na}^+$ ,  $\text{Ca}^{2+}/\text{Fe}^{2+}$ , and  $\text{Sr}^{2+}/\text{Ca}^{2+}$ ) were plotted against depth to investigate the relationship of molality to geopressuring. Among these,  $\text{Ca}^{2+}/\text{Na}^+$  and  $\text{Cl}^-/\text{Ca}^{2+}$  show the best correlation with the pressure regime. The  $\text{Ca}^{2+}/\text{Na}^+$  ratio ranges widely in the hydropressured interval, from 0.002 to 1.7 and shows no distinct trend or perhaps a decrease to the top of geopressure. Here there is a slight shift to lower ratios and then a uniform increase in values in excess of that for seawater (0.022) (fig. III-13), reflecting the effects of  $\text{Ca}^{2+}$ -generating diagenetic reactions. Variation in the  $\text{Cl}^-/\text{Ca}^{2+}$  ratio is largest (about 5 to 510) between 8,000 and 11,000 ft (2,440 and 3,355 m), the transition zone between the hydropressured and geopressured intervals (fig. III-14). The smallest variation (5 to 20) is in waters deep in the hydropressured or geopressured interval. A similar correlation with geopressuring is shown by the  $\text{Cl}^-/\text{Mg}^{2+}$  and  $\text{Cl}^-/\text{K}^+$  ratios. The variation observed is attributed either to more active water-rock interaction or to diagenesis in the transition zone. The  $\text{Mg}^{2+}/\text{Ca}^{2+}$  ratio uniformly decreases from the top of geopressure downward, reflecting loss of  $\text{Mg}^{2+}$  in authigenic chlorite and calcite. Variation among hydropressured waters is large, from 0.002 to 1.0 (seawater equals 5.6). The  $\text{K}^+/\text{Na}^+$  ratio shows no correlation with pressure; it gradually increases with depth and may be controlled mainly by temperature-dependent water-rock interaction, such as albitization and breakdown of detrital illite. The latter source of  $\text{K}^+$  is suggested by the fact that the  $\text{K}^+/\text{Na}^+$  ratio continues to increase below the depth of K-spar albitization. Most  $\text{Cl}^-/\text{Na}^+$  ratios are approximately 1.0; however, ratios in South Texas waters exceed 1.0, ranging from greater than 1.0 to 4.4. Clearly, not all Frio waters can be attributed to halite dissolution.

Mineral transformations were correlated with geopressuring by plotting activity indices, derived from the diagenetic reaction pairs (table III-2), against depth. The intent was to relate specific reactions to geopressuring, to high-resistivity shale (cap rock) at the top of geopressure, and ultimately to brine evolution. One of these reactions is the Ca-Na-montmorillonite exchange. From the top of geopressure downward, roughly coincident with the 100°C isotherm, the  $\log[\text{Ca}^{2+}]^{.16}/[\text{Na}^+]^{.33}$  ratio uniformly increases whereas the variation for hydropressured waters is large (fig. III-15). Besides the exchange reaction, exchanging one  $\text{Ca}^{2+}$  for two  $\text{Na}^+$  ions, other  $\text{Ca}^{2+}$ -generating (and  $\text{Na}^+$ -consuming) reactions are probably reflected in the  $\log[\text{Ca}^{2+}]^{.16}/[\text{Na}^+]^{.33}$  ratio. Among these are Ca-montmorillonite = chlorite, Ca-montmorillonite = kaolinite, plagioclase = kaolinite, calcite = ferroan calcite, smectite = illite, and

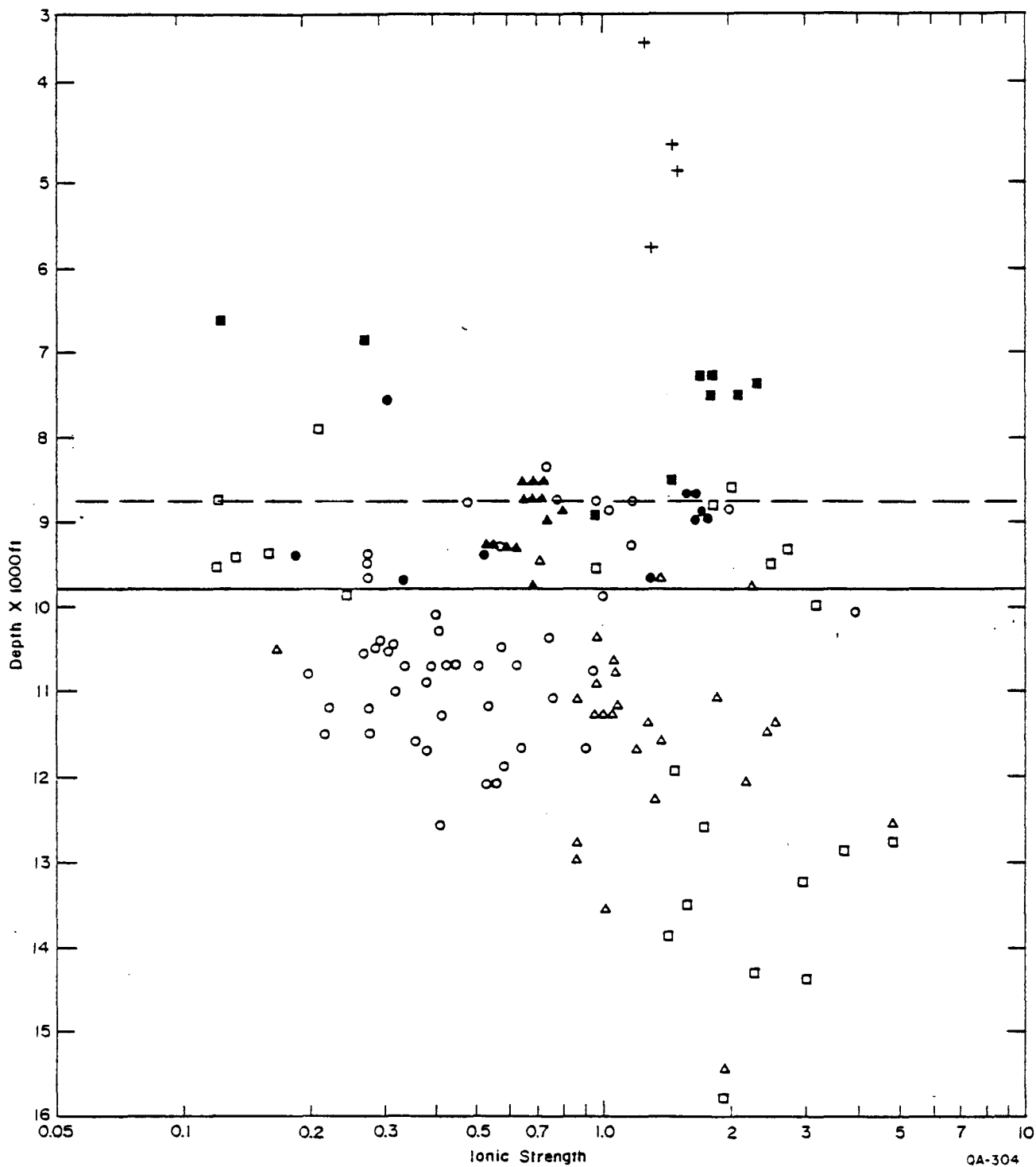


Figure III-12. Ionic strength versus depth,  $I = 0.7$  in seawater. Solid line designates approximate depth to deepest hydro pressured waters in upper and middle coast, and dashed line likewise in lower coast or South Texas.

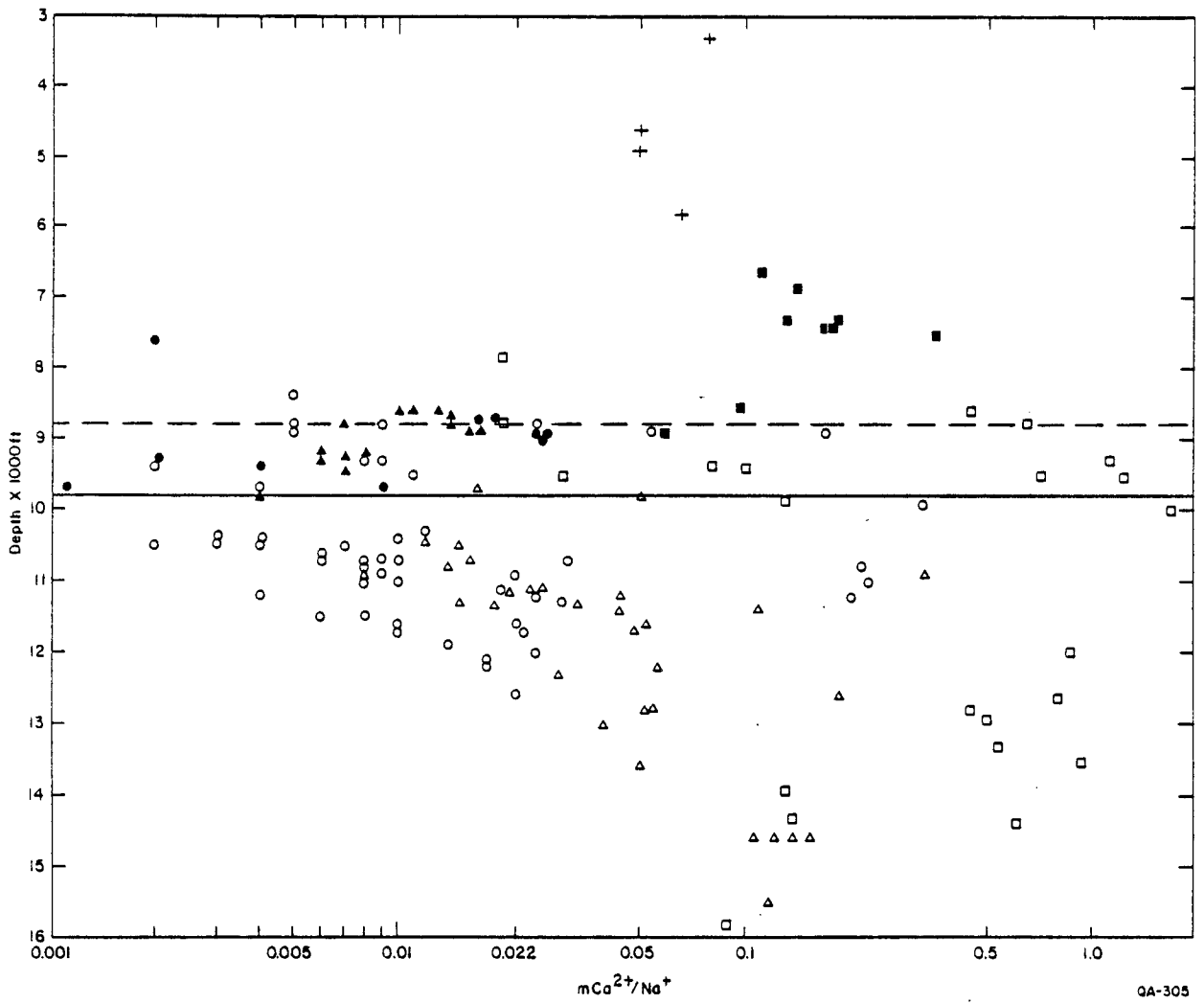


Figure III-13. Ca<sup>2+</sup>/Na<sup>+</sup> mole ratio versus depth; ratio = 0.022 in seawater.

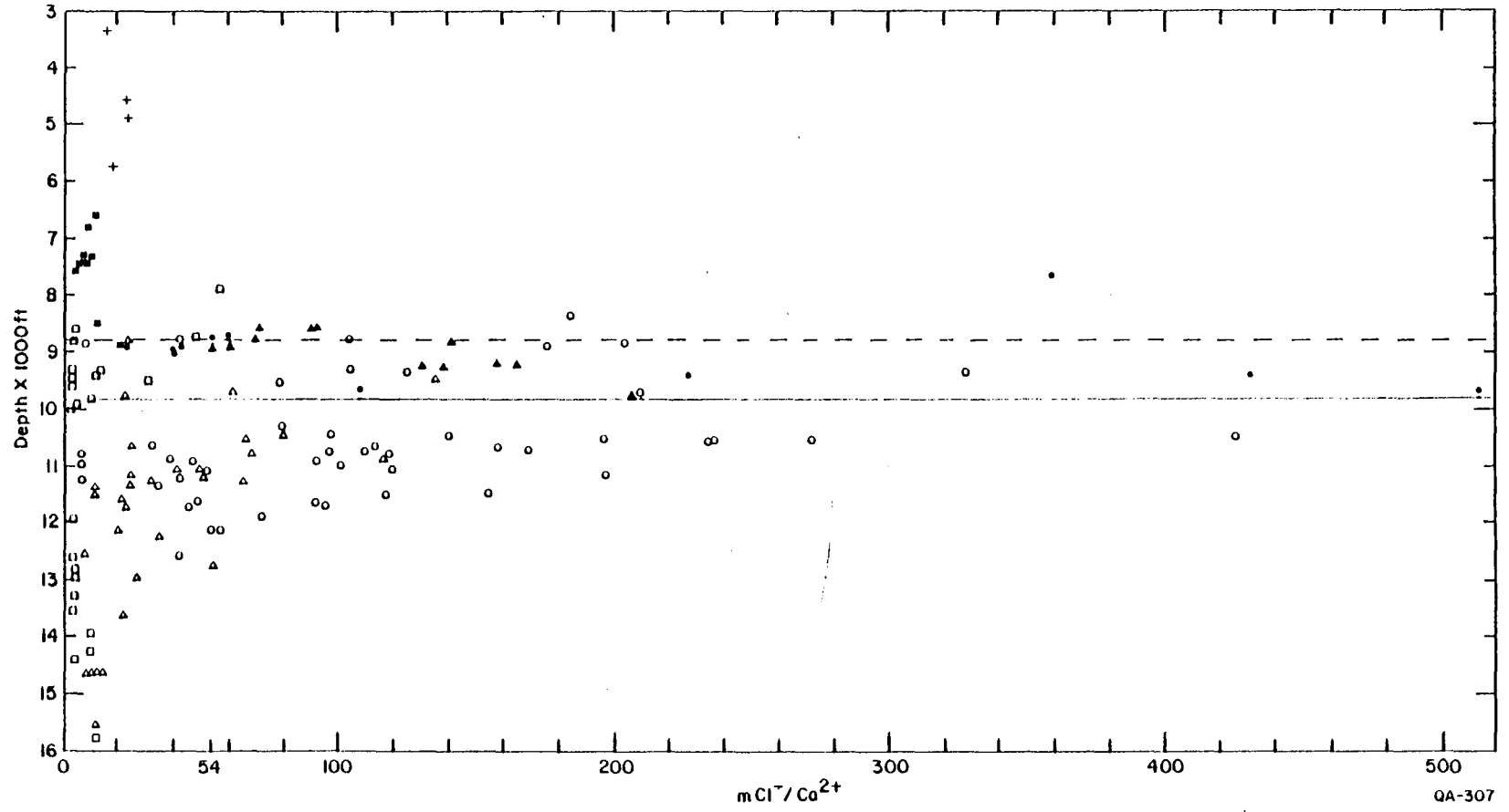
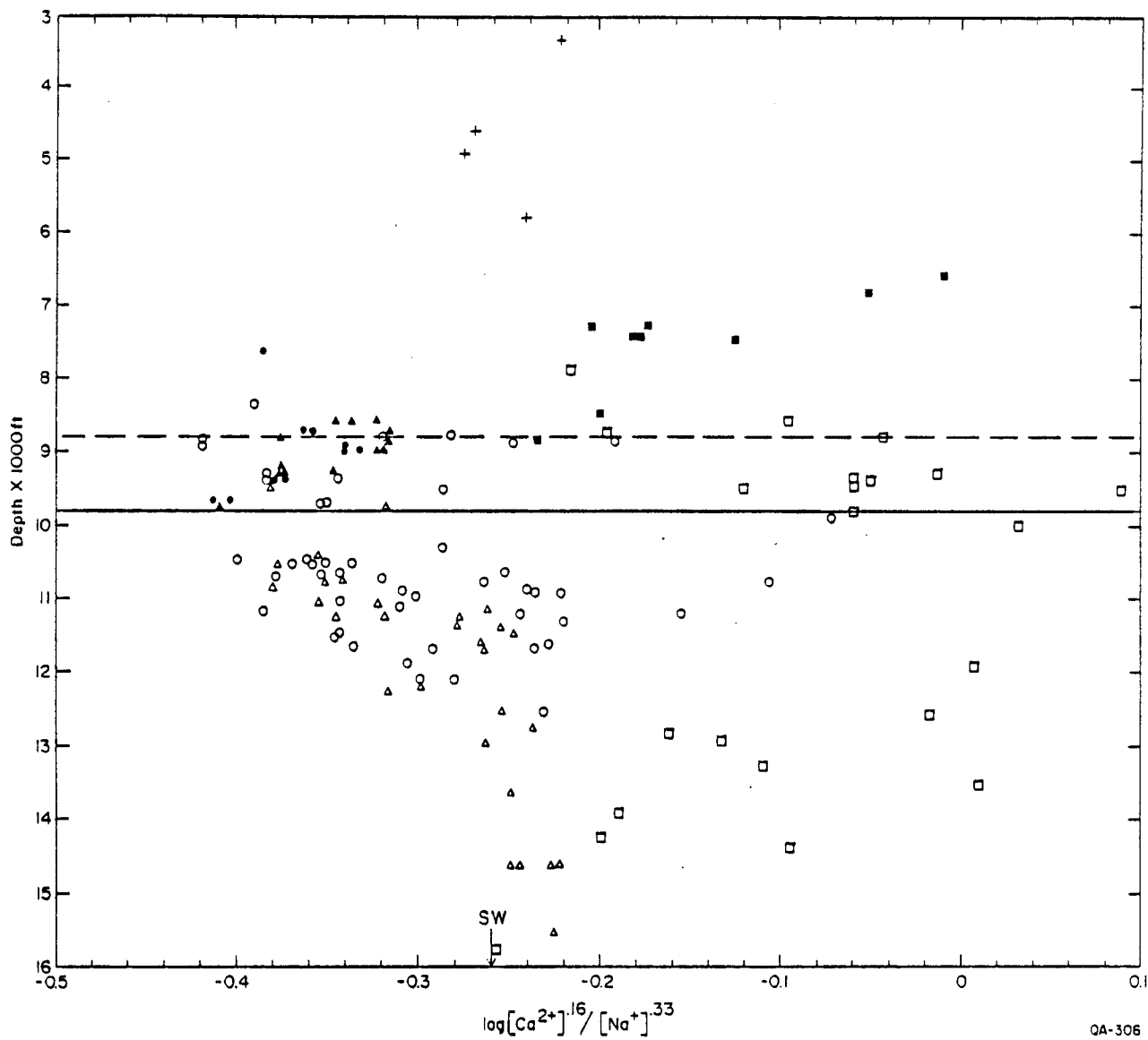


Figure III-14.  $Cl^-/Ca^{2+}$  mole ratio versus depth; ratio = 54 in seawater.



QA-306

Figure III-15.  $\log[\text{Ca}^{2+}]^{16} / [\text{Na}^+]^{33}$  ratio, derived from the reaction Ca-montmorillonite = Na-montmorillonite, versus depth. SW = log activity ratio in seawater.

albitization of plagioclase. The latter is an important source of  $\text{Ca}^{2+}$ ; however, total albitization of detrital plagioclase would probably release less than 50 percent of the  $\text{Ca}^{2+}$  necessary for diagenesis in the Frio Formation (Kaiser and Richmann, 1981). Clearly, additional sources of  $\text{Ca}^{2+}$  must be sought in chloritization, kaolinitization, and illitization reactions.

Plots of activity indices versus depth for the clay-mineral reactions discussed here display distinctive funnel-shaped patterns of data-distribution (fig. III-16). Variation in the activity index is largest between 8,000 and 11,000 ft (2,440 and 3,355 m), the hydropressure-geopressure transition zone. Considerably less variation is displayed by distinctly hydro pressured or geopressed waters. This implies that most of the diagenesis occurs in the transition zone. Activity indices converge on the top of geopressure and get larger or smaller, signaling favorability of one clay mineral over another. In figure III-16, the index gets larger, in effect converging on Ca-montmorillonite favorability. Chlorite either is unstable in the transition zone or is forming freeing  $\text{Ca}^{2+}$  and consuming  $\text{Fe}^{2+}$  and  $\text{Mg}^{2+}$ . With respect to montmorillonite, illite and kaolinite stability are favored in the transition zone, whereas montmorillonite, illite, and kaolinite are favored with respect to chlorite. Chlorite stability is favored in distinctly hydro pressured and geopressed waters, suggesting two stages of chlorite formation (fig. III-16).

## DIAGENETIC HISTORY

Major diagenetic events in the Frio Formation have been established petrographically by Loucks and others (1981) (fig. III-17). Within this diagenetic framework, solution-mineral equilibria can be used to sharpen our perception of carbonate equilibrium, relative mineral stabilities, and timing of diagenetic events. For instance, some petrographically unanswered questions concern episodic precipitation and leaching of authigenic calcite, timing of albitization, and stages of chlorite formation.

### Carbonate Equilibrium

Multiple generation of authigenic calcite is the rule in the Frio Formation. Major episodes of calcite precipitation occurred in several stages throughout the burial history. Leaching of calcite is also episodic and is responsible for most of the secondary porosity in Frio sandstones. These episodes are reflected in the presence of several distinctive calcite compositions at various depths (Loucks and others, 1981). Calcite sequencing is predictable from carbonate equilibrium and the trend of  $\log[\text{Ca}^{2+}]^{.05}/[\text{Fe}^{2+}]^{.05}$  ratio and  $\text{Ca}^{2+}/\text{Fe}^{2+}$

mole ratio with depth. To form non-ferroan calcite, the virtual absence of  $\text{Fe}^{2+}$  is required; waters having a  $[\text{Ca}^{2+}]/[\text{Fe}^{2+}]$  ratio of less than 10,000 will first yield ferroan calcite. Non-ferroan calcite is stable in surface seawater (fig. III-2) and probably would be favored in sulfide-rich hydro pressured waters before initiation of clay mineral transformations and release of  $\text{Fe}^{2+}$ . Ferroan calcite might be expected in sulfide-poor geopressed waters subject to deeper burial and higher temperatures. Ferroan calcite can also form at shallow depths in response to circulation of meteoric ground water. Indeed, in anaerobic fresh water,  $[\text{Fe}^{2+}]$  is commonly high relative to  $[\text{Ca}^{2+}]$  and siderite is stable. In addition, pure calcite might reappear at depth, even in the presence of some  $\text{Fe}^{2+}$  in very  $\text{Ca}^{2+}$ -rich and sulfide-rich waters, such as those that might be discharging from the underlying Mesozoic strata, as suggested by Galloway (1982). Timing and depth of calcite precipitation are directly affected by pH. Because pH generally decreases with depth in elisian (compactional) and abyssal (thermobaric) waters, calcite precipitation should be expected early in diagenesis.

Frio  $\log[\text{Ca}^{2+}]^{.05}/[\text{Fe}^{2+}]^{.05}$  ratios range widely, from 0.01 to 0.32, plotting deep in the ferroan calcite and calcite stability fields, respectively. Reflected, perhaps, is constant reequilibration with changing water chemistry or, in other words, multiple generation of calcite. Similarly, the  $\text{Ca}^{2+}/\text{Fe}^{2+}$  mole ratio displays a tremendous range of values, from 2 to 600,000. No obvious correlation is seen with geopressing. Late-stage ferroan calcite in South Texas is consistent with the trend of  $\log[\text{Ca}^{2+}]^{.05}/[\text{Fe}^{2+}]^{.05}$  ratio with depth; in these Frio waters it decreases. Likewise, a weak trend of decrease with depth is evident in the  $\text{Ca}^{2+}/\text{Fe}^{2+}$  mole ratio and also indicates that ferroan calcite is favored at depth.

#### Timing of Albitization

Albitization follows formation of quartz overgrowths, which precipitate at approximately  $60^{\circ}\text{C}$ . On the basis of microprobe data, regional geothermal gradients, and isotopic data, albitization occurs nearly contemporaneous with major kaolinite precipitation. Kaolinite cement is the last major authigenic mineral to form on the upper coast and either follows or coincides with major calcite leaching, a low-pH event (fig. III-17); kaolinite formed at approximately  $100^{\circ}\text{C}$ , as deduced from isotopic analysis (Loucks and others, 1981). Kaolinite cement is inferred to follow albitization because its temperature of formation, as calculated from isotopic data, is higher than that for initiation of albitization, which is estimated thermodynamically at less than  $100^{\circ}\text{C}$ . Furthermore, in view of the fact that plagioclase nucleates kaolinite cement, the relative stability of plagioclase with respect to albite and kaolinite is instructive. Relative to plagioclase, albite is thermodynamically favored over kaolinite; therefore, it is inferred that kaolinite cement followed albitization.

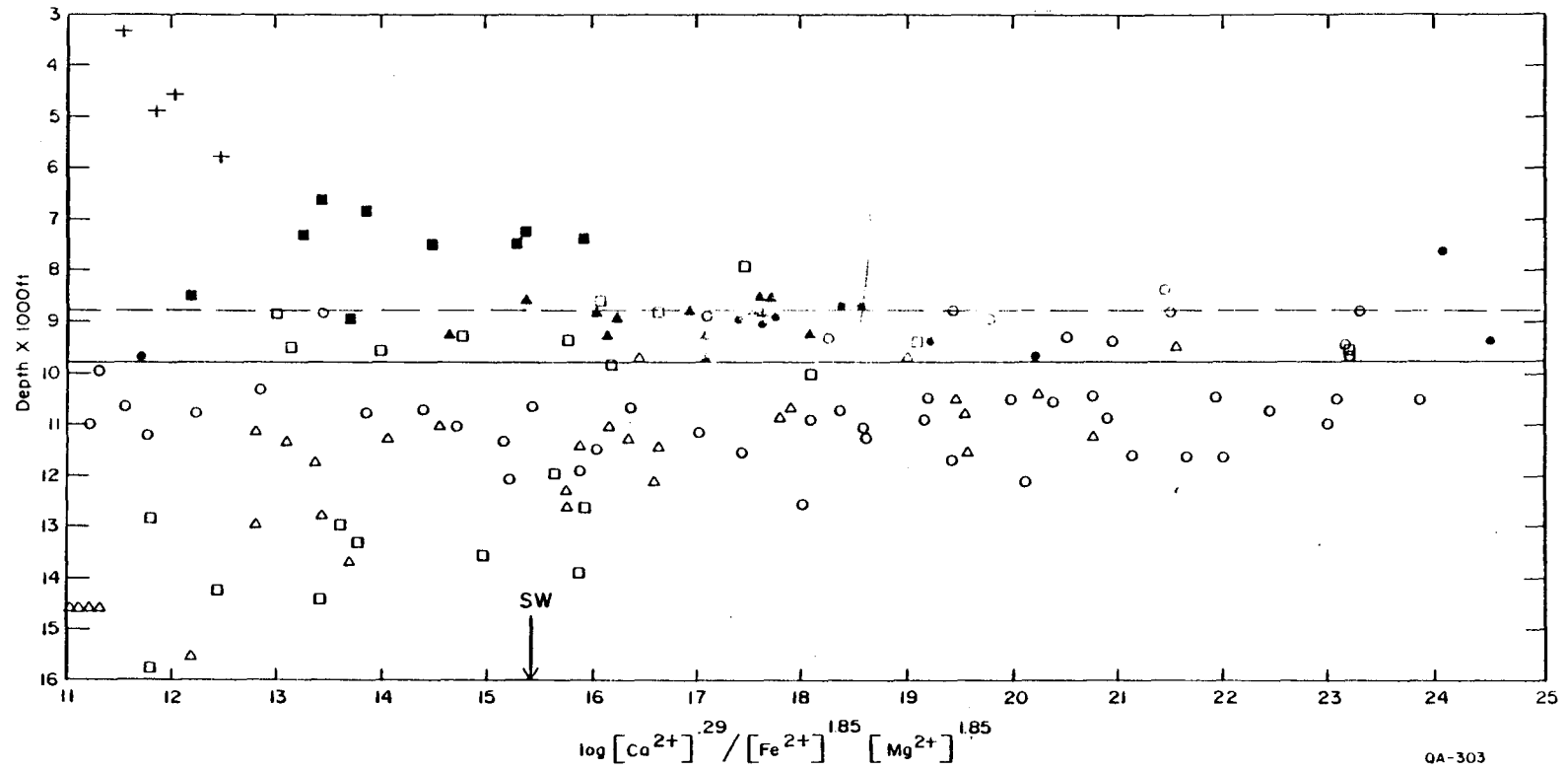


Figure III-16.  $\log [Ca^{2+}]^{.29} / [Fe^{2+}]^{1.85} [Mg^{2+}]^{1.85}$  ratio, derived from the reaction Ca-montmorillonite = chlorite, versus depth. Larger log ratios favor montmorillonite stability.

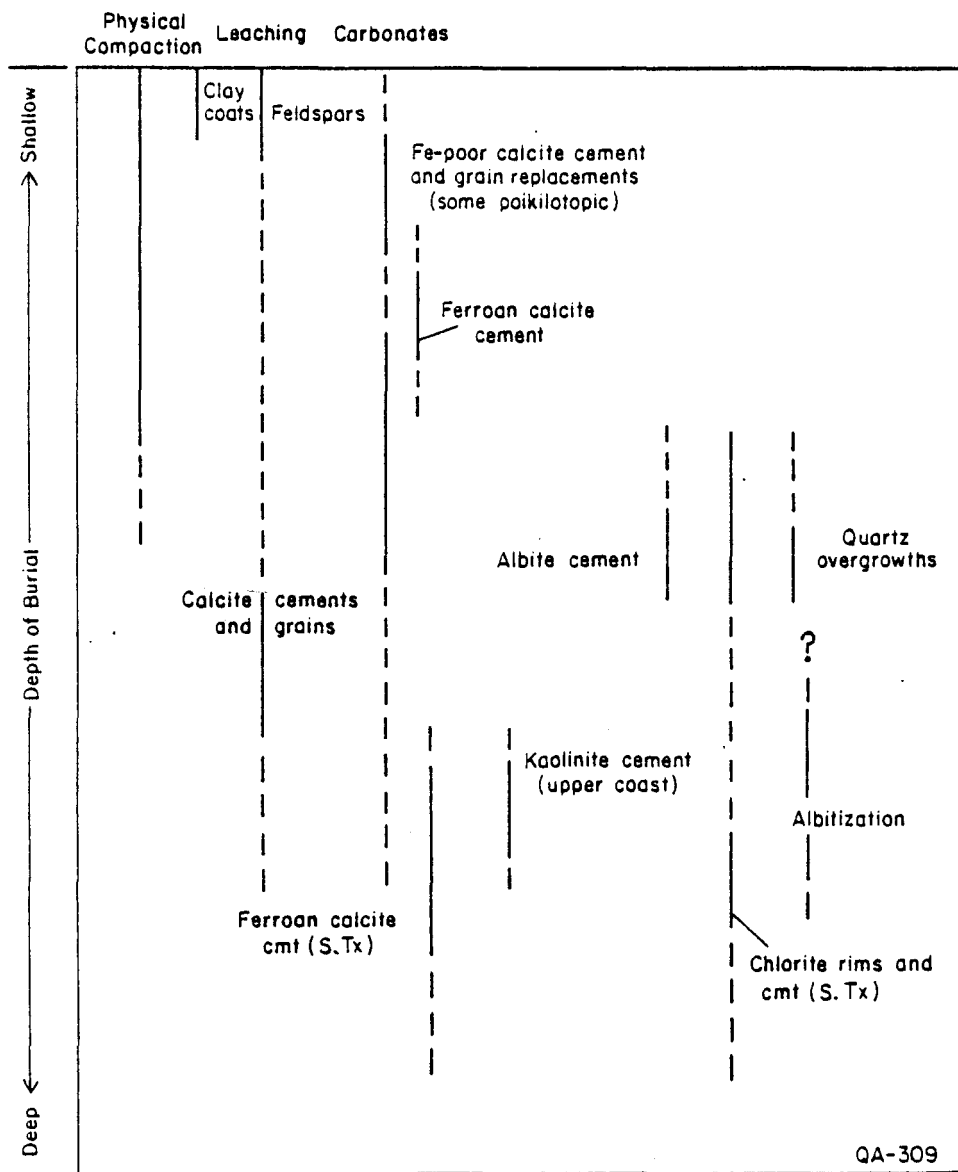


Figure III-17. Major diagenetic events in the Frio Formation (modified from Loucks and others, 1981).

## Chlorite Formation

Two stages of chlorite formation are proposed (fig. III-17). In the first stage, chlorite forms at the expense of Ca-montmorillonite clay coats to yield chlorite rims under hydro-pressured conditions at less than 75°C. Chlorite will appear early in those sediments or rocks that are rich in Fe<sup>2+</sup> and Mg<sup>2+</sup> (Velde, 1972), not unlike the volcanic-rich Frio sediments of South Texas. Certainly, chlorite, in particular 7Å varieties, would be favored in the Fe<sup>2+</sup>-rich and Mg<sup>2+</sup>-rich waters of South Texas. A second stage is postulated to form at the expense of kaolinite cement to yield chlorite cement under geopressured conditions at greater than 100°C, accounting for the absence of kaolinite in the deep Frio of South Texas.

## CONCLUSIONS

1. Diagenesis is mainly a function of temperature, pH, and pressure; it is only secondarily a function of mineral solubilities. Most diagenesis occurs in the transition zone between the hydro-pressured and geopressured interval.

2. Solution-mineral equilibria in hydro-pressured waters best reflect reservoir quality because most diagenesis occurs in the transition zone. Activity indices favoring chlorite and ferroan calcite stability and large  $\log[\text{Ca}^{2+}]^{.16}/[\text{Na}^{+}]^{.33}$  ratios are the best indicators of reservoir quality in deep Frio sandstone reservoirs.

3. Predictions about Frio diagenesis based on equilibrium thermodynamics are consistent with those established petrographically or from isotopic data, suggesting that estimated equilibrium constants ( $\log K_f$  and  $K_r$ ) are probably correct to one or two orders of magnitude. Chemical reality can be approximated in the Frio Formation.

4. Water-chemistry data complement petrographic data, adding insight on diagenetic sequence, in situ pH, and relative mineral stabilities. Carbonate equilibrium requires early precipitation of calcite in diagenesis. In situ pH's of geopressured waters are inferred to be 2 or 3 pH units lower than those measured at the wellhead. Low temperature and pH explain the general absence of chlorite in the upper Texas coast. Chlorite and illite are the stable layer silicates in deep Frio sandstones. The smectite/illite transformation is not the only clay mineral transformation of importance in diagenesis.

5. Predicting the course of diagenesis for whole basins or for individual reservoirs is possible armed with some knowledge of bulk composition, temperature and pressure gradients, and solution-mineral equilibria.

## ACKNOWLEDGMENTS

This research was funded in part by the U.S. Department of Energy, Division of Geothermal Energy, under Contract No. DE-AC08-79ET27111. The assistance of B. Dan Legett in the calculation of thermodynamic functions was invaluable. This study could not have been done without his calculations and computer program to determine  $\log K_f$  and  $\log K_r$  values. Many companies provided access to their properties for water sampling. James F. O'Connell collected Frio water samples, compiled water-chemistry data, and modified computer routines for plotting activity indices and mole ratios. Chemical analyses were done under the direction of Clara L. Ho, chemist-in-charge, Mineral Studies Laboratory of the Bureau of Economic Geology. The report was typed by Dorothy C. Johnson under the direction of Lucille C. Harrell. Illustrations were drafted by John T. Ames under the direction of Dan F. Scranton.

## REFERENCES

- Bebout, D. G., Loucks, R. G., and Gregory, A. R., 1978, Frio sandstone reservoirs in the deep subsurface along the Texas Gulf Coast, their potential for the production of geopressed geothermal energy: The University of Texas at Austin, Bureau of Economic Geology Report of Investigations No. 91, 92 p.
- Boles, J. R., and Franks, S. G., 1979, Clay diagenesis in Wilcox sandstones of southwest Texas: implications of smectite diagenesis on sandstone cementation: *Journal of Sedimentary Petrology*, v. 49, no. 1, p. 55-70.
- Brewer, R., 1964, Fabric and mineral analysis of soils, ch. 10, Pedological features I: Cutans: New York, John Wiley and Sons, p. 205-233.
- Carroll, D., 1970, Clay minerals: a guide to their x-ray identification: Geological Society of America Special Paper 126, 80 p.
- Eugster, H. P., and Chou, I. M., 1973, The depositional environments of Precambrian banded-iron formations: *Economic Geology*, v. 68, p. 1144-1168.
- Fisher, J. A., and Zen, E-An, 1971, Thermochemical calculations from hydrothermal phase equilibrium data and the free energy of H<sub>2</sub>O: *American Journal of Science*, v. 270, p. 297-314.
- Galloway, W. E., 1982, Epigenetic zonation and fluid flow history of uranium-bearing fluvial aquifer systems, South Texas uranium province: The University of Texas at Austin, Bureau of Economic Geology Report of Investigations No. 119, 31 p.
- Galloway, W. E., and Kaiser, W. R., 1980, Catahoula Formation of the Texas Coastal Plain: origin, geochemical evolution, and characteristics of uranium deposits: The University of Texas at Austin, Bureau of Economic Geology Report of Investigations No. 100, 81 p.

- Garrels, R. M., and Christ, C. L., 1965, Solutions, minerals, and equilibria, ch. 9, Effects of temperature and pressure variations on equilibria: New York, Harper and Row, p. 306-351.
- Helgeson, H. C., 1969, Thermodynamics of hydrothermal systems at elevated temperatures and pressures: *American Journal of Science*, v. 267, p. 729-804.
- Helgeson, H. C., Delaney, J. M., Nesbitt, H. W., and Bird, D. K., 1978, Summary and critique of the thermodynamic properties of rock-forming minerals: *American Journal of Science*, v. 278-A, 229 p.
- Hower, J., Eslinger, E. V., Hower, M. E., and Perry, E. A., 1976, Mechanism of burial metamorphism of argillaceous sediment: 1. mineralogical and chemical evidence: *Geological Society of America Bulletin*, v. 87, no. 5, p. 725-737.
- Kaiser, W. R., 1982, Predicting diagenetic history and reservoir quality in the Frio Formation (Oligocene) of Texas (abs.): Eleventh International Congress on Sedimentology, Hamilton, Ontario, McMaster University, Abstracts of Papers, p. 119-120.
- Kaiser, W. R., and Richmann, D. L., 1981, Predicting diagenetic history and reservoir quality in the Frio Formation of Brazoria County, Texas, and Pleasant Bayou test wells, in Sebout, D. G., and Bachman, A. L., eds., Proceedings, Fifth U.S. Gulf Coast Geopressured-Geothermal Energy Conference: Baton Rouge, Louisiana State University, p. 67-74.
- Kerrick, Y. K., and Darken, L. S., 1975, Statistical thermodynamic models for ideal oxide and silicate solid solutions with applications to plagioclase: *Geochimica et Cosmochimica Acta*, v. 39, p. 1431-1442.
- Kharaka, Y. K., and Barnes, I., 1973, SOLMNEQ: Solution-mineral equilibrium computations: Springfield, Virginia, National Technical Information Service Technical Report PB-215899, 81 p.
- Kharaka, Y. K., Callender, E., and Carothers, W. W., 1977, Geochemistry of geopressured geothermal waters from the Texas Gulf Coast, in Meriwether, J., ed., Proceedings, Third Geopressured-Geothermal Energy Conference: Lafayette, Louisiana, University of Southwestern Louisiana Center for Energy Studies, v. 1, p. GI 121-165.
- Kharaka, Y. K., Lico, M. S., Wright, V. A., and Carothers, W. W., 1979, Geochemistry of formation waters from Pleasant Bayou No. 2 well and adjacent areas in coastal Texas, in Dorfman, M. H., and Fisher, W. L., eds., Proceedings, Fourth U.S. Gulf Coast Geopressured-Geothermal Energy Conference: The University of Texas at Austin, Center for Energy Studies, v. 1, p. 168-193.
- Lindquist, S. J., 1977, Secondary porosity development and subsequent reduction, overpressured Frio Formation sandstone (Oligocene), South Texas: *Gulf Coast Association Geological Societies Transactions*, v. 27, p. 99-107.
- Loucks, R. G., Dodge, M. M., and Galloway, W. E., 1979a, Sandstone consolidation analysis to delineate areas of high-quality reservoirs suitable for production of geopressured geothermal energy along the Texas Gulf Coast: The University of Texas at Austin, Bureau of Economic Geology, Contract Report No. EG-77-5-05-5554 for U.S. Department of Energy, 97 p.

- Loucks, R. G., Richmann, D. L., and Milliken, K. L., 1979b, Factors controlling porosity and permeability in geopressured Frio sandstone reservoirs, General Crude Oil/Department of Energy Pleasant Bayou test wells, Brazoria County, Texas, in Dorfman, M. H., and Fisher, W. L., eds., Proceedings, Fourth U.S. Gulf Coast Geopressured-Geothermal Energy Conference: The University of Texas at Austin, Center for Energy Studies, v. 1, p. 46-82.
- \_\_\_\_\_ 1981, Factors controlling reservoir quality in Tertiary sandstones and their significance to geopressured geothermal production: The University of Texas at Austin, Bureau of Economic Geology Report of Investigations No. 111, 41 p.
- Morton, R. A., Garrett, C. M., Jr., Posey, J. S., Han, J. H., and Jirik, L. A., 1981, Salinity variations and chemical compositions of waters in the Frio Formation, Texas Gulf Coast: The University of Texas at Austin, Bureau of Economic Geology, Contract Report No. DOE/ET/27111-5 for U.S. Department of Energy, 96 p.
- Richmann, D. L., Milliken, K. L., Loucks, R. G., and Dodge, M. M., 1980, Mineralogy, diagenesis, and porosity in Vicksburg sandstones, McAllen Ranch Field, Hidalgo County, Texas: Gulf Coast Association of Geological Societies Transactions, v. 30, p. 473-481.
- Robie, R. A., Hemingway, B. S., and Fisher, J. R., 1978, Thermodynamic properties of minerals and related substances at 298.15K and 1 bar ( $10^5$  Pascals) pressure and at higher temperature: U.S. Geological Survey Bulletin 1452, 456 p.
- Saxena, S. K., 1973, Thermodynamics of rock-forming crystalline solutions: New York, Springer-Verlag, 188 p.
- Tardy, Y., and Garrels, R. M., 1974, A method of estimating the Gibbs energies of formation of layer silicates: *Geochimica et Cosmochimica Acta*, v. 38, p. 1101-1116.
- Velde, B., 1972, Phase equilibria for dioctahedral expandable phases in sediments and sedimentary rocks: Assoc. Internat. pour l'Etude des Argiles, Internat. Clay Conf., Madrid, June 25-30, 1972, preprints, v. 1, p. 285-300.
- Wood, B. J., and Fraser, D. G., 1976, Elementary thermodynamics for geologists, ch. 3, Multicomponent solids and fluids: New York, Oxford University Press, p. 81-126.

## Section IV

# DISTRIBUTION AND POSSIBLE DIAGENETIC ORIGIN OF HIGH-RESISTIVITY CAP ROCK SHALE, FRIO FORMATION, TEXAS GULF COAST

*By Robert J. Finley*

*Assisted by S. L. Hallam and S. W. Speer*

### ABSTRACT

The distribution of high-resistivity shale, known as cap rock in Gulf Coast Tertiary sequences, coincides with the transition zone between hydro pressured and geopressed regimes wherein significant clay mineral diagenesis takes place. Cap rock within the Oligocene Frio Formation in Texas occurs at depths where temperatures are generally between 75° and 90°C and pressure gradients are between 0.465 and 0.7 psi/ft (10.5 and 15.8 kPa/m). Analyses of cap rock shales show 2 to 3 percent increases in silica content relative to shallower non-cap rock samples but no increase in carbonate mineral content. Cap rock had previously been attributed to precipitation of calcite derived from leaching in the geopressed zone.

Instead, clay mineral transformations such as smectite-illite and smectite-chlorite may contribute to cap rock formation by release of diagenetic silica. The latter reaction releases more silica than the former and is favored in the Lower Texas Gulf Coast by higher pH of formation waters and greater availability of Mg<sup>2+</sup> and Fe<sup>2+</sup>. Cap rock appears unrelated to depositional facies and, consequently, to the types and amounts of organic matter that may be present in coeval Frio deltas. From north to south along the Texas Gulf Coast, increased cap rock development correlates with conditions suitable to chlorite stability and with poor reservoir quality related to a mineral assemblage containing abundant unstable constituents.

### INTRODUCTION

High-resistivity shale, known as cap rock in Gulf Coast Tertiary clastic sequences, has been attributed to authigenic carbonate minerals derived from leaching at depth in geopressed intervals (Magara, 1981). However, little direct evidence of excess carbonate cementation in cap rock relative to non-cap rock has been presented to date, and geochemical controls on cap rock distribution are not understood. Schmidt and McDonald (1979), and other authors as

well, have shown that dissolution of carbonate minerals is an important diagenetic process leading to development of secondary porosity. Any possible relationship between cap rock development and secondary porosity may lead to a useful indicator of reservoir conditions at greater depths, should cap rock occurrence be clearly related to dissolution of preexisting authigenic cements. To understand the nature of cap rock and its potential as an indicator of reservoir quality, an analysis of cap rock in the Oligocene Frio Formation of the Texas Gulf Coast was initiated. Cap rock distribution was mapped and petrographic and chemical analyses of cap rock shales were undertaken, supported by extensive previous work on diagenesis of Frio sandstones (Loucks and others, 1977; Loucks and others, 1981; Milliken and others, 1981). Results reported here are not conclusive with regard to the origin of cap rock shales but do suggest that an origin related to clay mineral transformations, rather than to dissolution and reprecipitation of carbonate minerals, is likely.

As part of the studies of Bebout and others (1978), Loucks and others (1979), and Gregory and others (1980), detailed investigations of reservoir quality revealed complex diagenetic histories of Tertiary sandstones, including sandstones of the Frio Formation. Many episodes of precipitation and leaching of authigenic carbonate cements occurred, leading to a variable distribution of secondary porosity (Loucks and others, 1977; Loucks and others, 1981; Milliken and others, 1981). Within the Frio Formation, reservoir quality depends on relationships among depositional environment, sediment composition, pore fluids, and prior compaction, cementation, and leaching. Deeper Frio reservoirs display secondary porosity resulting from leaching of feldspars, volcanic rock fragments, and calcite cements. Secondary porosity is poorly developed in the Lower Texas Gulf Coast but improves toward the Upper Texas Gulf Coast, in part because the mineralogy of the sandstones shifts toward a more quartzose and chemically stable assemblage. Also, fewer carbonate rock fragments are present in the Frio of the Upper Texas Gulf Coast than of the lower coastal area, where they are thought to act as nuclei for carbonate cementation (Lindquist, 1977; Loucks and others, 1977).

#### CAP ROCK DISTRIBUTION

Gregory and others (1980) used the method of Hottman and Johnson (1965) to derive formation fluid pressures from shale-resistivity data in the assessment of entrained methane in geopressured reservoirs of the Texas Gulf Coast. The amplified short-normal resistivity curves from induction electrical logs were used to plot shale resistivity as a function of depth. Normal compaction curves were fitted by a least-squares regression method, and a composite normal compaction curve was generated for most counties of the Texas Gulf Coast. Cap rock is defined as an interval having shale resistivity in excess of that predicted by the normal compaction curve (Fertl, 1976; Gregory and others, 1980).

Cap rock was mapped using a regional data base of shale-resistivity versus depth plots for approximately 350 wells. A typical shale-resistivity plot includes the normal compaction curve, mud weights, calculated pressures, and measured pressures (fig. IV-1). Criteria were established for the recognition of cap rock from shale-resistivity plots (table IV-1). That part of the shale-resistivity plot representing the Frio Formation was determined from stratigraphic cross sections constructed by Dodge and Posey (1981) and modified by Galloway and others (1982). Where present, cap rock is found at depths shallower than the 90°C isotherm and in the transition between the hydro pressured ( $\leq 0.465$  psi/ft [10.5 kPa/m] pressure gradient) and abnormal pressure regimes.

Each data point on figure IV-1 represents a shale interval generally 30 ft (10 m) thick, although thinner intervals were used when necessary. Data points A through H define a cap rock interval approximately 800 ft (240 m) thick. This depth zone, as defined from each resistivity plot, includes sandstones and shale and therefore is termed the cap rock interval in this study.

### Thickness

Mapping of the cap rock interval within the Frio Formation shows a few small areas of cap rock in the Upper and Middle Texas Gulf Coast and larger areas having greater thicknesses in the Lower Texas Gulf Coast (fig. IV-2). In the upper coastal region, cap rock is found in scattered wells in Brazoria and Galveston Counties and in Jefferson County. However, only four wells have a cap rock interval more than 600 ft (180 m) thick, and only one well contains as much as 900 ft (275 m). The Galveston - Brazoria County area, and to a lesser extent the Jefferson County area, show some spatially contiguous cap rock development in Miocene strata downdip of the Frio occurrences, but these are not included in figure IV-2.

In the Lower Texas Gulf Coast, areas of cap rock are present where many wells penetrate high-resistivity intervals more than 700 ft (210 m) thick, and some wells contain intervals 1,100 to 1,400 ft (340 to 430 m) thick. The greatest areal extents of cap rock are in Kleburg and Kenedy Counties, Hidalgo County, and a coast-parallel trend in Cameron and southeastern Willacy Counties (fig. IV-2). No zero isopach is shown on figure IV-2 because wells outside the 300-ft (90-m) isopach may contain thin intervals of high-resistivity shale and because interpretation of the shale-resistivity plot is increasingly subjective in cases of poor cap rock development.

### Peak Resistivity

Where Frio cap rock was found, the maximum resistivity occurs in the cap rock interval (fig. IV-1, point F). Even without cap rock development, resistivities within an individual well

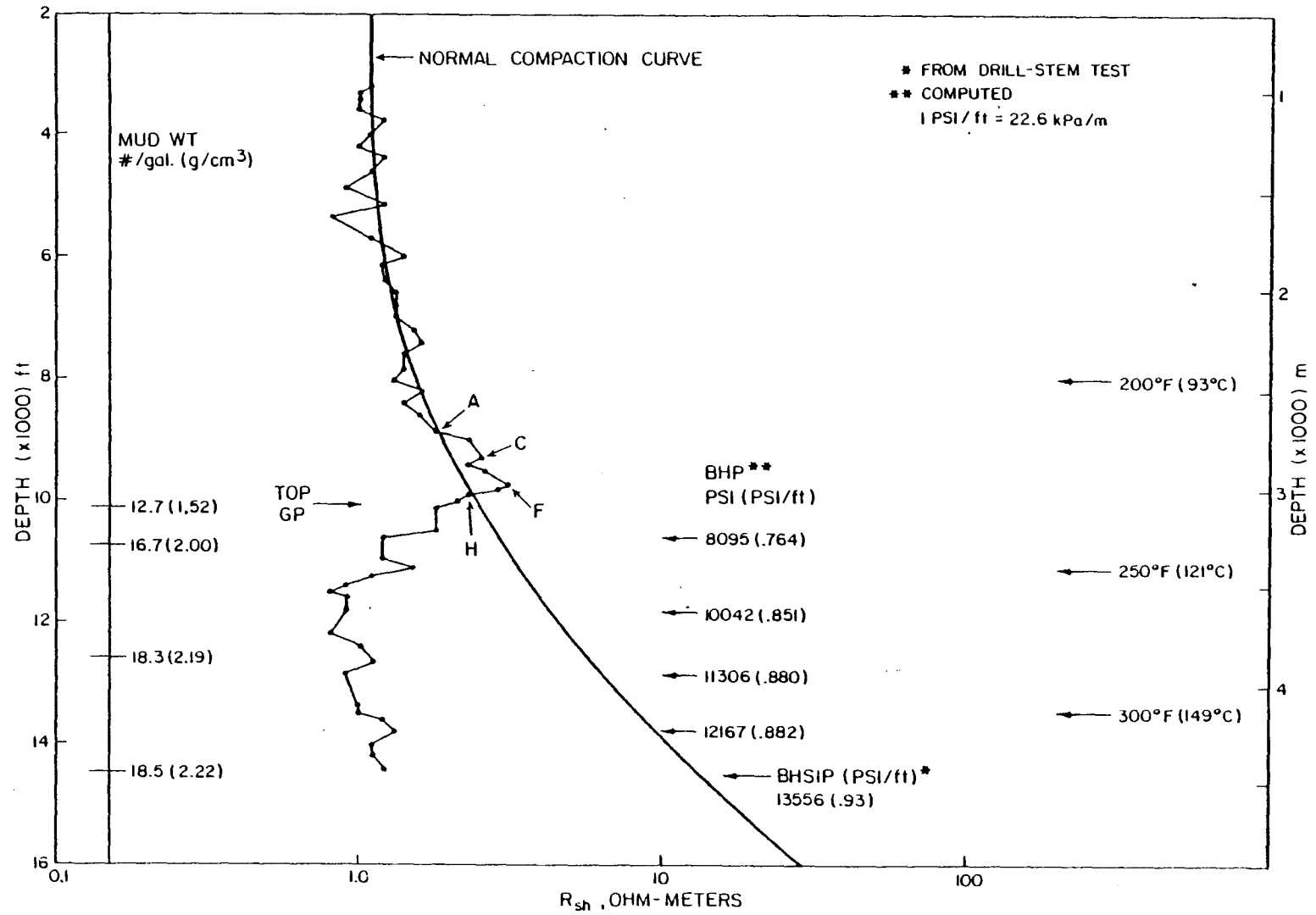


Figure IV-1. Shale-resistivity plot for the Humble Oil and Refining Company No. B-23 S. K. East well in Kenedy County, Texas.

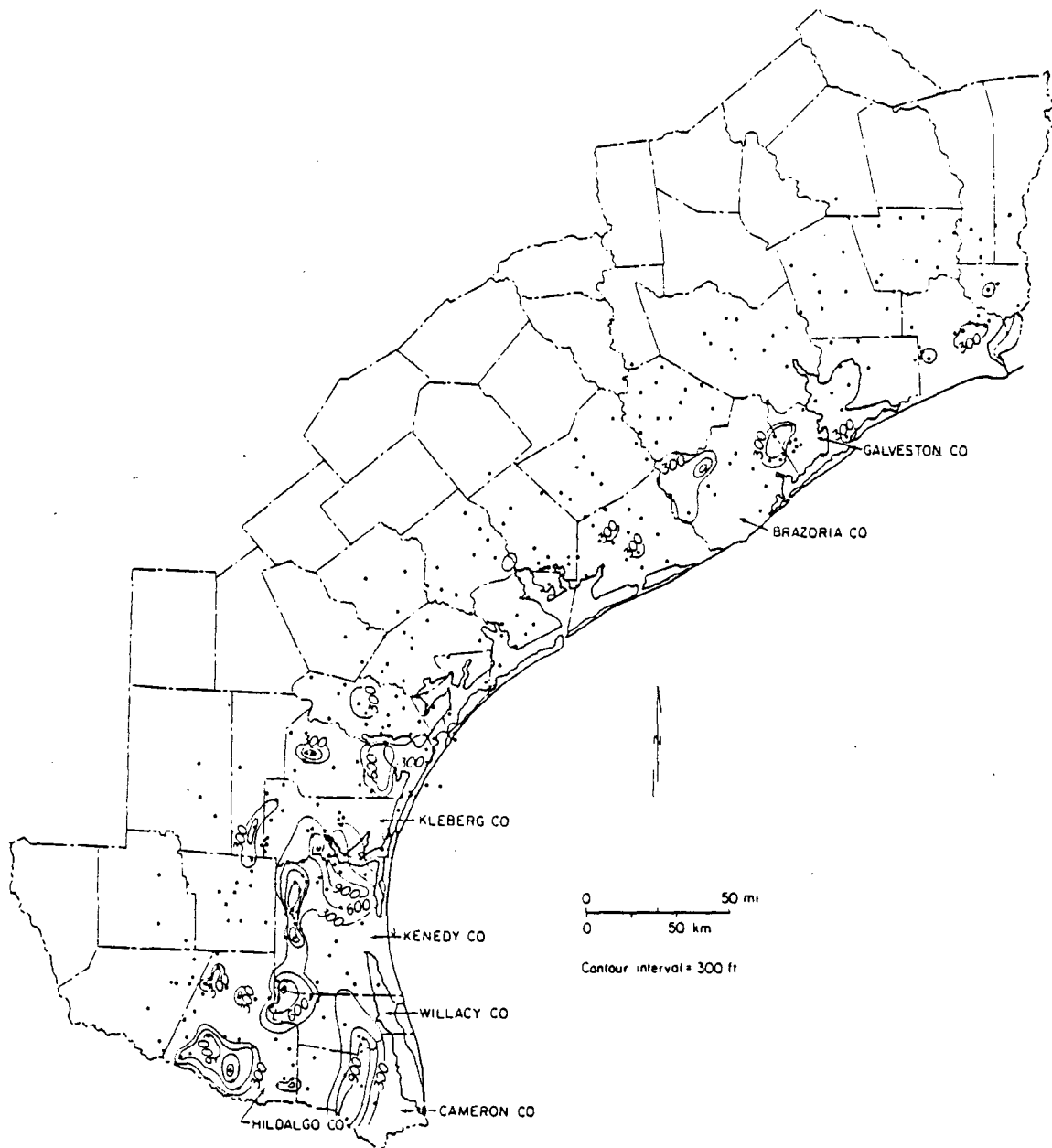


Figure IV-2. Thickness of cap rock intervals within the Frio Formation of the Texas Gulf Coast.

**Table IV-1. Criteria for defining cap rock using shale-resistivity plots derived from geophysical well logs.**

1. Shale intervals selected for reading of resistivity must show an SP response as close to baseline as possible and must generally be 30 ft (9 m) thick. Thinner intervals may be used if necessary; resistivity is read from the amplified short-normal trace of the induction electrical log.
2. The distribution of shale resistivity versus depth must be compared to the normal compaction curve based on resistivity of hydro pressured shales in a given county (see Gregory and Backus, 1980).
3. Two or more data points that exceed the normal compaction curve on the shale resistivity plot are considered necessary to define a cap rock interval. Single high values may be noted separately.
4. If irregular low-amplitude SP deflection occurs within a resistive interval, a tight silty or sandy shale (or hydrocarbons) may be indicated. Such a zone is not considered cap rock.

reach a maximum at the lowest point along the normal compaction curve just before encountering lower resistivities of undercompacted shales within the geopressed zone (if such a zone is present in a well). The Upper and Middle Texas Gulf Coasts are characterized by maximum Frio shale resistivities of less than 2.0 ohm-meters except near limited cap rock development (fig. IV-3). The coastwide trend is one of increasing maximum shale resistivity from north to south; peak values are approximately 6.0 ohm-meters in wells penetrating cap rock in the Lower Texas Gulf Coast (fig. IV-3).

#### Delineation of Study Area

Because regional studies showed that cap rock in the Frio Formation is best developed in the Lower Texas Gulf Coast, an area including parts of Kenedy and Kleberg Counties was selected for detailed study (fig. IV-4). The study area overlies part of a major Frio delta where drilling for geopressed Frio gas reservoirs has provided well control to depths of 12,000 to 17,000 ft (3,700 to 5,200 m).

#### CAP ROCK - FACIES RELATIONSHIPS

The Frio Formation consists of four major depositional systems in the Texas Gulf Coast: (1) the Houston delta system of the upper coast, (2) the Greta/Çarancahua barrier/strandplain system of the middle coast, (3) the Choke Canyon/Flatonia coastal lake/streamplain system of the middle coast, and (4) the Norias delta system of the lower coast (Galloway and others, 1982) (fig. IV-4). Facies interpretations of regional cross sections by Dodge and Posey (1981) show that cap rock has developed predominantly in the delta-front-slope facies of the Norias delta system (figs. IV-4 and IV-5) (Finley, 1982). Evidence will be presented to show that the formation of cap rock is likely to be a diagenetic process; therefore, this apparent facies relationship is not considered significant. Within the study area, the delta-front-slope facies is simply a volumetrically significant facies that occurs within a depth range (temperature and pressure regime) believed to be favorable to cap rock formation. Furthermore, the development of cap rock in the Norias delta system and the lack of cap rock in the Houston delta system imply that cap rock is not related to maturation of CO<sub>2</sub> in organic-rich deltaic sediments.

#### ANALYSIS OF CAP ROCK

Sidewall core and whole core of cap rock intervals were obtained for compositional analysis from three wells in Kenedy County, Texas, through the courtesy of Exxon Company,

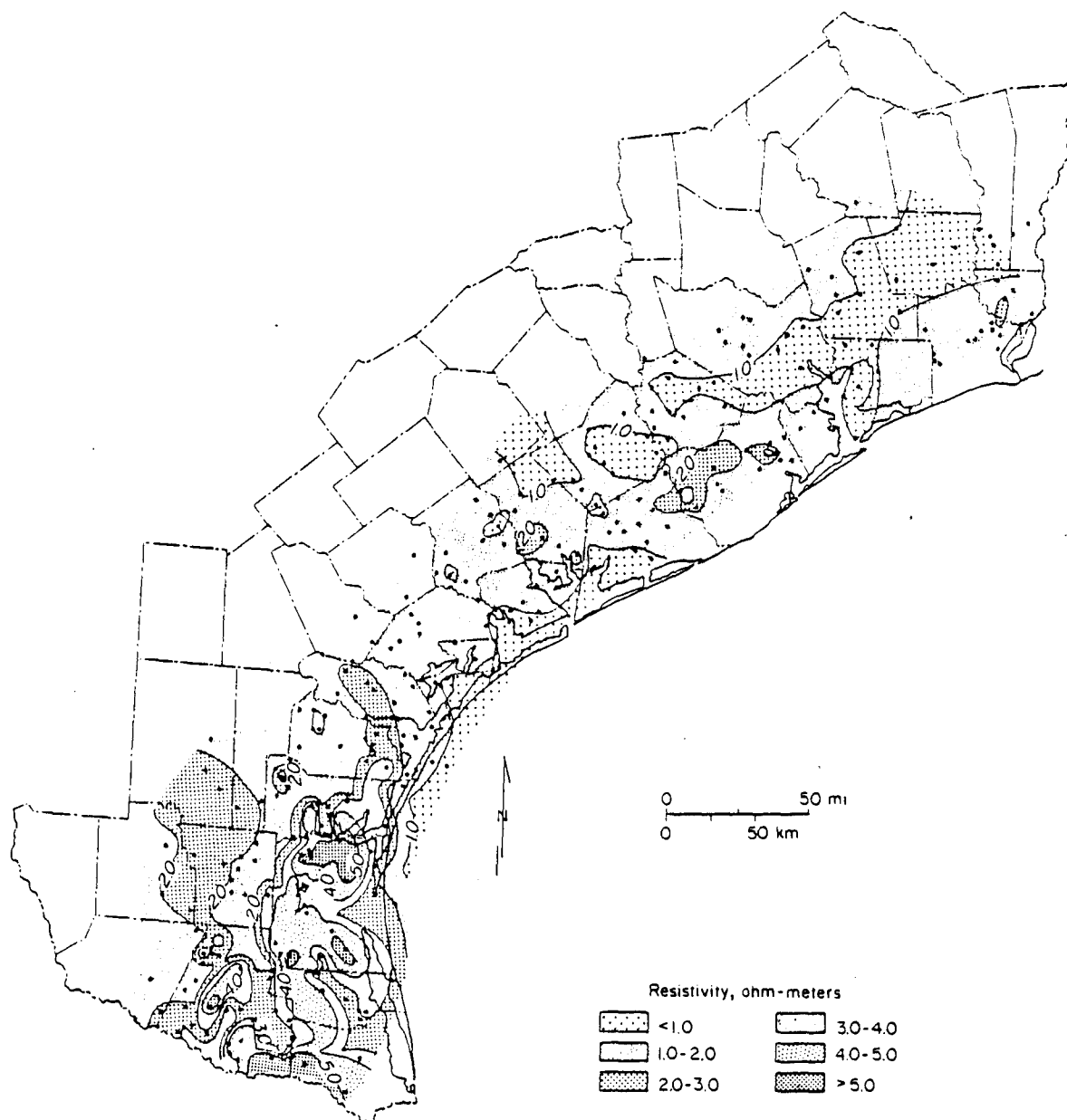


Figure IV-3. Maximum shale resistivity within the Frio Formation of the Texas Gulf Coast.

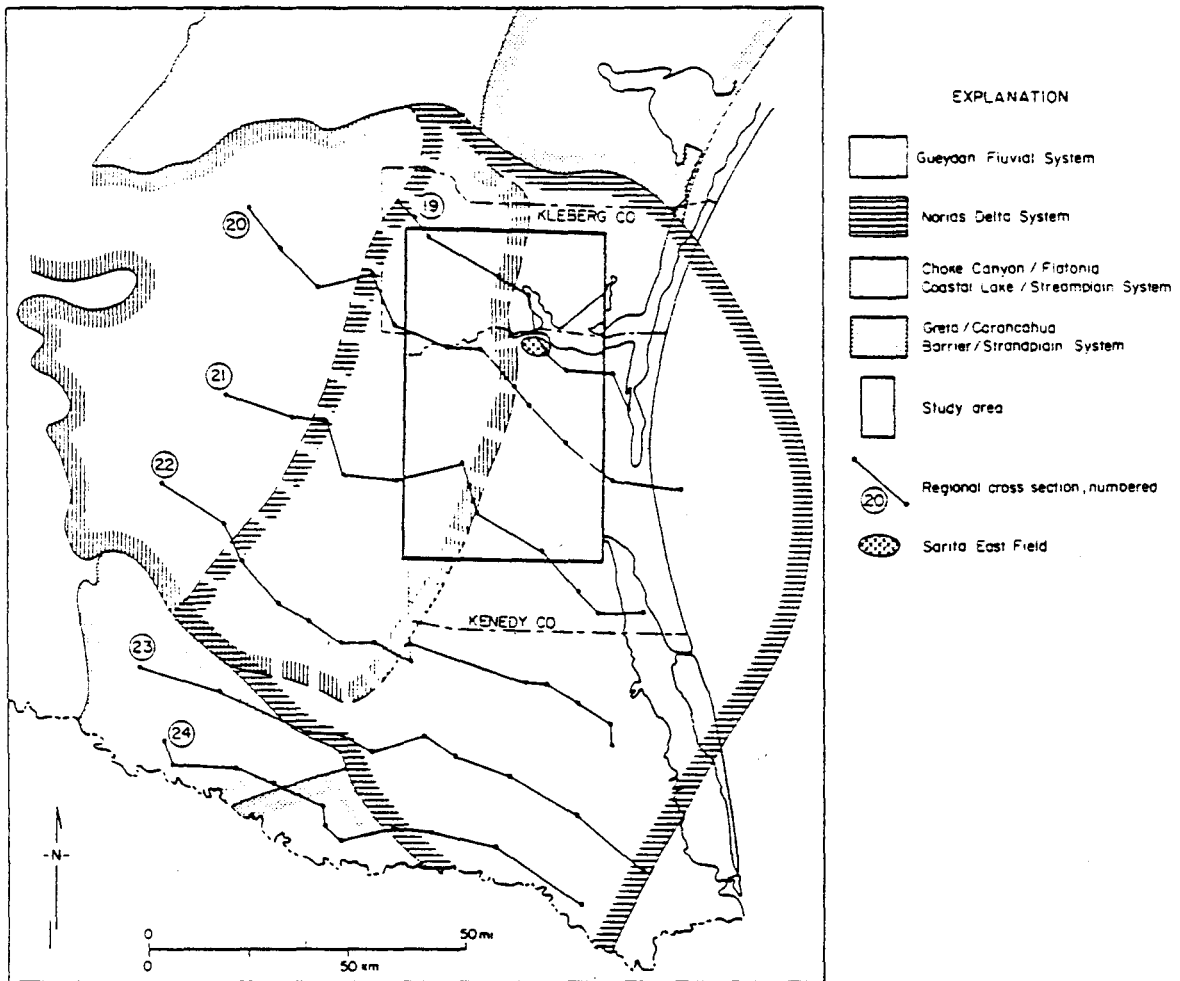


Figure IV-4. Major depositional systems of the Frio Formation in the Lower Texas Gulf Coast and location of regional cross sections in an area of more detailed study, which includes Sarita East field.

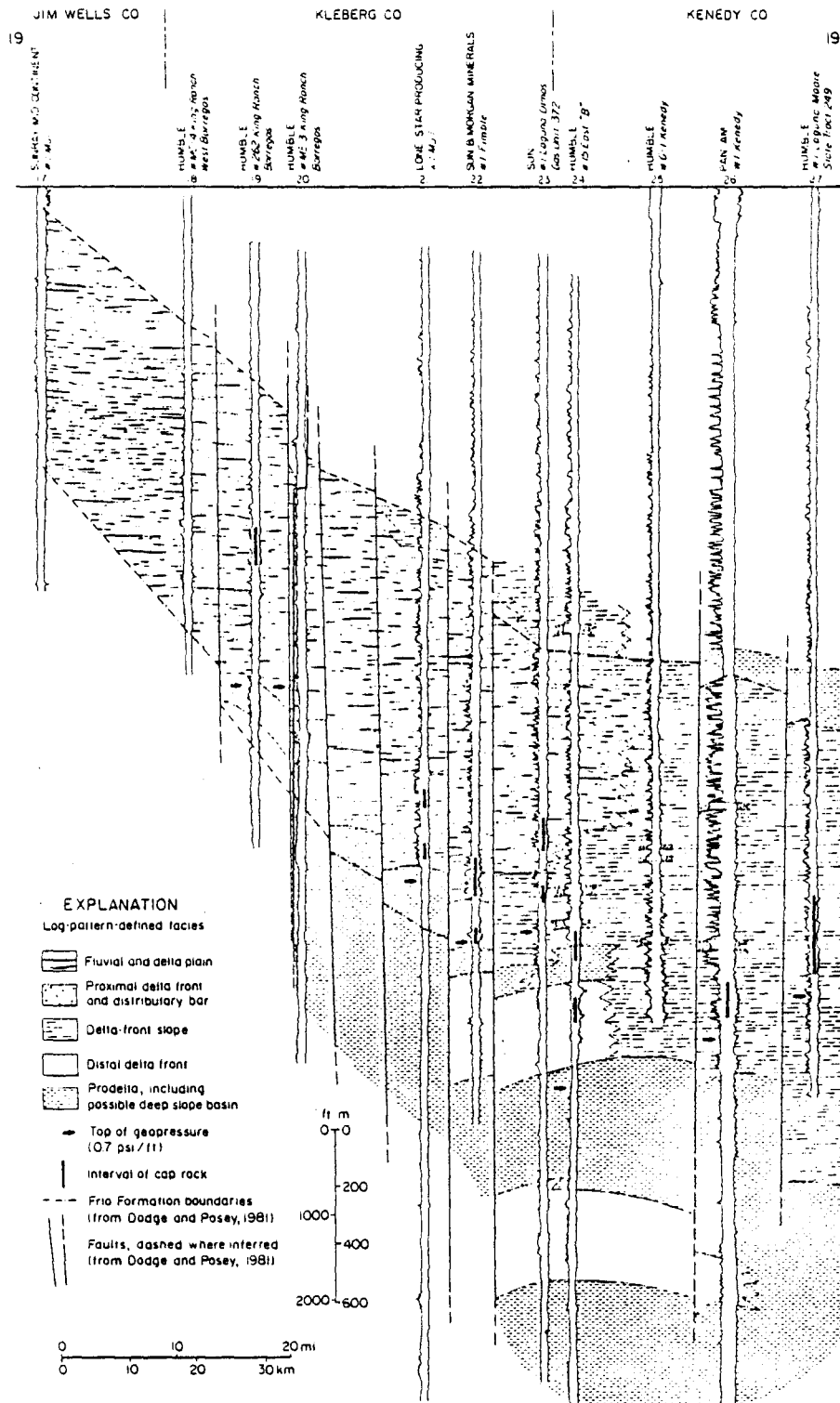


Figure IV-5. Facies interpretation of part of regional cross section 19 (from Dodge and Posey, 1981). See figure IV-4 for location.

U.S.A. In the Exxon No. B-39 S. K. East well in Sarita East field (fig. IV-4), sidewall cores of sands and shales were obtained from non-cap rock and cap rock intervals for analysis of total carbonate by CHN analyzer, for multi-element analysis by inductively coupled plasma atomic emission spectroscopy, and for mineralogy by X-ray diffraction. Morphology of shales was investigated using a scanning electron microscope (SEM) supplemented by energy dispersive analysis. Similar studies were made on whole core from part of the cap rock interval of the Humble Oil and Refining Company No. G-3 (No. 24) S. K. East well and from a non-cap rock core from the Humble Oil and Refining Company No. 17 S. K. East well. The latter wells are to the south of Sarita East field and are located 15 mi (24 km) apart in separate major fault blocks.

The sidewall core samples are a unique data set in that the cores, including samples of shales, were obtained specifically for cap rock studies by picking sidewall coring points at the wellsite immediately upon completion of geophysical logging. Sidewall core recovery included five non-cap rock shales, six cap rock shales, and sandstones both shallower than (five samples) and within (three samples) the cap rock interval. Mechanical problems affected the number and distribution by depth of samples recovered; therefore, sample spacing is uneven and strata shallower than 7,000 ft (2,100 m) are poorly represented.

#### Total Carbonate

Total carbonate in cap rock and non-cap rock intervals shows substantially no difference (tables IV-2 and IV-3). Precision of the analysis varied from less than 0.1 to 0.3 percent on the basis of replicate analyses. However, variation in total carbonate between closely spaced samples in a 1-ft (0.3-m) depth interval was up to 1.6 percent (10,312 ft A, B, C; table IV-3).

#### Silica and Multi-Element Analysis

In shale samples from the Exxon No. B-39 S. K. East well, percent total SiO<sub>2</sub> is generally 2 to 3 percent more in cap rock than in non-cap rock (table IV-4). Differences between cap rock and non-cap rock in other elements are not well defined, but the number of samples is small for the discrimination of trends (table IV-4). Within shale samples from whole core, an average 1.4 percent greater silica content was found in the non-cap rock samples (table IV-5). However, because the cap rock and non-cap rock samples come from the limited depth range of a single cored interval and from widely spaced wells, comparisons cannot be readily made with the suite of samples from a single well. Furthermore, the non-cap rock samples from the Humble No. 17 S. K. East well are from immediately below the cap rock interval of that well, not from above the interval as in the Exxon No. B-39 S. K. East, and this affects relative

Table IV-2. Percent total carbonate in non-cap rock and cap rock interval sediments in Exxon No. B-39 S. K. East well, Kenedy County, Texas.

Sandstone				Shale			
Non-Cap Rock		Cap Rock		Non-Cap Rock		Cap Rock	
Depth (ft)	%	Depth (ft)	%	Depth (ft)	%	Depth (ft)	%
4,802	6.2	9,877	2.6	3,493	5.1	9,821	3.1
7,997	5.0	10,565	6.3	7,247	5.5	9,961	5.7
8,816	*	10,566	9.5	7,738	4.0	9,962	6.5
9,395	4.9			8,164	5.0	10,004	5.7
				9,180	11.5	10,768	5.8
				N = 5		11,030	4.3
				$\bar{X} = 6.2$		N = 6	
				SD = 3.0		$\bar{X} = 5.2$	
						SD = 1.3	

\*Insufficient amount of sample.

Table IV-3. Percent total carbonate in non-cap rock and cap rock shales in two wells in Kenedy County, Texas.

Humble No. 17 S. K. East Non-Cap Rock Shale		Humble No. G-3 (No. 24) S. K. East Cap Rock Shale	
Depth (ft)	%	Depth (ft)	%
10,969	7.2	10,150 A	7.0
10,990	5.8	10,150 B	6.4
10,993	4.7	10,156	6.6
11,052	5.6	10,232	4.7
11,056	6.4	10,235	5.6
11,065	2.4	10,237	1.6
	N = 6	10,241	8.4
	$\bar{X}$ = 5.4	10,251	11.6
	SD = 1.7	10,276	5.8
		10,304	5.4
		10,312 A	3.1
		10,312 B	4.6
		10,312 C	4.1
			N = 13
			$\bar{X}$ = 5.8
			SD = 2.5

**Table IV-4. Multi-element analysis of non-cap rock and cap rock shales in Exxon No. B-39 S. K. East well, Kenedy County, Texas. (Whole rock basis is expressed as equivalent percent of oxide.)**

Depth (ft)	Non-Cap Rock					Cap Rock					
	3,493	7,247	7,738	8,164	9,180	9,821	9,961	9,962	10,004	10,768	11,030
SiO <sub>2</sub>	55.05	56.01	56.79	56.87	46.15	59.71	59.39	50.24	59.41	59.52	59.06
Na <sub>2</sub> O	1.32	1.63	1.28	1.23	1.77	2.49	3.71	2.22	2.29	1.23	4.95
K <sub>2</sub> O	2.52	2.60	3.33	3.53	1.99	3.33	1.74	1.90	2.40	2.97	1.62
MgO	2.37	2.19	2.23	2.41	1.44	2.35	1.73	3.41	1.76	1.90	1.05
CaO	7.92	9.06	6.92	7.15	18.83	4.11	8.25	10.51	9.27	8.25	6.23
Al <sub>2</sub> O <sub>3</sub>	14.68	13.83	15.33	14.08	9.93	14.95	12.11	12.30	11.51	12.58	13.93
Fe <sub>2</sub> O <sub>3</sub> (T)*	5.03	5.35	5.94	6.35	3.68	6.06	3.91	8.09	3.78	4.26	2.23
TiO <sub>2</sub>	0.65	0.68	0.71	0.63	0.47	0.63	0.47	0.48	0.49	0.60	0.37
MnO <sub>2</sub>	0.08	0.05	0.06	0.06	0.14	0.03	0.05	0.09	0.05	0.04	0.04
SrO	0.05	0.04	0.03	0.03	0.05	0.03	0.04	0.04	0.04	0.05	0.04
BaO	0.13	0.05	0.06	0.04	0.26	0.32	0.14	0.43	0.12	0.40	1.00

\*Total iron expressed as Fe<sub>2</sub>O<sub>3</sub>.

Table IV-5. Percent total silica in non-cap rock and cap rock shales in two wells in Kenedy County, Texas.

Humble No. 17 S. K. East Non-Cap Rock Shale		Humble No. G-3 (No. 24) S. K. East Cap Rock Shale	
Depth (ft)	%	Depth (ft)	%
10,969	56.9	10,150 A	50.5
10,990	55.6	10,150 B	57.0
10,993	56.9	10,156	53.2
11,052	56.7	10,232	62.7
11,056	57.7	10,235	56.0
11,065	62.3	10,237	62.7
	N = 6	10,241	53.4
	$\bar{X} = 57.7$	10,251	48.0
	SD = 2.4	10,276	54.8
		10,304	56.7
		10,312 A	59.7
		10,312 B	57.1
		10,312 C	59.5
			N = 13
			$\bar{X} = 56.3$
			SD = 4.4

position in the diagenetic sequence. Note again the differences between samples from within a 1-ft (0.3-m) interval (10,150 ft A, B; 10,312 ft A, B, C) (table IV-5). Analyses of other elements listed in table IV-4 show little systematic variation between cap rock and non-cap rock in the cored wells.

### Clay Mineralogy

X-ray diffraction of the less than 2 $\mu$ m fraction of shales from the Exxon No. B-39 S. K. East well was completed for untreated, heated (550°C) and glycolated samples. Interpretation of peak heights for kaolinite, smectite-illite, illite, and chlorite show two important trends: (1) a decrease in mixed layer smectite-illite and an increase in "discrete" illite through the cap rock interval and (2) the development of chlorite within the cap rock interval (fig. IV-6). The increase in illite with a distinct 10 Å peak and the decrease in smectite-illite is an expected result of mixed layer smectite-illite diagenesis (Hower and others, 1976; Boles and Franks, 1979). The increase in chlorite within the cap rock interval is consistent with higher temperature gradients on the lower Texas coast and a mineralogy rich in unstable rock fragments capable of yielding Fe<sup>2+</sup> and Mg<sup>2+</sup> (Kaiser, section III, this report; Loucks and others, 1981). The mechanism of chlorite formation may also be tied to smectite diagenesis, as discussed below. The increase in kaolinite in the cap rock interval occurs in the transition from hydro pressured to geopressed conditions, where Kaiser (section III, this report) found maximum expansion of the kaolinite stability field.

### DIAGENETIC MECHANISMS

The smectite-illite transformation is a well-known aspect of burial diagenesis of shales that has been investigated in detail using Gulf Coast examples (Perry and Hower, 1970; Hower and others, 1976; Boles and Franks, 1979). Whether or not aluminum is considered an immobile constituent of the transformation, the illitization of smectite releases large quantities of Si<sup>4+</sup>, along with Mg<sup>2+</sup> and Fe<sup>2+</sup>, and the reaction is well underway at relatively low temperatures (50° to 60°C) (Boles and Franks, 1979). Hower and others (1976) indicated that some silica released from the conversion is precipitated within the shales. However, Boles and Franks (1979) suggested that determining whether shales are open or closed systems relative to sandstones is difficult because of low sand-shale ratios and unknown variations in original shale composition. Loucks and others (1981) found little evidence in favor of open shale systems, but they concluded that further highly quantitative data were necessary to resolve the question. There seems little doubt, however, that the smectite-illite transition offers a mechanism for

silica mobilization and potential enrichment in parts of the stratigraphic column in which silica is released.

Kaiser (section III, this report) shows that chloritization of smectite can be initiated at low temperatures (50° to 75°C) if pH is as high as approximately 8. The abundance of chlorite in lower coast Frio sandstones shows that the stability of chlorite is favored by higher pH, higher temperature, and a larger  $\log \text{Mg}^{2+} - \text{Fe}^{2+}$  activity product, reflecting the availability of these ions from volcanic-rich detritus of the Norias delta system. Where chloritization is thermodynamically favored, 58 percent more silica is released per mole of smectite in the conversion to chlorite than in the conversion to illite (Kaiser, section III, this report). A stage of silica generation due to chloritization under hydro pressured conditions and at a temperature range of 50° to 75°C would yield considerable quantities of silica beyond those expected from smectite-illite diagenesis. Thus, a mechanism for release of silica from more than one clay mineral transformation exists in the Frio Formation of the lower Texas coast that does not exist in the upper coast.

Furthermore, figure IV-6 shows that kaolinite content increases in the cap rock interval, possibly as a result of transformation of smectite to kaolinite. This reaction also releases silica. Kaiser's data (section III, this report) suggest that kaolinite and chlorite are stable under different temperatures and pH levels, which indicates a potential conflict in their occurrence in the cap rock interval. However, variations in pH may have occurred over time where cap rock occurs in the transition between hydro pressured and geopressured regimes, and the geothermal gradient may not have been constant. Most importantly, this transition is an active zone of clay mineral diagenesis, and the development of cap rock is coincident with this activity.

#### DISCUSSION AND IMPLICATIONS FOR CAP ROCK DEVELOPMENT

Chemical analysis of sidewall core and whole core from Kenedy County, Texas, indicates no increased concentration of carbonate minerals in cap rock shales of the Frio Formation. SEM studies failed to find any authigenic carbonate grains preferentially developed in cap rock and confirmed that carbonate microfossils were not concentrated in shales of the cap rock interval. These direct observations call into question the model of cap rock development proposed by Magara (1981) wherein carbonate cements, leached in the geopressured zone, are reprecipitated to form high-resistivity cap rock shale in the immediately overlying transition between the geopressured and hydro pressured regimes. Milliken and Land (1982) failed to find excess carbonate in a well cited by Magara (1981) as evidence of cap rock development. Magara's (1981) model implies that development of secondary porosity at depth would release

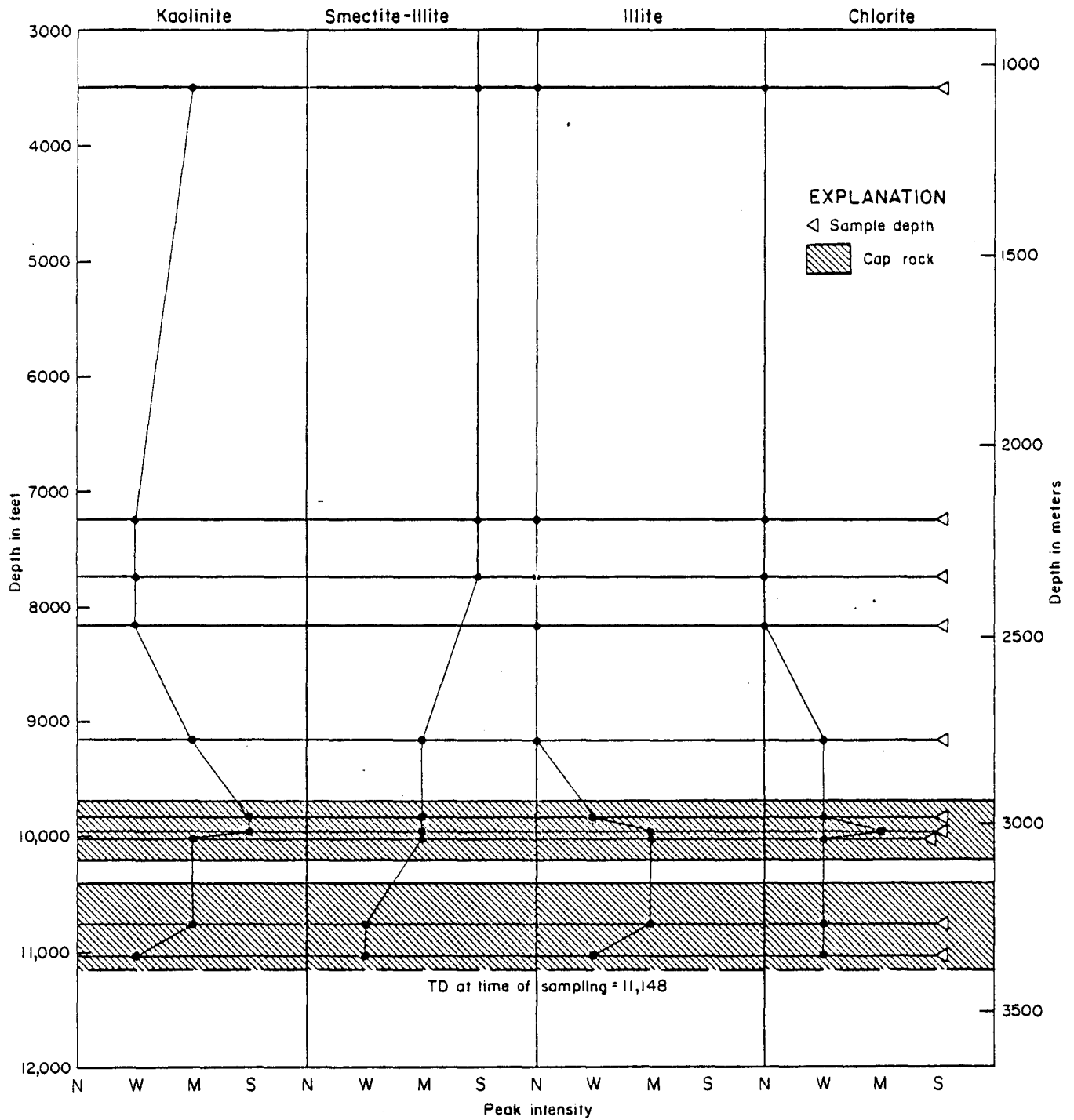


Figure IV-6. Qualitative interpretation of clay mineral distribution in the Exxon No. B-39 S. K. East well in Kenedy County, Texas, based on X-ray diffraction patterns. Relative intensity of peak heights was judged to be not present (N), weak (W), moderate (M), or strong (S). Uncorrected bottom-hole temperature at time of sampling was 87°C.

ions to subsequently precipitate as cap rock. If such were the case, regional trends of improved reservoir quality due to leaching would correlate positively with cap rock occurrence. Instead, within the Frio Formation, maximum cap rock development on the lower Texas coast correlates with reservoirs of low porosity and permeability wherein carbonate cements are ubiquitous. Improved reservoir quality, which petrographic studies have shown is largely owing to leaching of authigenic calcite, occurs on the upper coast (Loucks and others, 1981; Kaiser and Richmann, 1981); there, cap rock development is minimal (fig. IV-2). Cap rock development also cannot be tied to deltaic depositional facies, which might imply a connection between cap rock and terrestrial organic matter yielding potentially greater amounts of CO<sub>2</sub> than marine organic matter. Differences in cap rock development within coeval Frio deltaic depocenters argue against accumulation of a particular type of organic matter as a cause of cap rock development.

The distribution of cap rock in the Frio correlates with poor reservoir quality at depth, with a relatively unstable mineral assemblage rich in volcanic rock fragments, and with the higher geothermal gradient of the lower coast compared to the upper coast. A slight increase in silica content of cap rock relative to overlying shales and the initiation of the smectite-illite transition in a temperature range of 75° to 90°C suggest that clay mineral transformations are involved in cap rock genesis. Lack of cap rock throughout the Frio, however, indicates that the geochemical environment of the lower coast, in which chloritization is favored is also favorable to the formation of cap rock.

The mechanism postulated to be actually responsible for cap rock development is the generation of silica by clay mineral transformations, especially the chloritization of smectite if solution-mineral equilibria favor chlorite stability. The occurrence of cap rock in the transition from the hydro pressured to the geopressured interval ( $>0.465$  psi/ft [ $10.5$  kPa/m] pressure gradient) is probably favored by expulsion of fluids from the more highly geopressured interval below (gradients  $\geq 0.7$  psi/ft [ $15.8$  kPa/m]) (Magara, 1976). These fluids would contain some proportion of the silica released by clay diagenesis, as evidenced by the slight increase in total silica of the cap rock in the Exxon No. B-39 S. K. East well; clay mineral transformation having no mobilization of silica whatsoever would not change bulk chemistry from one interval to another. Apparently, the smectite-illite transition alone is not adequate to generate cap rock, although it may have a role in the development of geopressured intervals by reducing permeability in the interval of silica generation (Foster, 1981).

The non-cap rock shales of the Humble No. 17 S. K. East well (table IV-5) are deeper than the cap rock interval in that well. Thus, these shales may have undergone as much or more silica enrichment than cap rock shales and are not comparable to the non-cap rock shales of the

No. B-39 well (table IV-4). Comparison of the bulk chemistry of cap rock and non-cap rock must consider that true differences may be small in relation to natural variability and that differences may exist in the diagenetic history of individual major fault blocks that affect the distribution of cap rock.

As a result of the present study, further examination of clay mineral transformations in relation to the origin of cap rock appears warranted. New studies of Frio diagenesis have provided important information relevant to its possible origin (Kaiser, section III, this report). A plot of ionic strength versus depth for Frio waters (Kaiser, fig. III-12, this report) does not show a trend toward fresher waters in the transition between hydro pressured and geopressed regimes where cap rock occurs. Thus, the higher resistivity of cap rock shales does not appear to be related to fresher, more resistive formation fluids. No formation waters were available directly from a cap rock interval. Furthermore, if exsolved gas is capable of increasing formation resistivity in the cap rock interval, it is unclear why such a phenomenon should show regional variation that correlates with mineralogy and diagenetic history. More samples of cap rock must be analyzed to determine if the addition of diagenetic silica to the transition zone between hydro pressured and geopressed regimes is a viable cause of the increased shale resistivity that defines the cap rock interval.

#### CONCLUSIONS

1. Core samples of cap rock shales show slight enrichment in silica and no enrichment in carbonate relative to overlying non-cap rock shale.
2. The distribution of cap rock within the Frio Formation of the Texas Gulf Coast shows unequal development of cap rock in contemporaneous major deltaic depocenters and correlates with the relatively unstable mineral assemblage of the lower coast; cap rock is best developed overlying reservoirs of poor quality of the lower coast.
3. The temperature at which cap rock occurs and the vertical distribution of clay minerals suggest that the smectite-illite transformation may contribute to cap rock development. However, cap rock is dominantly developed where solution mineral equilibria favor the smectite-chlorite transition in a region of higher geothermal gradient and greater availability of  $\text{Fe}^{2+}$  and  $\text{Mg}^{2+}$ . Regionally, the development of cap rock correlates with the distribution of chlorite.

#### ACKNOWLEDGMENTS

This research was funded in part by the U.S. Department of Energy, Division of Geothermal Energy, under Contract No. DE-AC08-79ET27111. Exxon Company, U.S.A.,

graciously provided access to existing core and allowed collection of additional samples critical to this study. Larry Mack assisted with SEM analyses. Chemical and X-ray diffraction analyses were done under the direction of Clara L. Ho, Mineral Studies Laboratory of the Bureau of Economic Geology. Illustrations were prepared by Margaret Day, John Ames, and Jamie McClelland under the direction of Dan Scranton. The report was typed by Doris Tyler, Twyla J. Coker, and Jana McFarland under the direction of Lucille Harrell.

#### REFERENCES

- Bebout, D. G., Loucks, R. G., and Gregory, A. R., 1978, Frio sandstone reservoirs in the deep subsurface along the Texas Gulf Coast, their potential for the production of geopressured geothermal energy: The University of Texas at Austin, Bureau of Economic Geology Report of Investigations No. 91, 92 p.
- Boles, J. R., and Franks, S. G., 1979, Clay diagenesis in Wilcox sandstones of southwest Texas: implications of smectite diagenesis on sandstone cementation: *Journal of Sedimentary Petrology*, v. 49, p. 55-70.
- Dodge, M. M., and Posey, J. S., 1981, Structural cross sections, Tertiary formations, Texas Gulf Coast: The University of Texas at Austin, Bureau of Economic Geology Cross Sections.
- Fertl, W. H., 1976, Abnormal formation pressures: New York, Elsevier Publishing Co., 382 p.
- Finley, R. J., 1982, A preliminary assessment of high-resistivity cap rock shale in the Frio Formation of the Texas Gulf Coast: The University of Texas at Austin, Bureau of Economic Geology, report to the U.S. Department of Energy, Division of Geothermal Energy, Contract No. DOE/ET/27111-6, 28 p.
- Foster, W. R., 1981, The smectite-illite transformation: its role in generating and maintaining geopressure (abs.): *Geological Society of America Abstracts with Programs*, v. 13, no. 7, p. 454.
- Galloway, W. E., Hobday, D. K., and Magara, K., 1982, Frio Formation of Texas Gulf Coastal Plain: depositional systems, structural framework, and hydrocarbon distribution: *American Association of Petroleum Geologists Bulletin*, v. 66, p. 649-688.
- Gregory, A. R., and Backus, M. M., 1980, Geopressured formation parameters, geothermal well, Brazoria County, Texas, in Dorfman, M. H., and Fisher, W. L., eds., *Proceedings, Fourth United States Gulf Coast Geopressured Geothermal Energy Conference: Research and Development, Vol. 1*: The University of Texas at Austin, Center for Energy Studies, p. 235-311.
- Gregory, A. R., Dodge, M. M., Posey, J. S., and Morton, R. A., 1980, Volume and accessibility of entrained (solution) methane in deep geopressured reservoirs--Tertiary formations of the Texas Gulf Coast: The University of Texas at Austin, Bureau of Economic Geology, report to the U.S. Department of Energy, Division of Geothermal Energy, Contract No. DE-AC08-78ET01580, 390 p.

- Hottman, C. E., and Johnson, R. K., 1965, Estimation of formation pressures from log-derived shale properties: *Journal of Petroleum Technology*, v. 17, p. 717-723.
- Hower, J., Eslinger, E. V., Hower, M. E., and Perry, E. A., 1976, Mechanism of burial metamorphism of argillaceous sediment: 1. mineralogical and chemical evidence: *Geological Society of America Bulletin*, v. 87, p. 725-737.
- Kaiser, W. R., and Richmann, D. L., 1981, Predicting diagenetic history and reservoir quality in the Frio Formation of Brazoria County, Texas, and Pleasant Bayou test wells, in Bebout, D. G., and Bachman, A. L., eds., *Proceedings, Fifth U.S. Gulf Coast Geopressured-Geothermal Energy Conference*: Baton Rouge, Louisiana State University, p. 67-74.
- Lindquist, S. J., 1977, Secondary porosity development and subsequent reduction, overpressured Frio Formation sandstone (Oligocene), South Texas: *Gulf Coast Association of Geological Societies Transactions*, v. 27, p. 99-107.
- Loucks, R. G., Bebout, D. G., and Galloway, W. E., 1977, Relationship of porosity formation and preservation to sandstone consolidation history--Gulf Coast lower Tertiary Frio Formation: *Gulf Coast Association of Geological Societies Transactions*, v. 27, p. 109-120.
- Loucks, R. G., Dodge, M. M., and Galloway, W. E., 1979, Sandstone consolidation analysis to delineate areas of high-quality reservoirs suitable for production of geopressured geothermal energy along the Texas Gulf Coast: The University of Texas at Austin, Bureau of Economic Geology, report to the U.S. Department of Energy, Division of Geothermal Energy, Contract No. EG-77-5-05-5554, 97 p.
- Loucks, R. G., Richmann, D. L., and Milliken, K. L., 1981, Factors controlling reservoir quality in Tertiary sandstones and their significance to geopressured geothermal production: The University of Texas at Austin, Bureau of Economic Geology Report of Investigations No. 111, 41 p.
- Magara, K., 1976, Water expulsion from clastic sediments during compaction--directions and volumes: *American Association of Petroleum Geologists Bulletin*, v. 60, p. 543-553.
- Magara, K., 1981, Fluid dynamics of cap-rock formation in Gulf Coast: *American Association of Petroleum Geologists Bulletin*, v. 65, p. 1334-1343.
- Milliken, K. L., and Land, L. S., 1982, Fluid dynamics for cap-rock formation in Gulf Coast, discussion: *American Association of Petroleum Geologists Bulletin*, v. 66, p. 2685-2687.
- Milliken, K. L., Land, L. S., and Loucks, R. G., 1981, History of burial diagenesis determined from isotopic geochemistry, Frio Formation, Brazoria County, Texas: *American Association of Petroleum Geologists Bulletin*, v. 65, p. 1397-1413.
- Perry, E., and Hower, J., 1970, Burial diagenesis in Gulf Coast pelitic sediments: *Clays and Clay Minerals*, v. 18, p. 165-177.
- Schmidt, V., and McDonald, D. A., 1979, The role of secondary porosity in sandstones, in Scholle, P. A., and Schluger, P. R., eds., *Aspects of diagenesis*: Society of Economic Paleontologists and Mineralogists Special Publication No. 26, p. 175-207.

